



THE UNIVERSITY OF
WAIKATO
Te Whare Wānanga o Waikato

Research Commons

<http://researchcommons.waikato.ac.nz/>

Research Commons at the University of Waikato

Copyright Statement:

The digital copy of this thesis is protected by the Copyright Act 1994 (New Zealand).

The thesis may be consulted by you, provided you comply with the provisions of the Act and the following conditions of use:

- Any use you make of these documents or images must be for research or private study purposes only, and you may not make them available to any other person.
- Authors control the copyright of their thesis. You will recognise the author's right to be identified as the author of the thesis, and due acknowledgement will be made to the author where appropriate.
- You will obtain the author's permission before publishing any material from the thesis.

Effects of catastrophic coastal landslides on the Te Angiangi Marine Reserve, Hawke's Bay, New Zealand

A thesis submitted in partial fulfilment
of the requirements for the degree
of
Master of Science
in Earth & Ocean Sciences
at
The University of Waikato

by

Diana Julie Macpherson

The University of Waikato
2013



THE UNIVERSITY OF
WAIKATO
Te Whare Wānanga o Waikato

ABSTRACT

The Te Angiangi Marine Reserve protects 446 hectares of coastline considered to be representative of the nearshore marine environment of southern Hawke's Bay. It was established in 1997, and since then has been an area where human foraging and fishing has been discouraged through legislation, mindful of the fact that it is known that poaching does occur. The aim of protection in a general sense is to facilitate natural ecosystem functioning through protection of species that can influence habitat character with the desired outcome being a hypothesised return to a more robust and ecologically natural state. However, the main purpose of a marine reserve under current law is for scientific study so that the response and recovery of important marine ecosystems and their component species' can be studied and monitored after human predation stress has eased.

The Te Angiangi Marine Reserve was subjected to a large-scale sedimentation event in April 2011, when 650 mm of intense rain fell over a four day period in the Hawke's Bay region, which resulted in a significant amount of sediment being delivered to the coast through catastrophic coastal landslides. An accompanying trigger was a M4.5 earthquake centred only 10 km offshore from Pourerere at a depth of 20 km. The bounding hills in which the landslides occurred consist of soft, jointed, smectite clay-rich mudstone of the late Miocene Mapiri Formation. The joints enhance water penetration and the swelling (wetting) and shrinkage (drying) of the expandable smectite clay component. Spheroidal weathering releases variably sized joint blocks of mudstone which are very easily and effectively eroded further by the coastal hydrodynamic forces. In particular, persistent wave action at the coastline and over the intertidal platform releases the mainly fine and very fine sand, silt and clay sized particles which are readily dispersed offshore across and beyond the reserve. A subtidal sediment survey shows that the seabed in the reserve is dominated by fine and very fine sand and occasional reefs of bedrock mudstone with pronounced mud deposition occurring seaward of the marine reserve boundary at about 40 m depth.

The debris from the coastal landslides inundated the immediate intertidal platform adjacent to the hill side, which posed a serious threat to marine life both within and outside of the reserve. There was evidence of seagrass and marine organism mortality, especially in the upper intertidal zone. The occurrence of catastrophic scale landslide sedimentation across the interface of a coastal ecosystem comprising both protected and non protected habitats has provided a rare opportunity to examine the response and potential resilience of a marine reserve to a substantial physical disturbance event.

Internationally, empirical evidence for marine reserve resilience in the face of any form of disturbance is rare, particularly because most studies lack information prior to the event. Here, relevant intertidal data is available for the coastal region of interest, covering a number of years prior to the April 2011 storm events. The study is important since there are very few investigations which focus on the resilience of protected organisms to a physical disturbance that is relevant to examining likely increases in marine ecosystem stress associated with a changing climate. More extreme storms predicted under Climate Change modelling equate to more coastal sedimentation events. With the hypothesis that protection offered by a reserve allows biological interactions within the ecosystem to return to more balanced and natural states, the expectation is that an area under protection will have a better chance of recovery than one which may have important ecological imbalance. Hence the ecosystem within the Te Angiangi Marine Reserve will have a 'stronger' starting point for recovery.

Results from a preliminary intertidal survey of reserve and non-reserve organisms has indicated that reserve organisms are indeed showing hints of a resilience trend and reserve effect. This was unexpected given the relatively short time scale for this study (post sediment inundation) and also because the marine reserve covered a relatively small coastal area. Intertidal populations of paua (*Haliotis* spp.), kina (*Evechinus chloroticus*) and seagrass (*Zostera capricorni*) have generally indicated greater abundance and larger size in protected populations at Te Angiangi and adjacent areas, and a generally healthier reef platform compared with the non-reserve locations. The survey results provide an important contribution to the wider understanding of whether marine reserves increase the

resilience of protected populations although the author hastens to add that further work is needed.

The current study attempts to interrelate both Earth science and Biological science components of investigation for the purpose of more comprehensively examining the response of a marine reserve to sedimentation. Ideas and interrelationships between a large-scale sedimentation event and the observed response of the intertidal paua, kina and seagrass populations within and outside of a marine reserve are postulated.

ACKNOWLEDGEMENTS

First and foremost, I would like to thank my supervisors Professor Chris Battershill and Professor Cam Nelson. Chris has expressed undying enthusiasm for my project which in turn kept me motivated throughout, and his patience in explaining marine ecological aspects to me, and in waiting for my drafts (then reading them in a short amount of time) is gratefully acknowledged. I am appreciative of the resulting interesting feedback and input. I owe a huge amount of gratitude to Professor Cam Nelson, who despite retiring in mid 2012, continued to provide excellent and much needed support, knowledge, advice, and above all, his time. I am grateful for the time spent reading my rushed drafts, and the constructive feedback (the many cross-outs and notes made by his infamous red pen), which greatly improved many sections of this thesis. I'm truly grateful and honoured to have been counted as one of his students.

Field work was a very challenging aspect of this project and would not have been completed without assistance from Rod Hansen (DOC), whose knowledge of all aspects of the Te Angiangi Marine Reserve was paramount to my field work. Thanks to my many field assistants - Dudley Bell, Warrick Powrie (who is specifically thanked for finding everything that I had lost and doing the hard yards while mapping landslides), Courtney Foster, Chris Morcom, Josh de Villiers, Nicole Hancock (so much driving!), and Daniel (DOC). Many thanks to Wendy Bradley for providing accommodation at Blackhead, and Blair for providing accommodation at Aramoana, DOC for the use of their boat, the *Tiniwaka*, and Rod for skippering during sediment sampling. DOC are acknowledged for use of their survey data and providing some support funding, particularly Helen Kettles and Debbie Freeman. Special thanks to Barry Lynch and the Hawke's Bay Regional Council for providing landslide mapping information, Vicki Moon and Phil Ross for reading and providing feedback on some draft chapters, Kim Battershill for help with data input and organisation, Bernard Hegan (Tonkin & Taylor) for providing great aerial photographs, and Margaret Nelson for her company and providing amazing food during one field trip.

Special thanks to Janine Ryburn, who gave a huge amount of her time, advice and assistance with laboratory analyses. Also thanks to Annette Rogers for assistance with laser sizing and XRF, and Renat Radosinsky, Kirsty Vincent, and Ganqing Xu (XRD) for laboratory training and assistance. Thanks to Chris Morcom for giving me a crash course in ArcGIS and help with landslide aspects, and Josh de Villiers for help with statistics.

Last, but not definitely not least, I owe a huge thanks to my family and friends. To my parents, Karen and John Macpherson, your endless love, support and encouragement throughout my entire time at university (a long hard road for all of us!), it has helped me more than you know! Thanks to all the fellow MSc students, particularly to my office buddies Courtney and Erin, for the crazy adventures and incredible support over the last couple of years, it has been amazing. Also thanks to my tolerable flatmates who have listened to many a rant, donated food when I had none, and were always good at providing distractions. Lastly, thanks to my boyfriend Lance for taking the risks associated with dating a crazy Masters student, I am grateful for your support and understanding during the past year.

Funding for this project was provided by The Department of Conservation, the University of Waikato Masters Research Scholarship, the Broad Memorial Fund, and the Geoscience Society of New Zealand Hastie Award, all of which are gratefully acknowledged.

TABLE OF CONTENTS

ABSTRACT	III
ACKNOWLEDGEMENTS	VII
LIST OF FIGURES	XIII
LIST OF TABLES.....	XXI
Chapter 1 INTRODUCTION	1
1.1 Thesis motivation	1
1.2 Thesis objectives.....	2
1.3 Study area.....	3
1.4 Thesis format	7
Chapter 2 GEOLOGICAL SETTING	9
2.1 Tectonic and geological setting of the East Coast, North Island.....	9
2.1.1 Previous work.....	10
2.1.2 Regional structure.....	10
2.1.3 Regional stratigraphy and tectonic history.....	16
2.1.4 Study area geological setting.....	22
Chapter 3 THE MAPIRI FORMATION MUDSTONE	25
3.1 Introduction	25
3.2 Field methods	26
3.3 Laboratory methods	29
3.3.1 Carbonate content.....	30
3.3.2 X-ray diffraction (XRD)	32
3.3.3 X-ray fluorescence (XRF).....	41
3.3.4 Grain size analysis	45
3.4 Discussion	49
Chapter 4 SLOPE FAILURES	55
4.1 Introduction	55
4.2 Field work	55
4.3 Regional landslide susceptibility	56
4.4 Te Angiangi Marine Reserve landslides	59
4.4.1 Triggers	59
4.4.2 Type of slope failure	60
4.5 Volume and area estimates.....	68
4.5.1 Volume estimate.....	68
4.5.2 Area estimates	70
4.6 Discussion	74

Chapter 5	OFFSHORE SEDIMENTATION PATTERNS	75
5.1	Introduction	75
5.2	Background information	76
5.2.1	Sedimentation	76
5.2.2	Subtidal habitat types and bathymetry	79
5.2.3	Oceanography	81
5.3	Survey design	86
5.4	Field methods	87
5.5	Laboratory methods	89
5.5.1	Grain size analysis	90
5.5.2	Mineralogy	97
5.5.3	Carbon analysis	105
5.6	Discussion	110
Chapter 6	INTERTIDAL ECOLOGY	113
6.1	Introduction	113
6.2	Background information	115
6.2.1	Coastal sedimentation	115
6.2.2	Marine reserves in New Zealand	118
6.2.3	Marine reserve effectiveness and resilience	120
6.2.4	Biology of paua, kina and seagrass	122
6.2.5	Te Angiangi Marine Reserve previous survey work	127
6.3	Survey design	131
6.4	Field methods	135
6.4.1	Paua and kina	135
6.4.2	Seagrass	136
6.5	Statistical methods	138
6.6	Results	138
6.6.1	Intertidal 2011 survey results	138
6.6.2	Multi-year comparisons	146
6.7	Discussion	147
Chapter 7	DISCUSSION AND SUMMARY	151
7.1	Mapiri Formation mudstone	151
7.1.1	Important characteristics	151
7.2	Catastrophic landslides	152
7.3	Extent of significant sedimentation	153
7.4	Te Angiangi Marine Reserve response to sedimentation	154
7.4.1	Sedimentation and subsequent smothering of the intertidal platform	154

7.5 Pre-existing resilience in East Coast populations and a marine reserve effect	157
REFERENCE LIST	159
APPENDICES.....	169
Appendix 1. Geological timescale	169
Appendix 2. Bulk and clay mineralogy XRD charts	170
Appendix 3. XRD Mineralogy	179
Appendix 4. XRF Geochemistry	181
Appendix 5. Grain size results.....	183
Appendix 6. Sediment survey deployment information	184
Appendix 7. Subtidal sediment grain size data.....	187

LIST OF FIGURES

Figure 1.1. Locality map showing all place names and regions mentioned in the text. The red star marks the location of the Te Angiangi Marine Reserve.	3
Figure 1.2. The location and major features of the Te Angiangi Marine Reserve (modified from DOC, 2008).....	4
Figure 1.3. Blackhead township at the southern end of the reserve boundary. View is looking northwest.....	4
Figure 1.4. Aramoana township at the northern end of the reserve boundary. Many surficial slips are evident in the backing hills, similar to those typifying much of the inland hillsides. View is looking south.	5
Figure 1.5. The shoreline between Aramoana (bottom right) and Blackhead (top right). Sediment fans from the collapsed coastal hills within the reserve boundary extend onto the intertidal shore platform. Extensive landsliding is also evident on the coastal headland south of Blackhead. View is looking south.....	5
Figure 2.1. The location of the Australian-Pacific plate boundary in relation to the Hawke's Bay region and wider North Island. The Hikurangi Margin, the North Island axial ranges, and the Hikurangi Trough are also shown. The red star indicates the location of the Te Angiangi Marine Reserve (modified from Lee et al., 2011).....	11
Figure 2.2. Schematic cross-section of the east coast subduction margin (modified from Nyman et al., 2010).	12
Figure 2.3. Tectono-geomorphic structural features across the subduction margin (modified from Field et al., 1997).	12
Figure 2.4. Topographic relief map of the Hawke's Bay area showing some of the North Island axial ranges. The red star marks the location of the Te Angiangi Marine Reserve. ArcGIS database was used to derive the topographic relief map. White indicates regions of high elevation (adapted from Lee et al., 2011).	15
Figure 2.5. Geological map of the area inland from the Te Angiangi Marine Reserve in the southern Hawke's Bay region. The Pohatupapa folds and Porangahau-Pourerere Anticlinal Complex are also shown (modified from Lee et al., 2011).....	17
Figure 2.6. Geological legend for Figure 2.5.	18
Figure 2.7 Generalised panel diagram showing the Cretaceous to recent stratigraphy and depositional environments for the sedimentary rock column in southern Hawke's Bay. WM is the approximate stratigraphic position of the Whangaehu Formation mudstone, which contains tubular concretions, and which has many similar characteristics to the Mapiri Formation mudstone (taken from Nyman et al., 2010).....	19

Figure 2.8. <i>In situ</i> carbonate concretions protruding from the intertidal shore platform as a result of erosion of the surrounding softer host mudstone.	24
Figure 2.9. A section of the intertidal shore platform showing abundant randomly scattered concretions. Some landslide debris is also evident in the foreground....	24
Figure 3.1. Mudstone weathering process. Large jointed block of bedrock (left) from which clasts of variable sizes were released (middle) and further disintegrated into smaller rounded "spheroids" of cobble to pebble size (right)...	25
Figure 3.2. Mudstone and concretion sample locations. A - Sample DM2 was collected from the shore platform. B - Sample DM7 was collected from blocks of bedrock in the foreground. C - Sample DM3 came from a near <i>in situ</i> concretion. D - Sample DM1 was collected from a block of highly jointed bedrock in which the individual joint blocks exhibit prominent spheroidal weathering. Red arrows approximate sampling positions.	27
Figure 3.3. Rock sample locations (red dots) in the Te Angiangi Marine Reserve. Blue line marks the reserve boundary. Satellite image derived from ArcGIS database.	27
Figure 3.4. Flow chart of laboratory analyses carried out on samples.	29
Figure 3.5. The set up used to measure carbonate percentage.	31
Figure 3.6. The expected movement of primary (001) peak positions of the main clay minerals in untreated, glycolated and heated oriented sample mounts.	34
Figure 3.7. Bulk mineralogical XRD scan for mudstone sample DM1. S = smectite, C = chlorite, I = illite, K = kaolintie, P = plagioclase, Q = quartz, 001 = primary clay peak, 002 = secondary clay peak.	36
Figure 3.8. The average bulk mineralogical composition (relative abundances only) of the Mapiri Formation mudstone. A=abundant, C=common, S=some and N=absent.....	37
Figure 3.9. Bulk mineralogical composition of dolomitic concretion sample DM3. A=abundant, C=common, S=some and N=absent.....	37
Figure 3.10. Bulk mineralogical composition of calcitic concretion sample DM4. A=abundant, C=common, S=some and N=absent.....	38
Figure 3.11. General clay mineral composition and relative abundances in samples.	39
Figure 3.12. Sample DM1 mudstone untreated (air dried) oriented mount XRD scan. S = smectite, C = chlorite, I = illite, K = kaolintie, 001 = primary peak, 002 = secondary peak.	40

Figure 3.13. Sample DM1 mudstone ethylene glycolated oriented mount XRD scan. S = smectite, C = chlorite, I = illite, K = kaolintie, 001 = primary peak, 002 = secondary peak.	40
Figure 3.14. Sample DM1 mudstone heated to 550 °C oriented mount XRD scan. S = smectite, C = chlorite, I = illite, K = kaolintie, 001 = primary peak, 002 = secondary peak.	41
Figure 3.15. The average mudstone major element composition derived from XRF analysis of the three mudstone samples.	42
Figure 3.16. The element composition of dolomitic concretion derived from XRF results.	43
Figure 3.17. The element composition of calcitic concretion derived from XRF results.	43
Figure 3.18. Trace element composition of the average Mapiri Formation mudstone, the dolomitic concretion and calcitic concretion.	44
Figure 3.19. Histograms derived from GRADISTAT showing siliciclastic grain size distribution in all samples. Note the bimodality of samples DM1 and DM7. 47	47
Figure 3.20. Ternary diagram showing all samples plotted according to their sand-silt-clay content (derived from GRADISTAT, based on Folk (1954))......	48
Figure 3.21. Spheroidal weathering occurring within a boulder of mudstone. The boulder consists of many corestones, each one surrounded by concentric sheets or layers of weathering rock (examples outlined).	49
Figure 3.22. Spheroidal shaped pebbles derived from jointed clasts in the landslide debris litter the beach zone.	50
Figure 3.23. Major element composition comparison of the average Mapiri Formation mudstone with the global mudstone average derived from Boggs (2006)......	51
Figure 3.24. A Mapiri Formation tubular concretion exhibiting a central conduit which likely funnelled methane rich fluids upwards in a cold seep system in the Late Miocene.	54
Figure 4.1. Schematic of a landslide showing the aspects that were measured, if possible, during field work (modified from Selby, 1993)......	56
Figure 4.2. Approximate locations of the Waipoapoa and Ponui landslides, the Waitawhiti Complex, and the approximate western limit of gravitational collapse of the Kairakau-Waimarama Regional Slump (modified from Pettinga, 2004 and Lacoste et al., 2009)......	57
Figure 4.3. A - Some of the hill side within the reserve pre-April 2011 storm (photo taken in 2008). Outlined are obvious old landslide scarps. B - The same hill side post-April 2011 storm (photo taken in 2012). Main scarps of slips 7 to 11	

are outlined. Slip 7 is in the southern part of the reserve and slips 9 to 10 are directly opposite Stingray Bay. 61

Figure 4.4. Landslides in the northern half of the reserve. Main scarps of slips 7 to 14 are outlined. View is looking south. 62

Figure 4.5. Slope failures on hills south outside the reserve. 62

Figure 4.6. Main scarps of slips 1 to 9 are outlined. A - Slips 1 to 3 measure about 20 m in length along the scarps and are closest to Blackhead. Their estimated depths are ~1 m. B - Slip 4. The scarp length measures about 45 m, with an estimated depth of ~1 m. C - 'Slip' 5, which is characteristic of a debris flow, has an estimated depth of ~2 m. D - Slip 6. The scarp length measures about 156 and is the largest slip to occur heading north from Blackhead, with an estimated depth of ~4 m. E - Slip 7. The scarp length measures about 167 m, with an estimated depth of ~3m. F - Slips 8 and 9, both with estimated depths of ~3 m. The scarp length of slip 8 is about 400 m. 63

Figure 4.7. Main scarps of slips 10 to 14 are outlined. A - Slips 8, 10 and 11. 'Slip' 11 represents an area of multiple slope failures along ~ 200 m of hill side. B - Slip 10 has an estimated depth of ~3 m. C - Slips 12 (estimated depth of ~4 m), 13 (estimated depth of ~3 m) and 14 (refer to Figures 4.7 to 4.9 for some slip dimensions). D - Debris from slip 14. The black box outlines the location of E which shows the northern flank of slip 14 estimated at ~2 - 3 m deep..... 64

Figure 4.8. Debris measurements of slip 12, including the length around the debris frontal lobe, the maximum length (or extent) of the debris, and the width of the debris at the base of the hill. Also shown is the width near the top of the debris mass..... 65

Figure 4.9. Debris and scarp measurements of slip 13, including the scarp length at the crown, the length around the debris frontal lobe, the maximum length (or extent) of the debris, and the width of the debris at the base of the hill. 65

Figure 4.10. Debris measurements of slip 14, including the length around the debris frontal lobe, the maximum length (or extent) of the debris, and the width of the debris at the base of the hill. Also shown is the width near the bottom, and the width at the top, of the debris mass..... 66

Figure 4.11. Google Earth image showing the distribution of landslides directly adjacent to the reserve. The main scarp of each landslide is outlined, along with the length and width of the landslide scarps. These measurements were used to estimate an overall volume of sediment delivered into the reserve from these landslides. 69

Figure 4.12. Pre-storm mosaic of satellite images from the KiwiImage program. Dates the images were taken range from 2006-2010 (from Jones et al., 2011). The red line delineates their study area. The image scale is 1:850,000..... 71

Figure 4.13. Post-storm satellite images from the RapidEye system. Images were taken between 18-19 May 2011 (from Jones et al., 2011). The red line delineates the study area. 72

Figure 4.14. ArcGIS post-storm (RapidEye) satellite image with pre- and post-storm bare ground. The general boundary of the three stream catchments is outlined in black, and the purple represents post-storm bare ground present within the overall catchment boundary. The image scale is 1:50,000.....	73
Figure.5.1. Schematic showing marine sediments on the continental shelf and slope off the Te Angiangi Marine Reserve and the general southern Hawke's Bay and Wairarapa coastline (data from Lewis & Gibb, 1970 and Lewis, 1971).....	78
Figure 5.2. Nearshore subtidal biological habitat types in the vicinity of the study area (modified from Funnell et al., 2005).	80
Figure 5.3. The bathymetry of the nearshore area encompassing the Te Angiangi Marine Reserve (modified from Funnell et al., 2005).	81
Figure 5.4. Wave rose of significant wave height and mean wave direction (waves primarily travel to the north, as indicated by the bold arrow) offshore from the Te Angiangi Marine Reserve (from Oldman et al., 2006).	82
Figure 5.5. Coastal currents, eddies, water masses and fronts around New Zealand. The currents are the East Auckland Current (EAUC), West Auckland Current (WAUC), East Cape Current (ECC), D'Urville Current (DC), Westland Current (WC), Antarctic Circumpolar Current (ACC), Southland Current (SC) and the Wairarapa Coastal Current (WCC). The eddies are the North Cape Eddy (NCE), East Cape Eddy (ECE) and Wairarapa Eddy (WE). The water masses are Subtropical Water (STW), Subantarctic Water (SAW) and Circumpolar Surface Water (CSW). The fronts are positioned where the CSW and SAW meet - the Subantarctic Front (SAF), where the SAW and STW meet - the Subtropical Front (STF), and the Tasman Front, located in STW to the far north (image modified from http://www.shiningaspotlight.org.nz/31-the-oceanography-of-the-new-zealand-marine-ecoregion).....	84
Figure 5.6. Sediment sampling transect locations.	86
Figure 5.7. A - The ponar grab sampler. B - The ponar grab sampler being deployed using a pulley.....	87
Figure 5.8.A - A ponar grab sample being emptied into a container. B - Subsample of sediment being taken from the grab sample.....	88
Figure 5.9. Flow chart of laboratory analyses carried out on subtidal sediment samples.....	89
Figure 5.10. Grain size results for Transect 1. Samples are dominated by fine and very fine sand.	91
Figure 5.11. Grain size results for Transect 2. Samples are dominated by fine and very fine sand. This transect includes a beach sand sample (BH1) taken from Blackhead Beach.....	91

Figure 5.12. Grain size results for Transect 3. Samples are dominated by fine and very fine sand. With the exception of sample T3-9, the samples show a steady increase in mud content with depth, and T3-10 is mainly composed of silt.....	92
Figure 5.13. Grain size results for Transect 4. Samples are dominated by fine and very fine sand and increase in mud content with increasing depth. This transect includes a beach sand sample (SB1) taken from Stingray Bay.....	92
Figure 5.14. Grain size results for Transect 5. Samples are dominated by fine and very fine sand and increase in mud content with increasing depth.....	93
Figure 5.15. Grain size results for Transect 6. Samples are dominated by fine and very fine sand and increase in mud content with increasing depth. This transect includes a beach sand sample (ARA1) taken from Aramoana Beach.....	93
Figure 5.16. Grain size results for Transect 7. Samples are dominated by fine and very fine sand and increase in mud content with increasing depth.....	94
Figure 5.17. Grain size results for Transect 4. Samples are dominated by fine and very fine sand.....	94
Figure 5.18. Ternary diagram showing all samples plotted according to their sand-silt-clay content (derived from GRADISTAT, based on Folk (1954)).....	95
Figure 5.19. Grain size distribution along all transects based on Folk (1954) classification of all samples. Areas where no samples were taken are assumed to be hard substrate.....	96
Figure 5.20. Photomicrographs of samples BH1 and T6-7. A - Quartz and feldspar from sample BH1, B - XPL image of A showing quartz interference colours. C - A bioclast, possibly an echinoderm plate, from sample BH1, D - XPL image of A. Quartz (E) and feldspar (G and H) from sample T6-7, F - XPL image of E.....	102
Figure 5.1. Photomicrographs from sample T2-10. A - Calcite fragment, which could be a piece of a bivalve (i.e. oyster or pectinid), B - Calcite fragment under XPL. C - Quartz and plagioclase grains (plagioclase in the centre of image). D - Quartz and plagioclase under XPL. E - A benthic foram bioclast. F - Image showing the general size of grains in sample T2-10.....	103
Figure 5.22. Photomicrographs of rock fragments. A - Crushed mudstone fragments from sample DM1. B - rock fragments under XPL. C - An example of a suspected rock fragment from sample BH1. D - BH1 rock fragment under XPL.....	104

Figure 5.23. Total carbon results for all samples from the LECO method, with grain size (black lines) superimposed showing the increase in total carbon with decreasing grain size relationship.....	106
Figure 5.24. Inorganic carbon (IC) and organic carbon (OC) components of representative samples from the LOI method, with grain size (black lines) superimposed showing the increase in organic carbon with decreasing grain size relationship.....	107
Figure 5.25. The organic carbon results derived from the subtraction of inorganic carbon (from LOI) from total carbon (from LECO), compared to the organic carbon value derived from LOI.....	109
Figure 6.1. The effects of direct sediment deposition and suspended sediment concentration on a soft sediment ecosystem. As the disturbance regime increases, more effects are triggered (modified from Thrush et al., 2004).....	117
Figure 6.2. Marine reserves in New Zealand (from the DOC website).	119
Figure 6.3. The most common species of paua in New Zealand, the black-foot <i>Haliotis iris</i> (from nabis.govt.nz).	123
Figure 6.4. The New Zealand sea urchin, or kina <i>Evechinus chloroticus</i> (from forestandbird.org.nz).	124
Figure 6.5. Seagrass <i>Zostera capricorni</i> , surrounded by Neptune's necklace (<i>Hormosira banksii</i> top and bottom right corners of the photo) within a 0.25 m ² quadrat.....	126
Figure 6.6. Locations of non-reserve and reserve sites used in the 2011 intertidal survey.....	132
Figure 6.7. Paua on the underside of a rock about to be measured using callipers.	135
Figure 6.8. A 0.25 m ² quadrat used to measure seagrass parameters. Outlined in the red circle is a smaller 8 cm ² quadrat used to estimate shoot density.	136
Figure 6.9. Paua abundance and size at each of the low and middle shore heights for each site. Reserve (C, D, E, F) and non-reserve (A, B, G, H) sites are delineated by the black vertical lines. Shown is the total paua counted (A) and their average size (B). This total is divided into adult (>50 mm length) and juvenile number (<50 mm length; C and E respectively) and average size (D and F respectively).	139
Figure 6.10. Kina abundance and size at each of the low and middle shore heights for each site. Reserve (C, D, E, F) and non-reserve (A, B, G, H) sites are delineated by the black vertical lines. Shown is the total paua counted (A) and their average size (B). This total is divided into adult (>30 mm in size) and	

juvenile number (<30 mm in size; C and E respectively) and average size (D and F respectively).	141
Figure 6.11. Seagrass cover and average patch size at each site.	144
Figure 6.12. Seagrass quadrat results for each site. Shown is the percent of seagrass cover within the quadrat, and the percent of that seagrass which was green (A). B shows the average blade length and average shoot density (shoot density was estimated using small 3 x 8 cm ² quadrats). Reserve (C, D, E, F) and non-reserve (A, B, G, H) sites are delineated by the black vertical lines.	145
Figure 6.13. An estimate of paua density and average paua size at non-reserve locations Blackhead (BH) and Aramoana (ARA), and marine reserve location (MR), in years 1999 to 2003 (pre-event) and 2011 (post-event).....	146
Figure 6.14. An estimate of kina density and average kina size at non-reserve locations Blackhead (BH) and Aramoana (ARA), and marine reserve location (MR), in years 1999 to 2003 (pre-event) and 2011 (post-event).....	147
Figure 7.1. Schematic diagrams outlining the response to the 2011 sedimentation event on marine reserve populations. The blue 'P' (paua) and red 'K' (kina) are used to demonstrate the relative abundance of paua and kina in the low and mid shore before, during and after the event. Green patches of grass represent seagrass abundance before, during and after the event. Before the event (A), the reserve was functioning well and contained a presumably more robust ecological balance of interacting biological components. When the sedimentation event happened (B), landslide debris smothered a significant portion of the intertidal platform within the reserve and reduced paua and kina populations and seagrass abundance. The landslide debris began eroding into fine sized particles and being transported offshore. After the sedimentation event (C), the marine reserve populations began to recover, and landslide debris on the intertidal platform continues to rapidly reduce.	155

LIST OF TABLES

Table 3.1. Description of sample collections.	28
Table 3.2. Carbonate percentage results for mudstone (DM1, DM2 and DM7) and concretion (DM3 and DM4) samples.	32
Table 3.3. Important peak positions of some common minerals found in the mudstone and concretion samples.	35
Table 3.4. Statistical parameters derived from GRADISTAT for the acid insoluble siliciclastic fraction of all samples based on the Folk & Ward (1957) method. *Sorting, skewness and kurtosis results for samples DM1 and DM7 are biased due to their bimodal size distribution. % sand, silt and clay derived from raw data from Malvern laser sizer.	46
Table 4.1. Figures associated with each slip.	66
Table 4.2. The estimated volume of sediment derived from each landslide (excluding slip 4 and 11). The total volume has an error estimate of $\pm 75.02 \text{ m}^2$. ..	69
Table 5.1. Average sand, silt and clay contents of the sand, silty sand, muddy sand and sandy silt textural groups (see Figure 5.17).	96
Table 5.2. Detrital mineralogy data for Transect 2. Samples BH1 and T2-10 (highlighted) are representative intertidal sand and subtidal sand samples chosen for further mineralogical analysis.	98
Table 5.3. Detrital mineralogy data for Transect 4.	99
Table 5.4. Detrital mineralogy data for Transect 6. Sample T6-7 (highlighted) is a representative silty sand sample chosen for further mineralogical analysis.	99
Table 5.5. Key to abbreviations used for petrographic analysis in Tables 5.2 - 5.4.	99
Table 5.6. Comparison of LECO and LOI carbon results for selected samples.	108
Table 6.1. Pre-reserve and post-reserve surveys done on the reef platform, paua and kina, and seagrass, and their associated references.	128
Table 6.2. A list of sampling undertaken at each site. The number of seagrass transects sampled varied due landslide debris extending onto the intertidal platform, which reduced the area available for sampling. Sites E and F were severely impacted by debris, and therefore any area available was measured out and sampled.	133

Table 6.3. Human predation and sedimentation stressors acting upon areas to the south at Blackhead (BH), the marine reserve (MR) and to the north at Aramoana (ARA)..... 134

Table 6.4. Main paua and kina results for reserve and non-reserve populations sampled in the 2011 survey. 143

Table 6.5. Seagrass transect results. Shown is the total area sampled at each site, the area and percent of seagrass found within that area, and the mean patch size for each site. A comparison of the total percent seagrass cover between reserve and non-reserve sites is also shown. 144

Chapter 1

INTRODUCTION

This project involves studying the ecological resilience and response of a marine reserve to a severe coastal sedimentation event. In April 2011 much of the Hawke's Bay region in eastern North Island of New Zealand experienced several severe cyclonic storms resulting in catastrophic slippage of hillsides and coastal cliffs. It was the second wettest April recorded in 140 years in Napier, during which 878 mm of rain fell at Cape Kidnappers and 535 mm at Cape Turnagain (NIWA, 2011a). Furthermore, several earthquakes were felt in the region during the same month (GNS, 2011). A rather weak, blue-grey mudstone known as the Mapiri Formation (Lillie, 1953) constructs the coastal hills in southern Hawke's Bay, which have been cleared of vegetation for farming. The contribution of all these factors resulted in considerable large-scale slippage of the coastal cliffs along the length of the Te Angiangi Marine Reserve in southern Hawke's Bay, which delivered large volumes of muddy sediment directly into the offshore reserve. The hills have continued to collapse during subsequent storm events.

1.1 THESIS MOTIVATION

It had been anticipated that the April 2011 coastal sedimentation event, along with ongoing remobilisation of the landslide deposits, might negatively impact the marine reserve ecosystem (which was functioning well before the sedimentation event) and adjacent coastline. Consequently, the event has provided marine ecologists with an excellent opportunity to study the resilience and response of marine organisms from inside a marine reserve to such a major environmental disturbance, particularly so because information exists about the coastal ecology inside and outside the reserve prior to the event.

Marine reserves are established to not only conserve areas of significant biodiversity, but also for the purposes of scientific study (DOC, 2003), and the opportunity to observe if marine organisms from within a marine reserve are more resilient to a disturbance is of particular interest to marine ecologists. Thus a primary motivation for this project comes from a marine ecological perspective.

However, to better interrelate causes and effects, it is pertinent to also investigate the various physical environmental aspects (geology, geomorphology, engineering properties, climate, sediment types, ocean wave and current conditions) associated with the biological elements. Thus an interdisciplinary approach between marine ecology and Earth sciences is the best way to comprehensively address this topic.

1.2 THESIS OBJECTIVES

There are four main objectives of this project. Three of them address the physical aspects of the project, and the fourth involves reconnaissance examination of the response of the marine ecology to sedimentation.

1) Examine the geology of the coastal area immediately adjacent to the Te Angiangi Marine Reserve, and to determine the structures (bedding, joints, faults, folds), texture, chemical composition and mineralogy (especially clay mineral types) of the dominant mudrock lithology.

2) Describe (including gathering estimates of the volume of new sediment suddenly introduced into the coastal environment) and classify the slope failures along the coastal hills adjacent to the Te Angiangi Marine Reserve.

3) Investigate the present and likely future erodability of the slip material, and the ensuing sediment dispersal mechanisms and depositional patterns across and along the coastal platform and nearshore region encompassing the marine reserve. This could help explain any spatial and temporal response of the marine organisms to sedimentation, as it is hypothesised that nearshore currents flowing to the north could carry and deposit sediment in the coastal zone north of the reserve.

4) The material derived from the landslides has extended out onto the intertidal shore platform, posing a serious threat to the intertidal marine organisms living on the platform, and also beyond into the subtidal zone. A preliminary survey of the intertidal marine ecology from within and outside the reserve has been made in order to assess the impact on the marine organisms in response to the high sedimentation events. There is considerable pre-April 2011 ecological information

with which the results of this survey can be compared in order to detect any changes in the size and abundance of organisms.

1.3 STUDY AREA

The Te Angiangi Marine Reserve is located in the southern Hawke's Bay region on the east coast of the North Island, about 30 km east of Waipukurau and Waipawa townships (Figure 1.1). The reserve extends one nautical mile offshore from the high water mark and in total covers approximately 446 hectares, an area which is considered representative of the wider southern Hawke's Bay coastal marine environment (Figure 1.2). It is bordered by the coastal villages of Blackhead (Figure 1.3) in the south and Aramoana (Figure 1.4) in the north with about 2.7 km of shoreline between the two villages (Figure 1.5).

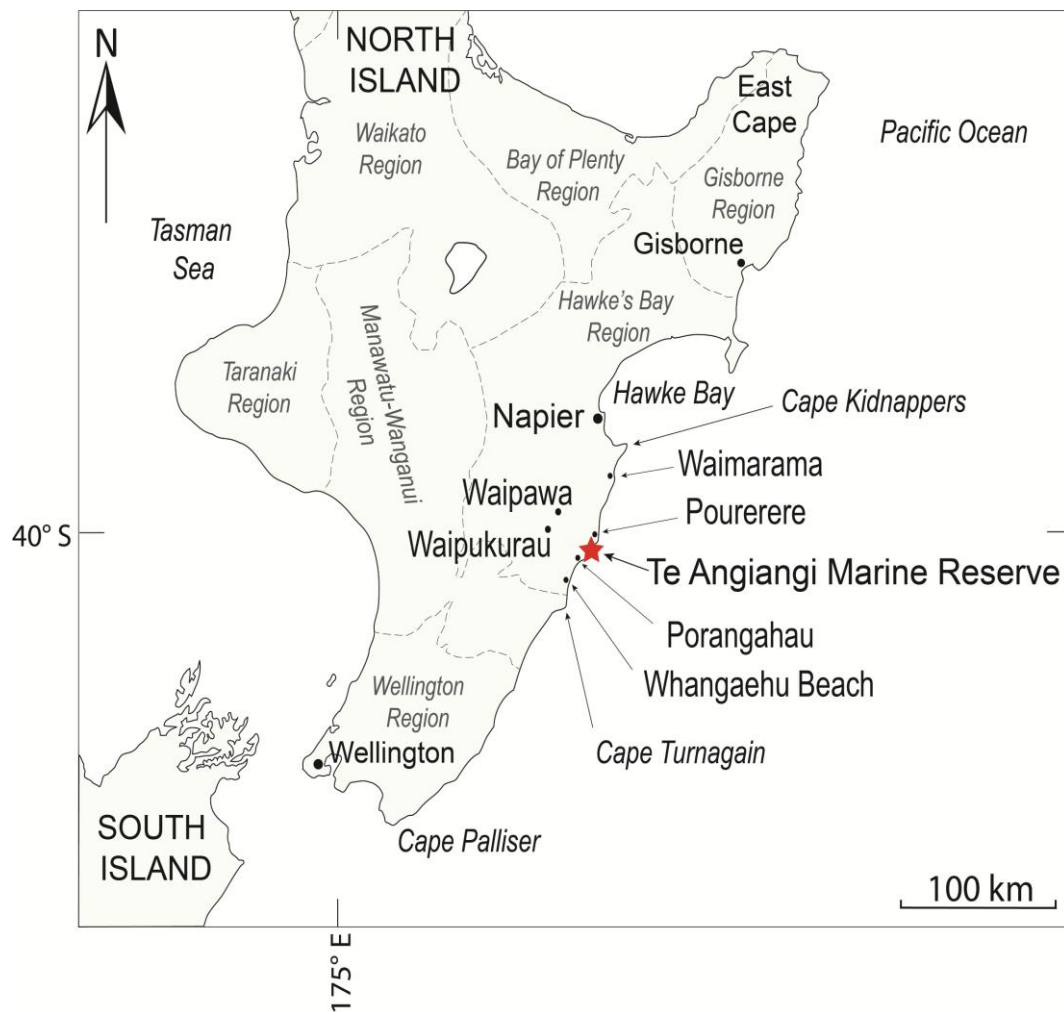


Figure 1.1. Locality map showing all place names and regions mentioned in the text. The red star marks the location of the Te Angiangi Marine Reserve.

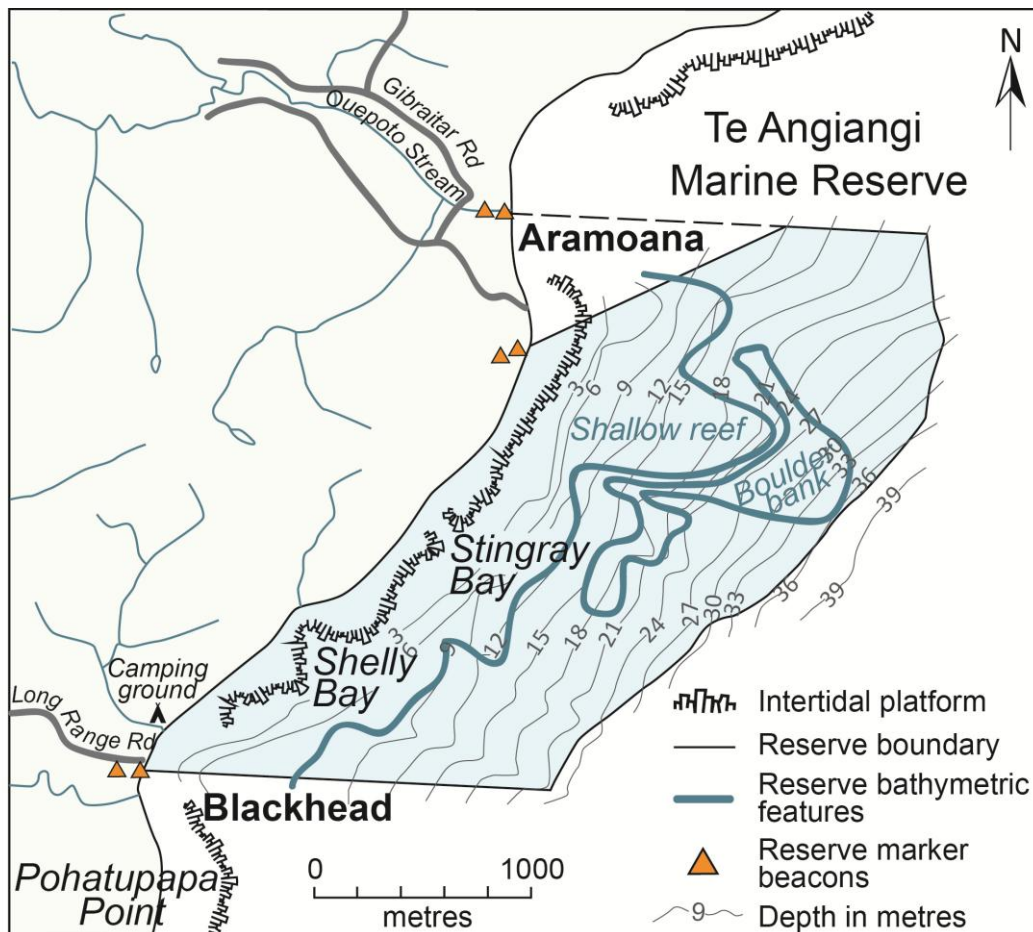


Figure 1.2. The location and major features of the Te Angiangi Marine Reserve (modified from DOC, 2008).



Figure 1.3. Blackhead township at the southern end of the reserve boundary. View is looking northwest.



Figure 1.4. Aramoana township at the northern end of the reserve boundary. Many surficial slips are evident in the backing hills, similar to those typifying much of the inland hillsides. View is looking south.



Figure 1.5. The shoreline between Aramoana (bottom right) and Blackhead (top right). Sediment fans from the collapsed coastal hills within the reserve boundary extend onto the intertidal shore platform. Extensive landsliding is also evident on the coastal headland south of Blackhead. View is looking south.

The reserve features an c. 100 m wide intertidal mudstone platform or "reef" which is fully submerged at high tide and fully exposed at low tide, and which extends most of the length of the reserve. The platform is characterised by turfs of coralline algae (*Corallina officinalis*), Neptune's necklace (*Hormosira banksii*), and patches of seagrass (*Zostera capricorni*), all of which provide important feeding areas for wading birds (DOC, 1994a). The platform and bordering coastal hills - private land which has been cleared of vegetation for the purpose of farming - are made up of locally concretionary, soft Late Miocene mudstone (Lillie, 1953) which is typically massive or homogenous so that the platform morphology is smooth and flat apart from the occasional carbonate concretion. About mid-way along the reserve there is a break in the platform which forms a pool at low tide known as Stingray Bay (Figure 1.2 and 1.5).

Subtidally, the reserve substrate is mostly featureless soft sediment, with siltstone reefs and a 'boulder bank' in the northern sector of the reserve (Figure 1.2). It is suspected that these boulders are mainly carbonate concretions, the same as those found protruding out of the mudstone platform. The water depth in the reserve is mainly less than about 24 m, but reaches 36 to 40 m at its seaward boundary (DOC, 2008).

Te Angiangi Marine Reserve was established in August 1997 and is a Marine Protected Area (MPA). This means it is a complete no take zone - the removal or disturbance of marine organisms from within the reserve is strictly prohibited (DOC, 2001). The main purpose of the reserve is scientific study which is oriented toward the effect that the protection offered by a MPA might have on organisms and overall ecosystem functioning. MPAs allow individuals and ecosystems to recover by reducing selection pressure on larger organisms through preservation, and allow rehabilitation of the ecosystem, which may have become degraded by human activities, such as harvesting pressure, input of polluted terrestrial run-off and the introduction of marine pests (DOC, 2001, DOC, 2003). The opportunity to observe if marine organisms from within a marine reserve are more resilient to some major disturbance is of particular interest to marine ecologists (Allison et al., 1998; Parker & Weins, 2005; Airoldi, 2003; Game et al., 2008; Micheli et al., 2012).

1.4 THESIS FORMAT

This thesis is formatted so the physical aspects of the project are addressed first, which then lead into the biological aspects, before finishing with an overall synthesis and discussion chapter. Chapters 2 to 5 deals with the geological and sedimentation aspects of the project. Chapter 2 provides the tectonic and geological setting and history of the Hawke's Bay region, as well as background information on the origin, age, structural and geological characteristics of the dominant lithology present in the study area. Chapter 3 presents in some detail the geological characteristics of the dominant mudstone lithology which make up the coastal hills in the study area. Chapter 4 addresses landsliding aspects, in particular the suspected triggers of slope failures, the distribution and nature of the landslides, and the estimated volume of sediment released into the marine environment due to landsliding. Chapter 5 outlines the possible offshore depositional patterns of the sediment released by the landslides into the marine environment. It includes a description of the physical oceanography and bathymetry in the area, along with results from an offshore sediment sampling exercise. Chapters 6 deals with the biological aspects of the project, and includes previous marine ecological work carried out in the Te Angiangi Marine Reserve. It then describes the marine intertidal survey carried out after the 2011 storm event, the results of this survey, and uses the results to compare and create multi-year patterns with previous comparable surveys. Chapter 7 attempts to integrate the results from all previous chapters to gauge any interrelationships between the catastrophic sedimentation event and the ecological resilience of organisms within the marine reserve.

To allow the reader to progress through the thesis with ease, and because of the segmented nature of the thesis, field and laboratory methods will be addressed in their relevant chapters, so there is no single chapter outlining all the field and laboratory methods. Most chapters are formatted to include introduction, aims, background information, field and laboratory methods, results and discussion sections.

Chapter 2

GEOLOGICAL SETTING

This chapter describes the tectonic and geological setting of the Hawke's Bay region which aids understanding of the physical aspects of the project.

2.1 TECTONIC AND GEOLOGICAL SETTING OF THE EAST COAST, NORTH ISLAND

It is relevant to examine the geological setting, including the historical to present day tectonics, structure and stratigraphy, of the Hawke's Bay region for two reasons: (1) to know the depositional paleoenvironmental conditions of the mudstone bedrock underpinning the reserve, and put this into a regional tectonic context; and (2) to appreciate the historical to present day structural forces impacting on the region. Such information will allow for further understanding and characterisation of the mudstone, and assist in proposing likely causes of slippage, and the effects this slipped mudstone might have on the marine reserve environment.

The section begins by providing a regional context for the Hawke's Bay geological structure and stratigraphy, followed by more specific examination of the lithology and structures in the vicinity of the Te Angiangi Marine Reserve itself.

2.1.1 Previous work

The earliest reference to the geology of the area south of Hawke's Bay was by Hochstetter (1867), where the Hawke's Bay Series was described as a group of limestone, sandstone and clay marls. The geology of the Dannevirke Subdivision, including the study area, was investigated in detail by Lillie (1953). This is one of the earliest and fundamental texts describing the geology of this region and was produced as part of a regional geological mapping survey of New Zealand, with the eventual aim of assisting with oil exploration activities. The most recent and up-to-date text describing Hawke's Bay geology and structure is by Lee et al., (2011), published as part of the new New Zealand 1:250 000 Geological Map Series (QMAP) produced by GNS Science. Many texts, such as Kamp (1992), Field et al., (1997), Bland & Kamp (2006), Barnes et al., (2010) and Lee et al., (2011), explain the tectonically active geological and structural setting of the Hawke's Bay region, sitting as it does within the Hikurangi Subduction Margin. The following section outlines the influence of the subduction margin on the region.

2.1.2 Regional structure

The Te Angiangi study area is located in the Hawke's Bay of eastern North Island (Figure 1.1), an area influenced geologically and structurally by the obliquely convergent Australian-Pacific plate boundary. The boundary runs in a southwest to northeast direction offshore along the North Island's east coast, almost parallel to the southern Hawke's Bay coastline where the Te Angiangi Marine Reserve is located (Figure 2.1). The plate boundary in this area is expressed in seafloor bathymetry as a subduction zone known as the Hikurangi Margin, where the dense oceanic crust of the Pacific Plate is obliquely converging and subducting beneath the more buoyant continental crust of the Australian Plate (Foster & Carter, 1997; Barnes et al., 2002; Lewis & Pettinga, 1993; Bland & Kamp, 2006). The Hikurangi Margin encompasses the area from where the plates converge in the east, to the axial ranges on the North Island landmass to the west (Figure 2.1). The Hikurangi Trough is part of the margin, otherwise known as the subduction trench, and is about 3000 m deep. It is where the Pacific Plate dips at an angle of about 3° for about 100 km before steepening beneath the North Island (Barnes et al., 2010; Figure 2.2). Subduction in the Hikurangi Margin began in the Early

Miocene (Rait et al., 1991; Field et al., 1997; Lee et al., 2011) and continues today at a rate of about 40-50 mm per year (Erdman & Kelsey, 1992; Barnes & Mercier de Lepinay, 1997; Beanland et al., 1998; Barnes et al., 2010; Lee et al., 2011). The leading edge of the Australian Plate, which includes the Hawke's Bay region, is undergoing deformation and uplift across the subduction boundary zone (Figure 2.2). In doing so, several major tectono-geomorphic structural elements have developed from east to west across the margin (Pettinga, 1982). These major features include: a) a subduction trench; b) an accretionary prism; c) a forearc basin; d) coastal ranges and e) axial ranges (Figure 2.3). Beyond is the active volcanic arc of the Taupo Volcanic Zone and the backarc region of western North Island.

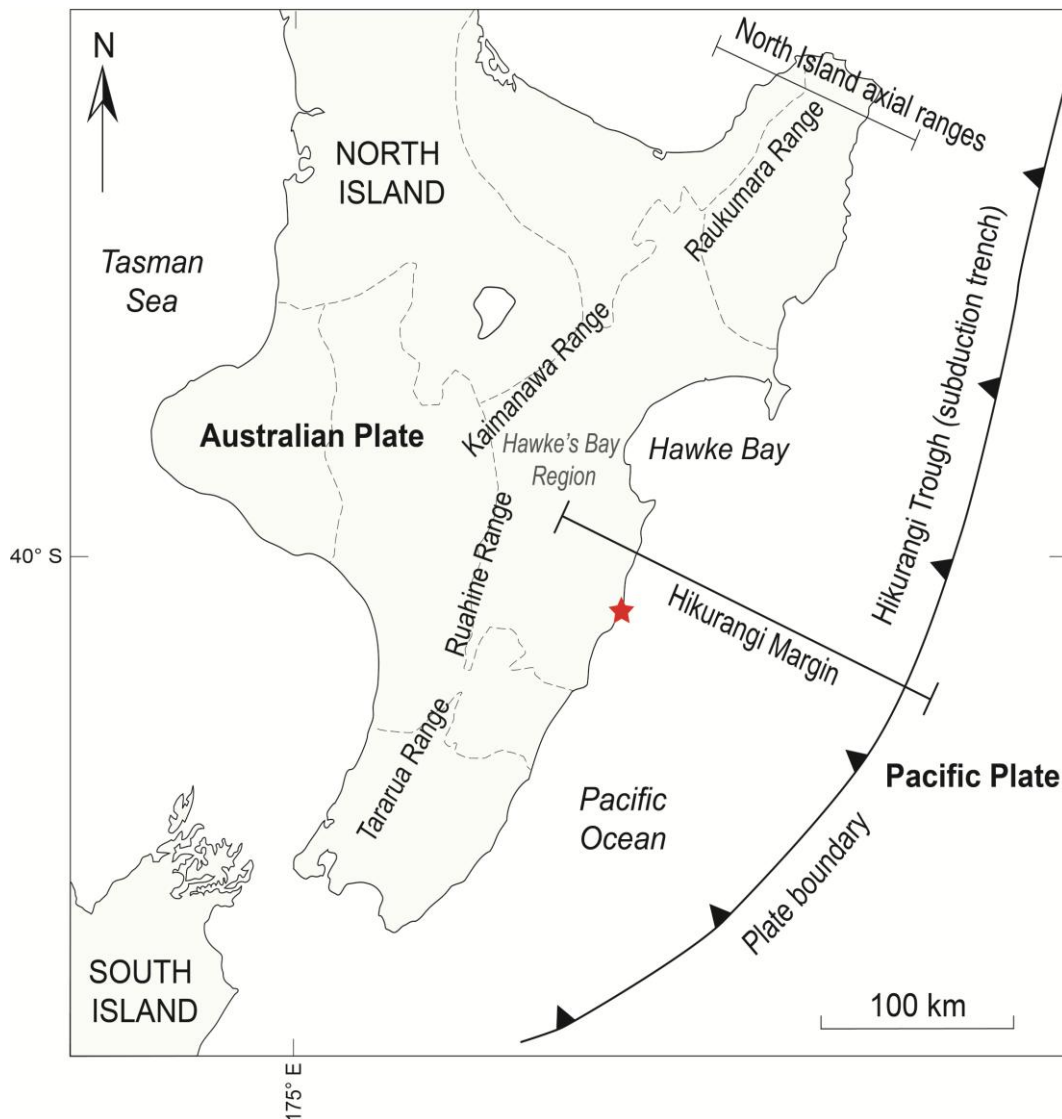


Figure 2.1. The location of the Australian-Pacific plate boundary in relation to the Hawke's Bay region and wider North Island. The Hikurangi Margin, the North Island axial ranges, and the Hikurangi Trough are also shown. The red star indicates the location of the Te Angiangi Marine Reserve (modified from Lee et al., 2011).

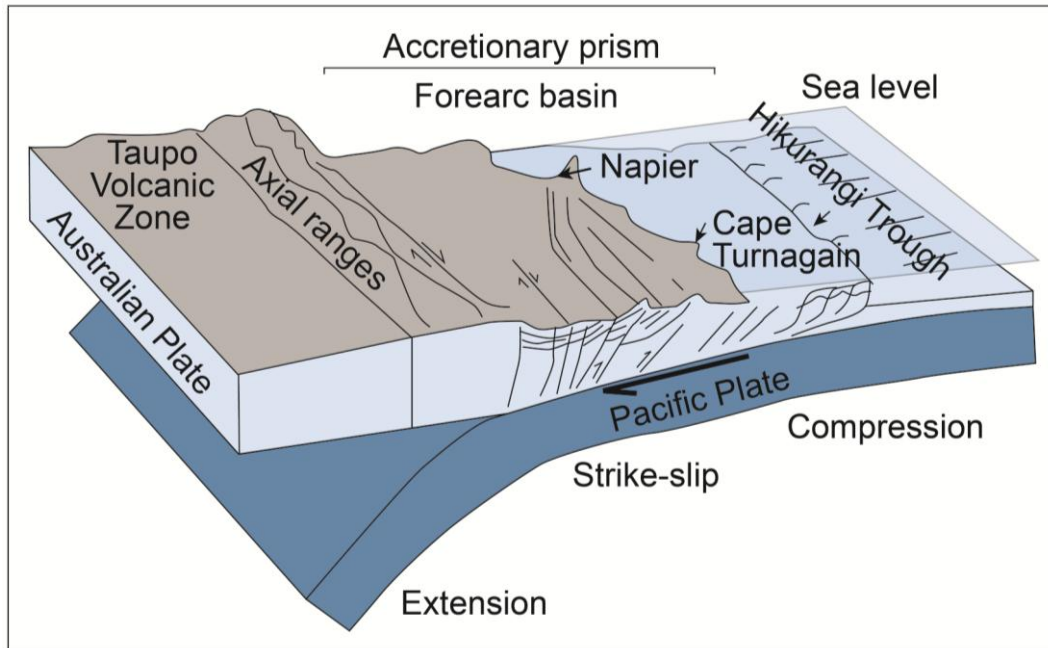


Figure 2.2. Schematic cross-section of the east coast subduction margin (modified from Nyman et al., 2010).

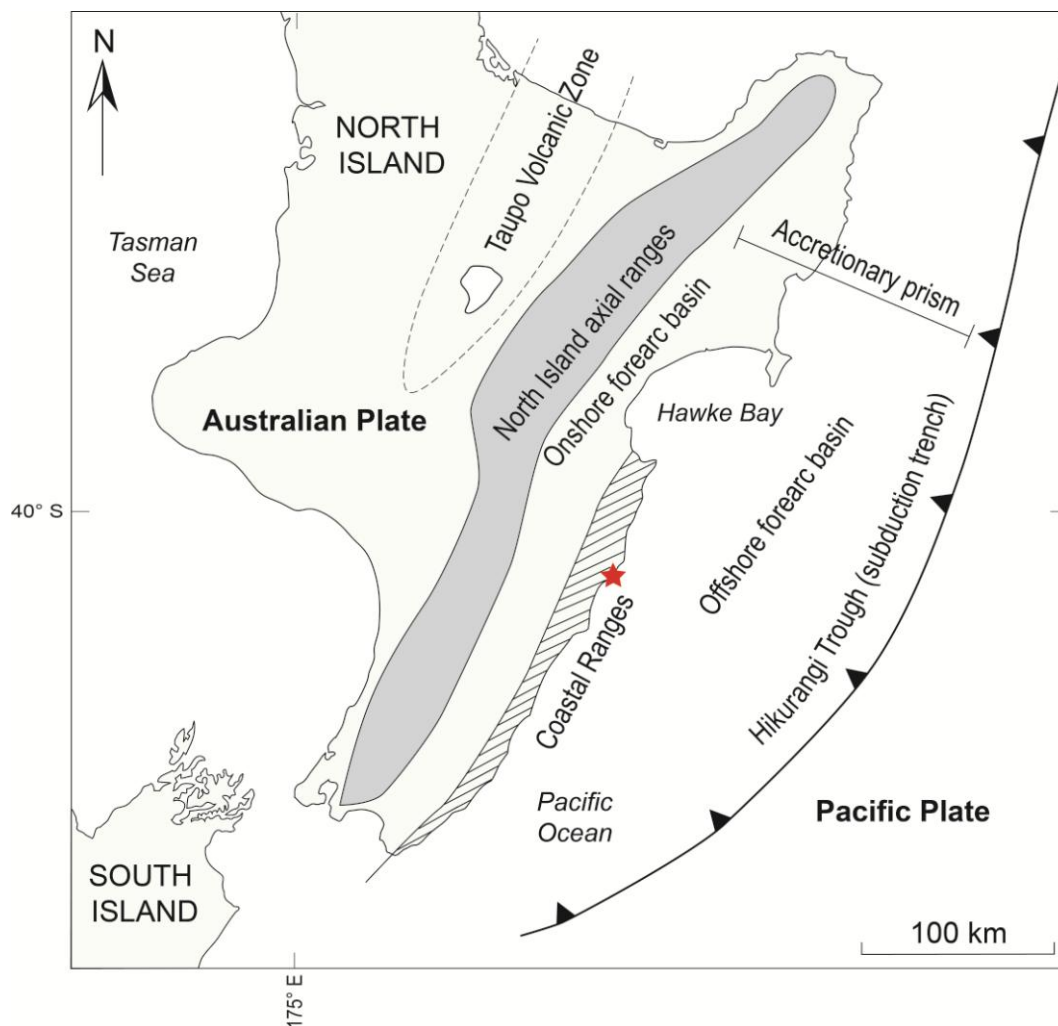


Figure 2.3. Tectono-geomorphic structural features across the subduction margin (modified from Field et al., 1997).

Subduction trench and accretionary prism

The subduction trench (the Hikurangi Trough) represents the region where initial subduction of the Pacific Plate occurs. It is the southern end of the Tonga-Kermadec-Hikurangi subduction zone of the western Pacific, a 3000 km long plate boundary where oceanic crust of the Pacific Plate is subducting obliquely beneath the continental crust (North Island) of the Australian Plate (Figure 2.2). In the area offshore from Hawke's Bay, rapid frontal accretion is occurring in the subduction trench, where more than 3 km of sediment has accumulated on the Pacific Plate (Barnes & Mercier de Lepinay, 1997; Barnes et al., 2002). The accretionary prism developing here as a result of collision and subduction of the plates, with up-doming of sediment due to lack of accommodation space, is mostly composed of Plio-Quaternary trench fill turbidites (Barnes & Mercier de Lepinay, 1997). Onshore Hawke's Bay is the semi-emergent section and marks the most eastern point of the accretionary prism, which extends landward from the subduction trench (Figure 2.3).

Forearc basin

Hawke's Bay lies within the onshore part of the forearc basin, which extends east offshore as far as the Hikurangi Trough. Onland it is a region of low-lying plains and rolling hills, bounded to the west by the North Island Mesozoic basement axial ranges (Beanland et al., 1998) and to the southeast by the coastal ranges composed of strata of Middle Cretaceous to early Neogene age (Pettinga, 1982; Figure 2.3). The forearc basin contains a 5 km thick sequence of marine and terrestrial sediments spanning the Neogene which rest unconformably on greywacke basement rocks (Field et al., 1997; Beanland et al., 1998). At the large scale the Neogene fill records marine regression from Miocene outer shelf and slope mudstones, through to shallow marginal marine sandstones and limestones, to terrestrial conglomerates deposited in the Pleistocene (Cashman et al., 1992; Beanland et al., 1998).

Coastal ranges

The coastal ranges are a structurally complex zone characterised by uplift, which began in the earliest Pliocene by contraction in the accretionary wedge. This, along with extensional (in some areas) tectonics produced pronounced northeast-southwest trending faults and anticlinal and synclinal structures (Pettinga, 1982; Cashman et al., 1992; Beanland et al., 1998). The study area is located within the coastal ranges and is influenced structurally by a series of complex folds and faults (Figure 2.3).

Axial ranges

The North Island axial ranges are a series of north-northeast trending ranges, including the Ruahine, Kaweka, Kaimanawa, and Ahimanawa ranges (Figure 2.4). They are composed of weakly metamorphosed Mesozoic sandstone and mudstone, otherwise known as greywacke basement rocks, all part of the Torlesse Terrane (Lee et al., 2011). The ranges are fault bounded, where the major Mohaka and Ruahine oblique-slip faults, part of the North Island Fault System (otherwise known as the North Island Shear Belt; Bland & Kamp, 2006), allow basement rocks to lie adjacent to much younger Neogene 'cover' rocks. The North Island axial ranges act as the western border of the forearc basin and extend continuously from Cape Palliser in the Wellington region in the south to East Cape in the north. There is some distinction made between the Tararua and Ruahine ranges in the south, within the axial ranges, which strike north-northeast, and the Kaimanawa and Ruakumara ranges in the north, which strike northeast (Field et al., 1997; Figure 2.1). The uplift history of the axial ranges probably started in the Early Miocene or early Middle Miocene as a result of the onset of oblique convergence of the Australian and Pacific plates. The rate of uplift probably picked up during the Plio-Pliocene, and remains ongoing as is evident from the elevations of marine terraces and the depth of incision of rivers in river valleys (Field et al., 1997).

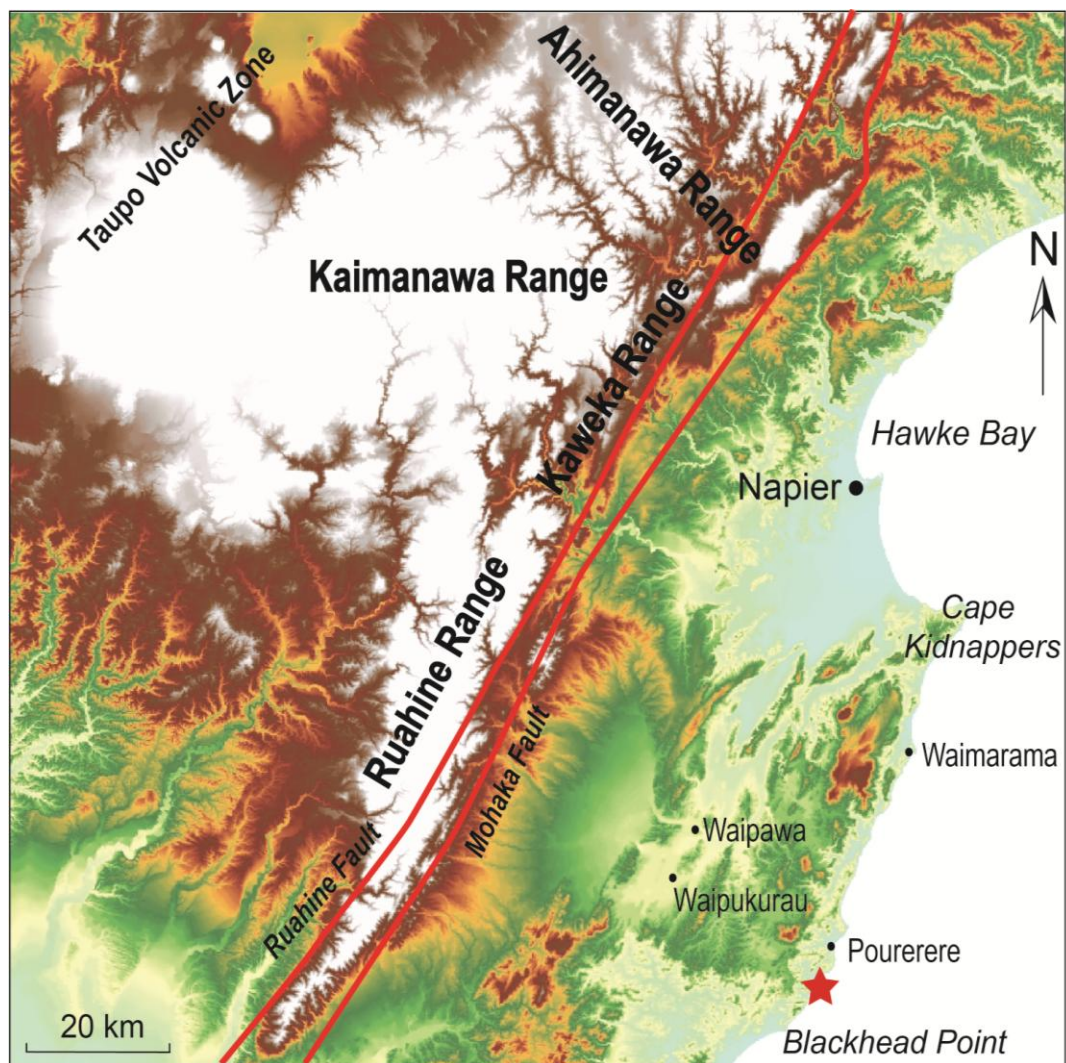


Figure 2.4. Topographic relief map of the Hawke's Bay area showing some of the North Island axial ranges. The red star marks the location of the Te Angiangi Marine Reserve. ArcGIS database was used to derive the topographic relief map. White indicates regions of high elevation (adapted from Lee et al., 2011).

2.1.3 Regional stratigraphy and tectonic history

The Late Cretaceous to Neogene tectonic history and stratigraphy are described in this section (refer to the New Zealand geological timescale in Appendix 1). A geological map of the inland area from Te Angiangi Marine Reserve in Figure 2.5 and a stratigraphic panel is shown in Figure 2.7.

Early to Middle Cretaceous

Throughout the Cretaceous the East Coast region (including the Hawke's Bay region) was positioned along the Pacific margin of Gondwana. In the Early Cretaceous (105 to 95 Ma), sediments of the Torlesse Terrane were accreted along this margin (Field et al., 1997; Lee et al., 2011). In the Middle Cretaceous regional convergence ceased or slowed, and was followed by crustal extension in some areas, which represented the rifting of New Zealand (Zealandia) from the Australian and Antarctic eastern side of Gondwana (Field et al., 1997).

Middle Cretaceous to Paleocene

In the Late Cretaceous-early Cenozoic, crustal extension in Zealandia was underway, which led to the isolation of New Zealand from Gondwana with the opening of, and seafloor spreading in the Tasman Sea (Field et al., 1997; Lee et al., 2011). Associated with the opening of the Tasman Sea was a change from a subduction-dominated to a passive margin setting during the early Late Cretaceous in eastern North Island (Lee et al., 2011). By the Paleocene seafloor spreading ceased. In the east of the Wairarapa - Hawke's Bay districts, the Late Cretaceous Glenburn Formation is present east of the Omakere Fault (Figure 2.5) and is well exposed along the Waimarama coast. The formation consists of well bedded, carbonaceous, alternating sandstone and mudstone with concretionary sandstone and conglomerate lenses that has an inferred depositional environment of outer shelf to upper bathyal (100 - 600 m depth) in a submarine fan setting (Lee et al., 2011).

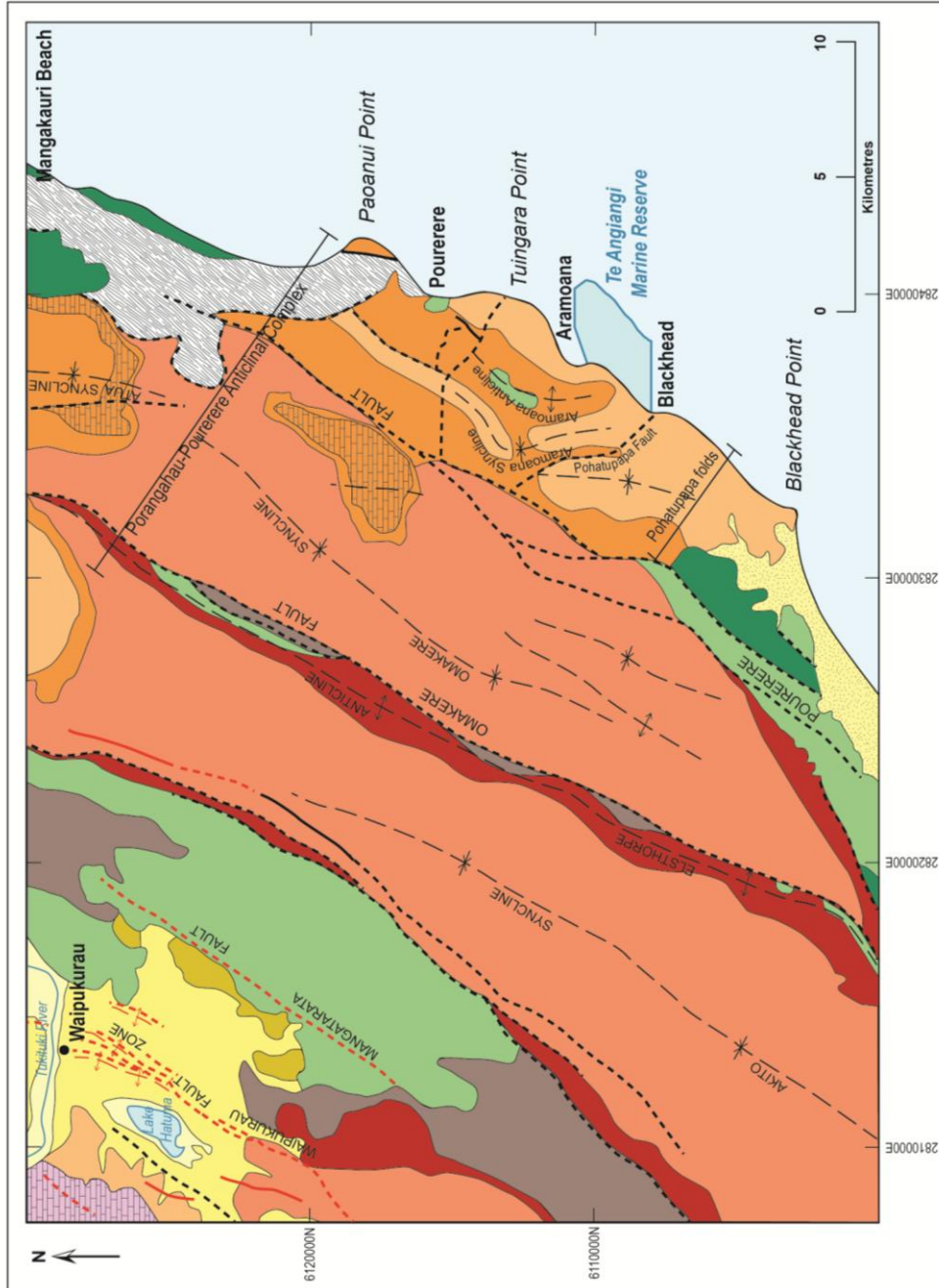


Figure 2.5. Geological map of the area inland from the Te Aniangi Marine Reserve in the southern Hawke's Bay region. The Pohatupapa folds and Porangahau-Pourerere Anticlinal Complex are also shown (modified from Lee et al., 2011).

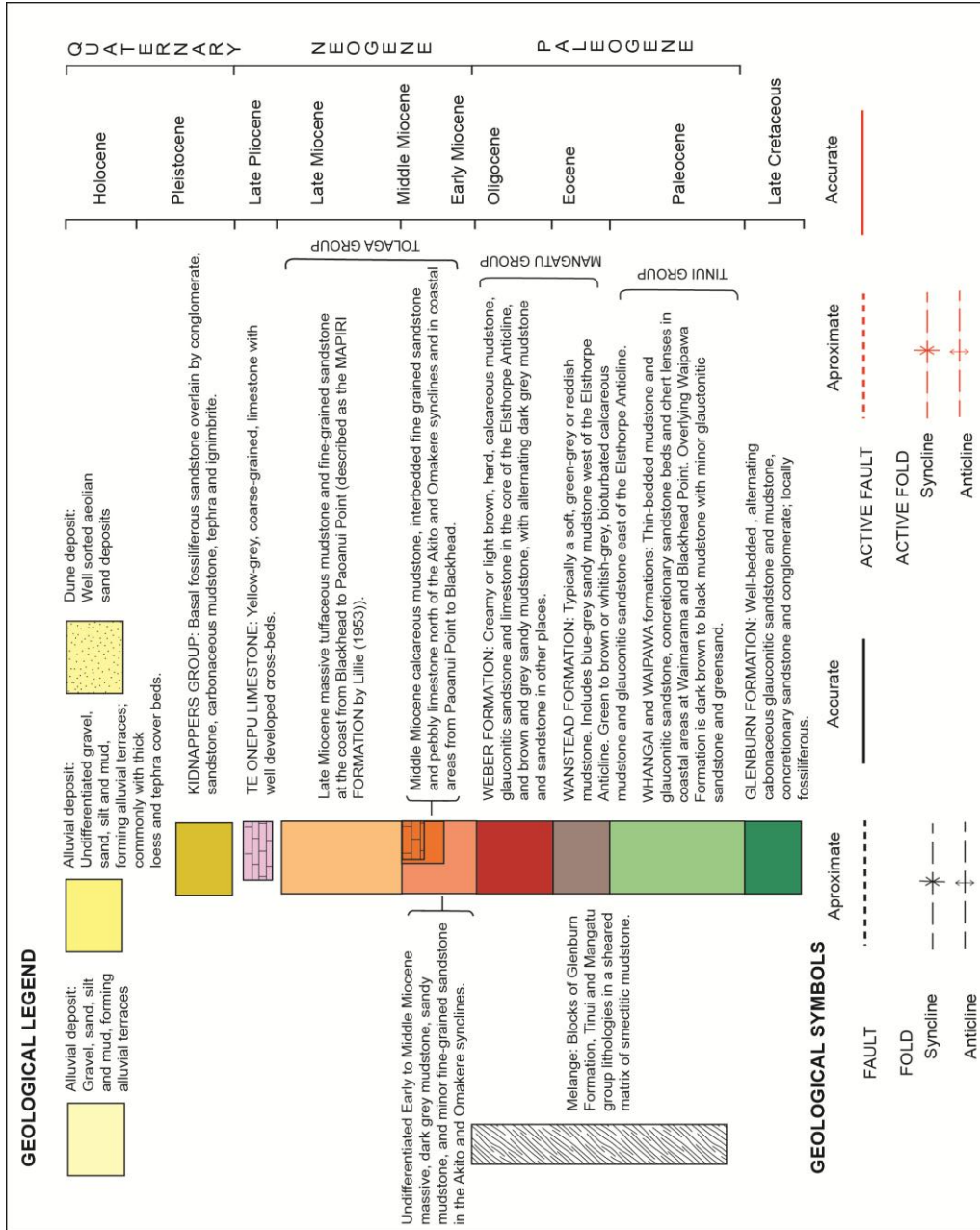


Figure 2.6. Geological legend for Figure 2.5.

The lower contact of the Glenburn Formation is unknown, while the upper contact is overlain by the widespread Tinui Group, of Late Cretaceous to late Paleocene age (Figure 2.6), that includes the Whangai and Waipawa Formations (Figure 2.7). The Tinui Group represents a stable to slowly subsiding depositional environment, as indicated by a decreasing content of terrigenous material, increasing amounts of glauconite, and an upward fining grain size. The Whangai Formation is a light and dark banded, well bedded mudstone with intercalated bands of glauconitic sandstone, and is conformably overlain by the Waipawa Formation, a dark brown to black carbonaceous mudstone, also with glauconitic sandstone. Both formations are present inland from the study area, with the Waipawa Formation well exposed southeast of Waipukurau (Figure 2.5). The Whangai Formation was deposited in shelf to bathyal depths, as indicated by microfossil assemblages, and the Waipawa Formation in an outer shelf to upper slope basin environment (Lee et al., 2011; Figure 2.7).

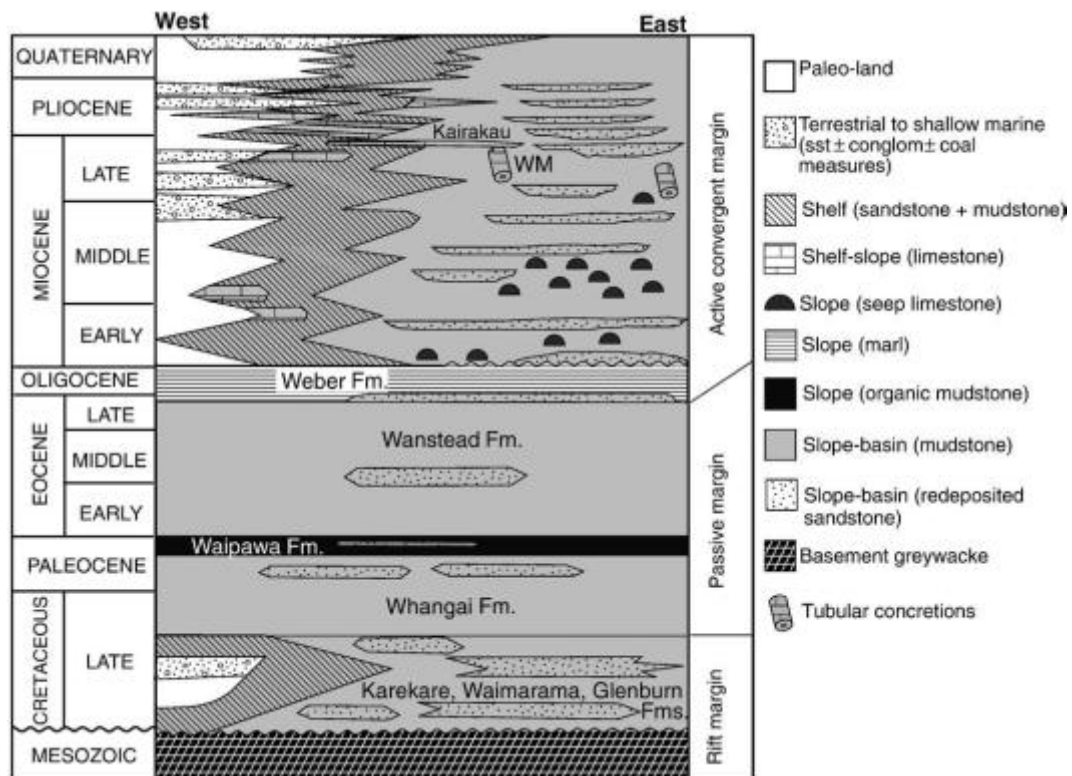


Figure 2.7 Generalised panel diagram showing the Cretaceous to recent stratigraphy and depositional environments for the sedimentary rock column in southern Hawke's Bay. WM is the approximate stratigraphic position of the Whangaehu Formation mudstone, which contains tubular concretions, and which has many similar characteristics to the Mapiri Formation mudstone (taken from Nyman et al., 2010).

Paleocene to Oligocene

The Wanstead Formation is a green-grey or reddish mudstone and in the study area it contains smectite clays which swell when wet, causing erosion and slope instability. This formation has a thickness of about 300 m (Lillie, 1953); it is inferred to have a Middle Eocene age, with a mid to lower bathyal-abyssal depositional environment. Widespread deposition of mudstone and sandstone in the region indicates that shelf to bathyal depositional environments continued into the Oligocene (Lee et al., 2011). The Weber Formation was deposited in slightly shallower (mid bathyal) water depths, and consists of alternating light brown and grey calcareous mudstone and well bedded sandstone, that can be difficult to distinguish from the Wanstead Formation (Lillie, 1953). Foraminifera are used to distinguish the two formations, and provide an Early Oligocene to earliest Miocene age range (Lillie, 1953; Lee et al., 2011). These formations were deposited as a result of thermal relaxation subsidence as eastern New Zealand continued to drift away from the Tasman Sea spreading ridge. Late in the Oligocene tectonism along the Hikurangi Margin commenced with development of the Australian-Pacific plate boundary (Lee et al., 2011). Since the beginning of active subduction along the plate boundary at about 25 Ma, up to 80 km of material has been added to the Hikurangi Margin (Field et al., 1997; Barnes et al., 2010).

Neogene-Quaternary

Early Miocene

In the Early Miocene, the Hikurangi Margin became active from as far north as Northland through to Marlborough, marked by volcanism in Northland, a change from slow carbonate-dominated deposition to rapid terrigenous sedimentation, and the beginning of a period of intense deformation. Evidence of deformation in the southern Hawke's Bay is seen through strike-slip thrust faults with up to tens of kilometres of displacement (Field et al., 1997).

At this time a change in the style of sedimentation becomes evident in the Hawke's Bay region, with widespread flysch deposition heralding the change from a passive to active margin (Lee et al., 2011). In fact, throughout the entire Miocene, episodic uplift and subsidence occurred at the same time in different parts of the region, resulting in bathyal mudstone to shelf limestone and

sandstone. The widespread Tolaga Group (Figure 2.6) consists of massive calcareous mudstone and some sandstone, and ranges in age from Early Miocene to Early Pliocene.

Middle Miocene

Regional uplift in the Middle Miocene affected the Wairarapa and Marlborough areas, resulting in erosion of Neogene 'cover' rocks to expose the underlying basement rocks. In southeastern Hawke's Bay, calcareous mudstone with interbedded fine-grained sandstone and pebbly limestone facies are present which unconformably overlie Early Miocene rocks in the Omakere and Akitio synclines (Figure 2.6).

Late Miocene

During the Late Miocene, tectonically produced rapid subsidence occurred in the region, and most places were submerged by this time. Faults along the axial ranges are inferred to have taken up most of the vertical component of movement at this time. Subsidence allowed the deposition of thick mudstone and flysch sequences (Lee et al., 2011), which lie conformably or gradationally on Early and Middle Miocene rocks in the southeastern Hawke's Bay (Lillie, 1953). Poorly bedded massive mudstone (the Mapiri Formation, explained in detail in the next section) and fine-grained sandstone are well exposed in, and comprise, the coastal cliffs from Blackhead to Pourerere, adjacent to the marine reserve (Figure 2.6). Further up the coast to the north, between Waimarama and Paoanui Point, melange consisting of crushed Glenburn Formation, Tinui Group, and smectitic mudstone is present (Lee et al., 2011; Figure 2.6).

Plio-Pleistocene

The Plio-Pleistocene is associated with changes in relative plate motion, marked by periods of deformation and uplift, in-between periods of quiescence (Field et al., 1997). The southern Hawke's Bay area was subjected to episodic uplift which began in the earliest Pliocene, with initial compressional forcing reactivating reverse faults in the region. The Ruahine Ranges were uplifted in the latest Pliocene, probably due to movement on the Ruahine Fault. This uplift was associated with deposition of conglomerates and deformation of soft sediments (Lee et al., 2011). Tephra beds and ignimbrites deposited in the Pleistocene

throughout the region represent volcanic activity from the developing Taupo Volcanic Zone. The Kidnappers Group (well exposed at Cape Kidnappers) was deposited during this time, and reflects a marginal marine depositional environment. Much of the region had emerged by this time as the regional uplift rate increased (Lee et al., 2011).

2.1.4 Study area geological setting

The Te Angiangi Marine Reserve is located within the coastal range zone, otherwise known as the coastal fault zone (Figure 2.3), where strata are deformed due to much faulting and subsequent folding. Topography in the area adjacent to the reserve, and in much of the coastal range zone, typically consists of rounded undulating hills composed of uplifted Middle Cretaceous to early Neogene sediments. Generally, Late Miocene sandstone and mudstone are present immediately adjacent to the reserve and Cretaceous to Paleogene sediments in other areas (Lee et al., 2011; Figure 2.5).

Major faults and folds west of the coast include the Pourerere Fault, which is the closest and most prominent fault in the immediate area, the Pohatupapa Fault, the Omakere and Atua Synclines and, further west, the Omakere Fault and Elsthorpe Anticline (Lee et al., 2011; Figure 2.5). Lillie (1953) describes strata to the east of the Pourerere Fault as being affected by anticline and syncline structures, along with both strike and cross-faults, collectively called the Pohatupapa folds which are part of the Porangahau-Pourerere Anticlinal Complex (Figure 2.5). The Pohatupapa folds are structurally very complex and are difficult to determine. Some folds are clearly visible but others are inferred on little evidence and, due to later faulting, are offset and no longer continuous. The folds are not strongly symmetrical and generally strike to the north (Lillie, 1953). There is a small anticline directly adjacent to the reserve, called the Aramoana Anticline (Figure 2.5).

The dominant lithology of these hills, according to Lillie (1953), is mudstone of the Mapiri Formation, usually containing fragments of pumice and bands of white tuff (thought to be derived from the Coromandel volcanic area (Field et al., 1997)). It is a massive, blue-grey, sandy mudstone with occasional carbonate

concretions. The formation has a Tongaporutuan Stage (Late Miocene) age, determined from its upper Tongaporutuan faunas, and is therefore equivalent to the Whangaehu Formation mudstone mentioned in Figure 2.7. However, there exists some uncertainty about the differentiation of Middle and Late Miocene formations in the area because they are lithologically very similar. Hence, biostratigraphy is necessary to differentiate the rocks. Foraminifera also suggest a bathyal environment of deposition for the mudstones. The Mapiri Formation is estimated to be 600 m thick in the vicinity of the reserve, although there may be undetected structural repetition. Any bedding is difficult to discern, although occasional interbeds suggest a gentle dip of about 10° to the ESE in the vicinity of the Te Angiangi Marine Reserve.

Field et al., (1997) reviewed the work by Lillie (1953) about the Mapiri Formation, but did not add to his description. Lee et al., (2011) support Lillie's description of the Late Miocene rocks, and state that Late Miocene rocks in the area east of the Omakere Fault-Elsthorpe Anticline unconformably overlie Early to Middle Miocene Tolaga Group rocks. The Late Miocene rocks in this area are, as described by Lee et al., (2011), shelf to bathyal undifferentiated massive mudstone, massive sandstone, tuffaceous mudstone, flysch beds, and concretionary sandstone.

An interesting feature of the Mapiri Formation is the occurrence of *in situ* carbonate concretions, well seen protruding from the intertidal mudstone platform (Figures 2.8 and 2.9). The concretions are quite abundant and well exposed on the intertidal platform to the south of Blackhead and to the north just before Aramoana, but scattered between Aramoana and Pourerere. Most of the concretions tend to align along major joints in the mudstone platform, although some appear to be scattered randomly. Recent work by Nyman et al., (2010), studying the nature and origin of tubular carbonate concretions present in the Late Miocene Whangaehu mudstone, immediately north of Cape Turnagain to the south of the Te Angiangi Marine Reserve (Figure 1.1), provides some insights into the character of the concretions found in the Mapiri Formation, addressed in a later section.



Figure 2.8. *In situ* carbonate concretions protruding from the intertidal shore platform as a result of erosion of the surrounding softer host mudstone.



Figure 2.9. A section of the intertidal shore platform showing abundant randomly scattered concretions. Some landslide debris is also evident in the foreground.

Chapter 3

THE MAPIRI FORMATION MUDSTONE

3.1 INTRODUCTION

The aim of this chapter is to determine the characteristics of the Mapiri Formation mudstone present in the coastal area immediately adjacent to the Te Angiangi Marine Reserve. This includes determining the structures (bedding, joints, faults, folds), texture, mineralogy (especially clay mineral types) and chemical composition of the Mapiri Formation, the dominant mudstone lithology in the area. Some of these features were determined in the field and others were made following laboratory analysis. During field work it was observed that the mudstone exhibited an interesting weathering process, whereby the individual joint blocks of mudstone eroded in a spheroidal manner to release clasts of small to giant size (Figure 3.1 and Figure 3.2D). Once these clasts of mudstone reached the beach zone, waves acted to further disintegrate them and release the mudstone "spheroids" as smaller rounded gravel clasts of cobble to pebble size (Figure 3.1). Further observation showed that the jointed nature of the mudstone allowed water to seep into the cracks and assist in breaking down the blocks, a characteristic that would be fostered in the presence of wetting (expanding) and drying (contracting) smectite clay minerals, which are checked for in the laboratory analysis.



Figure 3.1. Mudstone weathering process. Large jointed block of bedrock (left) from which clasts of variable sizes were released (middle) and further disintegrated into smaller rounded "spheroids" of cobble to pebble size (right).

3.2 FIELD METHODS

Field work involved walking the length of the reserve observing the geomorphology and photographing, examining, and describing geological characteristics of the mudstone. The bedrock of the coastal cliffs exposed by the landslides was examined, as well as the landslides themselves and the resulting debris (described in the next chapter). Dip and strike measurements were made using a Silva compass on suspected bedding in the bedrock which was exposed by landsliding.

The reserve is easily accessible from the south at Blackhead and can be traversed at any tidal height, although best avoided under extreme weather conditions. However, the only way to walk the entire length of the reserve during high tide is on top of the slip debris, as the track used for vehicle access was covered by slip debris in the April 2011 storm. The shore platform is completely covered during high tide, but can be walked during low tide with care and consideration for the marine life on the platform. The reserve is also accessible from Aramoana, although vehicle access is slightly more difficult as the main route in is a gravel farm road.

After examination and description of the geology and landslide aspects, including examination of any bedding and joints in the mudstone bedrock, representative geological samples were collected for characterisation by laboratory analysis. A total of five large mudstone and carbonate concretion samples were collected from locations within the Te Angiangi Marine Reserve, three of mudstone and two of concretions (Figure 3.2, Figure 3.3 and Table 3.1). *In situ* samples were collected using a geological hammer and chisel, but collections were also made from fallen blocks on the shore platform. Care was taken to collect mudstone bedrock samples that were fresh and unaffected by weathering.

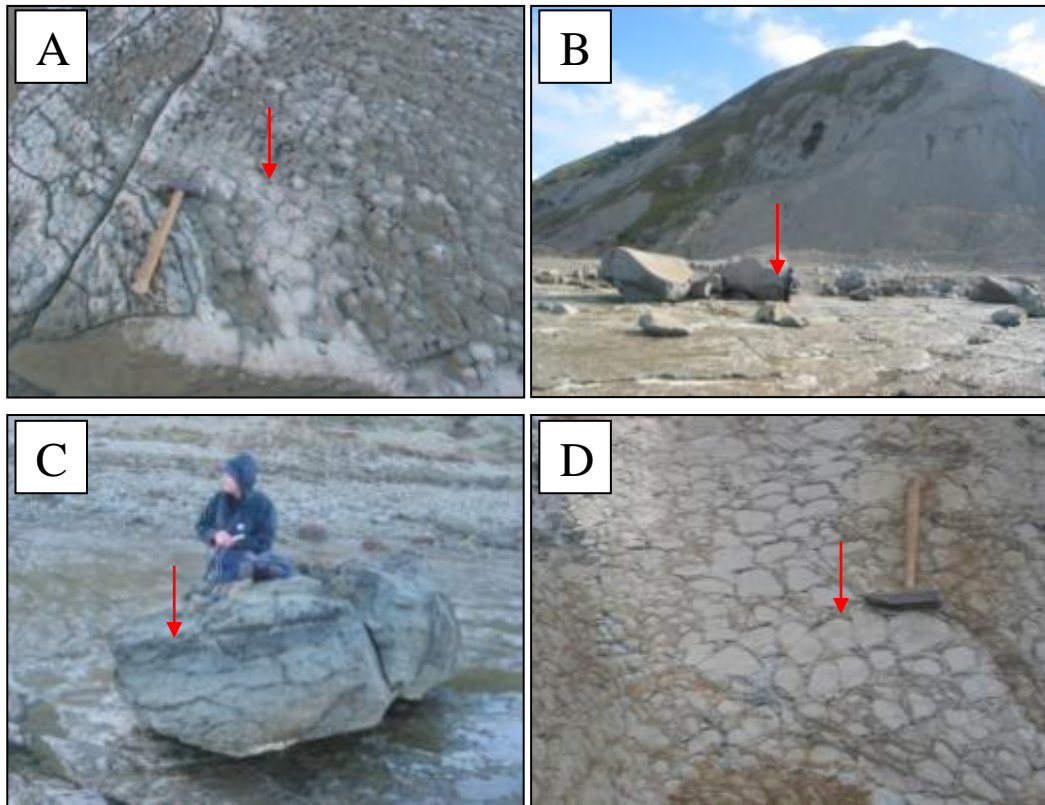


Figure 3.2. Mudstone and concretion sample locations. A - Sample DM2 was collected from the shore platform. B - Sample DM7 was collected from blocks of bedrock in the foreground. C - Sample DM3 came from a near *in situ* concretion. D - Sample DM1 was collected from a block of highly jointed bedrock in which the individual joint blocks exhibit prominent spheroidal weathering. Red arrows approximate sampling positions.



Figure 3.3. Rock sample locations (red dots) in the Te Angiangi Marine Reserve. Blue line marks the reserve boundary. Satellite image derived from ArcGIS database.

Table 3.1. Description of sample collections.

Sample code	Date collected	Description	Sample location	Comments
DM1	2/09/2011	Mudstone (2 or 3 large blocks).	Collected from large block of bedrock in slip debris in the middle of reserve. (40°9'32.18"S 176°50'26.72"E)	Block shows spheroidal weathering (progressive weathering from blocks to pebbles, Figure 3.2D).
DM2	2/09/2011	Mudstone (2 or 3 large blocks).	Collected from the shore platform at mid shore height in southern half of reserve. (40°9'51.22"S 176°50'4.13"E)	Platform here shows spheroidal weathering on a smaller scale (cm) due to smaller joints, not master joints (Figure 3.2A).
DM3	2/09/2011	Concretion (2 or 3 blocks).	Collected <i>in situ</i> (?) from shore platform at high shore height in southern half of reserve. (40°9'43.79"S 176°50'19.43"E)	Two concretions about 1.5 m long and 1.25 m across. Concretions have flagginess which may be bedding in the host mudstone. They may not be <i>in situ</i> (Figure 3.2C).
DM4	2/09/2011	One small tubular concretion with finger size hole through middle. Yellow-brown in colour, possibly due to weathering.	Collected from slip debris in the middle of reserve. (40°9'27.93"S 176°50'31.69"E)	Concretion may represent an avenue of past methane escape (based on similarities seen in Nyman et al., (2010) paper).
DM7	7/09/2011	Mudstone (2-3 blocks).	Collected from large block of bedrock in slip debris in the northern half of reserve. (40°9'7.57"S 176°50'49.24"E)	Block of bedrock shown in Figure 3.2B.

3.3 LABORATORY METHODS

A flow chart showing the laboratory analyses carried out on the rock samples collected is shown in Figure 3.4.

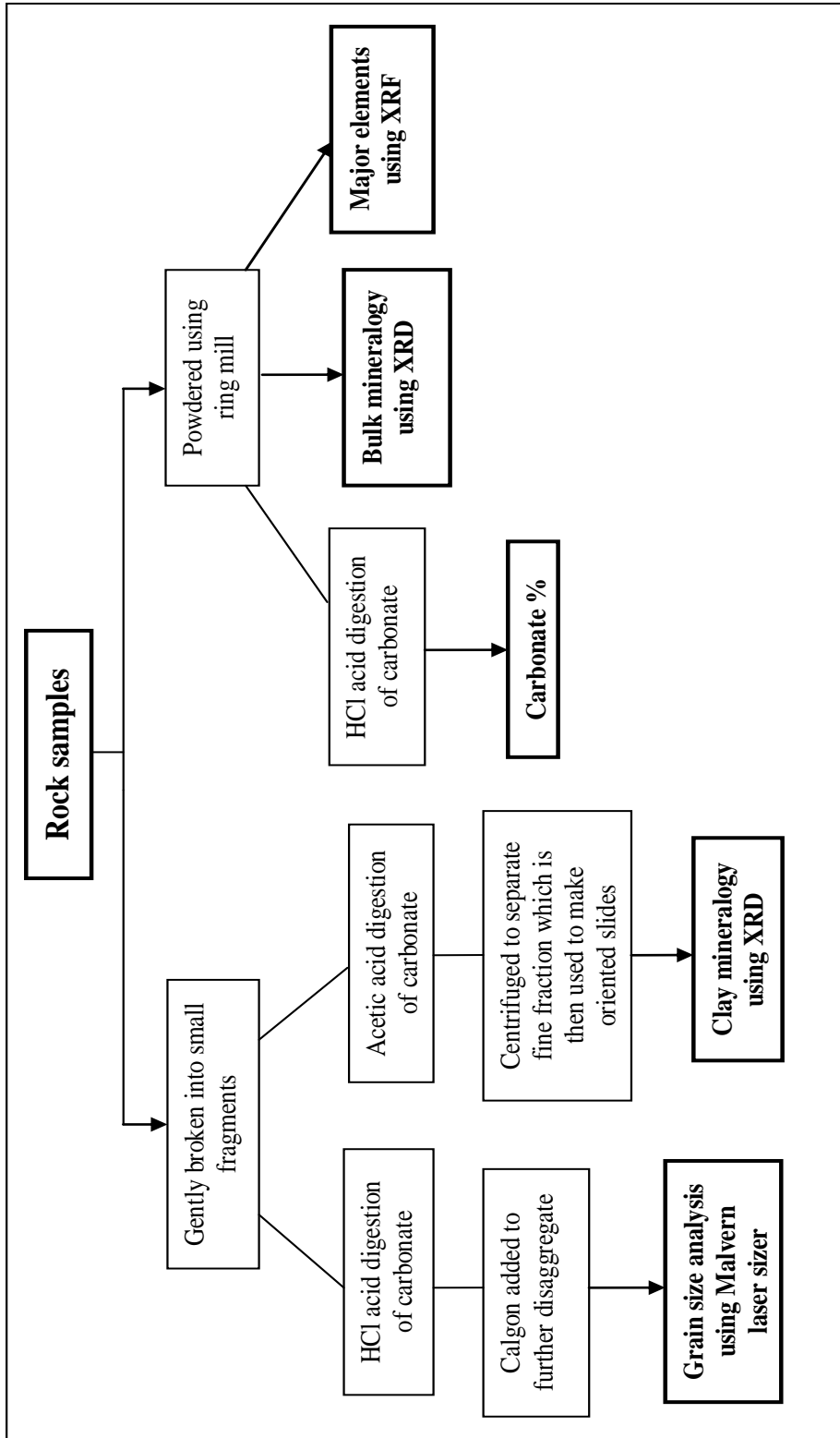


Figure 3.4. Flow chart of laboratory analyses carried out on samples.

3.3.1 Carbonate content

Carbonate percentage was determined for all samples to allow for a fuller description of the mudstone and further insight into the nature and origin of the concretions in the host mudstone.

Subsamples were taken of each rock sample and dried overnight in a 40°C oven. The samples were then powdered, to enable faster acid reaction time, using a tungsten carbide head in a ring mill at the University of Waikato. After the samples were powdered, about 5 g of dry powder was measured to four decimal places into labelled pre-weighed 250 ml beakers and dried overnight in a 40°C oven. Both the beaker and the powder held within the beaker were then re-weighed. The beakers were then placed into a fume hood and about 50 ml of 10% hydrochloric acid (HCl) (or enough to cover the sample in the beaker) was added, gently swirled and left to dissolve the carbonate overnight, stirring occasionally. To test if all the carbonate was dissolved, the sample was stirred and observed for any effervescence; if so, then more HCl was added and left for a further 2 hours. Five sheets of filter paper (Whatman No. 42 15cm) were folded and placed in a labelled pre-weighed small glass beaker and dried overnight at 40°C before weighing. The filter paper and the small beaker were held in a desiccator so the filter paper did not absorb any moisture while the powdered samples were digesting. The following day, three stands and five clamps were set up in a fume hood, with each of the clamps holding a glass funnel (Figure 3.5). A volumetric flask was placed beneath each of the funnels to collect waste acid. Once the acid digestion of the powdered samples was complete, one filter paper was placed into each of the glass funnels, making sure the small labelled glass beakers matched the filter papers with which they were weighed. The powdered sample was then diluted with deionised water and filtered through the filter paper using more deionised water.



Figure 3.5. The set up used to measure carbonate percentage.

The solution being filtered through the filter paper was tested with pH paper to check that the solution was at a neutral pH before being dried in the oven to prevent acid vapours being released while drying. Once the sample was filtered, the filter paper holding the insoluble remains of the sample was placed back into the matching labelled small beaker and placed into a 40°C oven overnight to dry. Once dry, the filter paper with the remains and small beaker was weighed.

Carbonate percentage by weight was determined by first calculating the difference between weight of the filter paper and corresponding small beaker after being dried initially, and the weight of the filter paper with insoluble remains and corresponding small beaker after being dried. The weight difference is the amount of insoluble remains. By subtracting the initial sample weight from that of the insoluble remains gives the amount of carbonate that was dissolved during acid digestion. This value was then converted into a weight percent (Table 3.2).

3.3.1.1 Results

Carbonate content results are shown in Table 3.2. Typically, the mudstone contain about 10% carbonate, while the concretions contain a significantly higher amount of 45 to 60%.

Table 3.2. Carbonate percentage results for mudstone (DM1, DM2 and DM7) and concretion (DM3 and DM4) samples.

Sample	Sample wt after drying (g)	Small beaker + filter paper after initial drying (g)	Small beaker + filter paper with insoluble remains after drying (g)	Insoluble remains (g)	Carbonate (g)	% Carbonate by weight
DM1 mst	5.0189	51.041	55.6328	4.5918	0.4271	8.5
DM2 mst	5.1027	41.375	46.1128	4.7378	0.3649	7.2
DM7 mst	5.176	51.0086	55.5785	4.5699	0.6061	11.7
DM3 concret	5.3396	46.907	49.1136	2.2066	3.133	58.7
DM4 concret	5.2049	47.484	50.3238	2.8398	2.3651	45.4

3.3.2 X-ray diffraction (XRD)

The bulk and clay mineralogical composition of all samples was analysed by a Philips X'Pert X-Ray Diffraction (XRD) machine with X'Pert HighScore software. In particular, the XRD technique would confirm field suspicions that the mudstone samples contained swelling clays.

Bulk mineralogy

In order to determine bulk mineralogy, a subsample of the powdered bulk sample was pressed into a small metal disc, placed into the sample holder and scanned from 2 - 42° 2 θ . These samples were unoriented and provided a representative mineralogical composition for each sample.

Clay mineralogy

Initial XRD runs for bulk mineralogy identified the need to further examine the samples in order to better identify the clay minerals present. Oriented samples were created and glass slide mounts were made for this purpose. These were made by firstly dissolving out the cement from a teaspoon of crushed rock sample using 1:4 acetic acid. Acetic acid was used rather than HCl, as HCl can distort clay mineral lattices (Carroll & Starkey, 1971). The samples were left for three days to allow the reaction to complete, aided by occasional stirring. After digestion of the cement was complete, the samples were transferred into a centrifuge tube and centrifuged for three minutes at 2000 rpm to remove the acetic acid from the

samples. The supernatant was decanted and discarded before re-dispersing the sample by adding about 40 ml of deionised water and mixing. The samples were centrifuged again for three minutes at 2000 rpm in order to remove any dissolved salts and prevent flocculation of the clay particles. The supernatant was decanted and the process repeated once more to ensure removal of all salt. A small amount of deionised water was then added to re-disperse the sample. The dispersing agent Calgon was then added to promote dispersion and prevent flocculation by reversing the normally positive charges through the adsorption of phosphate ions on the edge of the clay minerals (Moore & Reynolds, 1997). The samples were left overnight to allow the Calgon to react and then centrifuged for one minute at 300 rpm to separate out the fine sized particles ($<5 \mu\text{m}$). These particles held in the supernatant were decanted, and this suspension was used to make oriented mounts on glass slides. Using an eye dropper, some of the suspension was dropped onto a glass slide and left to dry overnight. Three slides per sample were made in order to analyse the clay minerals fully. One was air dried, the second was heated in a muffle furnace for one hour at 550°C , and the third was placed in a desiccator holding ethylene glycol and exposed to its vapour for 24 hours.

Heating eliminates any kaolinite present and collapses the primary smectite peak position to become concealed within the primary illite peak position, while ethylene glycol helps identify the presence of smectite by shifting its primary peak position to a higher \AA value. The air dried slide remains untreated. The slides were then scanned from $2 - 25^{\circ} 2\theta$, as this range encompasses most important clay peaks, including the non-basal peak for all samples at $19.9^{\circ} 2\theta$ seen in the initial bulk scans. The identification of clay mineral types becomes positive following the above treatments (Figure 3.6).

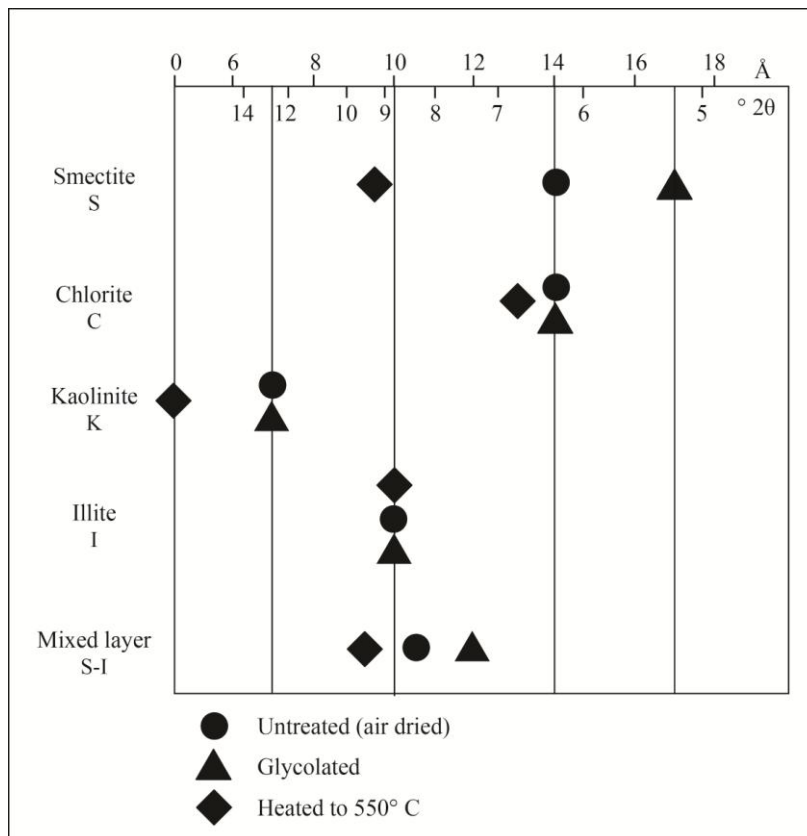


Figure 3.6. The expected movement of primary (001) peak positions of the main clay minerals in untreated, glycolated and heated oriented sample mounts.

3.3.2.1 Results

Bulk mineralogy

The end result of each scan by XRD is a chart showing peaks (all XRD charts are included in Appendix 2), with different peaks at different Å or °2θ positions. The positions of the primary peaks corresponds to a specific mineral, or a secondary peak of another mineral. Primary and secondary peak positions of some common clay and non-clay minerals are shown in Table 3.3. The intensity of each peak can be related broadly to the relative abundance of the mineral in a sample, allowing for a rough semi-quantitative estimate of its importance in that sample.

Table 3.3. Important peak positions of some common minerals found in the mudstone and concretion samples.

Mineral	Degrees 2θ	Angstroms (Å)
Quartz	26.62	3.35
Plagioclase	27.94	3.19
Low-magnesium calcite	29.42	3.04
High-magnesium calcite	30.0	2.97
Aragonite	26.22	3.40
Dolomite	30.9	2.89
Total clays	19.9	4.46
Illite 001	8.94	9.93
Illite 002	18.9	4.69
Chlorite 001	6.26	14.25
Chlorite 002	12.54	7.08
Kaolinite 001	12.34	7.19
Kaolinite 002	24.9	3.57
Smectite 001	6.0	14.0
Smectite 002	12.02	7.37

Figure 3.7 shows the XRD trace for mudstone sample DM1 as an example of bulk mineral analysis. The bulk mineralogy results for the mudstone samples were fairly consistent. All show relatively abundant clay minerals (the peak at about 4.5 Å represents total clays), with common quartz (peak at about 3.34 Å), some to common plagioclase (peak at about 3.19 Å), with some low-magnesium calcite (peak at about 3.04 Å; Figure 3.8). Peaks in these bulk mineralogical scans of unoriented powders suggest the clay minerals are likely illite and some combination of kaolinite, smectite and chlorite. More specific identification of the clay minerals present was achieved by creating oriented mounts under the different treatments mentioned earlier.

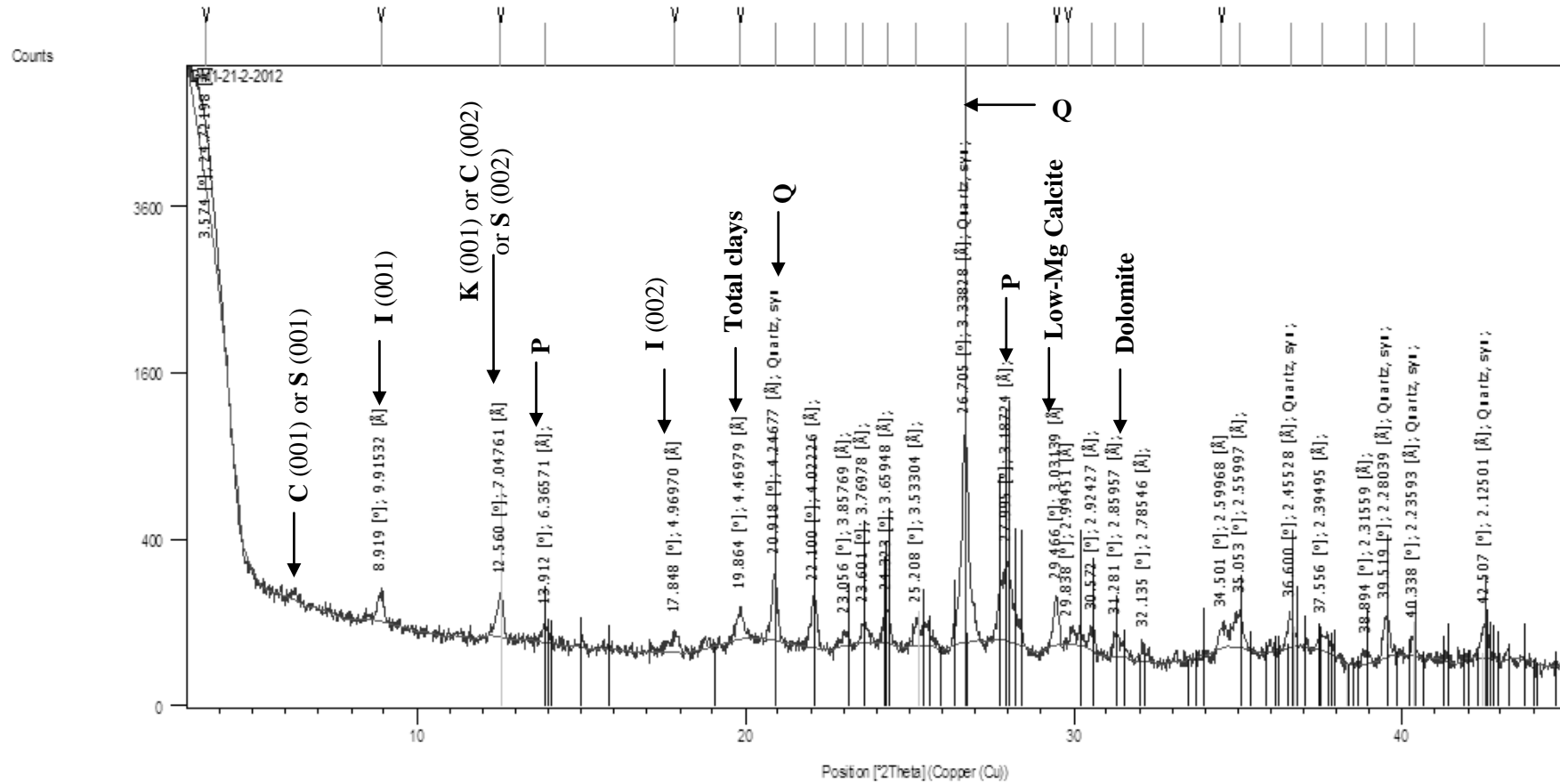


Figure 3.7. Bulk mineralogical XRD scan for mudstone sample DM1. S = smectite, C = chlorite, I = illite, K = kaolintie, P = plagioclase, Q = quartz, 001 = primary clay peak, 002 = secondary clay peak.

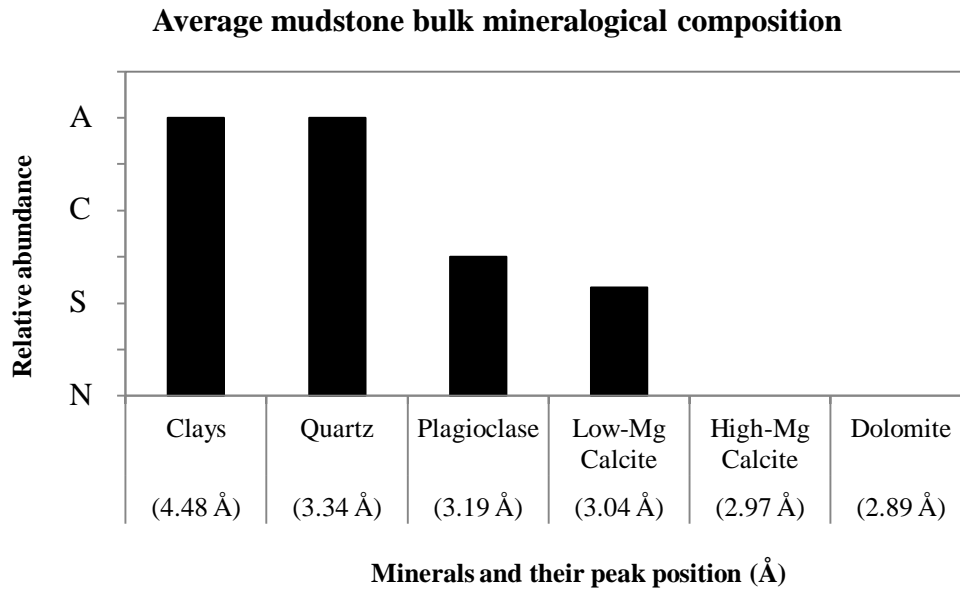


Figure 3.8. The average bulk mineralogical composition (relative abundances only) of the Mapiri Formation mudstone. A=abundant, C=common, S=some and N=absent.

Concretion samples were less consistent in their results. Both show relatively abundant clay minerals, common quartz, and some plagioclase. Sample DM3 (block taken from a possible *in situ* concretion) results suggest abundant dolomite, but any form of calcite is absent, so that it is a dolomitic concretion (Figure 3.9) whose carbonate content is near 60% (Table 3.2). Sample DM4 (tubular concretion) results suggest common low-magnesium calcite and some high-magnesium calcite (peak at about 2.97 Å), and also some dolomite (peak at about 2.89 Å; Figure 3.10). Concretion sample DM4 is therefore a calcitic concretion with a carbonate content of about 45% (Table 3.2).

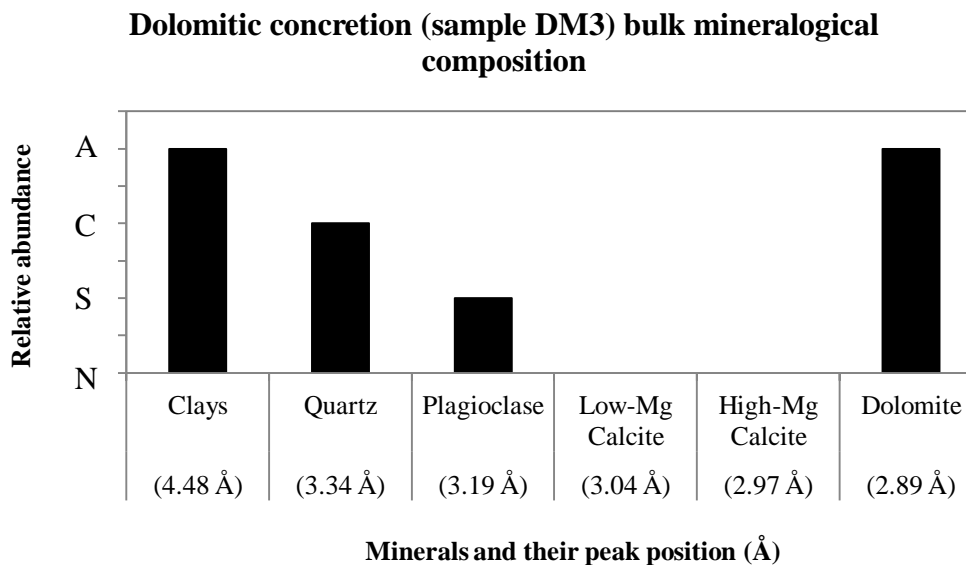


Figure 3.9. Bulk mineralogical composition of dolomitic concretion sample DM3. A=abundant, C=common, S=some and N=absent.

Calcitic concretion (sample DM4) bulk mineralogical composition

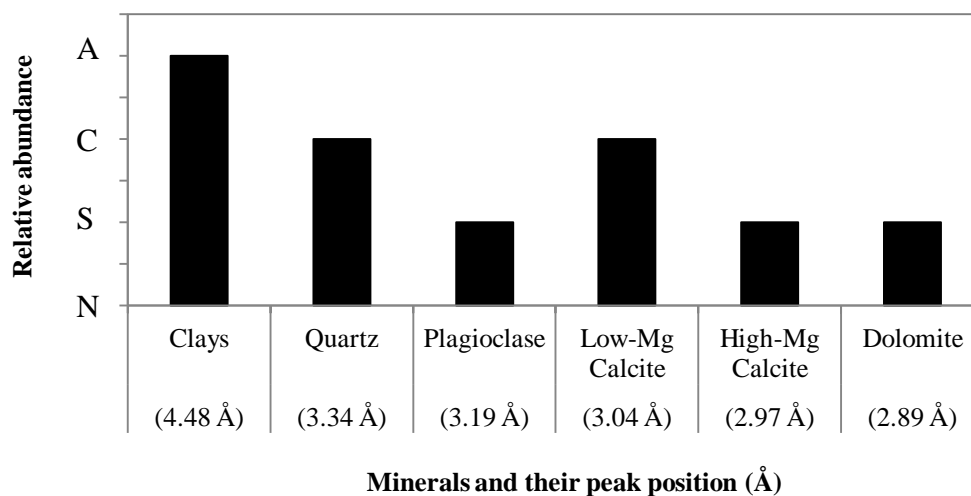


Figure 3.10. Bulk mineralogical composition of calcitic concretion sample DM4.
A=abundant, C=common, S=some and N=absent.

Clay mineralogy

Overall, the clay mineral composition based on primary (001) peak positions and peak intensities for all the samples indicates the presence of abundant illite, and smectite, some kaolinite, and rare chlorite (Figure 3.11). Appendix 3 contains a summary of clay mineral results for both oriented and unoriented mounts.

Illite appears persistently in all samples at about 10 Å and, as expected, glycolated and heated samples show no movement in the illite peak position. The persistence of a peak at about 14 Å corresponds to smectite in all untreated samples, because in the glycolated samples the smectite peak position shifts close to 17 Å, while in the heated samples the peaks shifts to about 9-10 Å to become concealed within the primary illite peak. A peak at about 7 Å persists in all untreated and glycolated samples, but disappears in all heated samples, therefore characterising kaolinite. The presence of chlorite is suspected due to a peak persisting at about 14 Å in all heated samples. However, curiously, the chlorite peak is not significantly present in the glycolated scans but appears in the heated ones, a feature needing future study. Figures 3.12 - 3.14 show sample DM1 as an example of clay mineral results on untreated and treated oriented mounts.

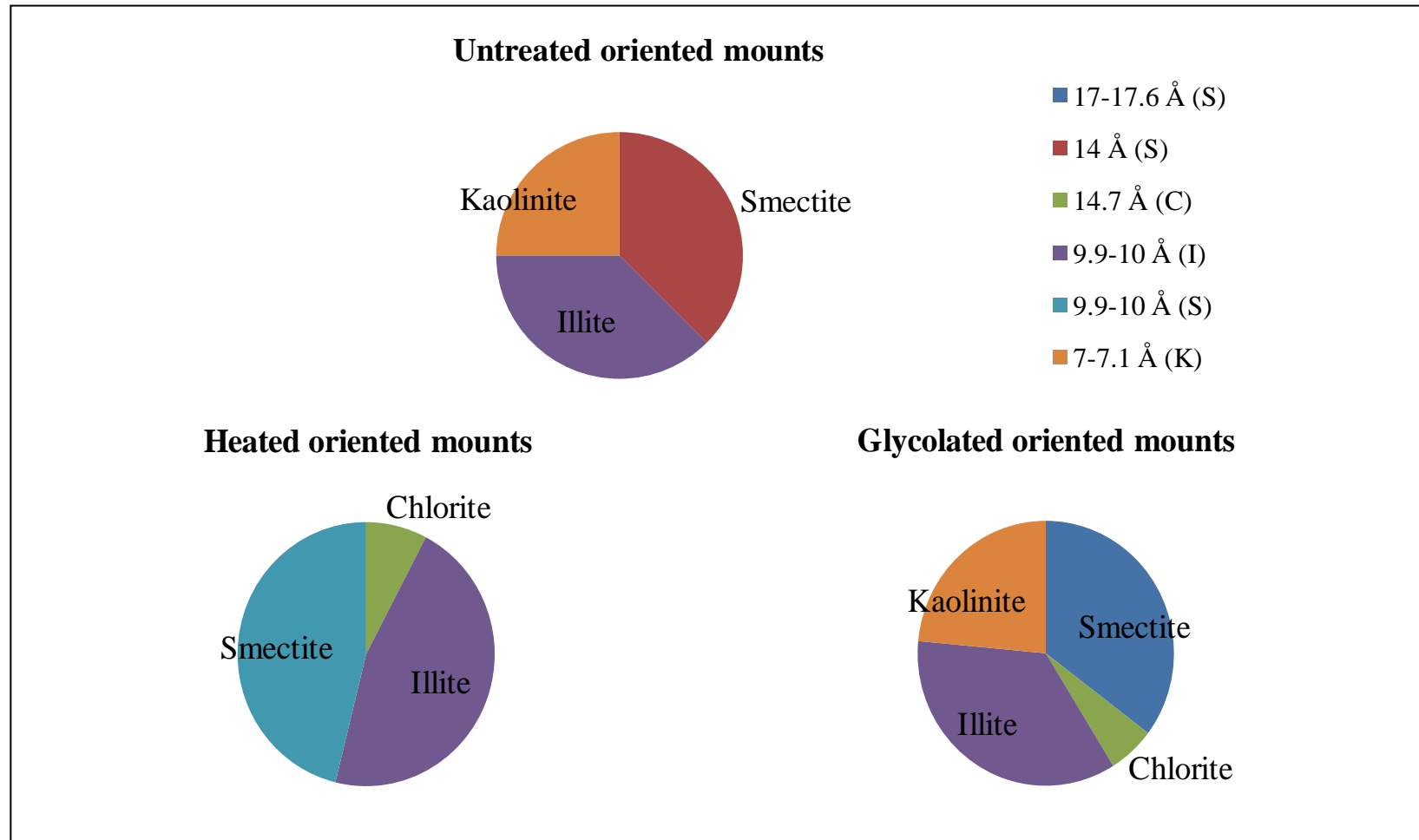


Figure 3.11. General clay mineral composition and relative abundances in samples.

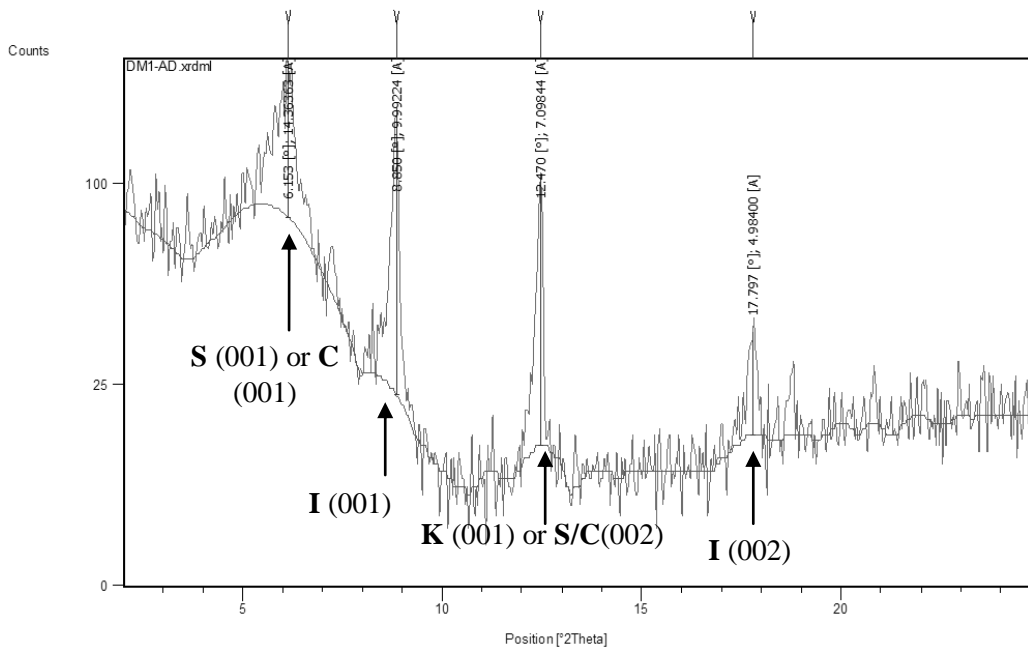


Figure 3.12. Sample DM1 mudstone untreated (air dried) oriented mount XRD scan. S = smectite, C = chlorite, I = illite, K = kaolintie, 001 = primary peak, 002 = secondary peak.

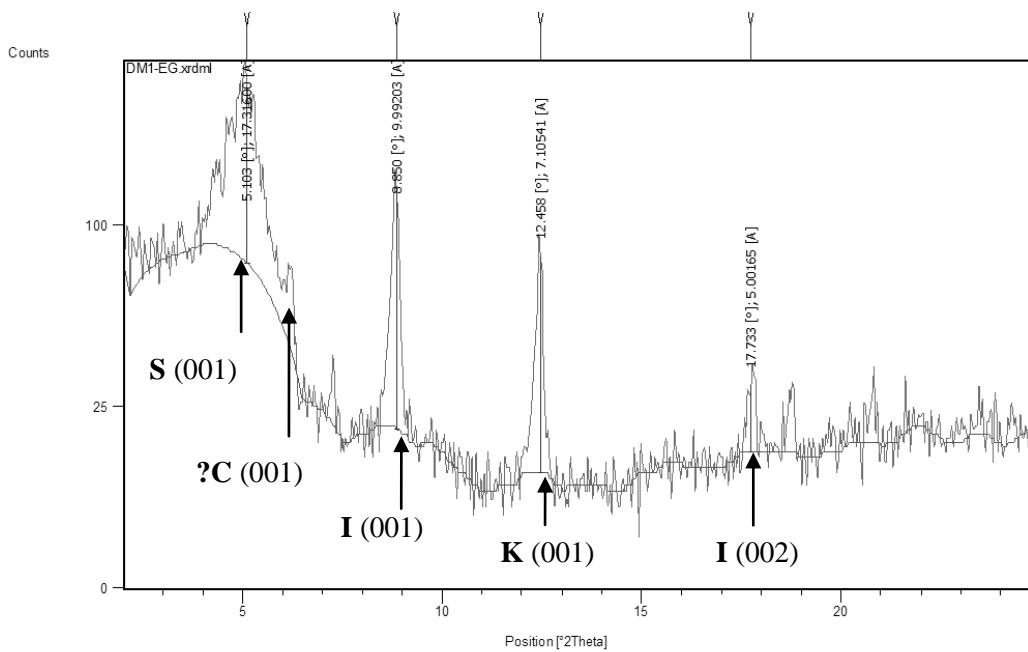


Figure 3.13. Sample DM1 mudstone ethylene glycolated oriented mount XRD scan. S = smectite, C = chlorite, I = illite, K = kaolintie, 001 = primary peak, 002 = secondary peak.

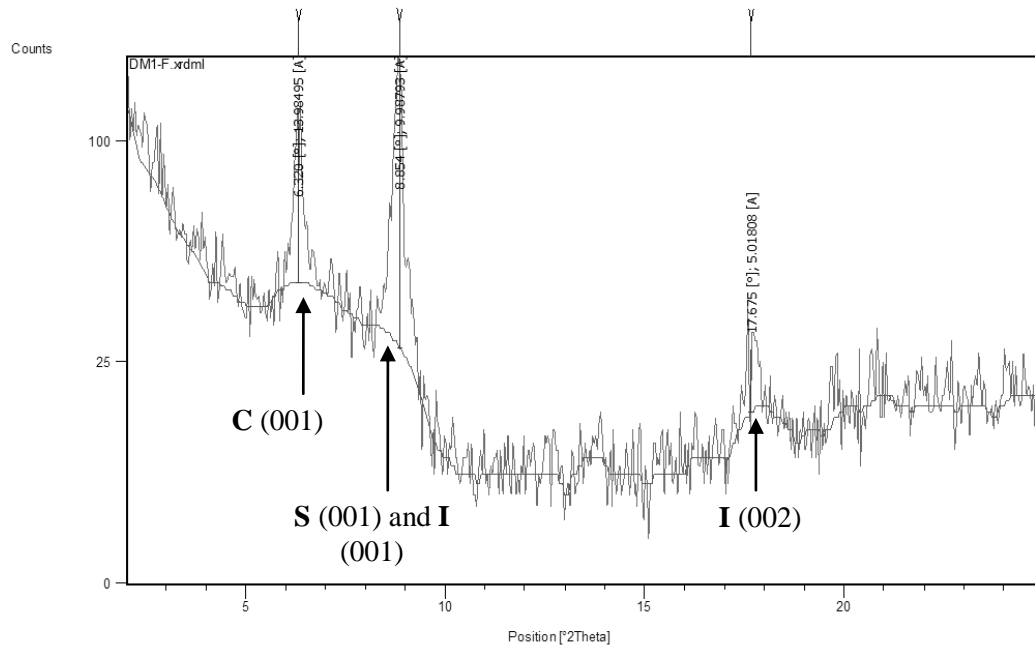


Figure 3.14. Sample DM1 mudstone heated to 550 °C oriented mount XRD scan. S = smectite, C = chlorite, I = illite, K = kaolintie, 001 = primary peak, 002 = secondary peak.

3.3.3 X-ray fluorescence (XRF)

The geochemistry of all samples was determined using the SPECTRO X-LAB 2000 XRF instrument at the University of Waikato. The pressed pellet method was used to yield bulk major and trace element compositions for all mudstone and concretion samples.

About 5 grams of powdered sample were weighed into a paper cup along with 10 drops of PVA binder and mixed together using a wooden spatula. The sample was then transferred into a pre-weighed aluminium holder and the holder placed onto a clean metal base that fitted into a cylinder which then allowed a plunger to be inserted for the purpose of pressing the holder containing the sample. The entire unit was then loaded into a hydraulic press and compressed to 90 pressure bars. The resultant pressed pellets were then dried in an oven at 70°C for two hours in order to evaporate the PVA binder, cooled, then weighed (with the weight of the aluminium holder tared) and the sample weight recorded. The pressed pellets were then ready to be analysed by the XRF machine.

3.3.3.1 Results

XRF major and trace element results for all samples are shown in Appendix 4. The XRF results for mudstone samples were averaged and are displayed in Figure 3.15. The chemical composition of the samples is a direct reflection of their mineralogical composition. Figure 3.15 shows that on average just over 60% of the mudstone is composed of SiO_2 , and along with the relatively high content of Al_2O_3 (15%), reflects the abundance of quartz, feldspar and clay minerals in the mudstones. Fe_2O_3 at an abundance of 5.2 % (which is total Fe and includes FeO) is supplied by iron oxide minerals, including smectite clay. K_2O , Na_2O and MgO content, all in relatively small amounts, relate again to the abundance of clay minerals, while some Mg is also tied to the carbonate mineral calcite. The CaO content also reflects the presence of calcite, there being no dolomite present in the mudstones (Figure 3.8).

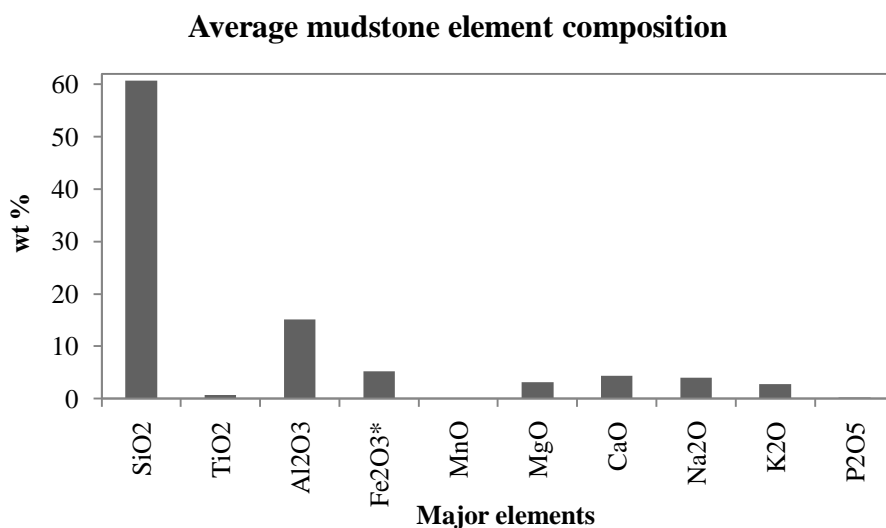


Figure 3.15. The average mudstone major element composition derived from XRF analysis of the three mudstone samples.

The major element compositions of the concretions are shown in Figures 3.16 and 3.17. The CaO contents are higher in the concretion samples, reflecting their high carbonate content (Table 3.2). The high MgO values in the concretion samples can be related to the presence of high Mg calcite and/or dolomite (Figures 3.9 and 3.10).

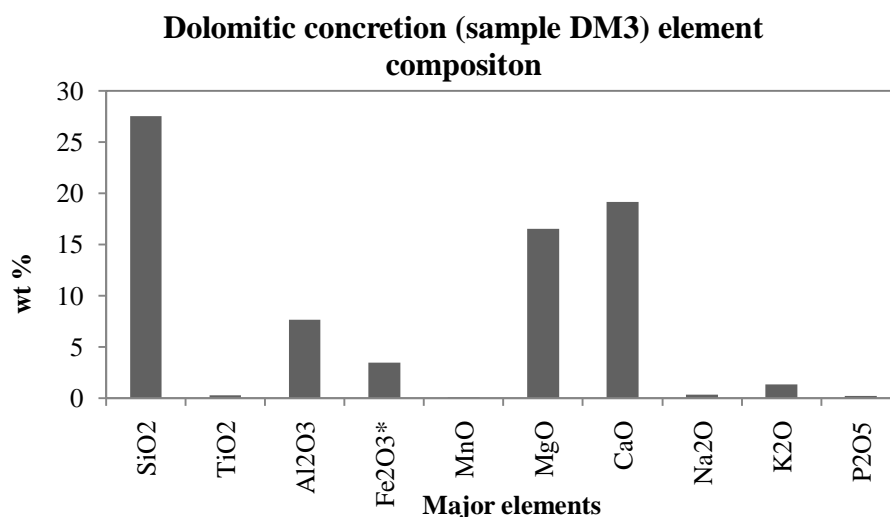


Figure 3.16. The element composition of dolomitic concretion derived from XRF results.

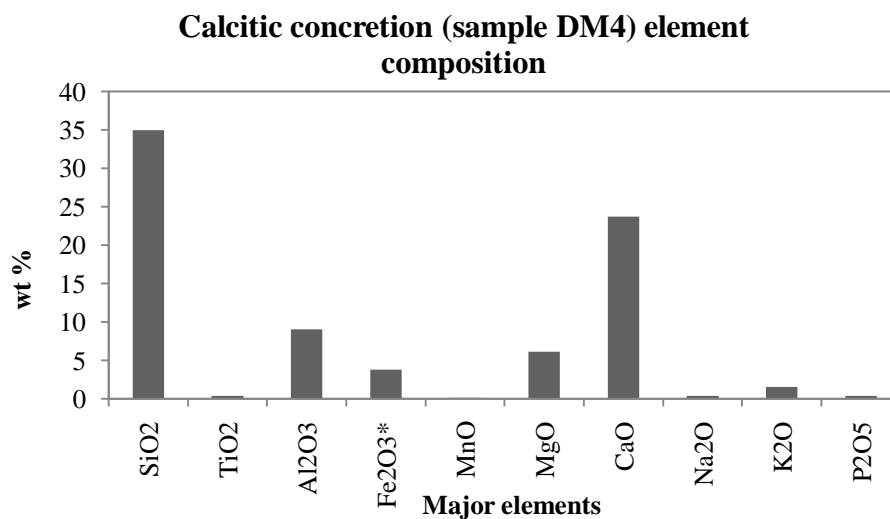


Figure 3.17. The element composition of calcitic concretion derived from XRF results.

Trace elements in the mudstones are dominated by S and Cl, with relatively common Sr, Ba, Zr and Rb. Those in the concretions are not notably different apart from their lower S and higher Cl contents (Figure 3.18).

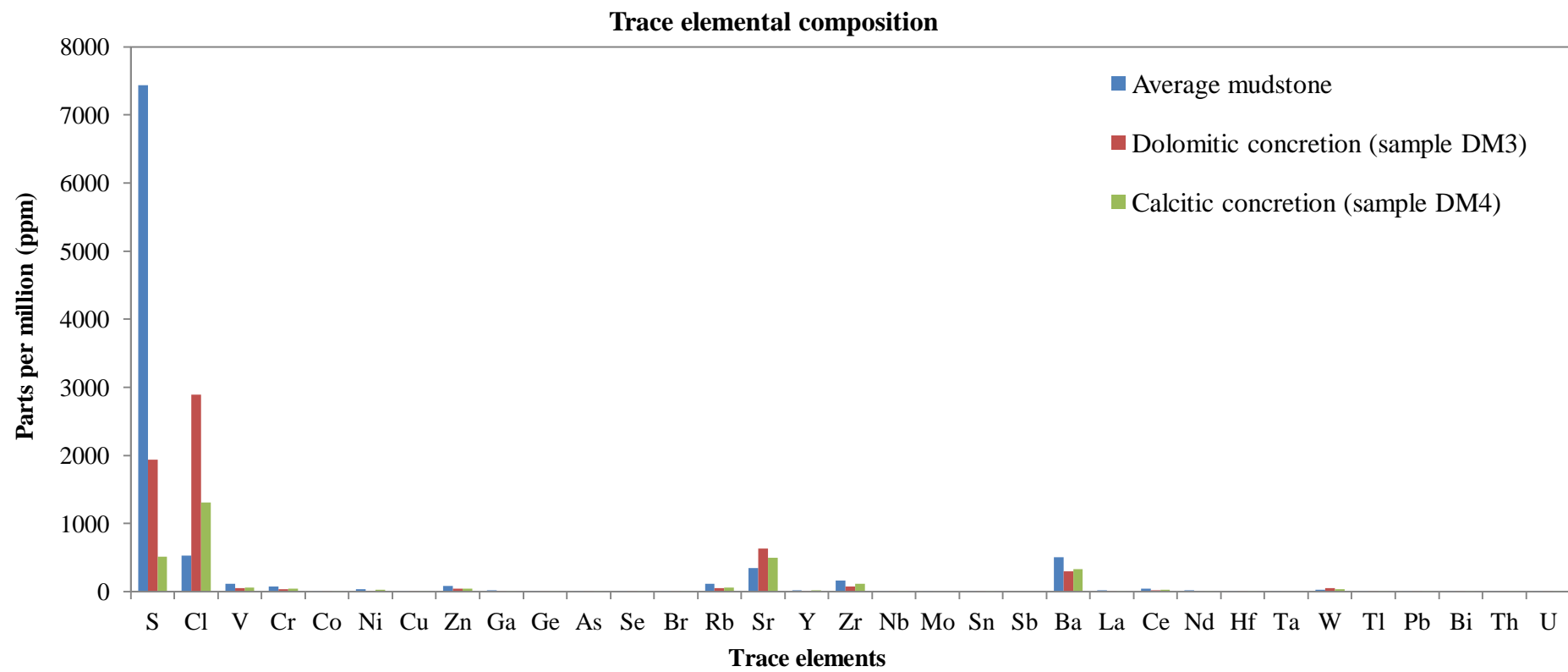


Figure 3.18. Trace element composition of the average Mapiri Formation mudstone, the dolomitic concretion and calcitic concretion.

3.3.4 Grain size analysis

Determining grain size characteristics of the mudstone and concretion units may allow for a more refined understanding of their depositional mechanisms and for a more precise lithological description.

Rock samples were gently crushed into small chips (they were not powdered as this would modify the original size of the grains). The carbonate cement was removed by adding 10 ml of HCl, gently swirling, then allowing the reaction to complete (or until effervescence had ceased). Samples were then put on a hotplate at 60°C to increase reaction time and to ensure any dolomite would be dissolved. This process was repeated twice more to ensure all carbonate was removed. During the process, a glass rod stirrer was used to gently prod the rock chips to aid in their chemical disaggregation. After acidification, de-ionised water was added along with 5 drops of Calgon to further disperse the individual grains in the sample. The result was a murky sediment suspension, of which about 5 to 10 drops were used for analysis in a Malvern laser sizer instrument in the Earth and Ocean Sciences Department at the University of Waikato.

3.3.4.1 Results

Raw data received from Malvern laser sizer software were entered into GRADISTAT (Version 4.0) grain size distribution and statistics package (Blott & Pye, 2001) for statistical analysis (Table 3.4). Parameters were derived from Folk & Ward (1957) equations and classifications (Appendix 5). Histograms showing the grain size distribution of insoluble material of all samples are shown in Figure 3.19. Figure 3.20 shows a ternary plot of the samples according to their sand-silt-clay content.

Table 3.4. Statistical parameters derived from GRADISTAT for the acid insoluble siliciclastic fraction of all samples based on the Folk & Ward (1957) method. *Sorting, skewness and kurtosis results for samples DM1 and DM7 are biased due to their bimodal size distribution. % sand, silt and clay derived from raw data from Malvern laser sizer.

		DM1	DM2	DM7	DM3	DM4
	SAMPLE TYPE	Bimodal, very poorly sorted	Unimodal, poorly sorted	Bimodal, very poorly sorted	Unimodal, poorly sorted	Unimodal, very poorly sorted
	SEDIMENT NAME	Medium sandy coarse silt	Very fine sandy very coarse silt	Medium sandy coarse silt	Very fine sandy coarse silt	Very fine sandy coarse silt
FOLK AND WARD METHOD (µm)	MEAN	45.85	31.57	51.63	19.68	13.78
	SORTING	5.778*	3.556	6.082*	3.604	4
	SKEWNESS	-0.006*	-0.25	-0.0238*	-0.155	-0.215
	KURTOSIS	0.83*	1.138	0.848*	1.137	1.052
FOLK AND WARD METHOD (Description)	MEAN	Very coarse silt	Very coarse silt	Very coarse silt	Coarse silt	Medium silt
	SORTING	Very poorly sorted*	Poorly sorted	Very poorly sorted*	Poorly sorted	Very poorly sorted
	SKEWNESS	Symmetrical*	Fine skewed	Symmetrical*	Fine skewed	Fine skewed
	KURTOSIS	Platykurtic*	Leptokurtic	Platykurtic*	Leptokurtic	Mesokurtic
MODE 1 (µm):		23.30	48.50	34.00	23.30	23.30
MODE 2 (µm):		325.0	-	325.0	-	-
% VERY FINE SAND		9.88	17.48	10.37	9.10	4.13
% FINE SAND		13.73	6.21	13.37	2.19	1.36
% MEDIUM SAND		13.18	0.86	12.99	0.44	1.86
% COARSE SAND		2.98	0.00	6.20	1.04	0.55
% TOTAL SAND		39.77	24.55	42.92	12.77	7.89
% SILT		44.00	60.94	41.71	66.45	62.14
% CLAY		16.22	14.50	15.38	20.78	29.97

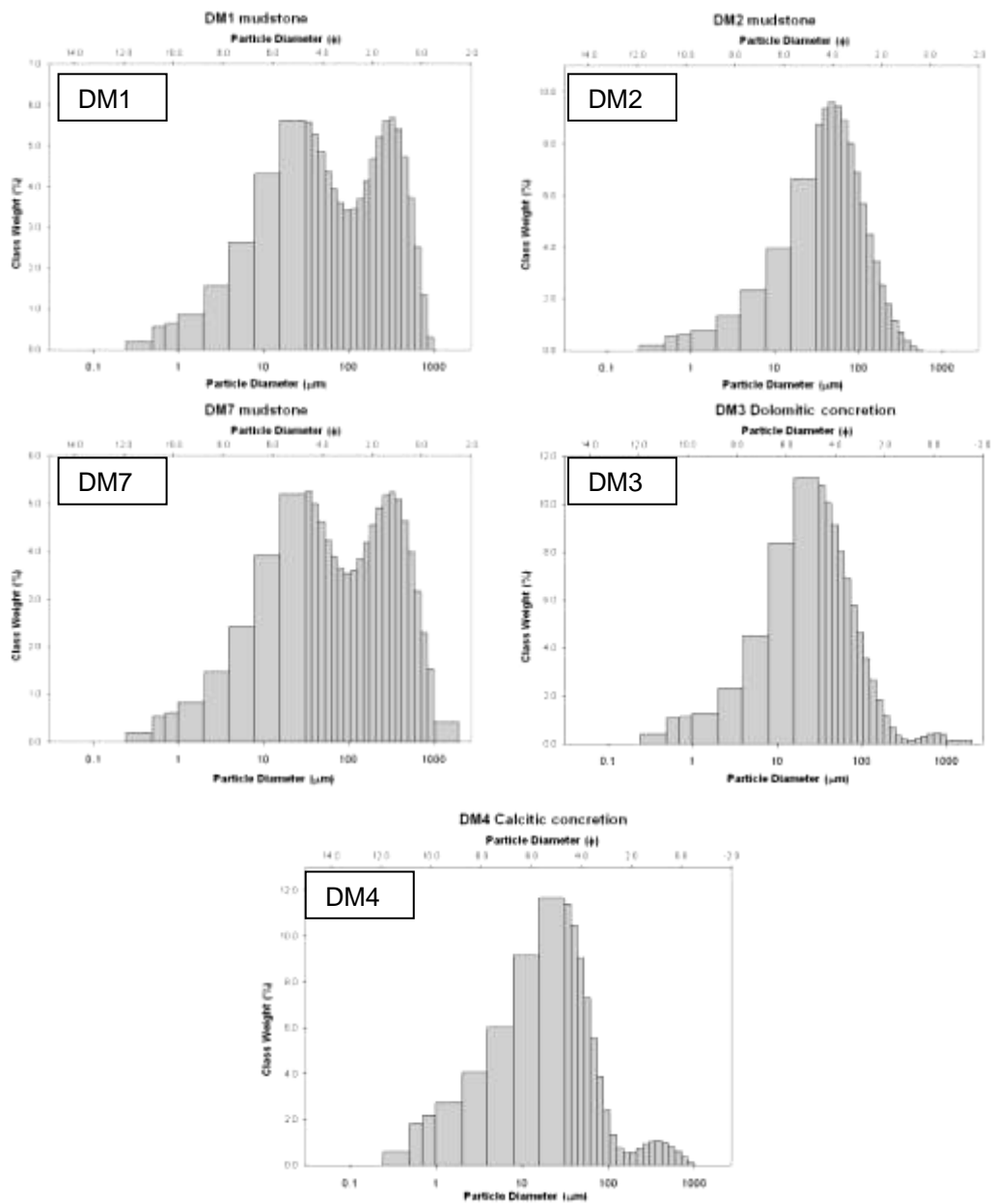


Figure 3.19. Histograms derived from GRADISTAT showing siliciclastic grain size distribution in all samples. Note the bimodality of samples DM1 and DM7.

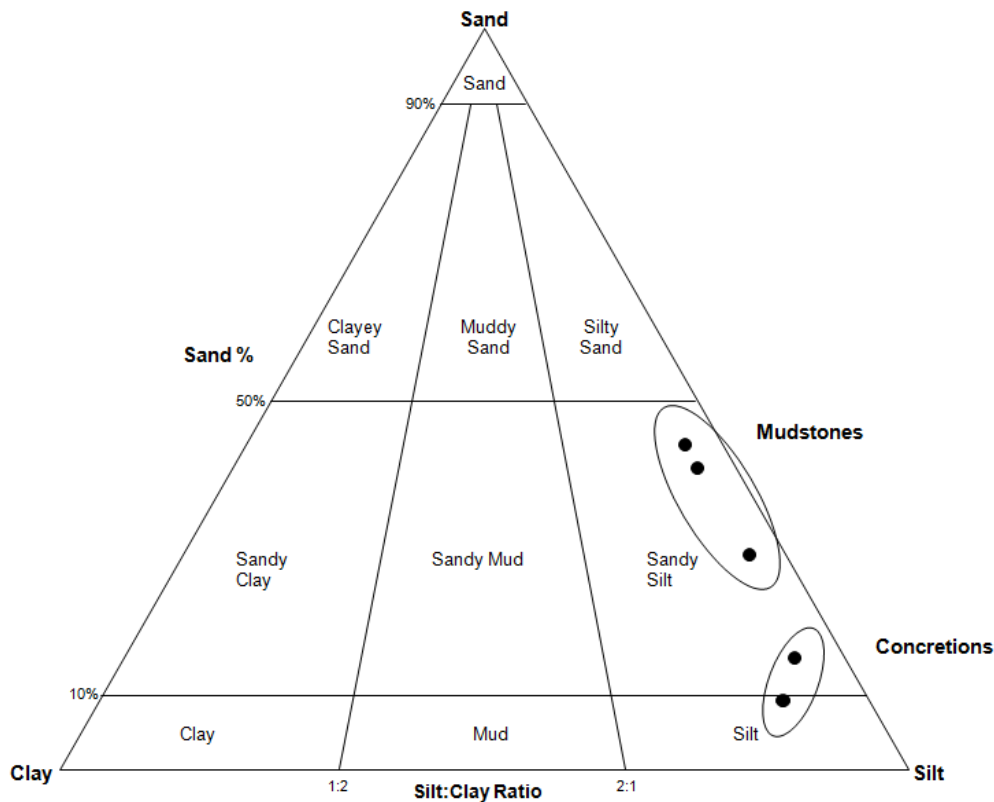


Figure 3.20. Ternary diagram showing all samples plotted according to their sand-silt-clay content (derived from GRADISTAT, based on Folk (1954)).

Grain size analysis demonstrates the mudstone samples are mostly composed of silt (44-61%), lesser sand (25-43%), and about 14-16% of clay sizes (Table 3.4), resulting in an overall classification of sandy silt (Figure 3.20). Sample DM2 is unimodal with the primary mode at about 48 μm (very coarse silt, Table 3.4). DM1 and DM7 mudstone samples show bimodal size distributions (Figure 3.19), with a primary mode of about 23 μm (coarse silt) and 34 μm (very coarse silt) respectively, and a secondary mode at 325 μm (medium sand). Bimodality in these mudstone samples could be indicative of more than one sediment source, or it could be that the rocks were insufficiently disaggregated before being analysed by the laser sizer. If the latter is the case, then the true grain size of the mudstones may be more accurately represented by the grain size composition of the concretions. The concretions have a higher clay percentage (20-30%), a higher silt content (62-67%), and only 7-13% sand (Table 3.4) in comparison to the mudstone. Both are unimodal, with size modes near 23 μm (coarse silt).

3.4 DISCUSSION

The field and laboratory analysis of the Mapiri Formation mudstone enables several conclusions to be drawn, which are discussed here.

Weathering

The spheroidal weathering process observed in the field, where breaking along complex joints liberates mudstone clasts which have crude spheroidal shape (Figure 3.21), is indeed facilitated the by presence of abundant swelling (and contracting) smectite clay minerals, as established by XRD clay mineralogical analysis.



Figure 3.21. Spheroidal weathering occurring within a boulder of mudstone. The boulder consists of many corestones, each one surrounded by concentric sheets or layers of weathering rock (examples outlined).

Exfoliation is a weathering term which encompasses spheroidal weathering. It is used when weathered boulders produce sheets of rock by a specific weathering process. Spheroidal weathering is used when corestones are present, and these corestones are surrounded by concentric layered shells, and the terms onion and concentric weathering are used as synonyms (Ollier, 1971). Spheroidal weathering is common in well jointed hard rocks, especially granite and basalt,

and less so in sandstone and other rocks (Ollier, 1971), but occasionally has been observed in mudstones. Spheroidal weathering has been observed in the Yager, Eel River and Rio Dell formations in the Eel River Valley area of California, and is observed in the massive, dark grey siltstone and mudstone layers of variable thicknesses, which lie between mainly sandstone layers. The mudstone in the Yager and Eel River formations are indurated, 'tough' massive mudstones, whereas the Rio Dell mudstone is generally softer and an intricate system of cross-fracturing and spheroidal weathering is commonly observed (Olge, 1953). The Mapiri mudstone may exhibit similarities with the Rio Dell mudstone, as both are soft, jointed rocks.

After spheroidal weathering releases clasts, or the corestones, they reach the water edge and develop into even smoother spheroidal shaped pebbles due to wave abrasion (Figure 3.21).



Figure 3.22. Spheroidal shaped pebbles derived from jointed clasts in the landslide debris litter the beach zone.

Such highly rounded shapes of pebbles on a shoreline would usually be indicative of a long period of transport in fluvial systems, but in this case the pebbles have already inherited a good degree of rounding (sphericity) upon release from the

mudstone bedrock, and then continued to be abraded and shaped through wave induced traction movement due to their relative "softness" (Figure 3.22). Fine sized particles are thought to be released during the spheroidal weathering process which upon entering the marine environment are at the mercy of the wave and current forces - the topic of Chapter 5.

XRD results indicate the average Mapiri mudstone is composed of abundant quartz, some to common plagioclase, some low-Mg calcite, and abundant clay minerals, the last of which consists of abundant illite and smectite, some kaolinite and rare chlorite. Carbonate analysis showed the mudstone contains between 7-12% (average of about 9%) carbonate. XRD results indicate this carbonate in the mudstones consists primarily of low-Mg calcite. XRF chemical results directly relate to the mineral composition, with the average mudstone containing about 60% SiO₂ and 17% Al₂O₃ (related to quartz, feldspar and clay minerals). Small amounts of MgO and CaO are related to the low-Mg calcite. When the major element composition of the average Mapiri mudstone is compared to an average global mudstone (Figure 3.23), the Mapiri mudstone exhibits no major differences. Nevertheless, special characteristics of the Mapiri mudstone (e.g. its swelling smectite clay, weak and jointed nature) and exposure to rapid subaerial erosion in the coastal cliffs have led to some very impressive slope failures - the topic of Chapter 4.

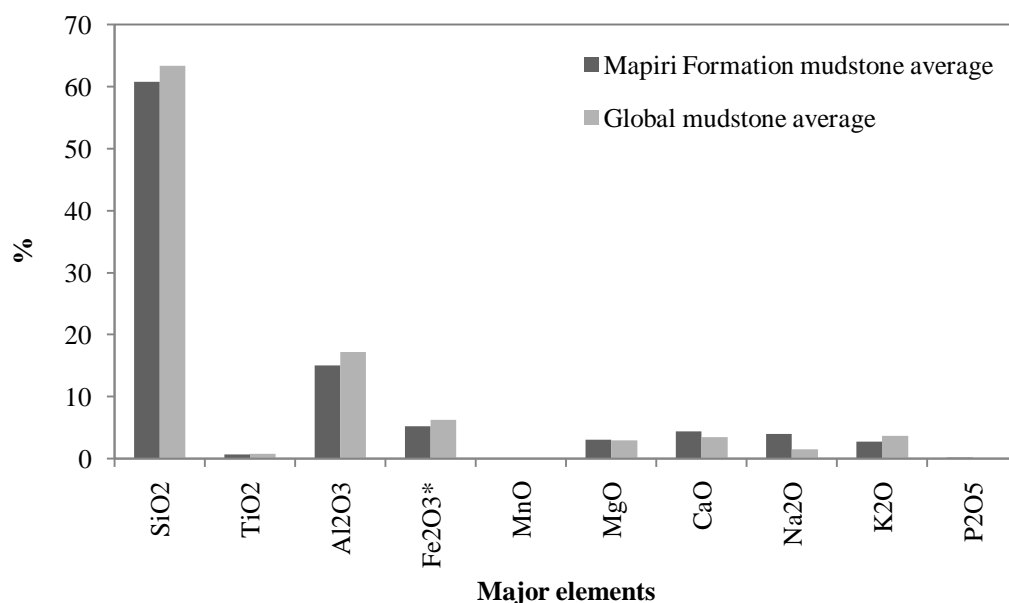


Figure 3.23. Major element composition comparison of the average Mapiri Formation mudstone with the global mudstone average derived from Boggs (2006).

Provenance

There are several factors impacting on and determining the composition of mudstones in general, which include tectonic setting, sediment source, depositional environment, grain size and diagenesis (Boggs, 2006). It is also important to note that mudstones form under environmental conditions in which fine sediment is abundant and water forces are small enough to allow fine sediment to settle out of suspension. They are characteristic of marine environments where the seafloor is deep enough to be out of the influence of waves and strong ocean currents (Boggs, 2006).

Clay minerals, along with quartz and feldspars are characteristic components of mudstones, and are mainly detrital, although siliciclastic minerals may also form or be altered into another mineral type during different stages of diagenesis. Commonly, clay minerals are derived as a weathering product of pre-existing rocks which contain feldspars. The Mapiri mudstone was likely deposited in a bathyal slope basin environment, and its siliciclastic material derived from erosion of older mudstones from the Paleogene to Neogene, and possibly even Cretaceous basement rocks. Some of these rocks have high abundance of clay minerals (e.g. the Wanstead Formation (Figure 2.7) contains smectite which is known to create slope instability and erosion in this formation), which are thought to have been released through erosion then transported into a bathyal slope environment, possibly into a slope basin formed as a result of thrust faulting during compression along the Hikurangi Margin. The presence of smectite is an important feature of this mudstone because of its ability to expand and contract, allowing the indurated mudstone to become weak through wetting and drying processes after subaerial exposure. The high abundance of illite is also noted. Illites, a common weathering product of feldspars, is often found in deeply buried muds in a temperate marine environment, formed by the transformation of smectite (and also from alteration of kaolinite) at temperatures ranging from 55 to 200°C (Li et al., 1997; Bjorlykke, 1998; Prothero & Schwab, 2003; Boggs, 2006).

Carbonate minerals form in mudstones during burial as cements, and the amount of carbonate formed relates to the amount of free pore space in the mud during burial diagenesis. As the degree of diagenesis increases, compaction due to pressure packs grains together tightly, decreasing the porosity. Carbonate in the

Mapiri mudstone, as derived from XRD analysis on the Mapiri concretions, is of both dolomitic and calcitic types, with contribution from calcitic microfossils.

Concretion formation

It is suspected, based on findings by Nyman et al., (2010), that tectonic setting has had the most important influence on the formation of concretions within the Mapiri mudstone. Nyman et al., (2010) found tubular concretions in the host Whangaehu mudstone (equivalent in age to the Mapiri mudstone) along the coastline of Whangaehu Beach, just north of Cape Turnagain (Figure 1.1). These concretions developed as a result of a shallow sub-seafloor plumbing network of a Late Miocene cold seep system, where methane rich fluid migrated towards the surface, altering the geochemical composition of the surrounding mudstone as it travelled. Thrust faults parallel to the coastline likely provided the pathways for this fluid to travel. Fluid migration due to overpressured sediment at depth occurs today in the Hikurangi Margin (at about 3000 m depth; Barnes et al., 2010) due to compaction and compressional tectonics. Nyman et al., (2010) infer that the same forces resulting in fluid migration occurred in the Late Miocene, resulting in localised fluid migration through the Whangaehu mudstone. Since this plumbing system is seen on a regional scale, there is valid reason to believe that the concretions seen in the Mapiri Formation could have been influenced by, or formed directly due to, the same cold seep system. Similarities between the Mapiri and Whangaehu concretions including their moderately high carbonate contents involving dolomite and calcite, and the presence of central conduits (Figure 3.24), lend support to this possibility.



Figure 3.24. A Mapiri Formation tubular concretion exhibiting a central conduit which likely funnelled methane rich fluids upwards in a cold seep system in the Late Miocene.

Chapter 4

SLOPE FAILURES

4.1 INTRODUCTION

The aim of this chapter is to describe and classify the slope failures along the coastal hills adjacent to the Te Angiangi Marine Reserve. A brief outline of the regional landslide susceptibility and occurrence is provided, before describing the slope failures that occurred sometime between the 25th and 28th April 2011 within and inland from the marine reserve. Intrinsic instabilities within the Mapiri mudstone, including its jointed and weak nature, and external triggering factors acting on the hill sides of the study area are outlined, and the slope failures directly adjacent to the reserve are identified individually and classified into their general types of failure. Estimates of (1) the volume of sediment produced from the larger slips directly adjacent to the reserve, and (2) the area of bare ground generated in the marine reserve stream catchments, are attempted.

4.2 FIELD WORK

Field work involved observing and describing the slope failures while walking the length of the reserve. The failures were separated from each other as accurately as possible, described and photographed individually. This involved estimating the dimensions of each, recording such properties as the depth, length, and width of the main scarp at the crown, and the length and width of the accumulated debris at the toe (Figure 4.1), and describing any other features, such as the type of failure, the presence of vegetation, and the size, sorting and composition of clasts in the accumulated debris. After the initial descriptions were made approximate measurements were carried out on the larger landslides using several measuring tapes and handheld GPS units (except for depth, which was estimated visually due to the inability in most cases to access the landslide scars for measurements with a measuring tape). In some cases, a GPS unit (with settings configured to 'track') was used to trace and measure the length of the main head scarp at the head of the landslide. The GPS continuously made waypoints as it was carried by a walker around the perimeter of the landslide. This was only done where it was safe to

walk on the hill side, and was therefore not used for tracing the larger areas of failure. In other cases, a walker measured various dimensions of the larger landslides (if safely accessible) using a measuring tape, while also using a GPS to mark occasional points in the landslide geometry. GPS points and tracks were downloaded from the handset into Google Earth. Google Earth allowed quick and easy viewing of the geographic distribution of landslides and could be used to make approximate measurements between points.

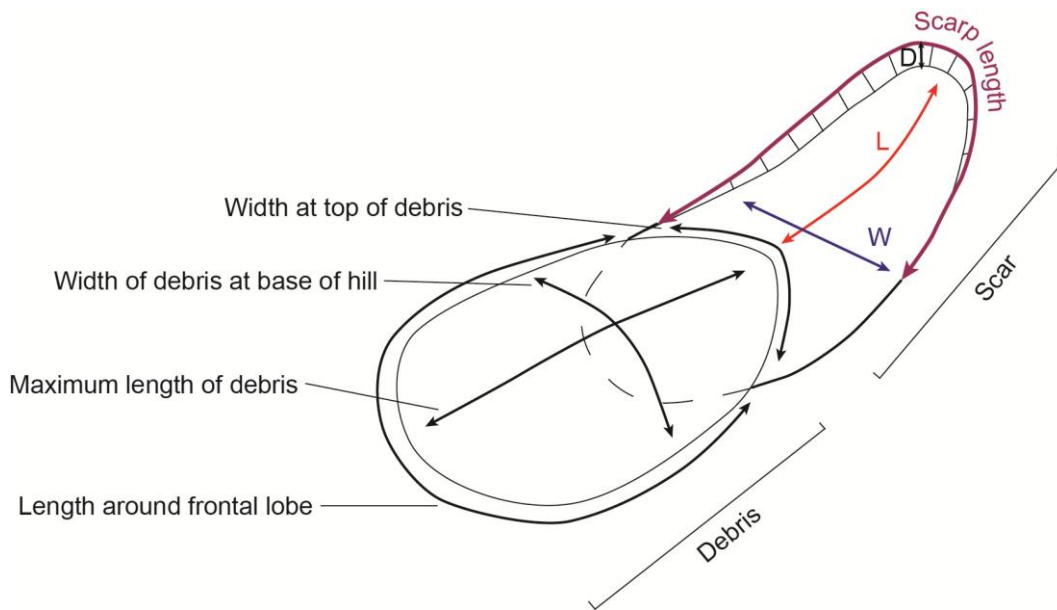


Figure 4.1. Schematic of a landslide showing the aspects that were measured, if possible, during field work (modified from Selby, 1993).

4.3 REGIONAL LANDSLIDE SUSCEPTIBILITY

The east coast of the North Island is well known for its landslide susceptibility (Selby, 1970; Gibb, 1978; Pettinga, 1980; Gibb 1981; Pettinga, 1987a, 1987b, 2004; Lacoste et al., 2009, Lee et al., 2011). All kinds of slope failures are common along this coastline and in the East Cape, and are seen particularly during seasonal rainfall and after storm events (e.g. Cyclone Giselle in 1968 and Cyclone Bola in 1988; Lacoste et al., 2009). For example, Gibb (1981) examined the Waiapu County coastline north of the Te Aniangi Marine Reserve (East Cape, North Island, Figure 1.1) using aerial photography in order to identify and quantify coastal hazard zones. Coastal landslides were recognised as prominent reoccurring features along this coastline, with large landslides occurring mostly in Late Cretaceous to Early Miocene rocks and smaller ones in Late Miocene deposits (equivalent in age to the Mapiri Formation at the Te Aniangi Marine

Reserve). The lithology of these rocks is mostly sandstone, siltstone and conglomerate. It was found for the Late Cretaceous to Early Miocene deposits in particular that once they were disturbed by gravitational sliding there was a change in their behaviour and they began to act like a soil and became prone to continual landsliding, aided by lubrication from interbedded bentonite deposits. The Mapiri Formation bounding the marine reserve likely exhibits similar landsliding characteristics, examined in a later section.

Large and complex areas of landsliding located slightly north of the marine reserve have been studied by Pettinga (1980, 1987a, 1987b), including the Waipoapoa and Ponui landslides, and the Waimarama-Kairakau Regional Slump (Pettinga, 2004), the latter also investigated by Crozier et al. (1992) (Figure 4.2).

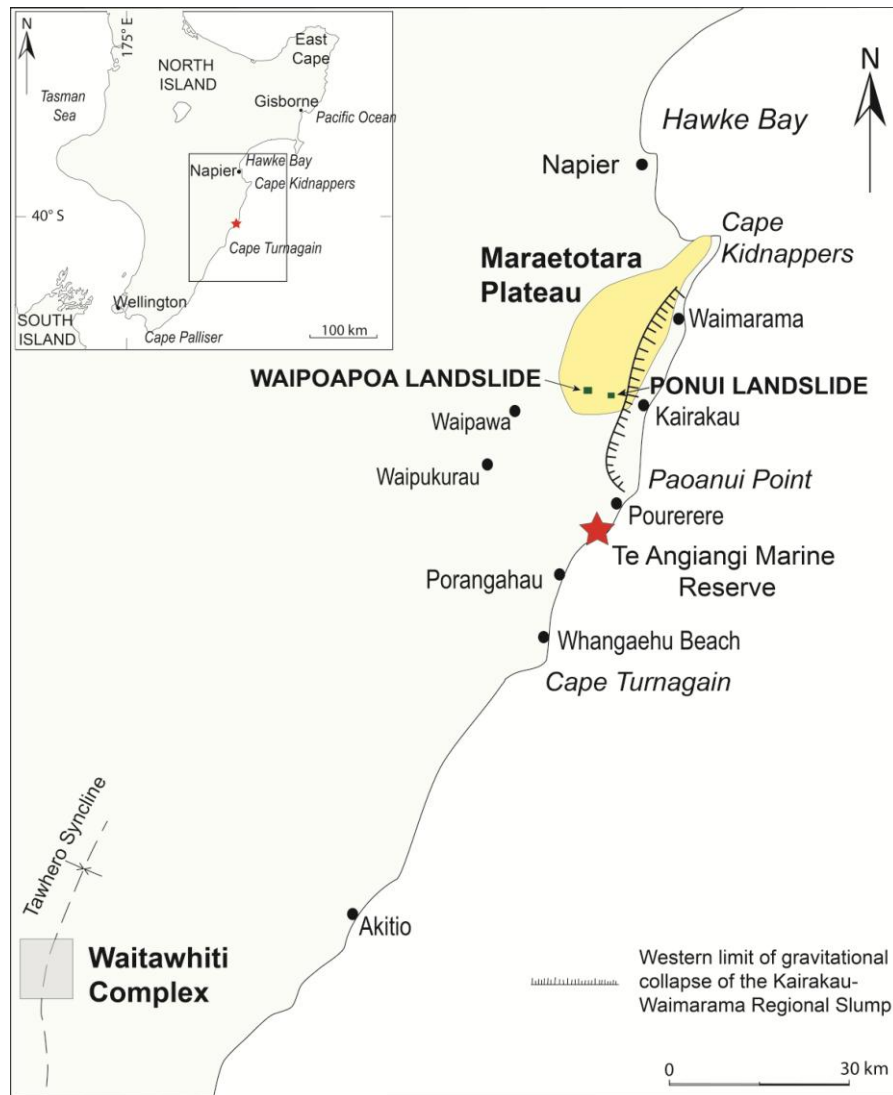


Figure 4.2. Approximate locations of the Waipoapoa and Ponui landslides, the Waitawhiti Complex, and the approximate western limit of gravitational collapse of the Kairakau-Waimarama Regional Slump (modified from Pettinga, 2004 and Lacoste et al., 2009).

The deep-seated Waipoapoa and Ponui landslides were reactivated on separate occasions during rainfall events in 1976, and are complex failures in weak, Late Miocene flysch deposits located in the Maraetotara Plateau in southern Hawke's Bay (Figure 4.2). The Waimarama-Kairakau Regional Slump is a massive regional gravitational collapse, stretching along the coast from Waimarama to Paoanui Point, that occurs within Neogene accretionary slope basin deposits - mostly undifferentiated mudstones and alternating sandstone and mudstone successions (Pettinga, 2004; Figure 4.2). A complex landslide area, called the Waitawhiti landslide complex, located 50 km south of Cape Turnagain (Figure 4.2), was investigated by Lacoste et al. (2009). Their study described possible factors that triggered landsliding in this area, including river incision at the base of hills, rainfall, vegetation, earthquakes and tectonic activity, fluid overpressure, and lithology. The geology of the Waitawhiti complex is Late Miocene (Tongaporutuan) in age and consists of fine grained sandstones and massive jointed siltstones, having very similar characteristics to the Mapiri Formation at the marine reserve.

There are several reasons for the extensive and numerous slope failures on the hill sides of the Hawke's Bay region. In particular, the coastal ranges in southern Hawke's Bay from Waimarama to Cape Turnagain consist of rounded undulating hills composed of fine-grained Miocene or Cretaceous to Paleogene mudstones and sandstones, with slope angles at the coast ranging from about 20 - 40° (slope angles ranging from 15 - 25° are described as steep, angles ranging from 25 - 35° are very steep, and angles ranging from 35 - 55° are precipitous (Moon, 2010)). The coastal ranges are not only steep, which increases the gravitational forces already acting on the slopes, but they are also in a tectonically very active region that is presently subjected to high uplift rates, from 0.5 to 2.3 mm/y⁻¹ (Pettinga, 1987a, 1987b, 1980; Lacoste et al., 2009). Associated earthquakes can contribute to landsliding by destabilising some slopes (Lacoste et al., 2009). Landsliding is also attributed to deforestation, which became a serious problem after European settlement about 170 years ago (Glade, 2003). Since then a considerable area of coastal land in Hawke's Bay has been converted to pastoral agriculture (Selby, 1970; Dymond et al., 2006; Lacoste et al., 2009). As a consequence, shallow regolith slides are common in the coastal ranges (Crozier et al., 1980) and generally result from intense rainfall and lack of vegetation cover (Lacoste et al.,

2009). In contrast, deep landsliding is more typically related to structural weaknesses in the bedrock lithology, and Neogene mudstones in the area are susceptible and succumb rapidly under weathering processes (Kennedy & Dickson, 2007).

4.4 TE ANGIANGI MARINE RESERVE LANDSLIDES

4.4.1 Triggers

In April of 2011 the east coast of the North Island was affected by a severe cyclonic storm, resulting in significant damage to buildings and farm land primarily due to landsliding (NIWA, 2011b). The storm affected a large section of the East Coast region, from Mahia in the north to Porangahau in the south, and included the area about 10 km inland from the coast (Jones et al., 2011). Heavy rain (up to 650 mm at the coast between Cape Kidnappers and Porangahau) fell from 25-28 April, with most falling on 26 April when 300 mm was recorded at Cape Turnagain (NIWA, 2011a), resulting in unusually wet soils for that time of year (NIWA, 2011b). Widespread shallow landsliding occurred within the affected area, and some pastoral farmers reported deeper-seated landslides than ever previously experienced (Jones et al., 2011). Intense rainfall during this storm is likely the main factor in triggering the extensive landsliding seen in the area, as the saturated soils led to an increase in pore-fluid pressure which in turn reduced the shear strength of the mudstone (Selby, 1993; Lacoste et al., 2009). A likely contributing factor in triggering the slope failures was the occurrence of a small earthquake Richter magnitude M4.5 on the evening of 26 April that was centred only 10 km offshore from Pourerere at a depth of 20 km (Jones et al., 2011). Typically the minimum magnitude for triggering landslides is suggested to be about M5, with significant landsliding occurring at M6 or greater (Jones et al., 2011). However, because of the highly saturated soil/rock conditions on the East Coast at the time of the earthquake, the lower magnitude may have been sufficient to trigger some landslides (Jones et al., 2011).

In the study area rather weak Miocene mudstone underlies the coastal hills, and landslides are common in these weakly cemented rocks (Lee et al., 2011). Although rock hardness was not directly measured in the Mapiri Formation mudstone, comparable Late Miocene to Early Pliocene mudstone at Cape

Turnagain near to the south yielded Schmidt hammer (both L and N type) rebound ('R') values of less than 10 in a study by Kennedy & Dickson (2007), which is below the detection level of the instruments but indicates that the mudstone is indeed very 'soft' or 'weak'. For example, Selby (1993) showed that even rebound values in the 10 to 35 range were characteristic of weathered and weakly compacted sedimentary rocks. Moreover, Gibb (1978) documented a maximum cliff retreat rate of 2.25 m/y^{-1} for mudstone cliffs at Cape Turnagain, one of the highest coastal cliff erosion rates at the time, supporting that these rocks are particularly susceptible to erosion, by both subaerial and marine processes.

The Mapiri mudstone includes a significant content of smectite clay minerals (see section 3.3.2 XRD clay mineral results), and it is also a highly jointed rock (Figure 3.2A). Jointed rocks are more susceptible to weathering because cracks provide access for water to enter which, in the presence of smectite minerals causes swelling of the rock and promotion of chemical decomposition. Swelling smectite minerals are particularly effective at adsorbing water and generally as more water becomes present the electrostatic forces between clay minerals and the surrounding water decreases, since more water separates the clay particles, resulting in weakening the overall rock cohesion (Selby, 1993). The jointed, smectite-rich nature of the mudstone means that it has inherent internal instabilities which combined with exposure to external triggering factors initiate slope failure. In the case of the Te Angiangi Marine Reserve area, the external triggering factor was the intense rainfall during the April 2011 storm, with a possible superimposed contribution from the small 'Pourerere' earthquake.

4.4.2 Type of slope failure

Slope failures are observed on hill sides in the vicinity of the Te Angiangi Marine Reserve, which between at least 2008 until the April 2011 storm showed little to no current active erosion (Figure 4.3A). However, there is certainly evidence of large landslides having occurred on these hill sides in the past, but in the lead up to April 2011 they supported reasonably continuous vegetation cover (Figure 4.3A).

Following April 2011 a total of 14 new individual slips, ranging from 1 to 4 m in depth, from 15 to 115 m in scar length and from 20 to 120 m in scar width, were identified within the marine reserve (Figure 4.3B and Figure 4.4). Large and relatively deep (~ 3 to 4 m) failures (possibly reactivated during the April 2011 storm) were also observed to the south outside the reserve (Figure 4.4), but no new significant failures were evident north of the reserve. Figures 4.6 and 4.7 show slips 1 to 9 and 10 to 14 respectively. They are numbered in order starting from slip 1 near Blackhead to slip 14 at Aramoana. The slips become larger (in width and length) and deeper with distance from Blackhead, presumably because the hills get progressively higher from south to north.

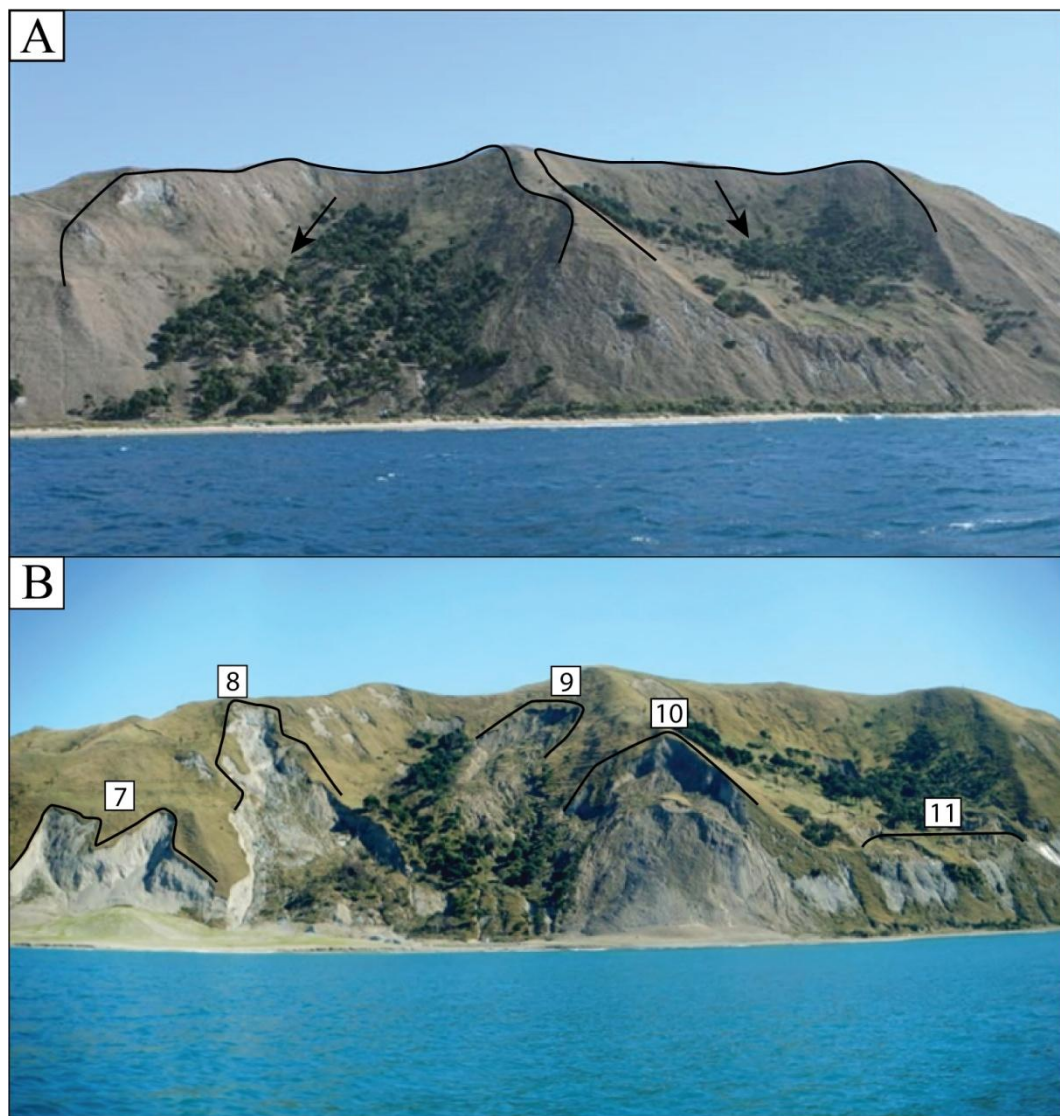


Figure 4.3. A - Some of the hill side within the reserve pre-April 2011 storm (photo taken in 2008). Outlined are obvious old landslide scarps. B - The same hill side post-April 2011 storm (photo taken in 2012). Main scarps of slips 7 to 11 are outlined. Slip 7 is in the southern part of the reserve and slips 9 to 10 are directly opposite Stingray Bay.

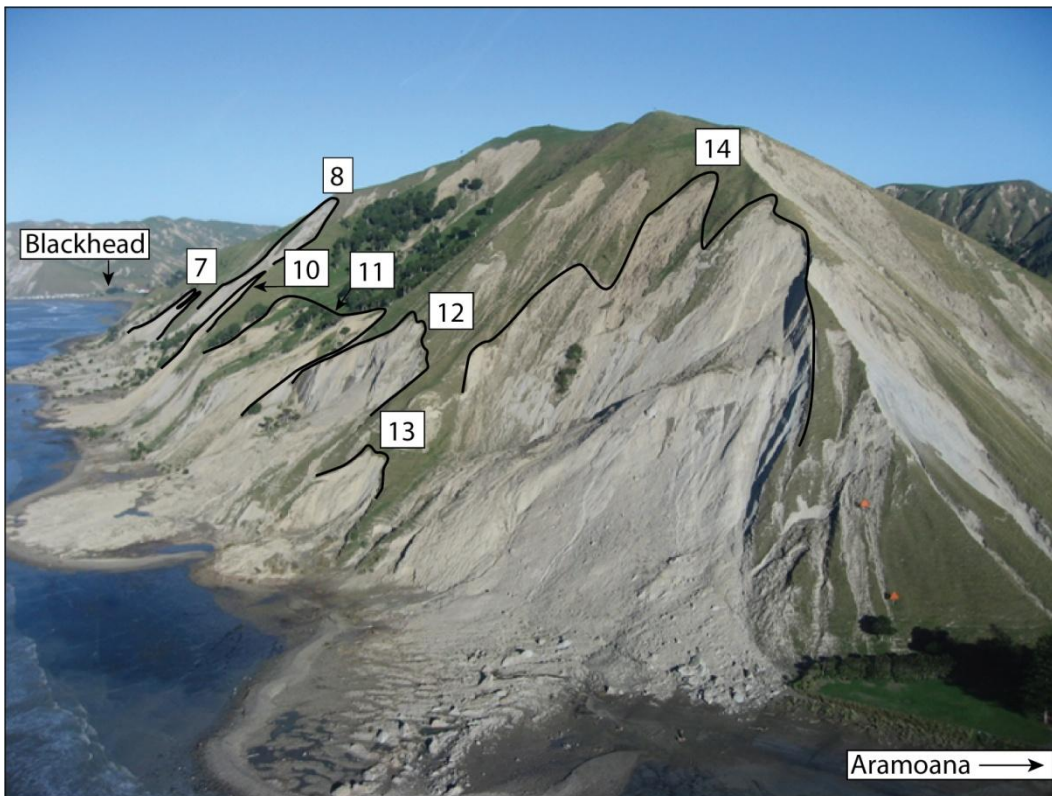


Figure 4.4. Landslides in the northern half of the reserve. Main scarps of slips 7 to 14 are outlined. View is looking south.



Figure 4.5. Slope failures on hills south outside the reserve.

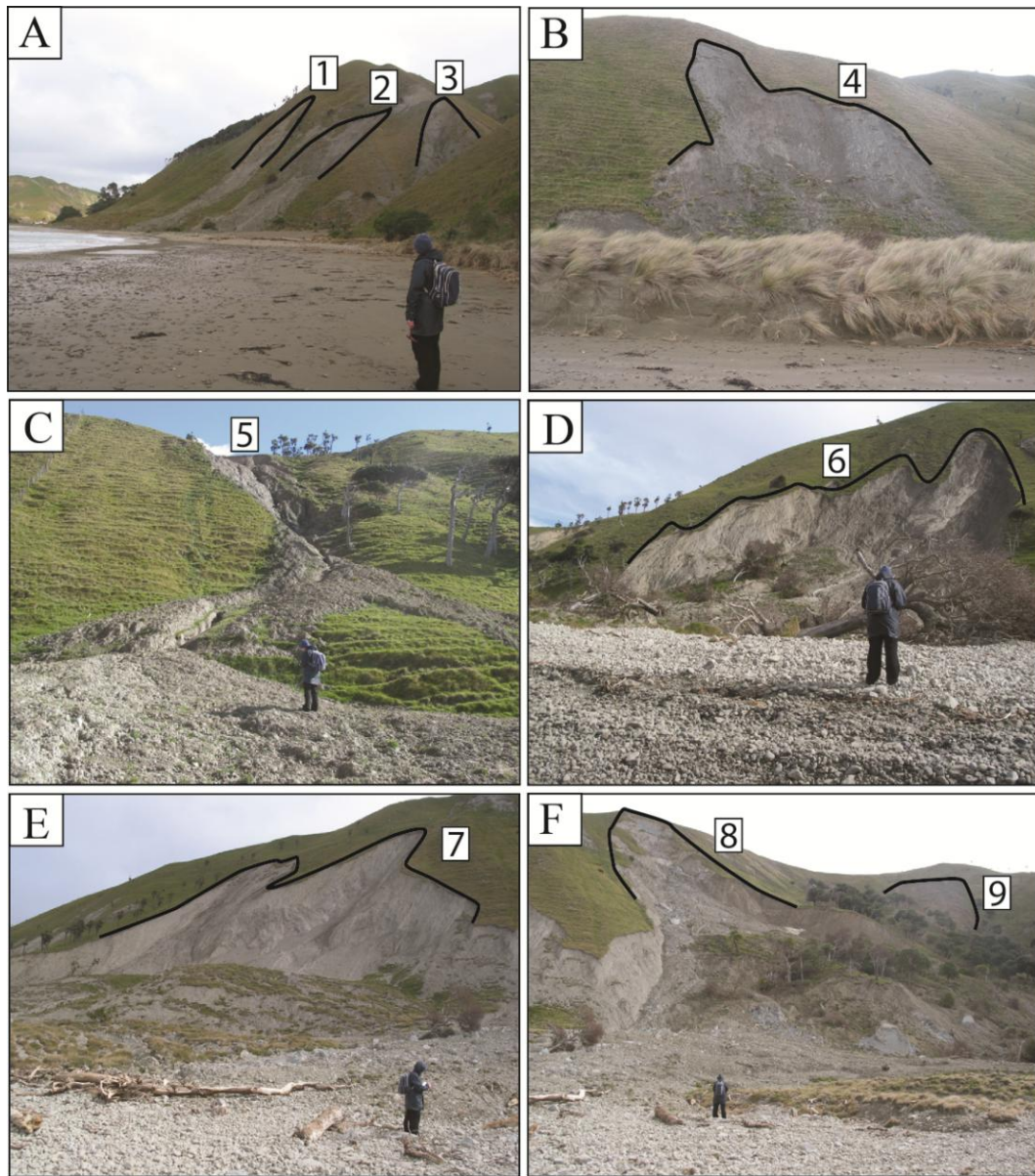


Figure 4.6. Main scarps of slips 1 to 9 are outlined. A - Slips 1 to 3 measure about 20 m in length along the scarps and are closest to Blackhead. Their estimated depths are ~1 m. B - Slip 4. The scarp length measures about 45 m, with an estimated depth of ~1 m. C - 'Slip' 5, which is characteristic of a debris flow, has an estimated depth of ~2 m. D - Slip 6. The scarp length measures about 156 and is the largest slip to occur heading north from Blackhead, with an estimated depth of ~4 m. E - Slip 7. The scarp length measures about 167 m, with an estimated depth of ~3m. F - Slips 8 and 9, both with estimated depths of ~3 m. The scarp length of slip 8 is about 400 m.

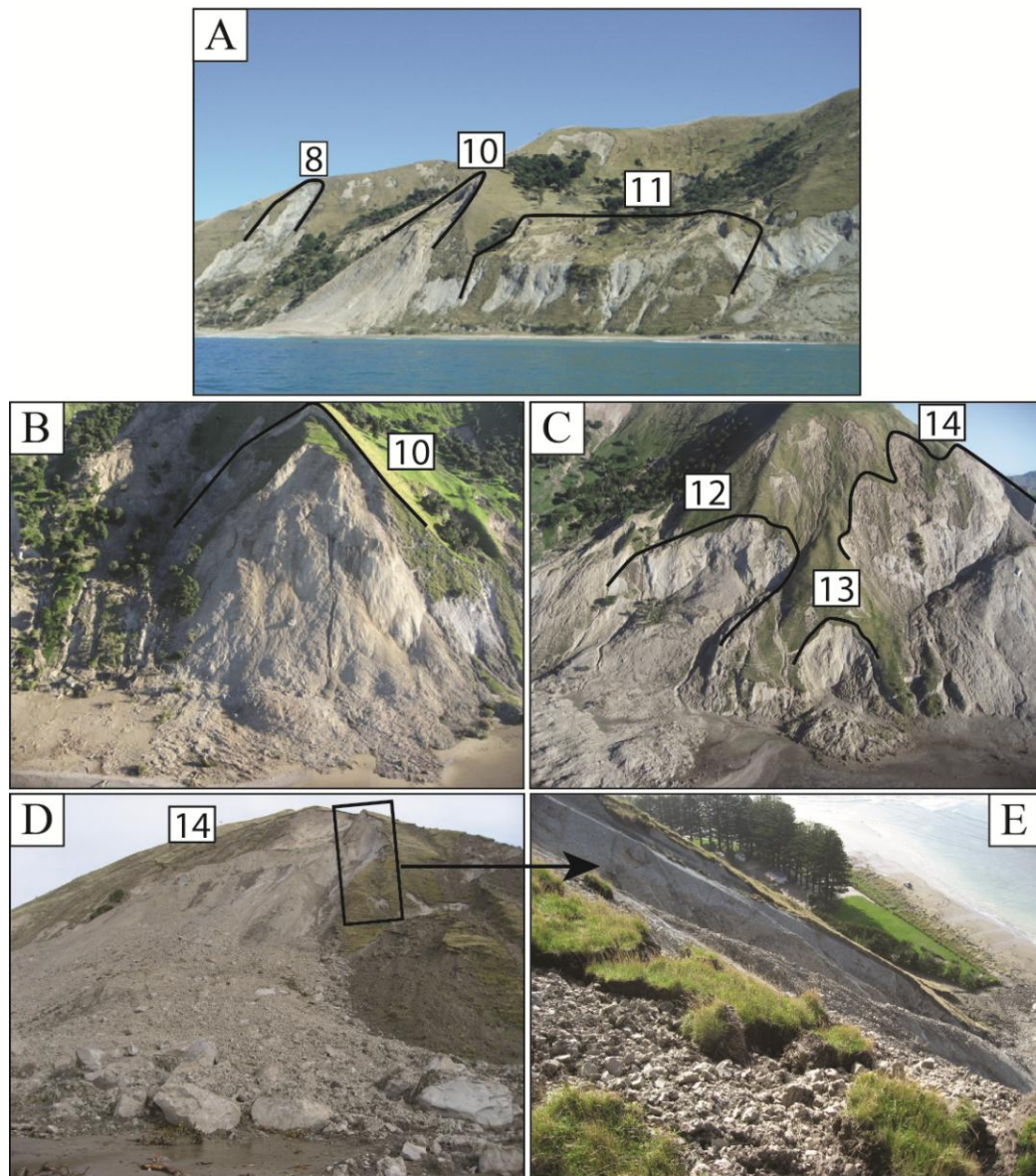


Figure 4.7. Main scarps of slips 10 to 14 are outlined. A - Slips 8, 10 and 11. 'Slip' 11 represents an area of multiple slope failures along ~ 200 m of hill side. B - Slip 10 has an estimated depth of ~3 m. C - Slips 12 (estimated depth of ~4 m), 13 (estimated depth of ~3 m) and 14 (refer to Figures 4.7 to 4.9 for some slip dimensions). D - Debris from slip 14. The black box outlines the location of E which shows the northern flank of slip 14 estimated at ~2 - 3 m deep.

Figures 4.8, 4.9 and 4.10 show the approximate dimensions of slips 12, 13 and 14 respectively.

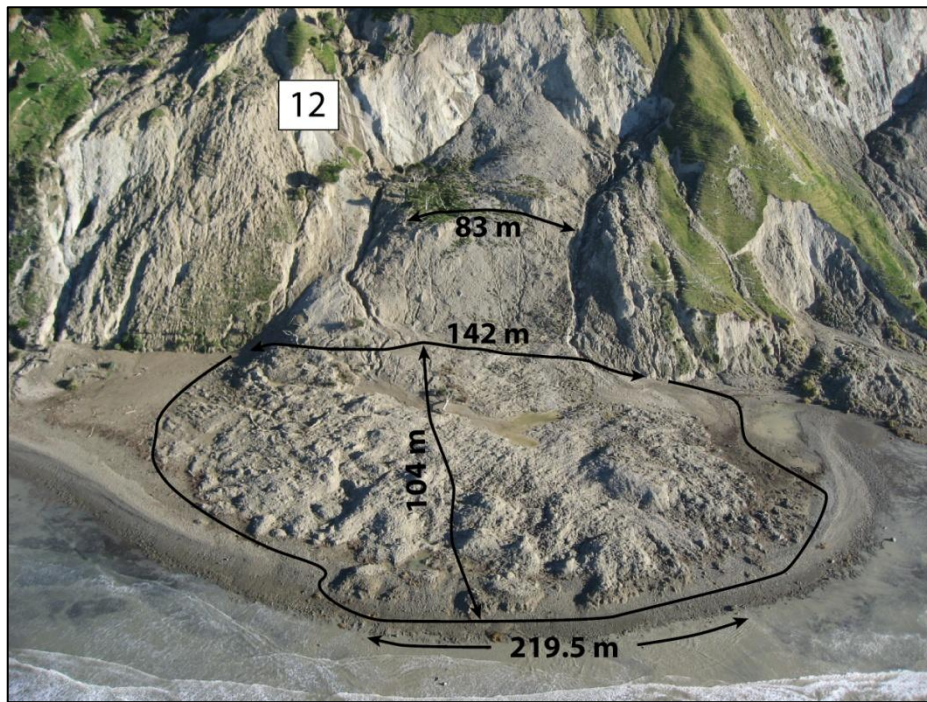


Figure 4.8. Debris measurements of slip 12, including the length around the debris frontal lobe, the maximum length (or extent) of the debris, and the width of the debris at the base of the hill. Also shown is the width near the top of the debris mass.

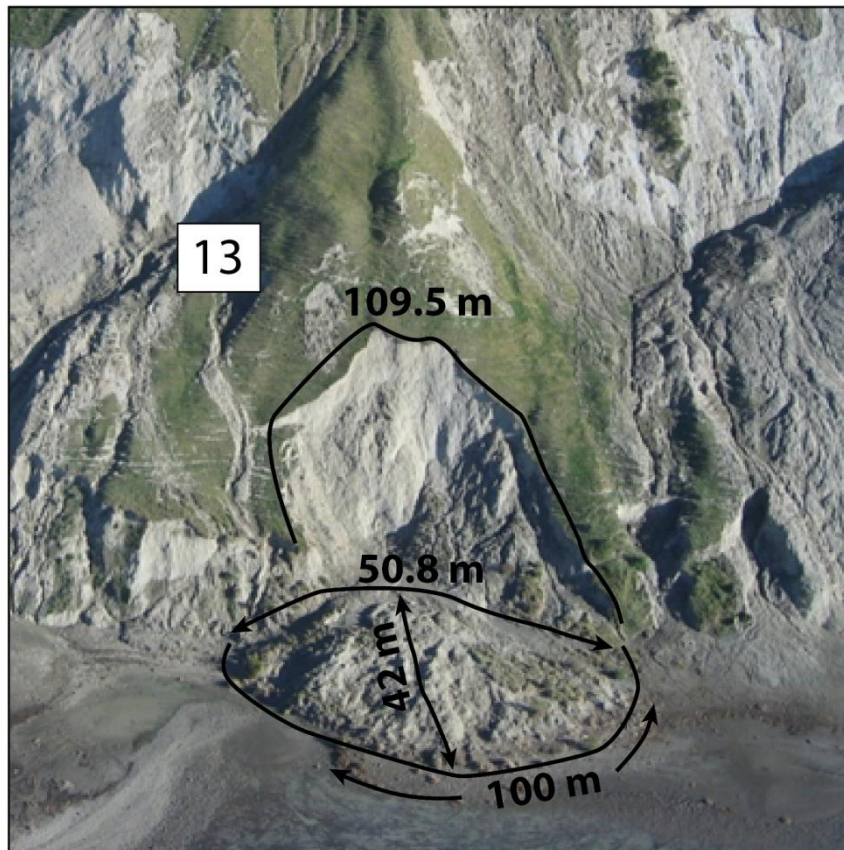


Figure 4.9. Debris and scarp measurements of slip 13, including the scarp length at the crown, the length around the debris frontal lobe, the maximum length (or extent) of the debris, and the width of the debris at the base of the hill.

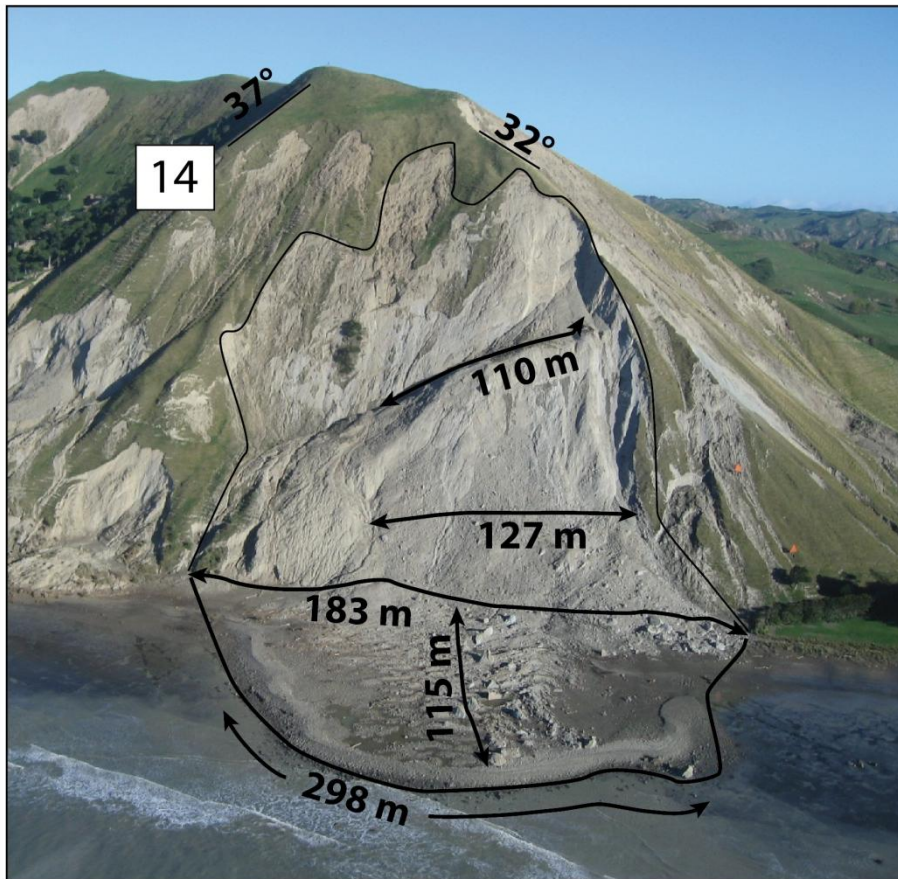


Figure 4.10. Debris measurements of slip 14, including the length around the debris frontal lobe, the maximum length (or extent) of the debris, and the width of the debris at the base of the hill. Also shown is the width near the bottom, and the width at the top, of the debris mass.

To make referring to Figures of the slips easier, Table 4.1 lists which Figures relate to each of the slips.

Table 4.1. Figures associated with each slip.

Slip	Figure	Slip	Figure
1	4.6A	8	4.3B, 4.4, 4.6F, 4.7A
2	4.6A	9	4.3B, 4.6F
3	4.6A	10	4.3B, 4.4, 4.7A, 4.7B
4	4.6B	11	4.3B, 4.4, 4.7A
5	4.6C	12	4.4, 4.7C, 4.8
6	4.6D	13	4.4, 4.7C, 4.9
7	4.3B, 4.4, 4.6E	14	4.4, 4.7C, 4.7D, 4.7E, 4.10

Translational slides are the most common form of landslide occurring in soils, and are likely the type of landsliding seen in these failures. Translational landslides are described as being shallow features (depth to the failure plane ranges from 1-4

m) that slide along a planar surface, with straight side flanks, and their length is usually greater than their depth. Additionally, translational slides tend to occur during heavy rainfall as the water table is raised to near the soil surface, by which stage any pre-existing surface cracks can also be filled with water. Water saturation allows pore pressure to rise substantially and weaken the soil strength, making the slope susceptible to failure (Selby, 1993). Following this explanation, along with the descriptions made in this section, and based on the Varnes (1978) classification of slope failures, it appears the majority of landslides adjacent to the reserve are characteristic of translational debris slides. Figures 4.3, 4.6 and 4.7 show the outlines of the main scarps of the slips, which generally show straight side flanks and greater lengths than depths. Slips 6, 7, 8, 9, 10, 12, 13 and 14, all with depths ranging from 2 to 4 m, are large debris slides, while slips 1, 2, 3, 4 and 11 are small to medium debris slides, with depths ranging from 1 to 2 m (see Table 4.1 for relating figures). Slip 5 is a debris flow. The more impressive failures (slips 7, 8, 9, 12 and 14) expose bedrock in the hill side and large boulders of bedrock are present in the accumulated debris. In most of these larger failures the debris appears to have been transported as a debris flow (e.g slip 12 and 14), as boulders of bedrock have been transported across the intertidal platform. Some other large failures have undeformed blocks of earth which have travelled down slope some distance (slip 10), while in others the debris consists of entire cabbage trees, clumps of grass, and a large size range of clasts (from boulder to pebble size - slips 6, 8, 9, 13). Generally the smaller and shallower failures have debris consisting of smaller sized and poorly sorted clasts made up of soil clumps and some bedrock (e.g. slip 5). The debris of the smallest failures consists of dislodged masses of soil and no clasts of bedrock (slips 1 to 4).

Based on Varnes (1978), further classification would deem most of the landslides as 'complex' failures as they generally appear to be a mix of translational debris sliding at the top and debris flow movement at the bottom, as characterised by the accumulated debris (as shown in slips 12 and 14 for example). Field observations and aerial photographs show evidence of flow lobes, coarse and poorly sorted sediment loads, and transported boulders of bedrock, which suggest that the saturated materials may have advanced by viscous flow following the initial sliding.

4.5 VOLUME AND AREA ESTIMATES

4.5.1 Volume estimate

A rough estimate of the volume of sediment produced from slips 1 to 14 was generated from measurements made using Google Earth (version 6.1.0.5001; Figure 4.11 and Table 4.2). This estimate is of some interest because these slips delivered sediment directly into the marine reserve environment during the April 2011 storm, and in some instances smothered the intertidal platform.

After GPS points were loaded into Google Earth, approximate measurements could be made between the points using the 'Path' tool (which has a measurement error of about 5%). A GPS track was created which traced the main scarp of slips 1 to 8, which then allowed approximate scar width and length measurements to be made. The positions of the main scarp of slips 9, 10, 12, 13 and 14 were estimated (tracks could not be made around these landslides for safety reasons) based on GPS points made in various positions about the debris geometry (Figure 4.11). The depth of each slip was estimated visually during field observations and in conjunction with later examination of aerial photography.

The volume estimates were produced by first calculating the area of the scar, by multiplying the maximum scar width by maximum scar length. Average measurements of the maximum length and width (at the base of the scar) of each scar from Google Earth was used. The area was then multiplied by the estimated depth of the scar to generate the volume estimates (Table 4.2).

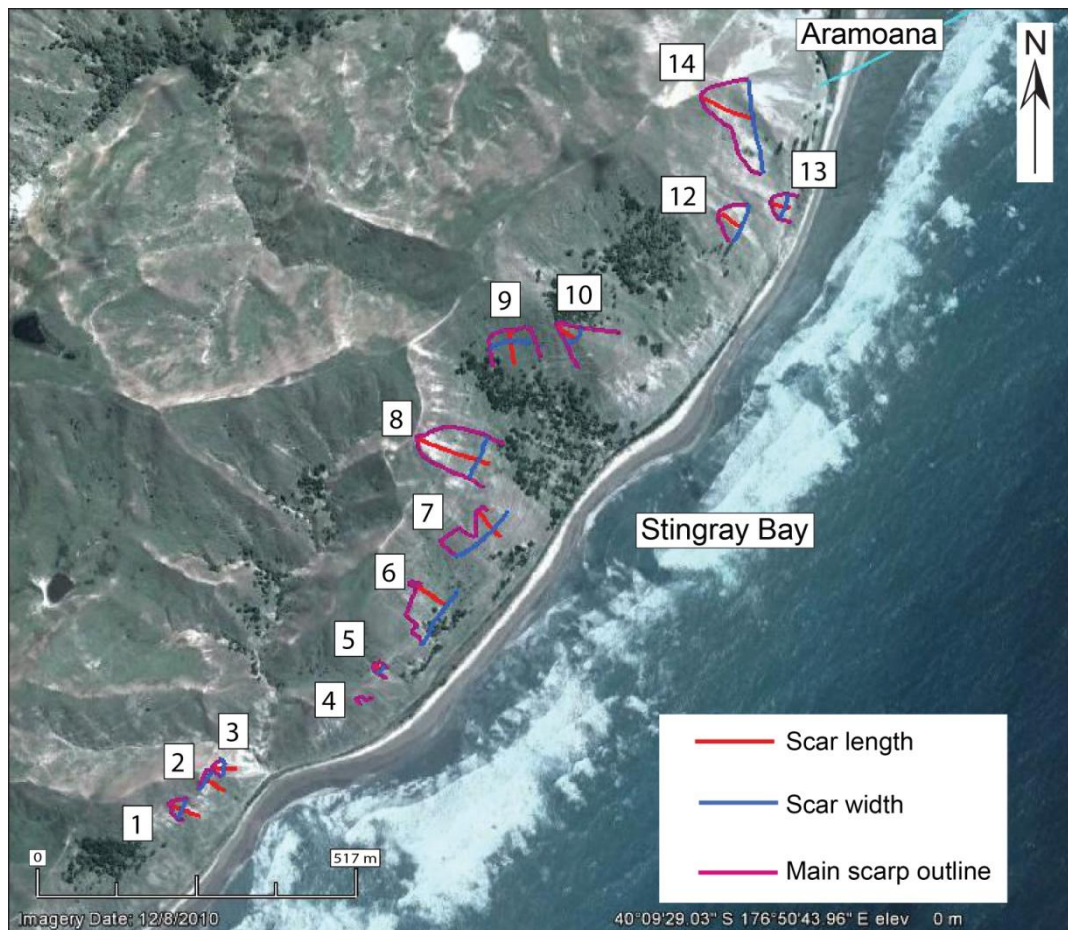


Figure 4.11. Google Earth image showing the distribution of landslides directly adjacent to the reserve. The main scarp of each landslide is outlined, along with the length and width of the landslide scars. These measurements were used to estimate an overall volume of sediment delivered into the reserve from these landslides.

Table 4.2. The estimated volume of sediment derived from each landslide (excluding slip 4 and 11). The total volume has an error estimate of $\pm 75.02 \text{ m}^3$.

Slip	Scar length (m)	Scar width (m)	Area (m^2)	Depth (m)	Volume (m^3)
1	50	38	1900	1	1900
2	41	32	1312	1	1312
3	42	31	1302	1	1302
5	15	20	300	2	600
6	64	115	7360	4	29440
7	56	120	6720	3	20160
8	115	66	7590	3	22770
9	70	60	4200	3	12600
10	36	38	1368	3	4104
12	40	70	2800	4	11200
13	35	40	1400	2	2800
14	90	155	13950	3	41850
Total:			50,202	Total:	150,038

Slip 4 was not included in the volume estimates in Table 4.2 because the debris from this slip did not reach the beach and was therefore out of influence of the marine environment. The area of hill side regarded as 'slip' 11 was also not included since the area was not accessible enough to allow GPS tracks or points to be made.

The analysis shows that about 150,000 m³ of sediment was produced from slope failures on the hill sides fronting the Te Angiangi Marine Reserve. The actual amount of sediment to enter the marine reserve as a result of landslides is likely to be much larger, because landslides are also locally present throughout the entire reserve catchment and are also abundant regionally.

4.5.2 Area estimates

Regional area estimate

Geological and Nuclear Science (GNS) were commissioned by the Hawke's Bay Regional Council to assess the proportion of land affected by landslides on a regional and individual farm basis along the Hawke's Bay coastal belt. They achieved this by processing, classifying and analysing satellite imagery from before and after the storm event by identifying the change in fresh bare ground in pre- and post-storm images. The study area included the 250 km stretch of coastline from Mahia to Porangahau and extended 10 km inland.

GNS acquired through the "All of Government" KiwiImage program a mosaic of pre-storm images taken over the period 2006-2010 (Figure 4.12). Post-storm images were acquired through the RapidEye system which is a constellation of five satellites that were able to image the Hawke's Bay area on 18-19 May 2011, shortly after the April 2011 storm (Figure 4.13). The images were then analysed by GNS using ENVI 4.8 and ArcGIS 10 software for identification of bare ground (Jones et al., 2011).

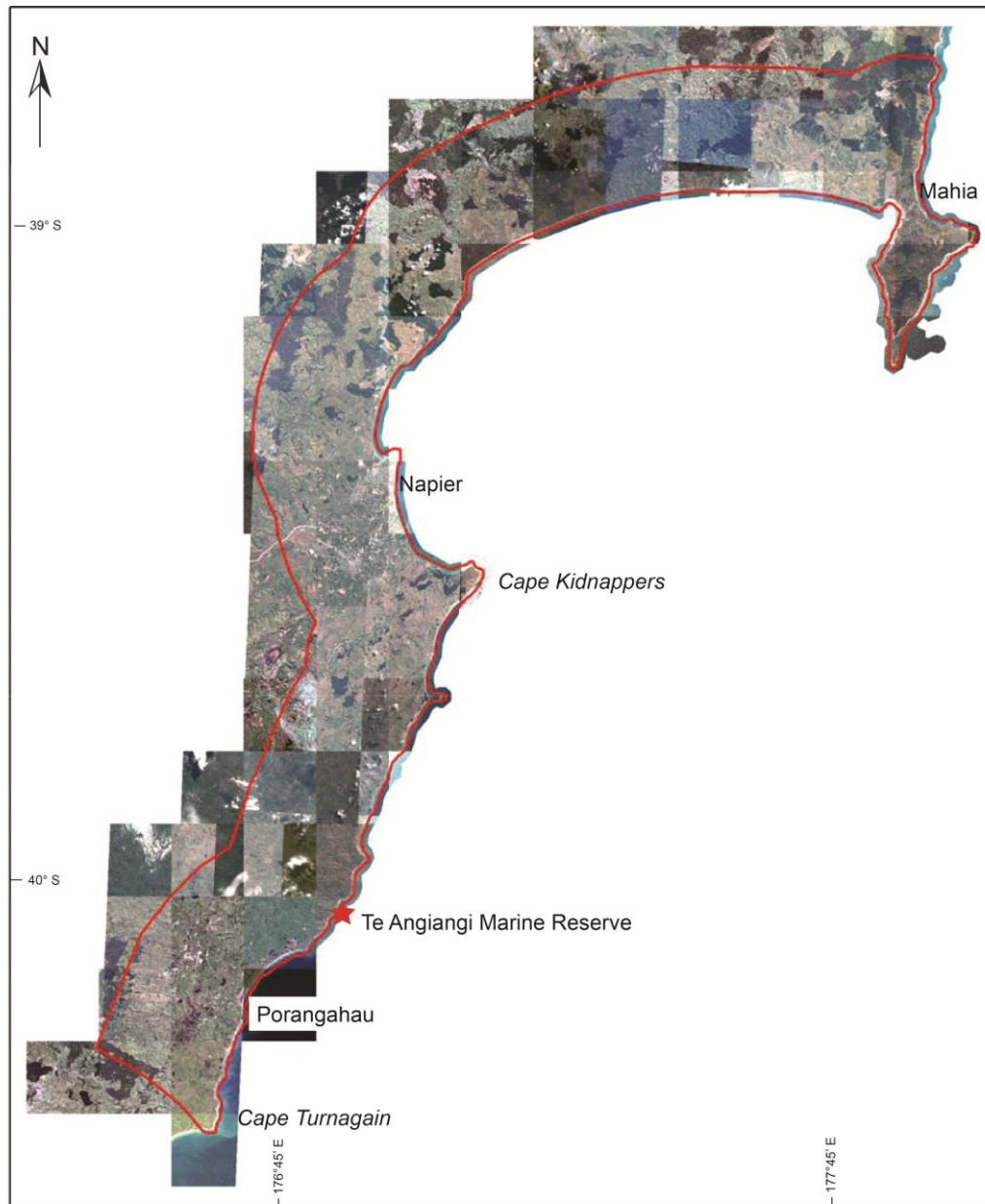


Figure 4.12. Pre-storm mosaic of satellite images from the KiwiImage program. Dates the images were taken range from 2006-2010 (from Jones et al., 2011). The red line delineates their study area. The image scale is 1:850,000.



Figure 4.13. Post-storm satellite images from the RapidEye system. Images were taken between 18-19 May 2011 (from Jones et al., 2011). The red line delineates the study area.

Out of the 5 900 km² area analysed in the post-storm imagery, 43 km² (0.73%) was classified as bare ground. When post-storm imagery was compared to pre-storm imagery, 86% was recognised as new bare ground, which is assumed to be a direct result of the April 2011 storm (Jones et al., 2011).

Land adjacent to the Te Aniangi Marine Reserve was included in this analysis. The information could therefore be used to determine the proportion of land in the area of the reserve affected by slope failures as a result of the April 2011 storm.

Te Aniangi catchment area estimate

An ArcGIS file received from GNS containing the bare ground data and a post-storm image for southern Hawke's Bay was examined and manipulated for the purpose of estimating the area affected by landsliding within the vicinity of the Te Aniangi Marine Reserve, something which had not been done in any detail by GNS. There are three streams which discharge in the vicinity of the reserve whose catchments were mapped in another overlying layer. This catchment layer was clipped to the bare ground layer, which isolated the bare ground polygons present within the catchments (Figure 4.14). Attached to each polygon is information regarding the polygon ID, its shape length (in metres) and shape area (in metres squared). After isolating all the polygons present in the catchment, information for

each polygon was retrieved and exported into an Excel file for further analysis. The shape area for each polygon was summed together to give an approximate area of bare ground present within the stream catchments. An approximate 1,594,196 m² of bare ground generated from the April 2011 storm was estimated out of a total catchment area of 19,843,073 m², resulting in a 12.4% increase in bare ground within the catchment.

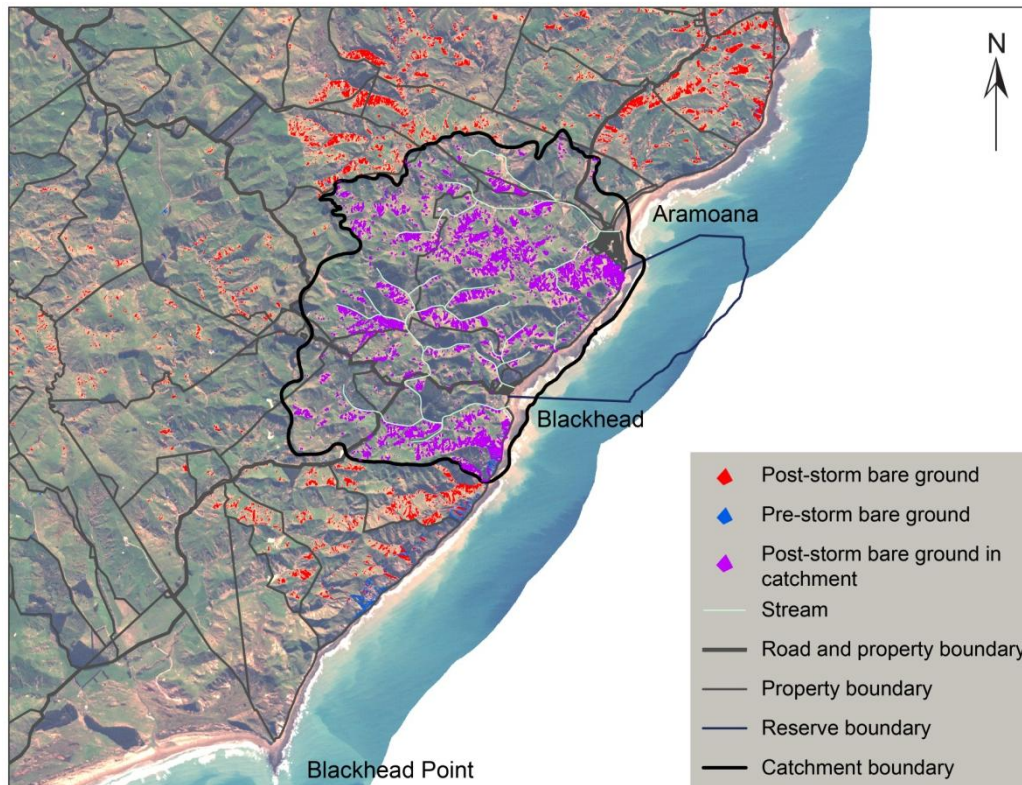


Figure 4.14. ArcGIS post-storm (RapidEye) satellite image with pre- and post-storm bare ground. The general boundary of the three stream catchments is outlined in black, and the purple represents post-storm bare ground present within the overall catchment boundary. The image scale is 1:50,000.

It is important to note that the bare ground polygons include both landslide scar and debris components, as the satellite imagery was of insufficient resolution to differentiate between the two (Jones et al., 2011). As a result, the area could be overestimated. However, it is also questionable as to whether the image classification identified all of the slips present directly adjacent to the reserve (slips 1 to 14), meaning that the area could also be underestimated.

4.6 DISCUSSION

After describing and classifying the slope failures in the vicinity of the Te Angiangi Marine Reserve, it is concluded that they are mostly translational debris slides triggered by intense rainfall during the April 2011 storm, with the possible contribution from a small earthquake (M4.5) which occurred at the height of the storm.

An estimated volume of about 150,000 m³ of sediment is thought to have been produced by the landslides directly adjacent to the marine reserve (Table 4.2). The figure is approximate because of: (1) small errors in establishing the dimensions of the landslide scars; (2) the measurement error associated with Google Earth; and (3) the scar area calculations. The scar area was assumed to be rectangular in shape when in reality they were more irregular. Also, the volume does not account for the complex area of landslides named slip 11.

Compared to the volumes of the Ponui and Waipoapoa landslides of 2,500,000 m³ and 8,350,000 m³ respectively the Te Angiangi landslide volume is relatively small. Moreover, the area of bare ground generated at the immediate coastline, of about 50,200 m² (Table 4.2) is tiny area compared with the approximately 1,594,196 m² of bare ground estimated to have been produced within the catchment as a result of the April 2011 storm. Such a large area could be more representative of the amount of sediment to reach the coastline, since it includes the input from sediment transported in streams. However, this presumes that all the sediment generated within the catchment was delivered to the coast. The rainfall which caused the slips very likely provided a medium for much sediment in the catchment to be transported to the streams and therefore delivered to the coast.

Sediment produced from landslides within the marine reserve catchment would have been transported by streams and eventually deposited at the coast, either within or just outside the reserve, whereas landslides at the coast delivered debris directly into the marine environment. The landslide sediment from slips 1 to 14 was delivered directly onto the intertidal shore platform, where at high tide it was exposed to erosion and transported by wave action. The offshore sedimentation patterns of this landslide sediment is the topic of Chapter 5.

Chapter 5

OFFSHORE SEDIMENTATION PATTERNS

5.1 INTRODUCTION

The aim of this chapter is to investigate sediment dispersal mechanisms and depositional patterns over the coastal platform and nearshore region encompassing the Te Angiangi Marine Reserve. A subtidal sediment survey was designed in an attempt to detect areas of deposition of the eroded mudstone detritus. The survey was carried out during field work in March and April 2012, and the results form the bulk of this chapter. Background information on the bathymetry and oceanography of the marine reserve are also provided.

Landslides at the coast pose a serious threat to marine organisms and overall ecological functioning. Landslide plumes of suspended sediment mainly affect localised offshore areas of the coast. In terms of ecological impacts, direct burial of sessile communities is a major impact, along with deposition of suspended fine sediment in plumes. Sediment plumes persist as waves erode away the fine material, until all that is left of the landslide debris is large boulders (Kiest, 1993). For the Te Angiangi Marine Reserve project, determining dispersal and depositional patterns could help explain any spatial and temporal response of the marine organisms to sedimentation, as it is hypothesised that nearshore currents might carry and deposit sediment on the reefs north of the reserve, and that landslide suspended sediment plumes could persist for some time after the initial landsliding.

After characterising the mudstone through field examination and laboratory work, and observing its pronounced wetting and drying spheroidal weathering pattern (Chapter 3), it is considered that fine sized particles are released during this process. As the eroded particles become finer, they become more easily transportable by wave action. The large volume landslide debris and long extension of the debris toes out onto the intertidal platform likely means that it will take a considerable time for the sediment to be fully dispersed. Sediment is going to be reworked continuously by wave action during tidal cycles until the

debris has been eroded back far enough to be out of wave reach. This means that for some time there will be ongoing dispersal of sediment and a possibly associated ongoing effect on marine organisms. This highlights the need for an offshore sediment survey which will provide insight into where the sediment from the landslide plumes is being dispersed and deposited.

5.2 BACKGROUND INFORMATION

This section provides background information on sedimentation along the east coast of the North Island, the habitat types and bathymetry, and oceanography of the nearshore region of the Te Angiangi Marine Reserve. The section is also relevant to the marine ecology chapters.

5.2.1 Sedimentation

Foster and Carter (1997) investigated mud sedimentation and Parra et al. (2012) investigated sand sedimentation on the continental shelf in Poverty Bay (Gisborne) in relation to the Waipaoa River source to sink sedimentary system, which is located north of the Te Angiangi Marine Reserve (Figure 1.1). Sediments on the continental shelf in eastern North Island are dominated by mud, which reflects the erodibility of the typically soft Tertiary sediments present in this area. The eastern coastline of the North Island, in both the Poverty Bay and Hawke's Bay areas, is subject to similar influences which affect mud sedimentation on the continental shelf, such as active tectonism, meteorological extremes, changing land use, and particularly, highly erodible sediments.

Foster and Carter (1997) focused on mechanisms by which sediment is received into the shelf environment and depositional patterns. They showed that suspended sediment is dispersed as plumes which are directed in response to the local prevailing wind-driven circulation pattern. Sediment is also delivered by fluvial suspended sediment plumes which can be dispersed by gravity and shelf currents. However, Parra et al. (2012) investigating sand dispersal and deposition, suggest that sand sedimentation is predominantly delivered onto the shelf by mass wasting from coastal cliffs and is transported offshore during storm waves and currents. Generally, mud and sand distribution is a function of delta and coastal process dynamics and margin configuration. However, the Poverty Bay shelf exhibited unique grain size distributions, where sand was found to be fining landward, not a

typical fan-like point source fluvial pattern where sediments become finer with distance offshore. This is in comparison to the southern Hawke's Bay and Wairarapa shelf, which is a typical graded shelf exhibiting a seaward fining grain size (Lewis & Gibb, 1970). Directly offshore the marine reserve, nearshore subtidal sediments are medium and fine sand dominated to about 20 m depth, and muddy sand (medium and fine sand with a >20% mud fraction) from 20 to about 40 m depth. Beyond 40 m depth the sediments become sandy mud (mud with a >20% medium and fine sand fraction). Beyond 100 m depth sediments are dominated by mud (Figure 5.1; Lewis & Gibb, 1970).

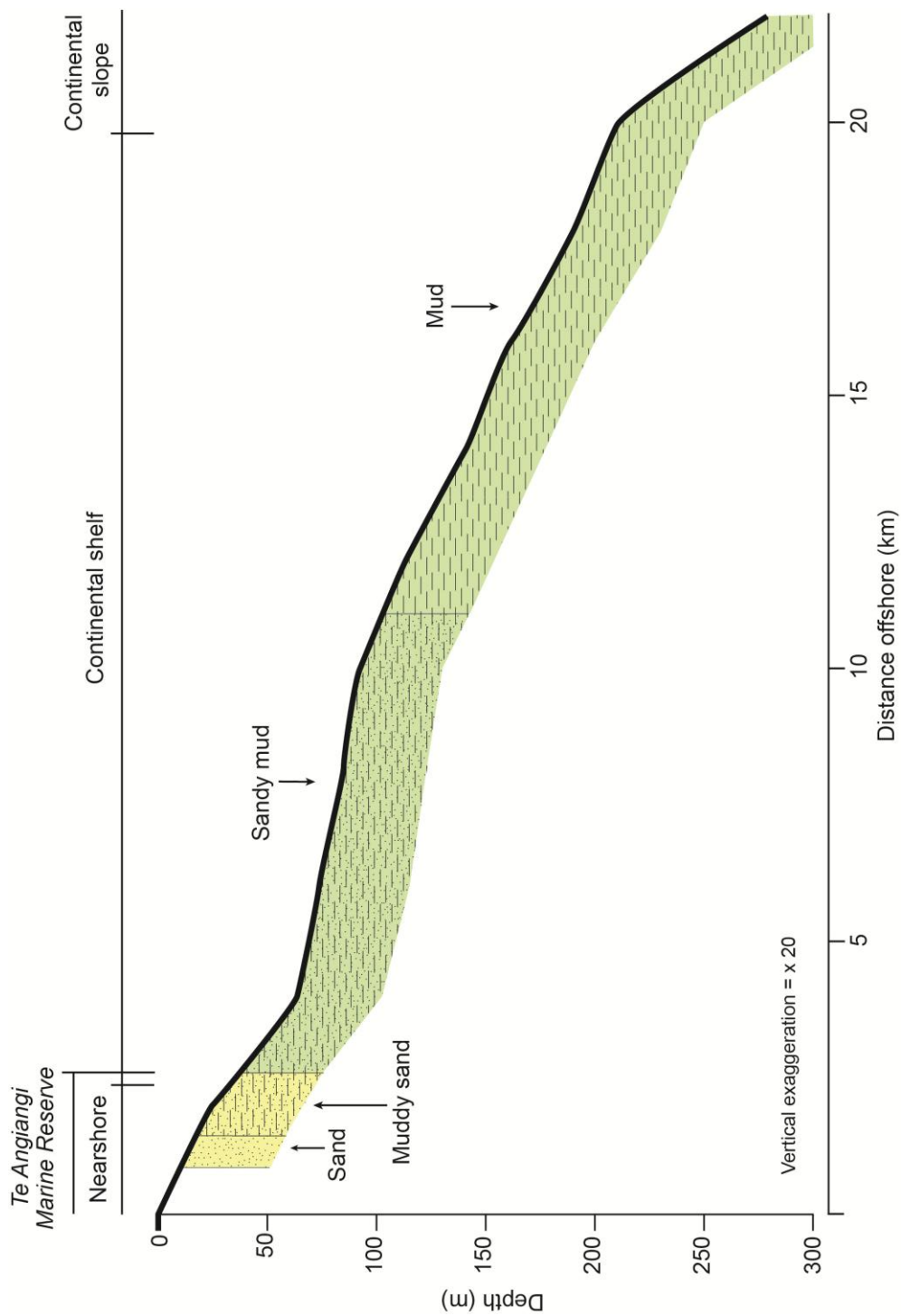


Figure.5.1. Schematic showing marine sediments on the continental shelf and slope off the Te Aniangi Marine Reserve and the general southern Hawke's Bay and Wairarapa coastline (data from Lewis & Gibb, 1970 and Lewis, 1971).

5.2.2 Subtidal habitat types and bathymetry

Funnell et al. (2005) carried out a nearshore subtidal biological habitat and substrate survey of the area between Blackhead Point in the south to Tuingara Point in the north, encompassing the Te Angiangi Marine Reserve. This was done using acoustic mapping and video techniques to collect side-scan sonar, bathymetry and subtidal video data. The information was collated to create a habitat map of the study area (Figure 5.2). Side-scan sonar images were analysed for differences in substrate and the results correlated well with drop camera video footage. Subtidal reef habitats were classified and mapped for the entire area based on these data. Based on the video footage it was visually concluded that most of the study area was soft substrate, composed of well sorted medium sand covered in medium sized ripples (of 1 to 3 cm high with a wavelength ~10 cm), with some areas of finer sand and mud. Where there was hard substrate (reef, boulders and cobbles of rock), the most common habitat in the area was encrusting invertebrates/sponge flat (15 to 50 m), followed by mixed algae (3 to 20 m) and *Ecklonia radiata* (kelp) forest (8 to 21 m). Shallow *Carpophyllum maschalocarpum* and *C. Plumosum* (brown algae; 3 to 6 m) is the least common habitat, but is likely underrepresented due to the inability to systematically manoeuvre the survey vessel in such shallow water.

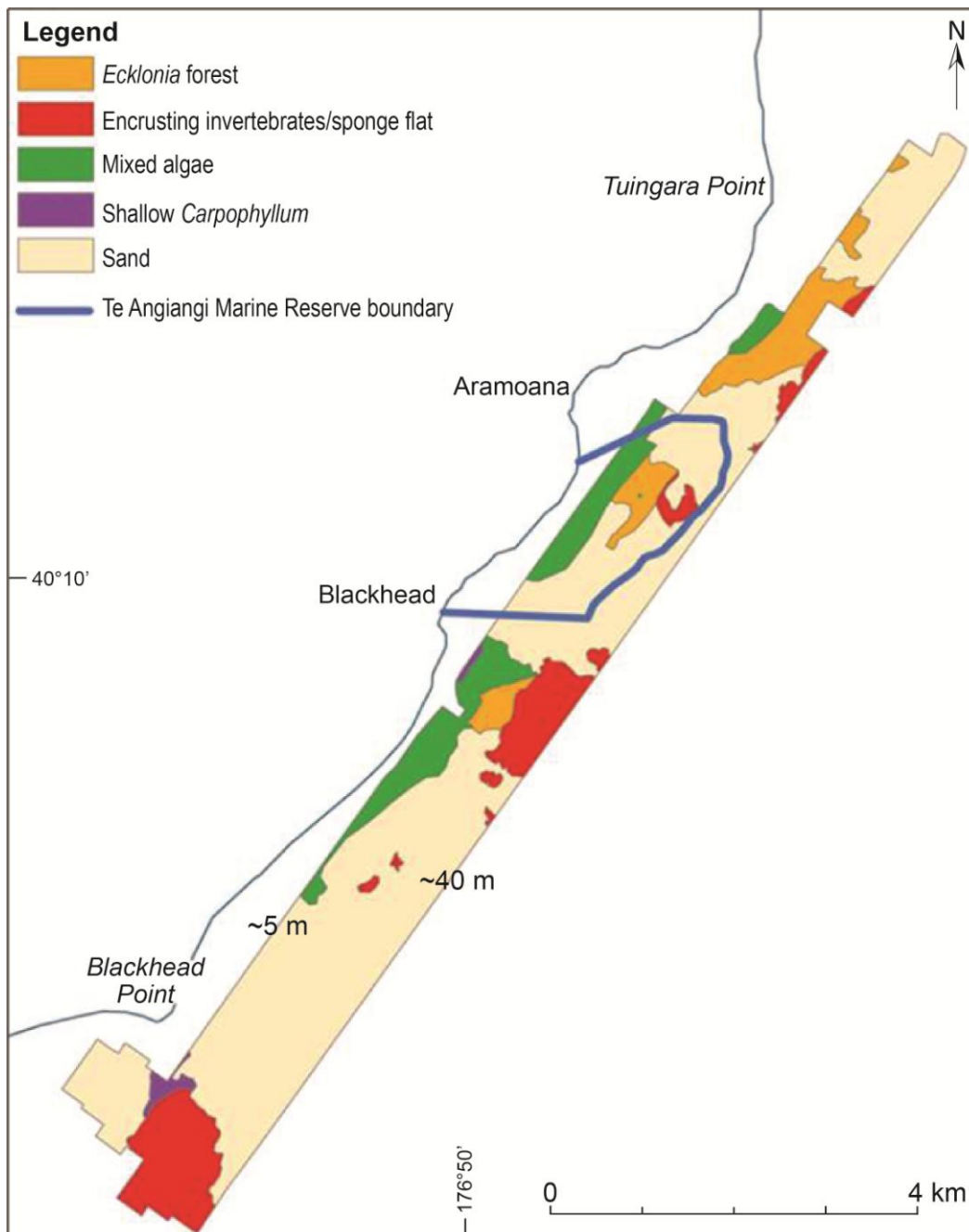


Figure 5.2. Nearshore subtidal biological habitat types in the vicinity of the study area (modified from Funnell et al., 2005).

Bathymetry was determined by obtaining survey depths and positions using differential GPS, single beam echosounder, motion sensor, and hydrographic software (Figure 5.3).

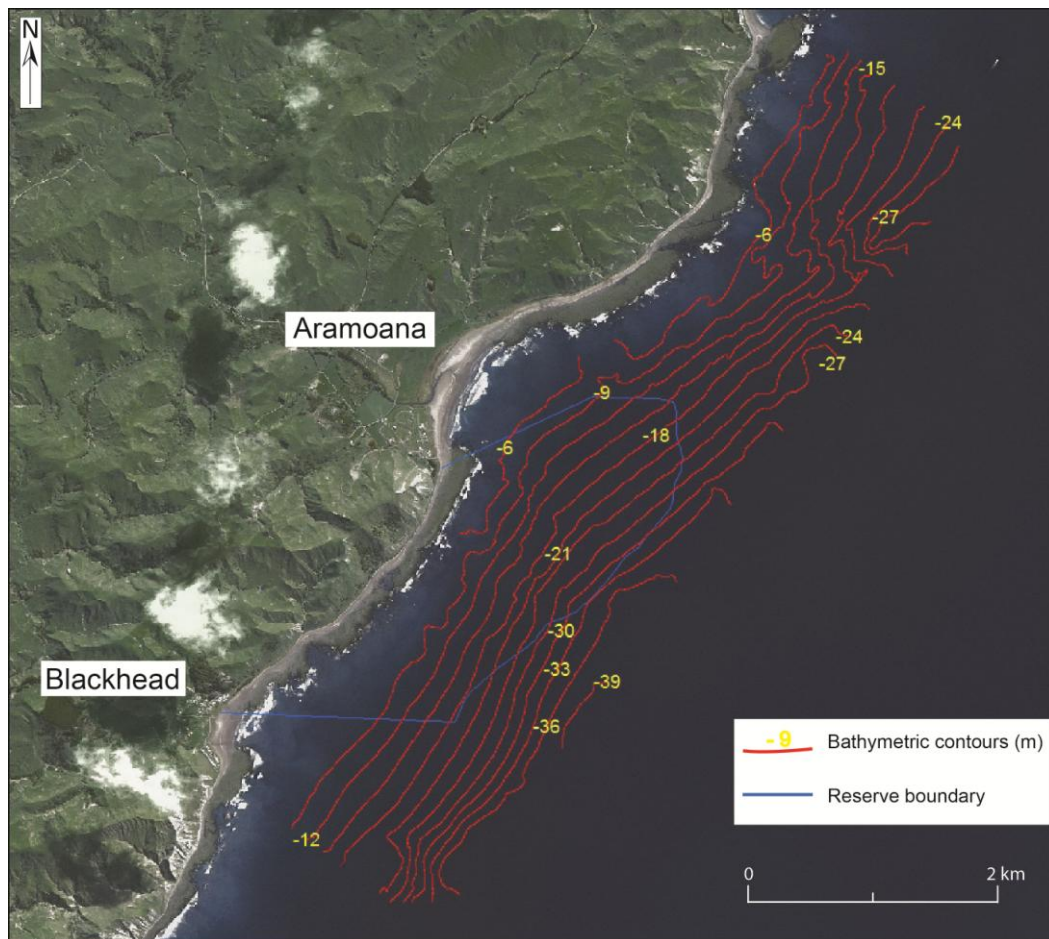


Figure 5.3. The bathymetry of the nearshore area encompassing the Te Angiangi Marine Reserve (modified from Funnell et al., 2005).

5.2.3 Oceanography

5.2.3.1 Wave climate

Ocean wave characteristics around New Zealand have been reviewed by Pickrill and Mitchell (1979), and highlight that the wave environment is dominated by westerly and southerly swell and storm waves generated in the temperate latitude belt of westerly winds. As a result the east coast is a high energy shoreline with a mixed wave climate. Predominantly, it has southerly swells derived from the westerlies south of New Zealand, and locally generated southerly and northerly storm waves. The prevailing wave conditions along the east coast are 0.5 to 2.0 m in height and 7 to 11 s in period. A weak seasonal patterns is noted from an increase in frequency of local northerly waves in the summer. Nearshore currents in the area are influenced to some extent by waves and therefore wave climate has an important role in the physical oceanography of the area.

The offshore wave climate, derived from the 20 year WAVes Model (WAM) wave generation and hindcast model, as outlined in Oldman et al. (2006), is characterised by a mean significant wave height of 1.9 m, a mean wave approach direction of 170° (south southeast), and a mean wave period of 6.9 s (Figure 5.4).

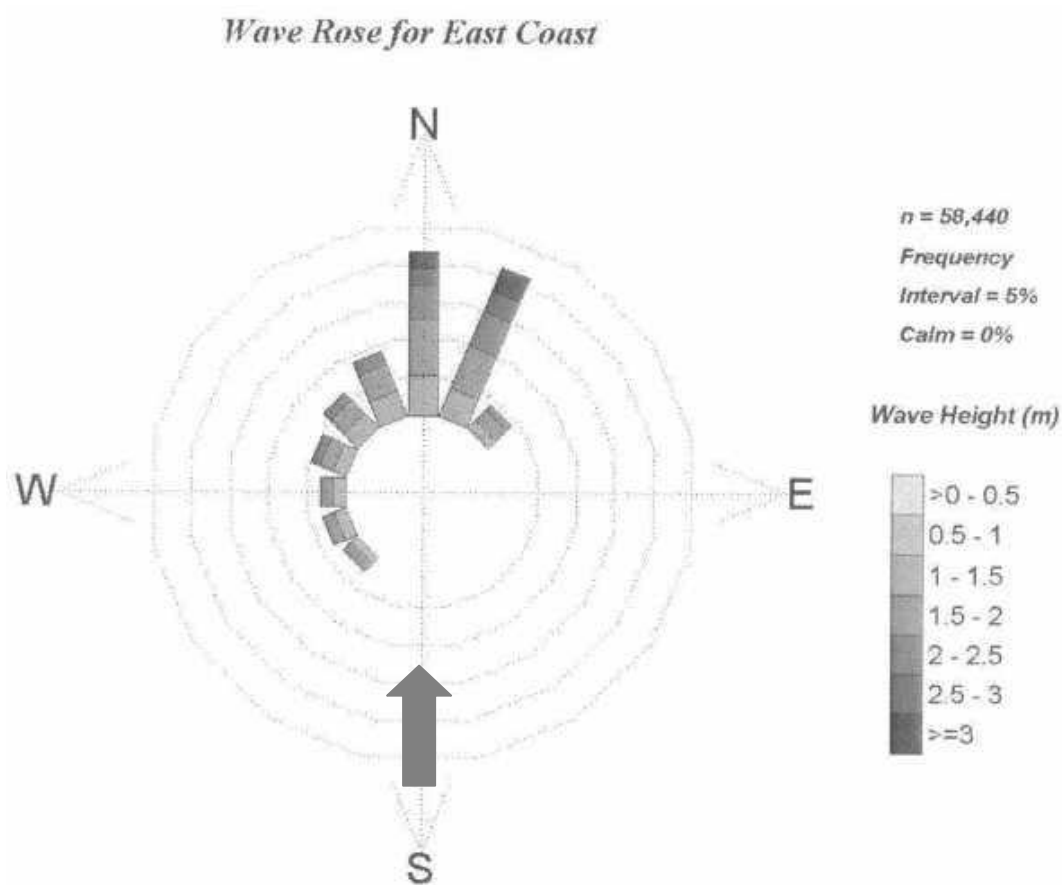


Figure 5.4. Wave rose of significant wave height and mean wave direction (waves primarily travel to the north, as indicated by the bold arrow) offshore from the Te Angiangi Marine Reserve (from Oldman et al., 2006).

The predominant storm waves (from the WAM model) are ones approaching from the south, with a significant mean wave height of 2.6 m, a mean wave direction of 184° (south), and a mean wave period of 6.8 s. Easterly storms also frequently occur and are characterised by waves approaching from the east or northeast, with a significant wave height of 2.1 m, a mean wave direction of 22° (east to northeast), and a mean wave period of 6.9 s.

Nearshore (< 30 m depth) wave conditions modelled by the Simulating WAVes Nearshore (SWAN) model were used to predict shallow water wave heights at the coast at the Te Angiangi Marine Reserve under the above average and storm wave

conditions by Oldman et al. (2006). For average and southerly storm wave conditions the wave height ranges from 1.5 to 2 m, and for easterly storm wave conditions the wave height ranges from 0.2 to 0.8 m at the coast.

5.2.3.2 Currents

Heath (1985) reviewed the physical oceanography of the seas around New Zealand and, along with earlier work by Brodie (1960) and Garner (1961, 1969), describes two main oceanic currents off coast between the East Cape and Wellington, namely the East Cape Current (ECC) and the Wairarapa Coastal Current (WCC; Figure 5.5; Chiswell, 2000). The ECC delivers warm water from the north, and the WCC delivers cool water from the south (water predominantly derived from the SC) from the Subtropical Front. This has significant influences on the marine biology of the area, especially in regard to how water temperature and water movement influence larval dispersal. An eddy called the Wairarapa Eddy (WE) is formed where the ECC turns offshore (Figure 5.5), and it is within this eddy that larvae, particularly rock lobster larvae, are retained long enough to allow development into later stages (Chiswell, 2003).

The SC flows north along and inshore of the shelf break off the South Island. It breaks away before flowing east due to the topographic high of the Chatham Rise, to become the Subtropical Front. Some of the SC persists and flows on to Cook Strait, combining into the D'Urville Current (DC). The flow then turns and continues northwards to become the WCC. The WCC flows north along the shelf at 40-50 km from the coast, extending as far north as Mahia Peninsula in northern Hawke's Bay (Chiswell, 2000). Current meter records show that the WCC nearly always flows northwards at an average speed of 20 cm/s (Oldman et al., 2006). The WE strongly influences the strength of the WCC so that, for example, intensification of the WE tends to push warmer water onto the shelf and weaken or cut off the WCC.

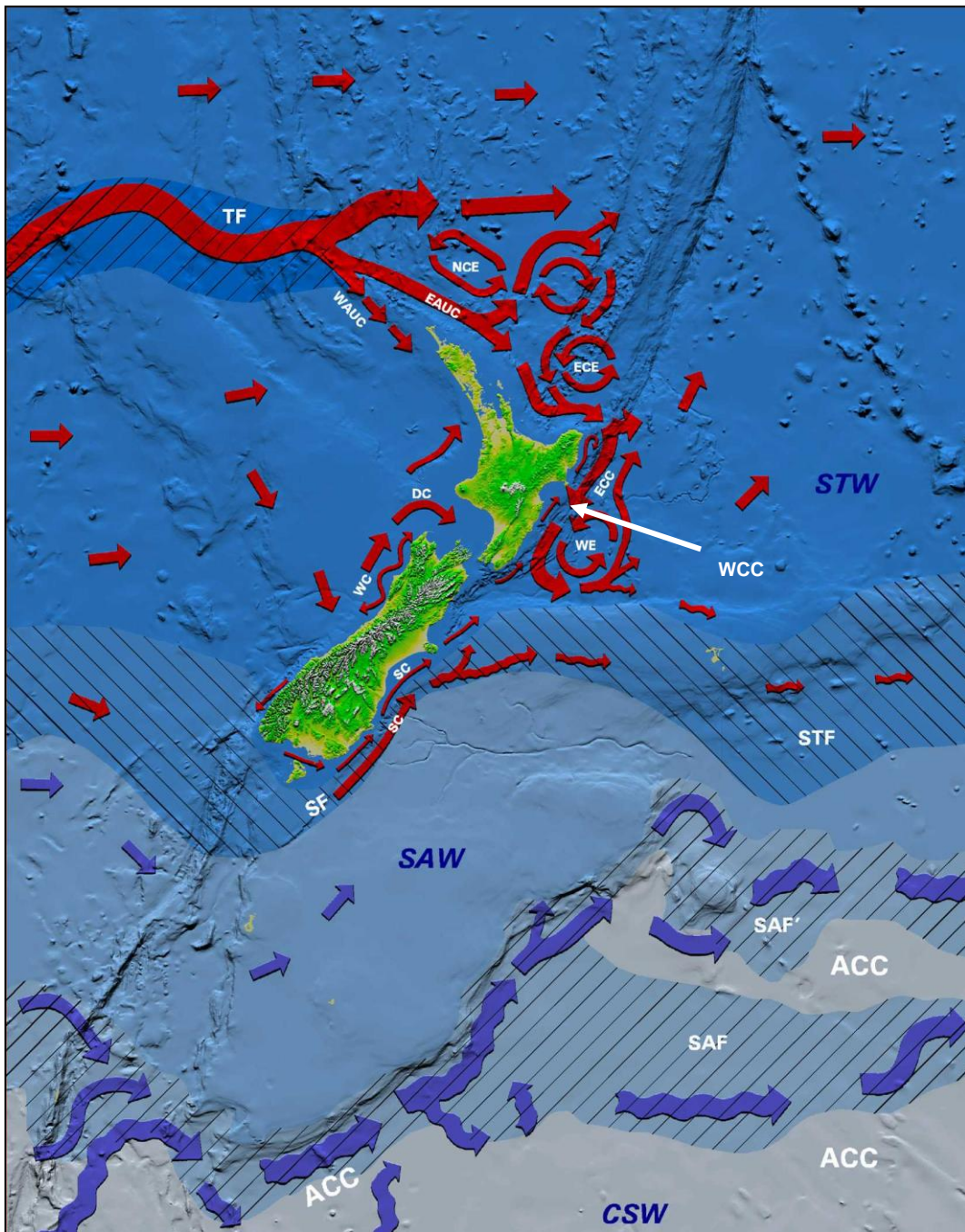


Figure 5.5. Coastal currents, eddies, water masses and fronts around New Zealand. The currents are the East Auckland Current (EAUC), West Auckland Current (WAUC), East Cape Current (ECC), D'Urville Current (DC), Westland Current (WC), Antarctic Circumpolar Current (ACC), Southland Current (SC) and the Wairarapa Coastal Current (WCC). The eddies are the North Cape Eddy (NCE), East Cape Eddy (ECE) and Wairarapa Eddy (WE). The water masses are Subtropical Water (STW), Subantarctic Water (SAW) and Circumpolar Surface Water (CSW). The fronts are positioned where the CSW and SAW meet - the Subantarctic Front (SAF), where the SAW and STW meet - the Subtropical Front (STF), and the Tasman Front, located in STW to the far north (image modified from <http://www.shiningaspotlight.org.nz/31-the-oceanography-of-the-new-zealand-marine-ecoregion>).

A hydrodynamic and dispersal model for the southern Hawke's Bay coastline was carried out by NIWA (Oldman et al., 2006). The model was used to examine the different types of forcing and resulting currents, and how they affect dispersal of different larval species along the coastline. Residual currents are the net movement of water over a tidal cycle, and are generally small to negligible along the Wairarapa coastline (they flow at < 5 cm/s). The WCC under different forcing conditions (weak, average, or strong flow conditions, defined from the model as opposed to true weak, average and strong measurement, since the current records for the WCC are limited), along with forcing by waves, tides and oceanic intrusion from the ECC, result in complex patterns of residual flow in the nearshore region (the area extending to around 30 m water depth) off the Te Aniangi Marine Reserve. The model predictions show that tidal forcing alone results in small residual currents, but with the superimposed influence of the WCC and waves the residual currents become much stronger (Oldman et al, 2006).

Depth-averaged hydrodynamics stimulated for the marine reserve included forcing by tides, ocean currents and wave radiation stresses. The results indicate the littoral currents set up by inshore wave radiation stress are very effective in ejecting larvae spawned in shallow inshore waters out into the broad-scale tidal and wind-induced flows.

At the marine reserve, residual currents flow to the south under wave influence alone, but flow to the north under tides, average to strong WCC, and average wave conditions, and are very weak for weak WCC conditions. They also flow to the north under strong WCC and southerly storm wave conditions, but at a higher speed. As a result, populations of the studied species, bull kelp (*Durvillaea*), kina (*Evechinus chloroticus*), limpets (*Cellana* spp.), paua (*Haliotis iris*) and bubu (*Turbo smaragdus* and *Cookia sulcata*), are thought to be self-recruiting, and any external recruits are thought to come from reefs immediately south of Blackhead. There is likely to be a large number of larvae derived from the marine reserve settling on reefs to the north of Aramoana (Oldman et al., 2006).

5.3 SURVEY DESIGN

The subtidal sediment survey was designed to detect areas of mud deposition and encompassed the offshore nearshore region from just north of Aramoana to just south of Blackhead. The survey was carried out within and just beyond the reserve boundary, both alongshore and offshore. A total of eight transects was sampled, four starting within the reserve boundary and four starting just outside the reserve boundary, two to the north and two to the south (Figure 5.6). This allowed a spread of subtidal samples to be collected from within and immediately adjacent to the reserve, which were then analysed for their mud content in order to gauge dispersal and depositional patterns of the fine sized particles derived from the landslide debris.

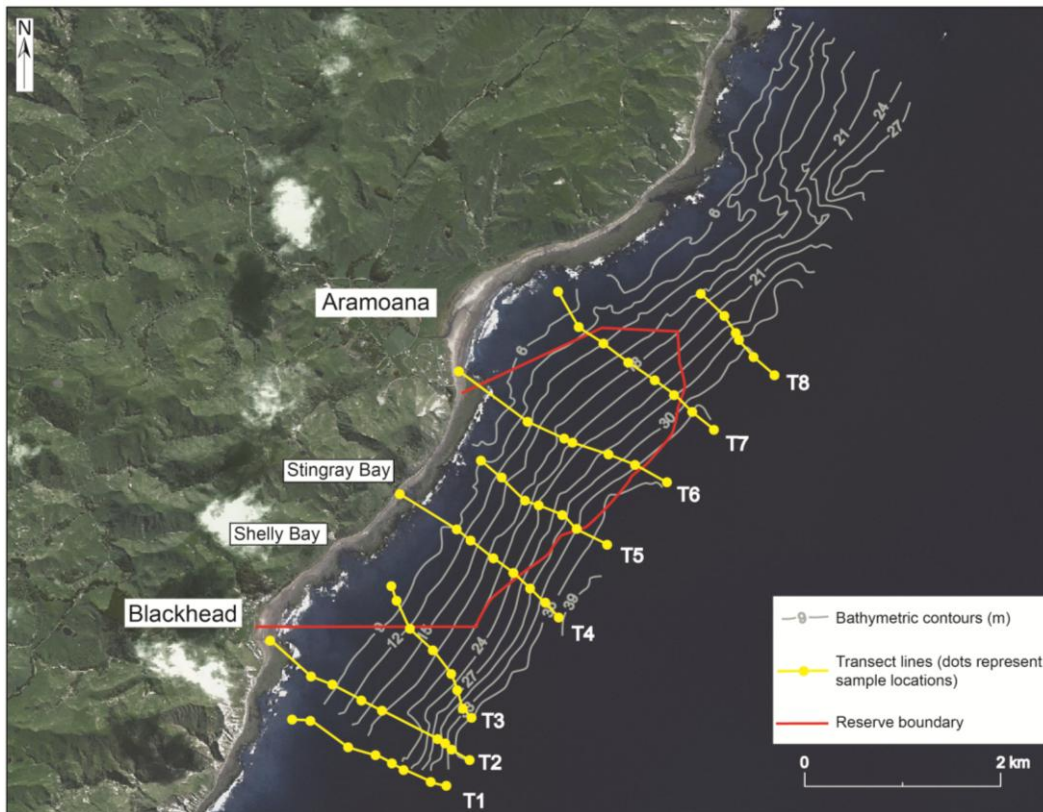


Figure 5.6. Sediment sampling transect locations.

The transects extended from 1800 to 2300 m offshore and ranged from 6 to 40 m depth (at 40 m depth the distance offshore was about 2000 m for all transects). Sediment samples were taken at 5 m water depth intervals where possible. The first sample was taken at 5 m depth and the last at 40 m depth, resulting in eight subtidal samples collected for each transect, a total of 64 subtidal samples for the

eight transects. Three intertidal sand samples were collected from Blackhead Beach, Stingray Bay and Aramoana Beach so that Transect 2 (generally in line with Blackhead Beach), Transect 4 (generally in line with Stingray Bay) and Transect 6 (generally in line with Aramoana Beach) could be extended onshore (Figure 5.6).

5.4 FIELD METHODS

Sediment samples were collected aboard a boat using a petite ponar grab sampler. Grab samplers are commonly used for quantitative sampling because a volume of sampled sediment can be calculated based on the dimensions of the sampler (Morrisey et al., 1998). However, the petite ponar grab was not used for quantitative purposes in this survey. Primary reasons for its use were: (1) it is easy to use because it is small and light; (2) it is effective at sampling soft surficial sediment; and (3) in the case of this survey, due to lack of available SCUBA divers, it was easier to manage compared to dive core sampling. The petite ponar grab sampler (Figure 5.7A) is considerably lighter than a standard ponar grab and allows hand line operation (Figure 5.7B). However, lighter weight grabs compromise the maximum depths in which it can be deployed because sea conditions must be calm (mild to moderate current conditions) for adequate use (Morrisey et al., 1998).

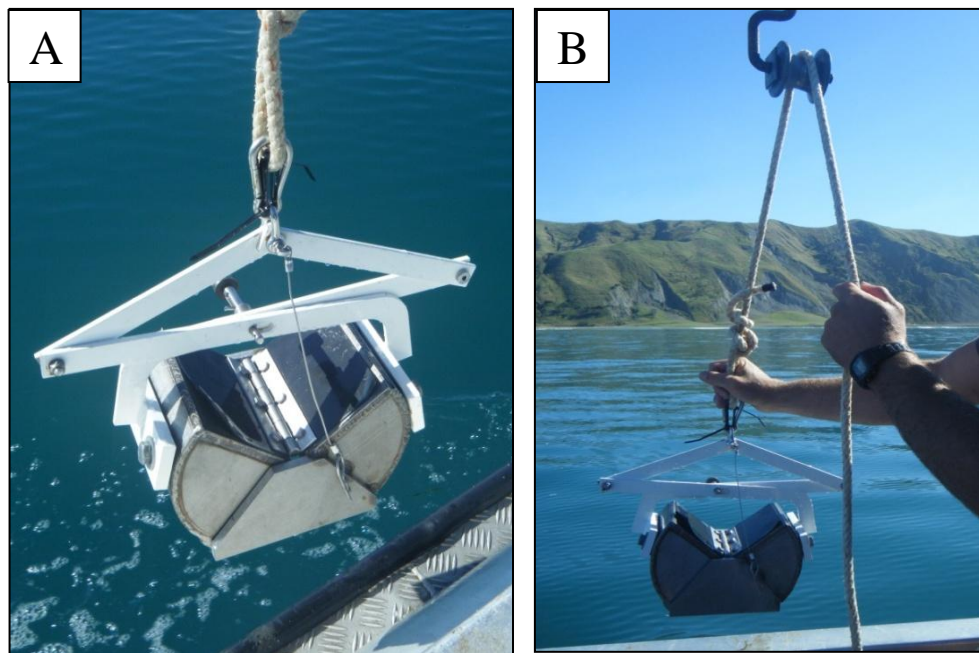


Figure 5.7. A - The ponar grab sampler. B - The ponar grab sampler being deployed using a pulley.

The ponar grab was deployed by hand using a simple pulley system (Figure 5.7B). The grab was attached to a rope with a clip, and also a cable tie in case the clip were to fail. It was deployed with the jaws held open with a catch bar and spring loaded pin, which is self-releasing. There are top screens covered by top flaps which allow water to flow through the device as it descends, consequently reducing the shock wave that precedes the sampler. When the grab hits the seafloor, the rope slackens and releases tension on the catch bar and the pin is released, which allows the jaws to close and 'grab' a sample of surficial sediment.

The ponar sampler was deployed at every 5 m depth interval down to 40 m depth along each transect. The coordinates of each deployment were recorded using a handheld GPS, shown by the yellow dots in Figure 5.6. The depth was determined using a GPS and sonar system onboard the boat. The coordinates, depth, and time were recorded at each deployment (Appendix 6). Samples could not be retrieved at several depths along the transects wherever reef or some other form of hard substrate was encountered. There were also difficulties in sampling in depths less than 10 m, which could be achieved only during very calm sea conditions. As a result, a total of 42 samples were collected out of the theoretical 64 number.

The sediment sample retrieved by the ponar grab was emptied into a container (Figure 5.8A), stirred, and a subsample obtained (Figure 5.8B). The small subsample (about 100 g) was collected into a plastic container. This sample was used for laboratory analysis of grain size and organic matter content, and was stored in a fridge to prevent microbial decay until analysis.

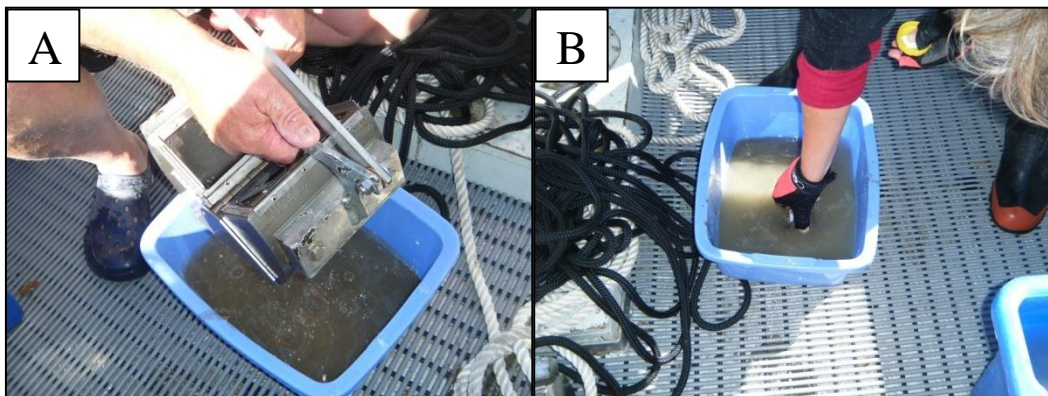


Figure 5.8. Ponar grab sample being emptied into a container (A). Subsample of sediment being taken from the grab sample (B).

Three surficial beach sand samples were collected from Blackhead Beach, Stingray Bay and Aramoana Beach. A ruler was used to measure about 2 cm into the sand, and then the top 2 cm of sand scooped into a plastic container. This sample was then used for laboratory analysis of grain size.

5.5 LABORATORY METHODS

A flow chart showing the laboratory analyses carried out on the sediment samples collected is shown in Figure 5.9.

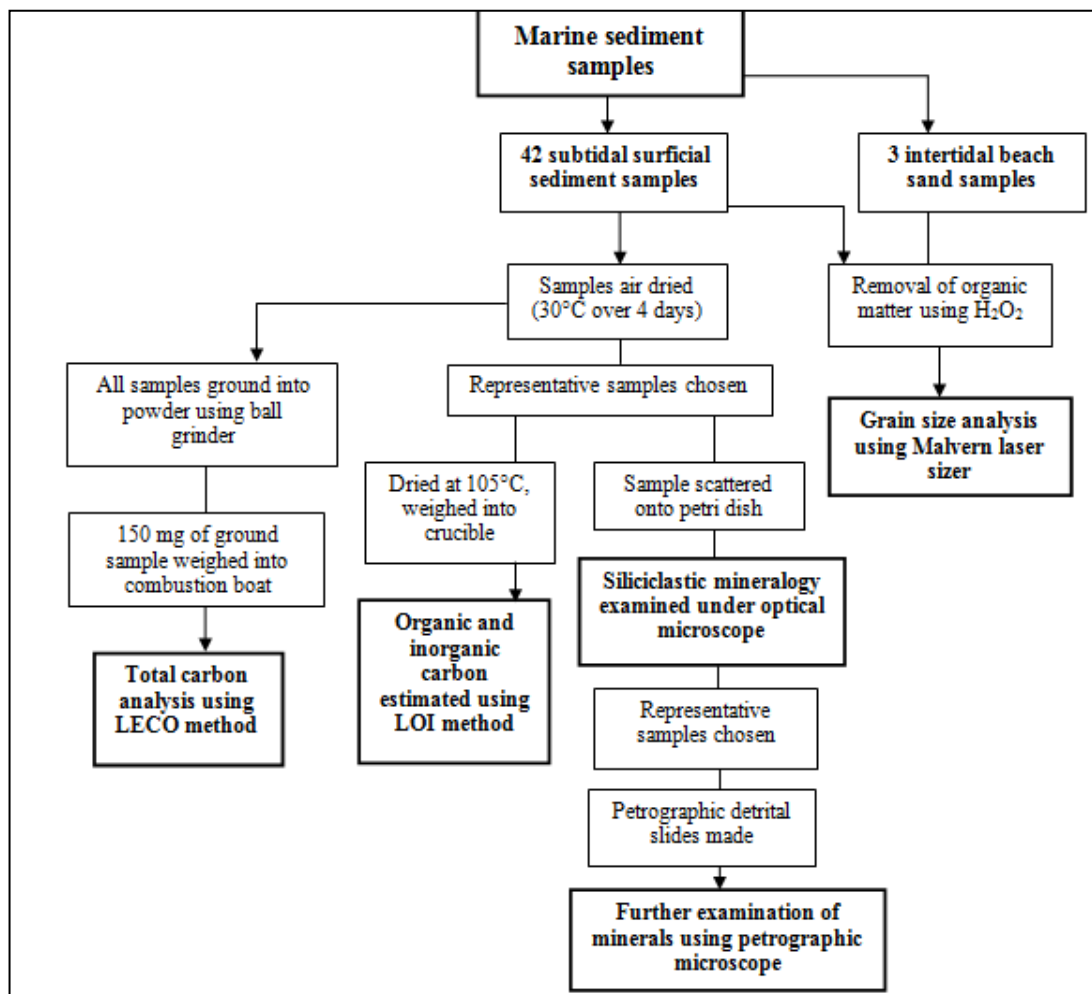


Figure 5.9. Flow chart of laboratory analyses carried out on subtidal sediment samples.

5.5.1 Grain size analysis

The grain size distribution of all 42 subtidal sediment samples and the three beach sand samples was analysed by the Malvern laser sizer in the Earth and Ocean Sciences Department at the University of Waikato. About 2 g of sediment was placed into a 50 ml glass beaker. Organic material was removed from the samples before being analysed by the laser sizer so the results were not misrepresented by organic particles. To remove organic material the samples were placed in a fume hood and enough 10% hydrogen peroxide added to cover the sample in the beaker. Samples were then stirred and left overnight. To ensure complete removal of organic material, they were then heated on a hotplate to remove spent peroxide and cooled, then fresh peroxide added and left overnight. More peroxide was added in one hour increments the next day until effervescence had ceased, then returned back to the hotplate to remove the spent peroxide. The samples were cooled fully, and a small amount of deionised water added along with 5 drops of Calgon to act as a chemical dispersing agent. Samples were left overnight to allow the Calgon to react. They were then ready for analysis. About 5 to 10 drops of sample was added to the sample chamber of the Malvern laser sizer.

5.5.1.1 Results

Raw data from the Malvern laser sizer software for all samples were entered into an Excel file for analysis. The sand, silt and clay percentages and sand sizes were calculated in Excel and graphed in STATISTICA (Version 11) statistical package. Figures 5.10 to 5.17 show grain size results for all samples and transects. The depth and distance from shore for every sample along every transect is plotted. The sand, silt and clay content and the sand size classes for each sample are shown, which can be related to its depth and distance from shore. Figure 5.18 shows a ternary plot of the samples according to their sand-silt-clay content, and classifies the sediment types based on the Folk (1954) sediment classification scheme.

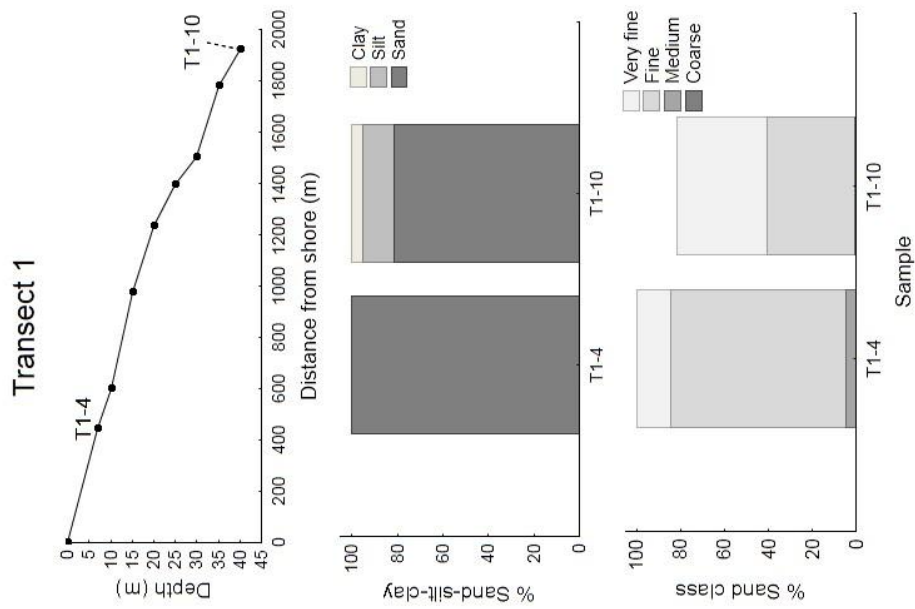


Figure 5.10. Grain size results for Transect 1. Samples are dominated by fine and very fine sand.

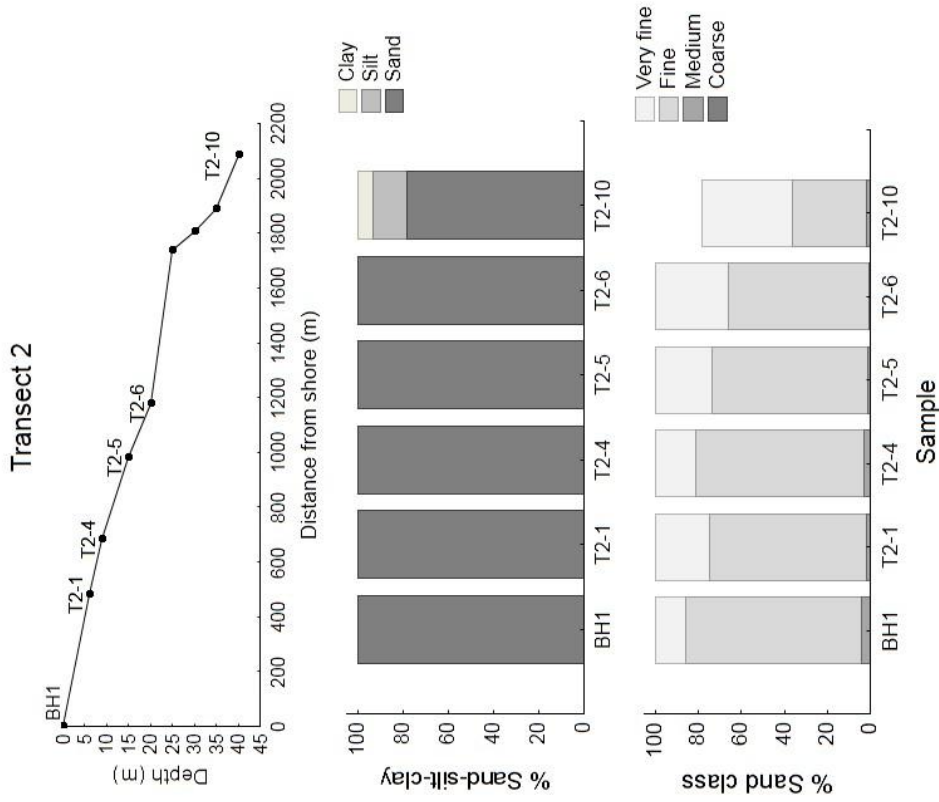


Figure 5.11. Grain size results for Transect 2. Samples are dominated by fine and very fine sand. This transect includes a beach sand sample (BH1) taken from Blackhead Beach.

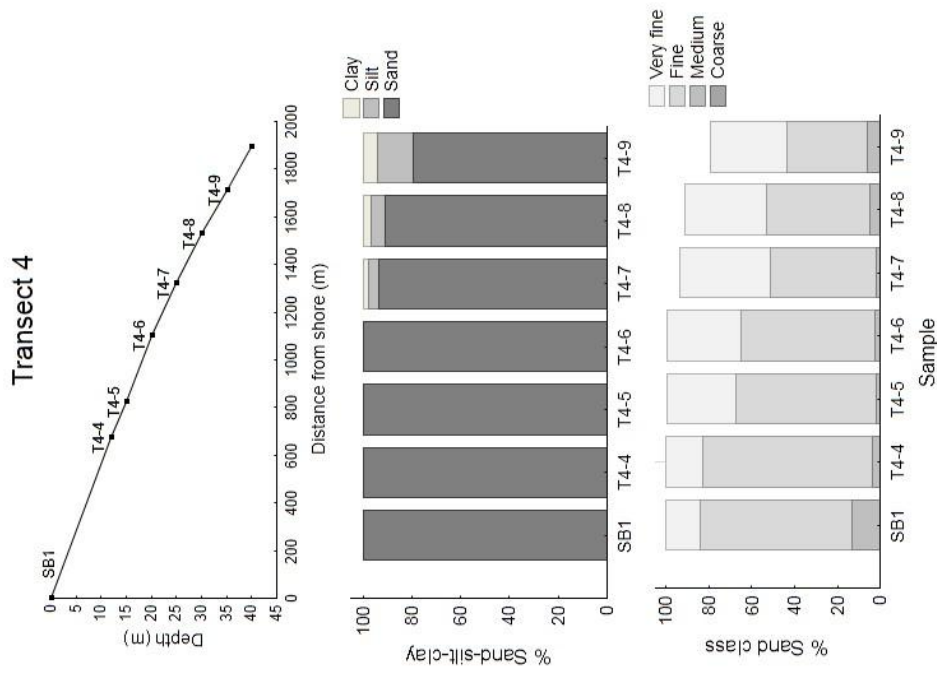


Figure 5.12. Grain size results for Transect 3. Samples are dominated by fine and very fine sand. With the exception of sample T3-9, the samples show a steady increase in mud content with depth, and T3-10 is mainly composed of silt.

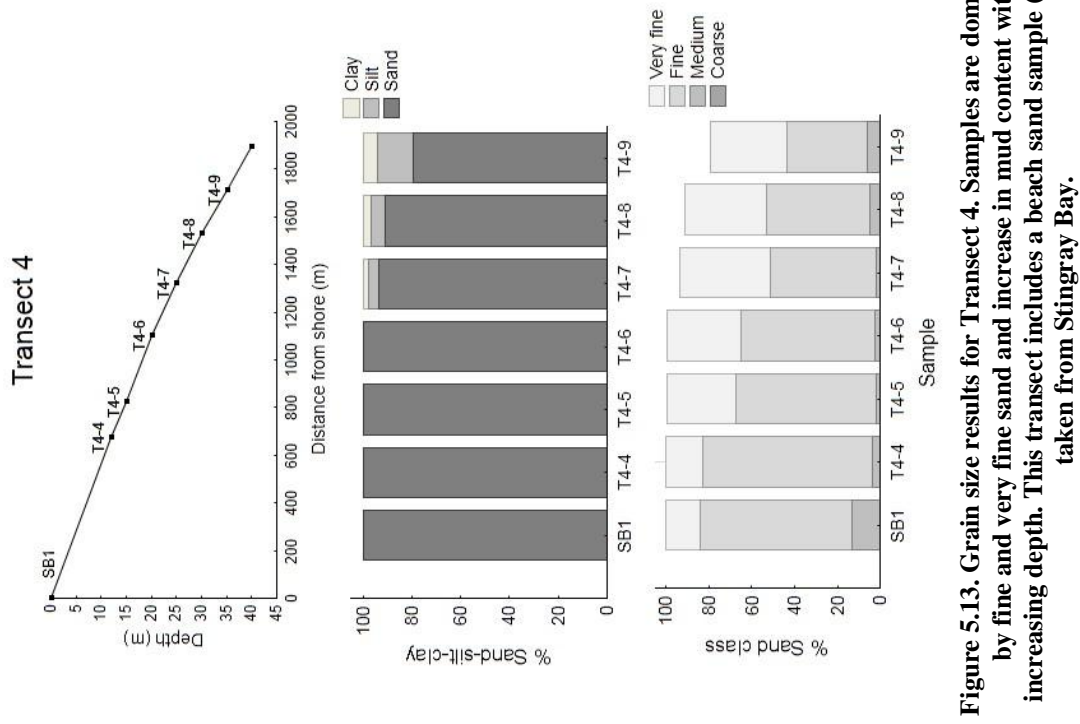


Figure 5.13. Grain size results for Transect 4. Samples are dominated by fine and very fine sand and increase in mud content with increasing depth. This transect includes a beach sand sample (SB1) taken from Stingray Bay.

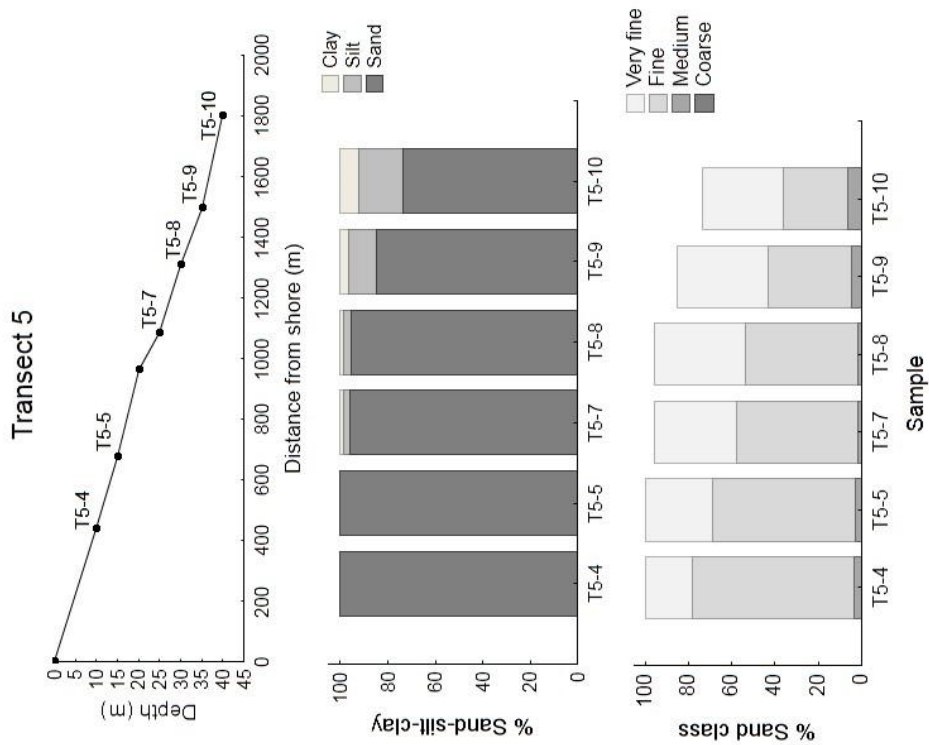


Figure 5.14. Grain size results for Transect 5. Samples are dominated by fine and very fine sand and increase in mud content with increasing depth.

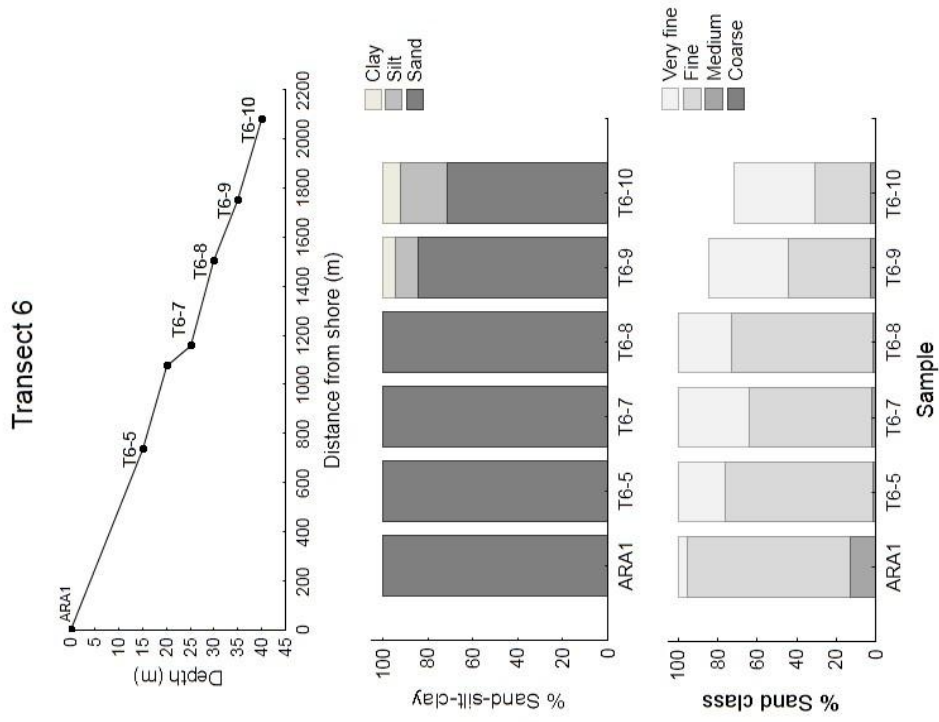


Figure 5.15. Grain size results for Transect 6. Samples are dominated by fine and very fine sand and increase in mud content with increasing depth. This transect includes a beach sand sample (ARA1) taken from Aramoana Beach.

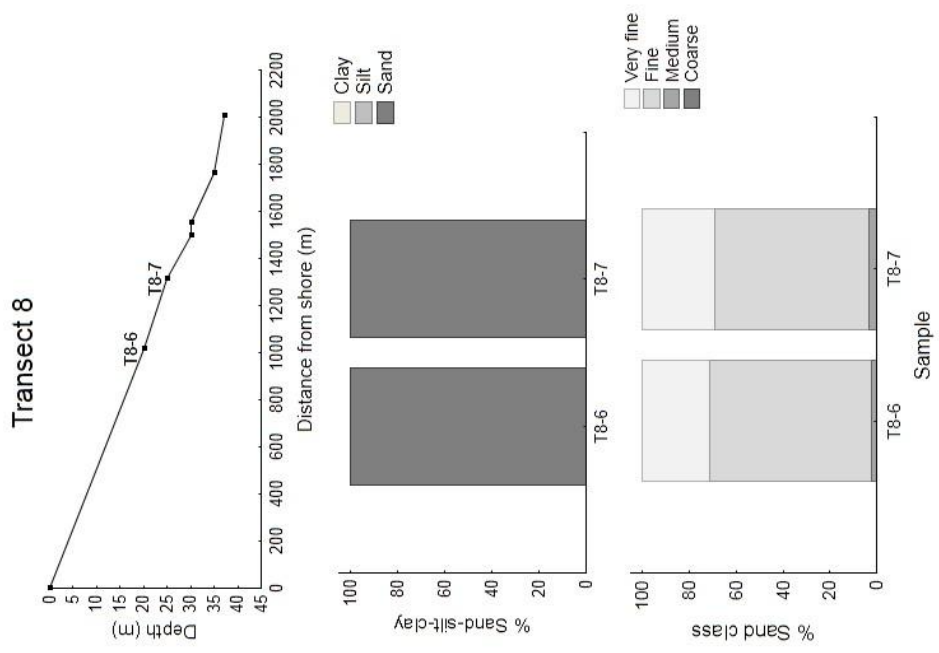


Figure 5.16. Grain size results for Transect 7. Samples are dominated by fine and very fine sand and increase in mud content with increasing depth.

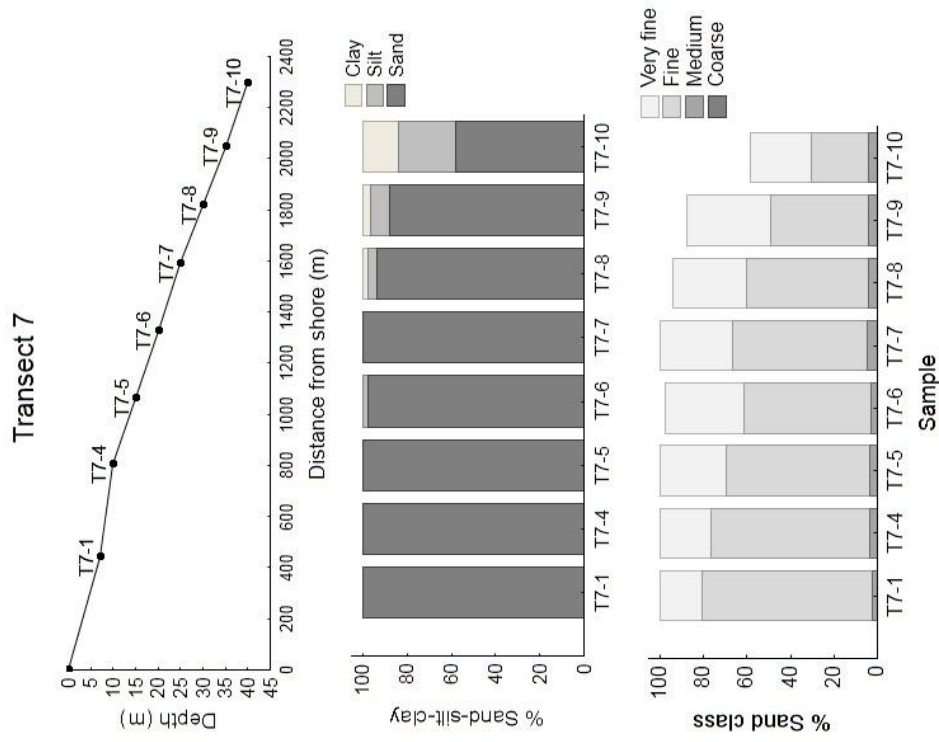


Figure 5.17. Grain size results for Transect 8. Samples are dominated by fine and very fine sand.

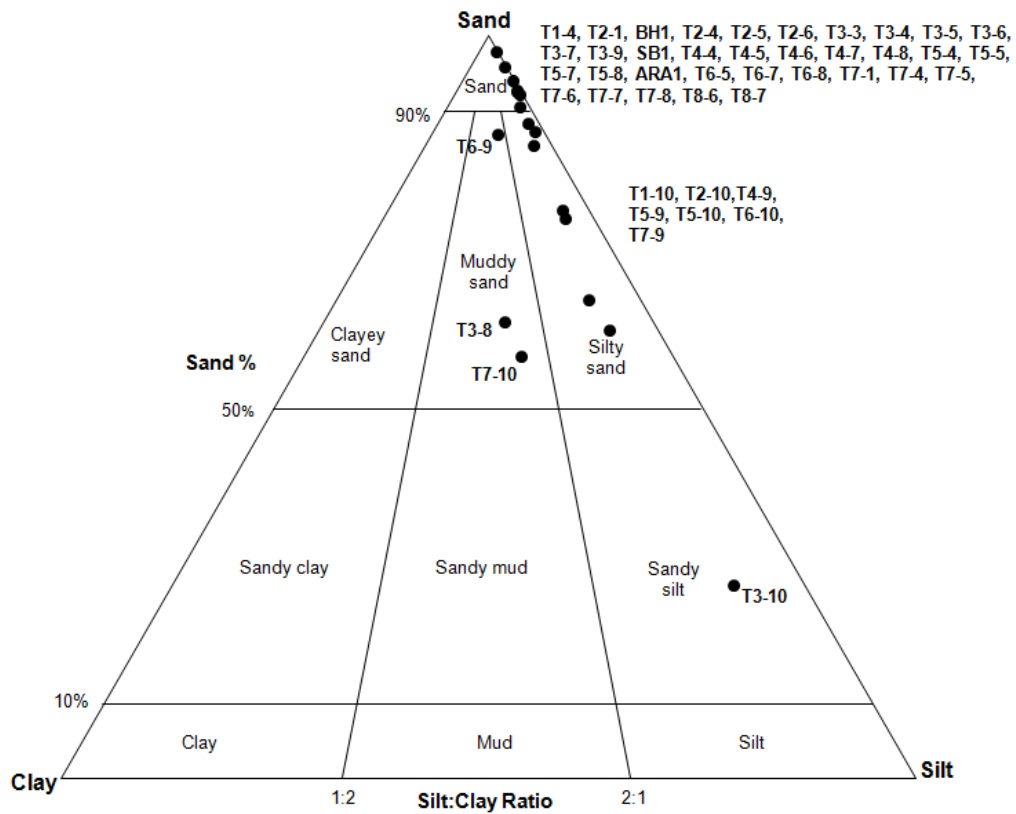


Figure 5.18. Ternary diagram showing all samples plotted according to their sand-silt-clay content (derived from GRADISTAT, based on Folk (1954)).

Grain size analysis in relation to depth and distance offshore of the sample location (Figures 5.10 to 5.17) shows a general trend amongst all samples and transects, where grain overall size fines with increasing depth and distance from shore. Despite this, most of the samples are classified as sand (about 73%; Figure 5.18), and the modes of these samples indicate they are predominantly fine or very fine sand (Appendix 7). The shallower samples mostly consist of fine sand and tend to increase in the component of very fine sand with increasing depth and distance offshore (Figures 5.10 to 5.17). There is no coarse sand in any samples, although there is medium sand present in varying amounts in most samples - intertidal sand contained between 4 to 13%, subtidal sand between 0.5 to 9.4%, silty sand between 0.9 - 6.2%, muddy sand between 2.7 to 4.4%, and sandy silt contained 0.9% medium sand. For Transects 2, 4 and 6, the three intertidal sand samples mainly consist of fine sand, and have a higher component of medium sand. Fine and medium sand amounts generally decrease as very fine sand, silt and clay increase with increasing depth and distance offshore. This supports the fining pattern observed in all other transects.

About 17% of the samples are classified as silty sand, a further three samples are classified as muddy sand, and one sample is classified as sandy silt (Figure 5.18). All of these samples were collected from depths of 35 to 40 m (about 2 km offshore) along most transects and have much higher amounts of silt and clay (Table 5.1).

Table 5.1. Average sand, silt and clay contents of the sand, silty sand, muddy sand and sandy silt textural groups (see Figure 5.17).

	Sand	Silty sand	Muddy sand	Sandy silt
%Sand	98.64	79.48	69.16	22.72
%Silt	0.88	14.89	18.31	55.40
%Clay	0.48	5.63	12.53	21.88

The distribution of sand, silty sand, muddy sand and sandy silt along all transects is shown in Figure 5.19. Since samples were not collected from every deployment (due to the grab sample being unable to collect a sample), it is assumed that the areas where no samples were collected are dominated hard substrate. The areas of hard substrate shown in Figure 5.19 are in the same general locations to the reef areas noted by Funnell et al. (2005) (Figure 5.2), and correspond to their subtidal habitat of mixed algae and *Ecklonia* forest.

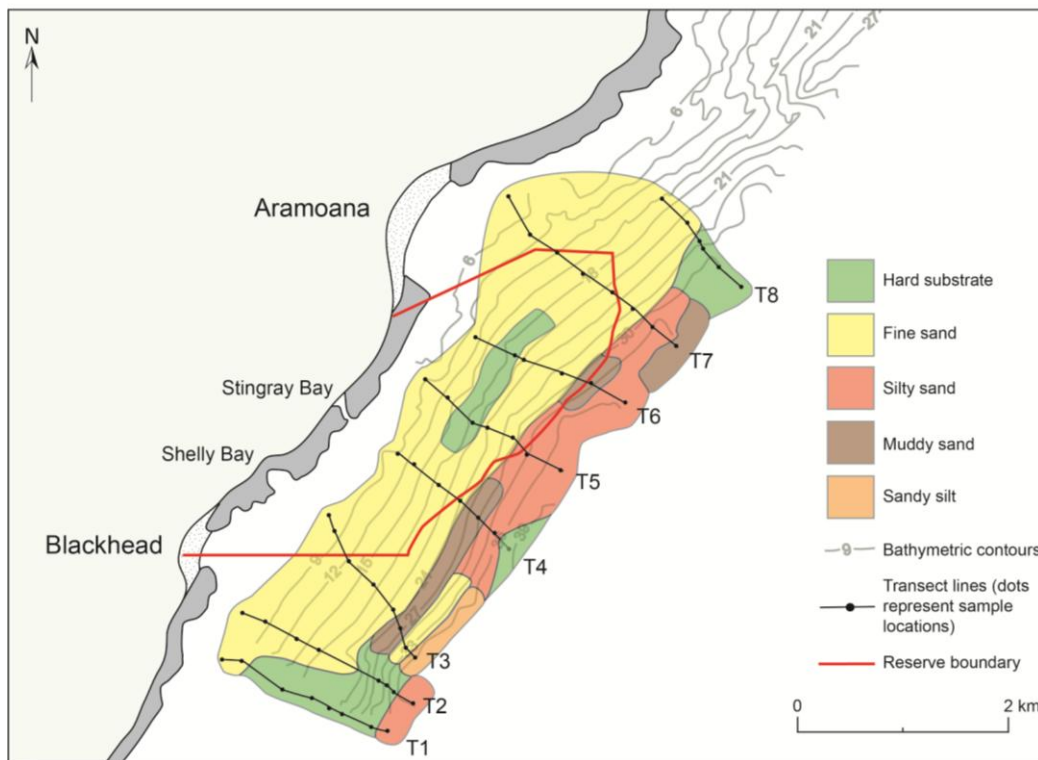


Figure 5.19. Grain size distribution along all transects based on Folk (1954) classification of all samples. Areas where no samples were taken are assumed to be hard substrate.

The primary result shown from the grain size distribution analyses is that mud (silt plus clay) occurs only near or beyond the seaward boundary of the marine reserve, indicating that the majority of the mud sized sediment has not settled within the marine reserve itself.

5.5.2 Mineralogy

It is assumed that the origin of the mud found in the nearshore region of the marine reserve is derived from weathering of the landslide debris material. However, it may also be derived from alongshore and/or onshore and offshore transport mechanisms. To aid in identifying the source of mud sized particles, mineralogical analysis was carried out on representative subtidal samples, the results of which can be compared with the mineralogical composition of the onshore mudstone rock samples tested in Chapter 3.

All samples from Transect 2 (BH1, T2-1, T2-4, T2-5, T2-6, T2-10), Transect 4 (SB1, T4-4, T4-5, T4-6, T4-7, T4-8, T4-9) and Transect 6 (ARA1, T6-5, T6-7, T6-8, T6-9, T6-10; Figure 5.6) were chosen for mineralogical analysis. These transects were selected to give three complete offshore transects covering both along and offshore directions.

Detrital mineralogical composition was determined by optical mineralogy methods. Firstly, the sediment samples were transferred into tin trays and air dried over four days in a 30°C oven. Once dry, a small amount of sample was scattered onto a clean petri dish and examined under a binocular microscope to determine general mineralogical composition. Further examination was then carried out on representative samples based on the results of the detrital mineralogy. Petrographic thin-section slides were made for samples BH1, T6-7, T2-10, and mudstone sample DM1 (refer to Chapter 3), and examined under petrographic microscope in order to further identify minerals that could not be accurately identified from the binocular microscope. Sample DM1 was used as a reference to help in identifying rock fragments. Thin-sections were made by firstly frosting one side of a glass slide using a Struers diamond Discoplan-TS precision cutting and grinding machine. Slides were rinsed with water and allowed to dry. For samples BH1, T6-7 and T2-10, the loose sediment was prepared by sieving

through a 500 μm mesh. For the mudstone sample DM1, the rock was crushed using a hammer and the resulting grains passed through a 500 μm mesh. Slides were labelled using a diamond tipped pencil. Resin was used to mount the <500 μm loose sediment to the frosted side of the glass slide. A small amount of resin was spread onto each slide using a wooden spatula and grains were sprinkled uniformly onto the resin to form a 'one grain thick layer' then dried on a hotplate at 40° for 24 hours, followed by grinding using a Discoplan-TS to a final thickness of about 0.025-0.035 mm. Slides were checked during grinding by viewing under a petrographic microscope to ensure samples were not ground too thinly. Grinding continued until an adequate thickness had been reached for petrographic analysis, which is typically when quartz showed pale yellow to grey interference colours. Slides were then polished using a Buehler Metaserv grinder-polisher. After removal of any surface discrepancies the thin-sections were ready for analysis under a petrographic microscope using a polarizing filter to examine them under both plane polarized light (PPL) and cross polarized light (XPL).

5.5.2.1 Results

Detrital mineralogy

The general siliciclastic mineralogical composition of sediment samples along Transects 2, 4 and 6 is shown in Tables 5.2 to 5.4. Also noted are the abundance of bioclasts, and the sorting, shape and size mode of the siliciclastic grains. Definition of the abbreviations used in these tables is shown in Table 5.5.

Table 5.2. Detrital mineralogy data for Transect 2. Samples BH1 and T2-10 (highlighted) are representative intertidal sand and subtidal sand samples chosen for further mineralogical analysis.

Sample:		BH1	T2-1	T2-4	T2-5	T2-6	T2-10
Siliciclasts	Quartz	A	A	A	A	A	A
	Feldspar	A	A	A	A	A	A
	Rock fragments	-	-	-	-	-	-
	Calcite	-	R	-	R	-	-
	Dark minerals	C	C	M	M	M	M
	Mica	-	-	-	R	-	-
	Clay	-	-	-	-	-	C
Bioclasts	Bioclasts	-	S	R	S	S	A
	Sorting	EW	W	W	W	EW	EW
	Shape	SR	SR	SR	SR	SR	SR
	Mode (μm)	195	176	187	174	166	140

Table 5.3. Detrital mineralogy data for Transect 4.

Sample:		SB1	T4-4	T4-5	T4-6	T4-7	T4-8	T4-9
Siliciclasts	Quartz	A	A	A	A	A	A	A
	Feldspar	A	A	A	A	A	A	A
	Rock fragments	M	-	-	-	-	-	-
	Calcite	-	S	R	R	R	R	R
	Dark minerals	VC	M	M	M	S	S	M
	Mica	-	-	-	-	-	-	R
	Clay	M	-	-	-	-	-	-
Bioclasts	Bioclasts	C	S	M	VC	A	A	A
	Sorting	MW	W	W	W	MW	MW	W
	Shape	SR	SR	SR	SR	SR	SR	SR
	Mode (µm)	206	191	169	168	155	161	153

Table 5.4. Detrital mineralogy data for Transect 6. Sample T6-7 (highlighted) is a representative silty sand sample chosen for further mineralogical analysis.

Sample:		ARA1	T6-5	T6-7	T6-8	T6-9	T6-10
Siliciclasts	Quartz	VA	A	A	A	A	A
	Feldspar	A	A	A	A	A	A
	Rock fragments	-	-	-	-	-	-
	Calcite	-	-	R	-	R	-
	Dark minerals	M	M	C	C	M	M
	Mica	-	-	-	-	R	R
	Clay	-	-	-	-	C	C
Bioclasts	Bioclasts	S	-	S	S	M	M
	Sorting	EW	W	EW	EW	EW	EW
	Shape	SR	SR	SR	SR	SR	SR
	Mode (µm)	225	179	167	173	153	127

Table 5.5. Key to abbreviations used for petrographic analysis in Tables 5.2 - 5.4.

Abundance		Sorting		Shape	
VA: >75	Very abundant	EW	Extremely-well sorted	A	Angular
A: 50-75	Abundant	W	Well sorted	SA	Sub-angular
VC: 25-50	Very common	MW	Moderately-well sorted	SR	Sub-rounded
C: 15-25	Common	M	Moderately sorted	R	Rounded
M: 5-15	Many	MP	Moderately-poorly sorted		
S: 1-5	Some	P	Poorly sorted		
R: <1	Rare				
-	Absent				

All the sediments consist of abundant quartz and feldspar (50-75%). They also contain some to common dark minerals, including magnetite (1-25%), some to abundant bioclasts (1-75%), and rare rock fragments (<1%). Calcite was present in rare to some amounts (<1 - 5%), mica (muscovite) in rare amounts (<1%), and clay in many to common amounts (5-25%). Rock fragments were only found in sample SB1, which was collected at the mid-tide mark directly opposite a large collection of landslide debris. This sample, along with muddy sand sample T6-9, and silty sand samples T6-10 and T2-10, contained 5-25% clay. Calcite was found in rare abundance, while bioclasts were generally more abundant in most samples from Transect 4. There is no obvious trend in dark mineral abundance along or offshore.

The samples ranged from moderately to extremely-well sorted and all grains were sub-rounded. The modal size for intertidal sand ranged from 195 to 225 μm , with the Blackhead and Aramoana Beach samples being extremely-well sorted and the Stingray Bay sand being moderately-well sorted. The mode for subtidal sand ranged from 155 to 191 μm with the sorting ranging from moderately to extremely-well sorted. The modal size for silty sand ranged from 127 to 153 μm with the Blackhead and Aramoana Beach samples being extremely-well sorted and the Stingray Bay sand being well sorted.

A weak alongshore trend in mineralogical composition is observed. Overall, Transect 4 samples were less well sorted than the other two transects, possibly because this transect was located directly opposite an area severely affected by landsliding. Transect 4 also contained rock fragments, generally more calcite, and a higher abundance of bioclasts. Samples from Transects 2 and 6 were similar, but Transect 6 contained more clay and mica. No obvious offshore mineral patterns were observed.

Due to several limitations with simple optical microscopy, mineral identifications may not be accurate. For example, rock fragments may have been incorrectly identified as dark minerals, and clay might have been incorrectly identified as crushed fine rock fragments, dark minerals, or quartz. Calcite may have been identified as mica, and vice versa. Consequently, some further examination was needed to better identify the minerals.

Thin-section mineralogy

A petrographic microscope was used to further identify minerals that could not be positively identified from the binocular microscope. Sample BH1 was chosen as a representative intertidal beach sand sample, sample T6-7 as a representative subtidal sand sample, and sample T2-10 as a representative silty sand sample. Samples that classified as sand and silty sand were chosen because they are the two main sediment types along Transects 2, 4 and 6 (Figure 5.18).

Petrographic analysis allowed better identification of some minerals that were suspected to be present based on the general mineral results (Tables 5.2 to 5.4). The intertidal sand sample BH1 mainly contained fractured quartz and feldspar (Figure 5.20A and B), rock fragments (Figure 5.22C and D) and bioclasts (Figure 5.20C and D). The subtidal sand sample T6-7 mainly contained quartz (Figure 5.20E, F and G), feldspar (mostly plagioclase; Figure 5.20H), and suspected rock fragments. Silty sand sample T2-10 mainly contained quartz and feldspar (mostly plagioclase; Figure 5.21C and D), bioclasts (Figure 5.21E) and some calcite (Figure 5.21A and B). The grains in this sample were notably smaller (10 to 60 μm ; Figure 5.21F) compared to the other subtidal sample examined (40 to 100 μm ; Figure 5.20E).

To clarify if some grains were rock fragments, thin-section DM1 was examined and the fragments of mudstone in this sample compared to an example of a suspected rock fragment from sample BH1 (Figure 5.22).

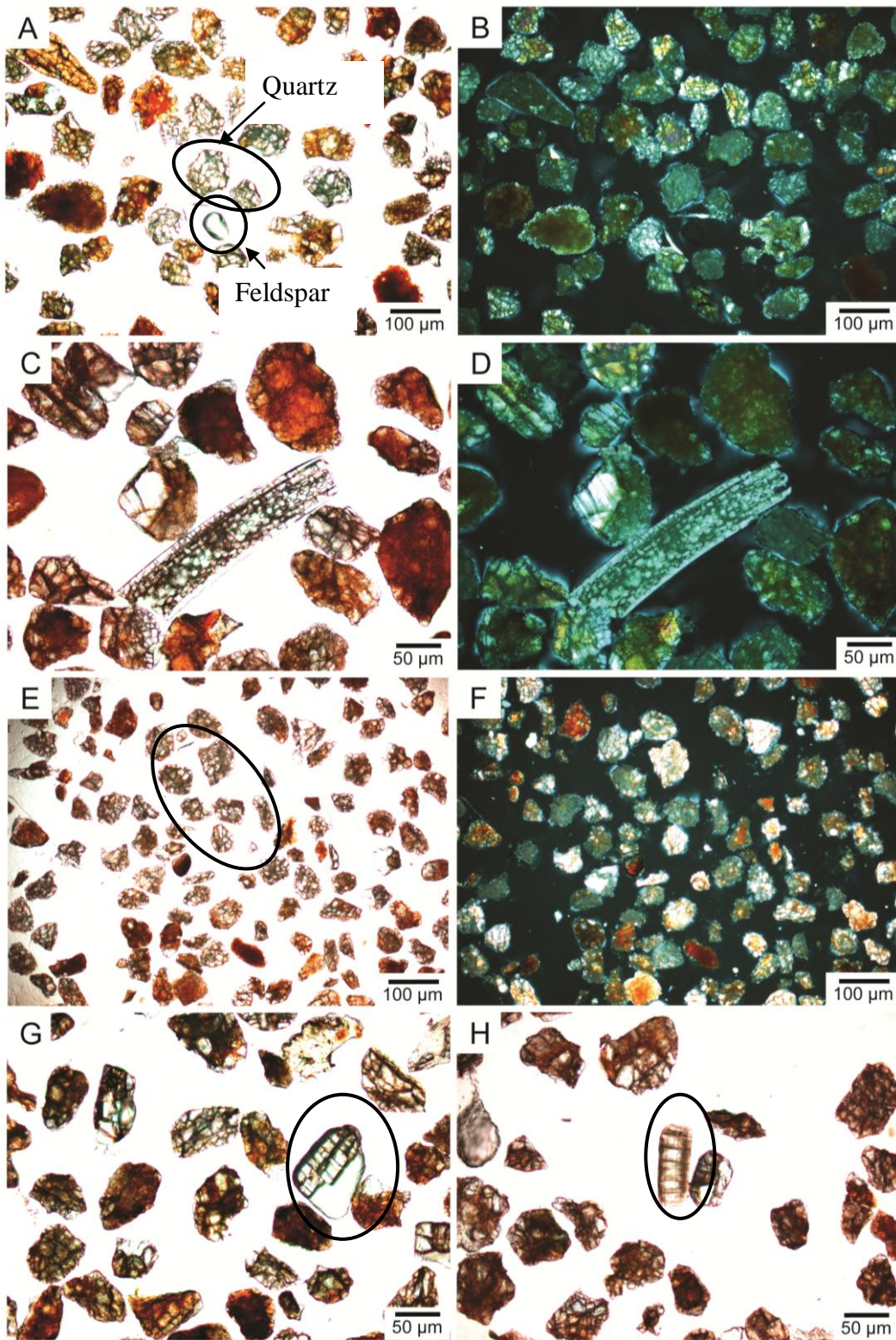


Figure 5.20 Photomicrographs of samples BH1 and T6-7. A - Quartz and feldspar from sample BH1, B - XPL image of A showing quartz interference colours. C - A bioclast, possibly an echinoderm plate, from sample BH1, D - XPL image of A. Quartz (E) and feldspar (G and H) from sample T6-7, F - XPL image of E.

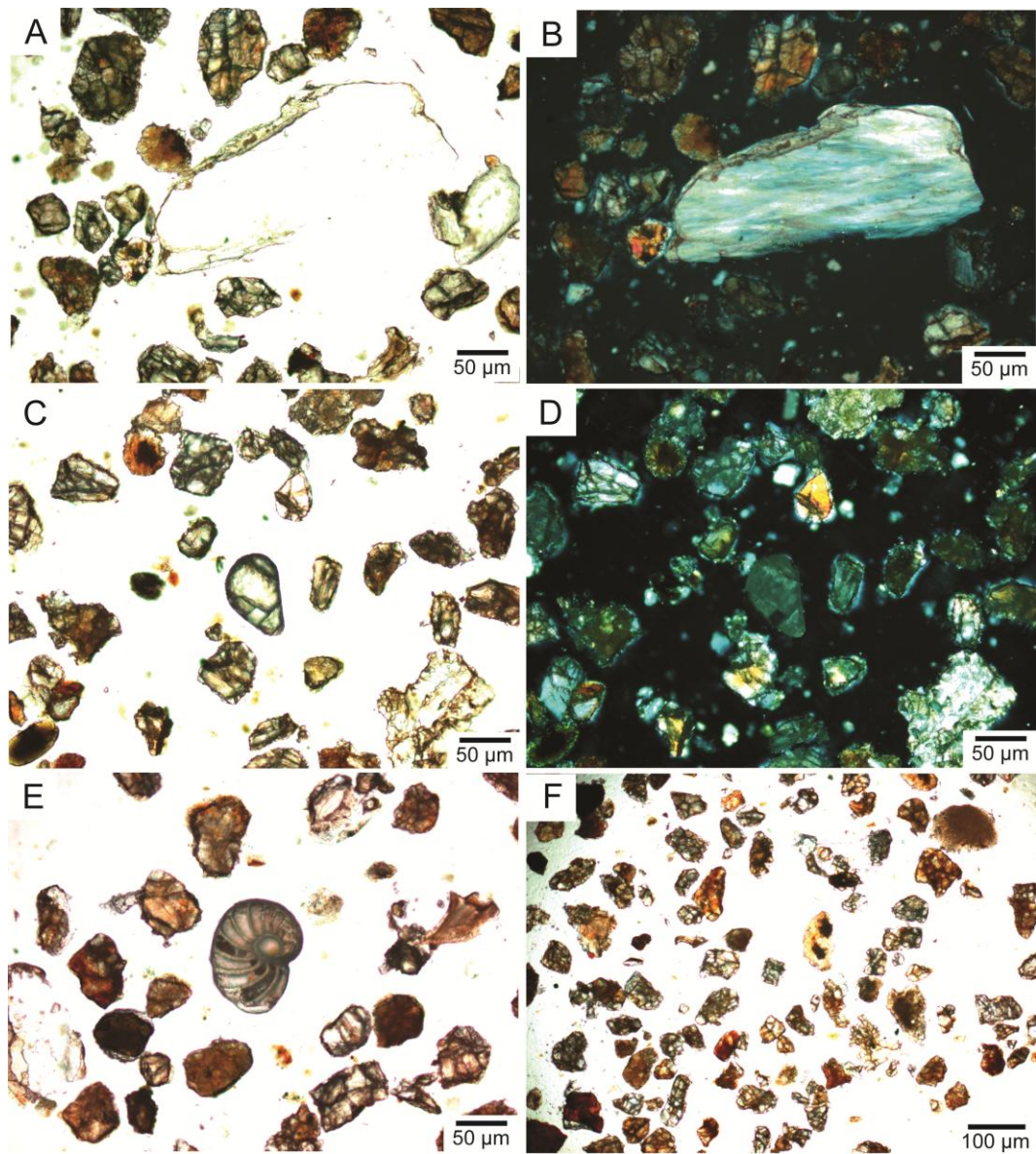


Figure 5.21. Photomicrographs from sample T2-10. A - Calcite fragment, which could be a piece of a bivalve (i.e. oyster or pectinid), B - Calcite fragment under XPL. C - Quartz and plagioclase grains (plagioclase in the centre of image). D - Quartz and plagioclase under XPL. E - A benthic foram bioclast. F - Image showing the general size of grains in sample T2-10.

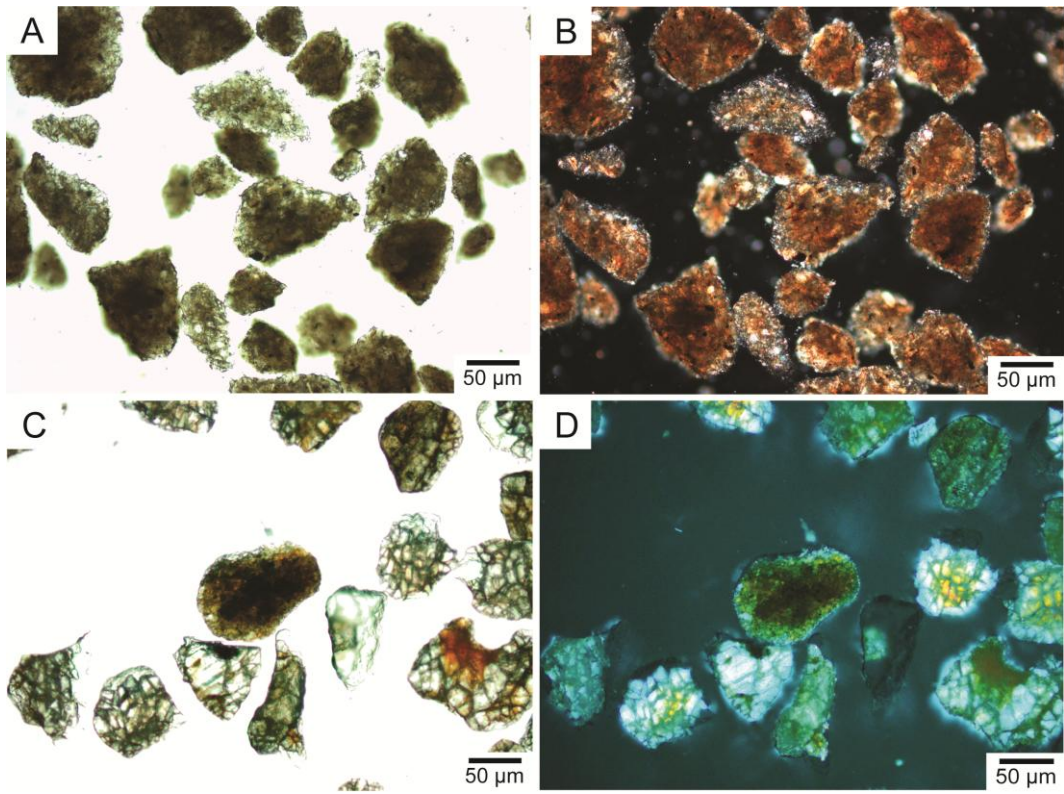


Figure 5.22. Photomicrographs of rock fragments. A - Crushed mudstone fragments from sample DM1. B - rock fragments under XPL. C - An example of a suspected rock fragment from sample BH1. D - BH1 rock fragment under XPL.

5.5.3 Carbon analysis

The organic carbon, or organic matter, content in subtidal surficial sediments can be used as an indicator of the benthic health for marine ecological purposes. The amount of carbon in sediments is often used as an indication of the amount of food available for benthic organisms, or as an indication of the amount and type of food settling to the sediments through the water column (Byers et al., 1978). The amount of organic material can also control the oxidation state of silicates in the sedimentary environment (Velde, 1992). Two methods (LECO and loss on ignition (LOI)) were trialled in order to determine the carbon content of the subtidal surficial sediment samples. A combination of LECO and loss on ignition (LOI) methods are often used to measure carbon in marine sediments (Byers et al., 1978).

5.5.3.1 LECO carbon analyser total carbon method

The first method used a LECO TruSpec CN Carbon/Nitrogen Determinator to measure the total carbon (TC = both inorganic and organic carbon components) within all subtidal sediment samples, which is used to approximate the percentage of organic carbon. 150 mg of dried, powdered sample was measured into tinfoil cups before being placed in a loading head. Samples were then combusted at 950°C in a temporary oxygen enriched atmosphere to convert carbon in the solid sample to gas form (CO₂). The combustion gases are passed through a secondary furnace at 850°C for further oxidation and particulate removal before then being passed through an additional furnace filter and two stage thermoelectric cooler, removing moisture, into a collection vessel known as the ballast. Carbon is then measured in the combustion gases as carbon dioxide by the CO₂ infrared detector.

Results

The percentage of total carbon based on weight is very small - from 0.6 to 1.8 %. However, a trend where total carbon increases with depth and distance offshore is observed along all the transects, and is particularly evident in Transect 5 (Figure 5.23). This increasing carbon with increasing depth and distance offshore trend is associated with grain size, and when total carbon is compared to the grain size mode of each sample (Figure 5.23), a strong relationship where total carbon increases with a decrease in grain size is evident.

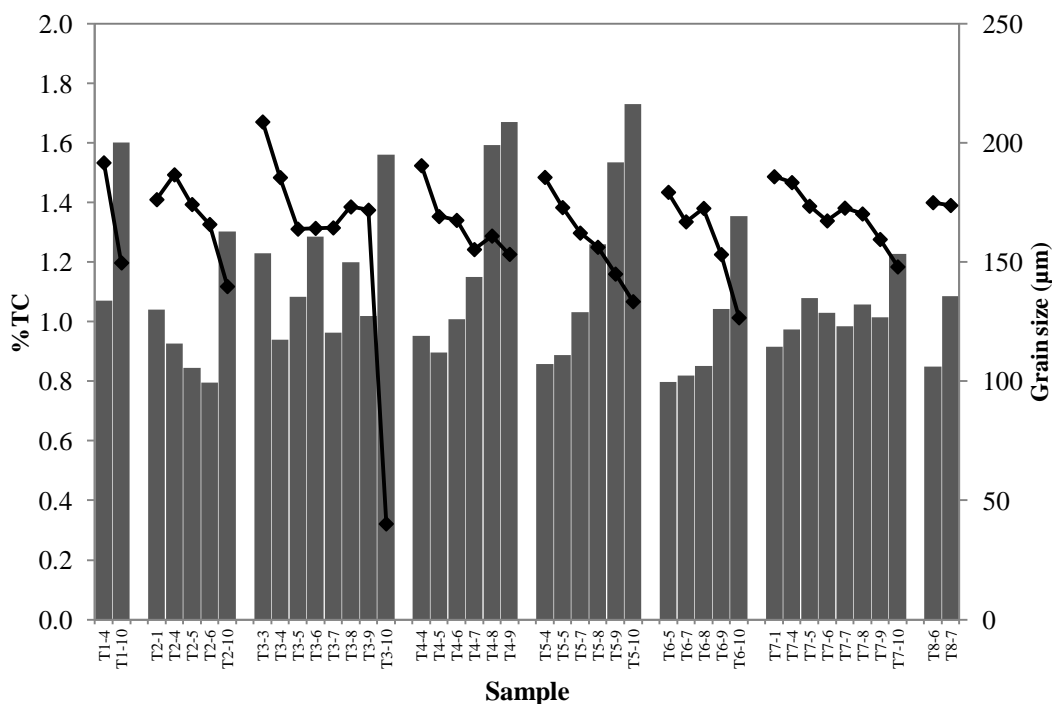


Figure 5.23. Total carbon results for all samples from the LECO method, with grain size (black lines) superimposed showing the increase in total carbon with decreasing grain size relationship.

5.5.3.2 LOI total carbon method

A representative group of 18 subtidal samples was chosen for loss of weight on ignition (LOI) to measure both inorganic and organic carbon components individually. 18 ceramic crucibles were pre-burned in a muffle furnace for 6 hrs at 900°C to remove any moisture and contaminants. They were then cooled inside a desiccator and weighed. About 2 g of air dry sediment sample was weighed into a crucible and placed in an oven set at 105°C overnight to remove any moisture, then cooled in a desiccator and weighed again. Samples were then placed into the muffle furnace set at 550°C for 6 hrs to removed organic carbon. They were then cooled in a desiccator, weighed, and returned to the muffle furnace now set at 900°C for 6 hrs, before cooling and weighing for a final time.

Results

The percentage of inorganic carbon (IC) and organic carbon (OC) based on weight is shown in Figure 5.24. A weak trend is noted along transects, where organic carbon increases with depth and distance offshore, and no obvious trend is observed in the content and distribution of inorganic carbon. Most samples have a higher abundance of inorganic carbon than organic carbon. The content of

inorganic and organic carbon is very small, varying from about 0.1 to 0.4%. When inorganic and organic carbon is compared with grain size, the comparison shows generally that, with the exception of sample T3-4, organic carbon increases with decreasing grain size, so the finer grained samples contain a higher amount of organic carbon compared to coarser grained samples (Figure 5.24).

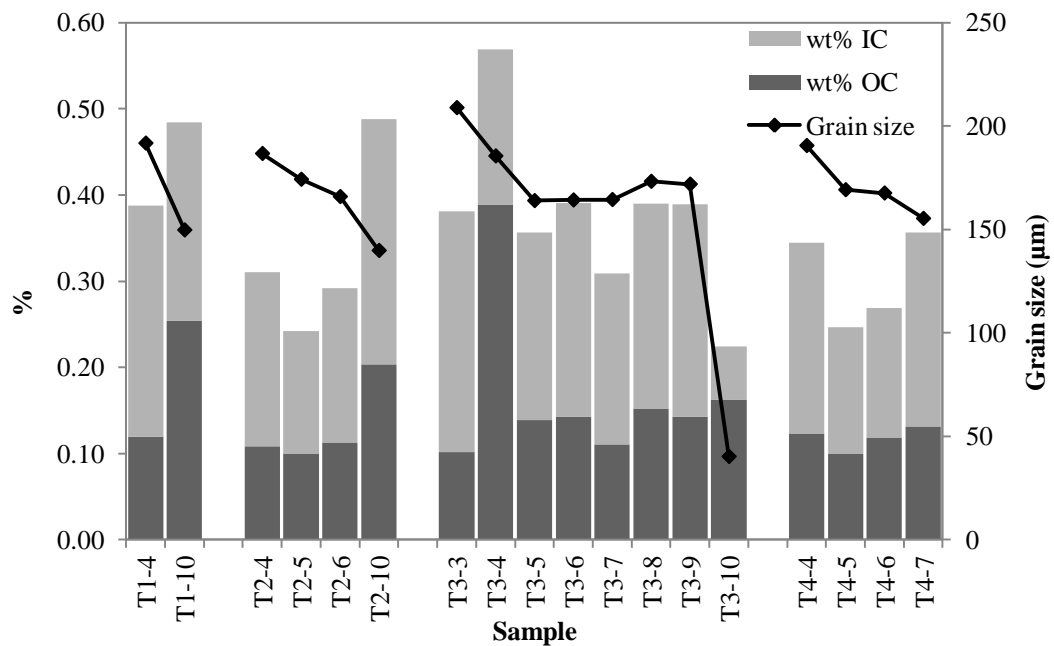


Figure 5.24. Inorganic carbon (IC) and organic carbon (OC) components of representative samples from the LOI method, with grain size (black lines) superimposed showing the increase in organic carbon with decreasing grain size relationship.

Organic carbon is present in higher amounts in finer sediments because during transport offshore they are sorted together, become bound since organic carbon is directly associated with mineral grains, and are deposited together in calmer waters (Chester, 1993). Organic carbon remains present in relatively higher amounts since the supply of oxidising agents to organic debris are more restricted to clay-rich deposits (Chester, 1993).

5.5.3.3 Overall results and comparison

The weight percent of inorganic carbon derived from LOI is subtracted from the total carbon percentage from LECO to give an estimate of organic carbon (Table 5.6), and is compared to the weight percent of organic carbon from LOI (Figure 5.25). These two values appear weakly comparable, as the LOI organic carbon values fluctuates in a similar manner to the estimated organic carbon content between samples. The already very small percentage of LOI inorganic carbon meant that subtracting this from total carbon values resulted in a tiny change in total carbon percent. The LOI organic carbon percent is therefore much smaller than the estimated organic carbon percent.

Table 5.6. Comparison of LECO and LOI carbon results for selected samples.

Sample	%C	wt% IC LOI	%OC (%C - wt% IC LOI)	wt% OC LOI
T1-4	1.07	0.27	0.80	0.12
T1-10	1.60	0.23	1.37	0.25
T2-4	0.93	0.20	0.79	0.11
T2-5	0.84	0.14	0.67	0.10
T2-6	0.79	0.18	0.51	0.11
T2-10	1.30	0.28	1.30	0.20
T3-3	1.23	0.28	1.05	0.10
T3-4	0.94	0.18	0.72	0.39
T3-5	1.08	0.22	0.84	0.14
T3-6	1.29	0.25	1.09	0.14
T3-7	0.96	0.20	0.73	0.11
T3-8	1.20	0.24	0.95	0.15
T3-9	1.02	0.25	0.96	0.14
T3-10	1.56	0.06	1.56	0.16
T4-4	0.95	0.22	0.80	0.12
T4-5	0.90	0.15	0.75	0.10
T4-6	1.01	0.15	0.78	0.12
T4-7	1.15	0.22	0.93	0.13

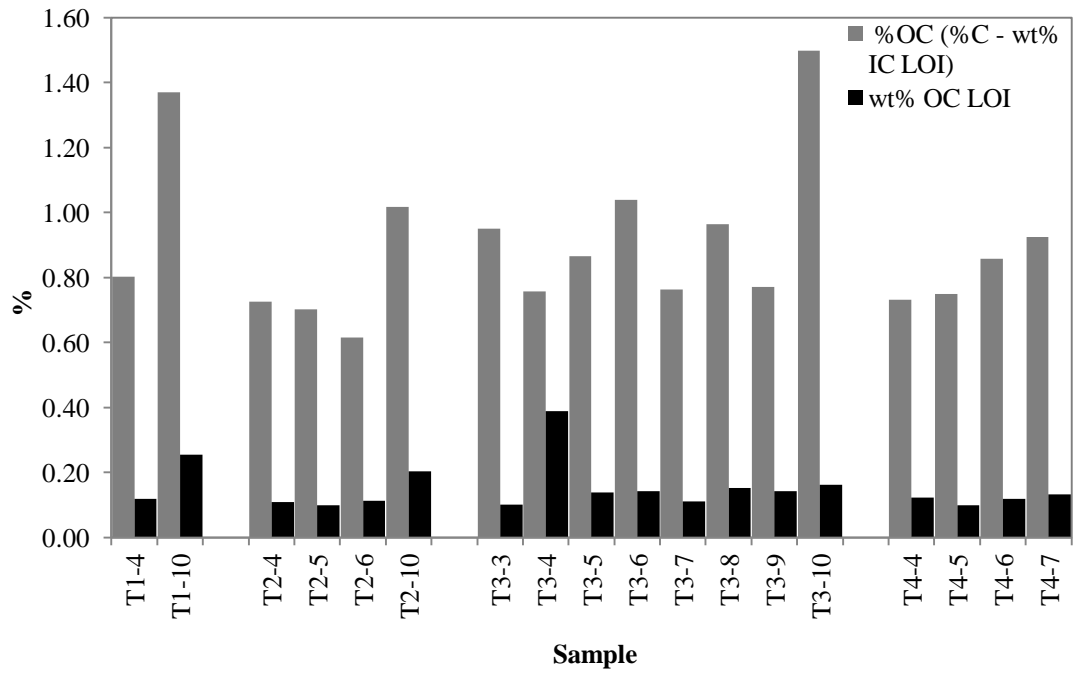


Figure 5.25. The organic carbon results derived from the subtraction of inorganic carbon (from LOI) from total carbon (from LECO), compared to the organic carbon value derived from LOI.

5.6 DISCUSSION

Mud origin

In carrying out this survey which was designed to detect areas of mud (silt plus clay) deposition, it was assumed that all the mud sized particles in the nearshore region were derived from the landslide material. A brief mineralogical analysis revealed that generally the samples contained abundant amounts of quartz and plagioclase of differing sizes (overall sample grain size modes varied from 127 to 225 μm) and the quartz appeared very fractured under the petrographic microscope. Also present were calcite and rock fragments. Rock fragments found in all samples under the petrographic microscope were compared to crushed mudstone sample DM1. The comparison showed similarities, particularly in the colour under PPL and the appearance of clumps of smaller grains within the rock fragment (Figure 5.21). The rock fragments appear to be composed entirely of finer grains, likely cemented clay minerals. General mudstone XRD results (see Chapter 3 Figure 3.8) showed abundant clay and quartz, common plagioclase and some to common calcite, which indicate there are similarities in the presence of these minerals between the mudstone DM1 and the subtidal sediment samples. It is also noted that the nearshore subtidal samples did not display any large (i.e. >1 mm) fragments or clumps of material, which might be expected from the landslide debris immediately offshore. This suggests that weathering and erosion of the landslide debris is very effective and results in fine grains which have been easily dispersed offshore. This is not conclusive evidence, but it seems that effective erosion of the mudstone landslide material results in fine grains and rock fragments, which may be present in the subtidal samples.

Mud deposition

An earlier survey by Funnell et al. (2005) stated that soft substrate in the marine reserve nearshore region is dominated by medium sized sand from visual video footage, with some areas of finer sand and mud. Subtidal sediments collected during the 2012 Te Angiangi Marine Reserve survey mainly contain fine to very fine sand, with only up to 10% medium sized sand present in the collected samples. It could therefore be considered that a layer of finer grained sediment derived from erosion of the landslide material could have been deposited and overlies a pre-existing medium sized sand deposit. For this reason, a sediment coring device for collection of the samples would have been more appropriate for

the purpose of this survey, because cores can show changes in grain size with sub-bottom depth (Morrisey et al., 1998), but for reasons already outlined core sampling was not possible.

Nearshore currents which predominantly flow to the north (Funnell et al., 2005) were thought to have a possible influence in transporting and depositing fine suspended sediment north, but this was not seen in the 2012 survey. Grain size appears uniformly fine sand distributed alongshore within the reserve boundaries (Figure 5.18), and no mud was detected in the northern extent of the survey. However, the survey may have detected mud deposition to the north, had it been extended further north. The grain size distribution does indicate that offshore transport mechanisms are important in transporting mud into deeper water, since mud is detected in increasing amounts with increasing depth and distance offshore. Suspended mud being transported in landslide plumes is therefore thought to by-pass the <30 m area altogether, drop out of suspension and settle in water depths >30 m, where it is assumed the surface wave effects on bottom sediment transport becomes negligible.

Sand origin

A possible explanation to the origin of the sand present in the study area is that it has been released from the adjacent mudstone due to erosion, since the Mapiri mudstone contains a significant amount of sand (about 40% based on mudstone bedrock samples DM1 and DM7; see Table 3.4). The main sand sizes are medium and fine sand (about 13% each), with a slightly smaller component of very fine sand (about 10%). Sand eroded from the mudstone bedrock is a likely source of fine sized sand present in the subtidal nearshore region, given the recent delivery of bedrock to the coast due to landsliding.

Carbon

Overall carbon analysis suggests that inorganic carbon is present in higher abundances than organic carbon, and overall total carbon comprises only a small portion of each sample (0.6 to 1.8 wt%). In these sediments inorganic carbon is likely made up of calcium carbonate derived from shell fragments, and perhaps a lesser amount from foraminifera and carbonate concretions which have eroded out of the mudstone debris at the coast.

Organic carbon is indicative of organic matter, which is an important benthic health indicator. Organic carbon content in marine sediments can vary considerably, but generally in nearshore sediments organic carbon accumulates at relatively fast rates, and usually makes up 1 to 5% percent of the sediment; but this value can be much higher in nearshore areas under high productivity (for example up to around 25%; Chester, 1993). The carbon results from the 2012 survey suggest there is little organic carbon settling on the seafloor from the water column and therefore available to benthic organisms. In relating these results to a broader continental shelf and margin scale, continental margins are generally characterised by high levels of organic carbon storage, with an estimated 80 to 85% carbon burial currently occurring, especially off river-dominated coasts. Brackley et al. (2010) measures changes in organic matter percentage along a floodplain to shelf to slope transect on the Poverty Bay Shelf on the east coast of the North Island. Initially, organic matter content decreases from the floodplain to deeper water (>36 m; this reflects the loss of terrestrial organic carbon as it becomes buried or transported further offshore), before increasing through addition of modern marine organic carbon in waters up to 56 m deep, then increasing again in water depths from 56 to 1428 m as this organic carbon is accumulated within pre-existing aged marine organic carbon (Brackley et al., 2010). The percent organic matter within the floodplain to 36 m part of the transect ranged from 0.2 to 0.8% (compared to Te Angiangi Marine Reserve subtidal sediments which ranged from 0.1 to 0.4% organic carbon based on LOI data or up to 1.8% total carbon from LECO). It is possible that the distribution of organic carbon in the reserve is similar to what is observed along the floodplain to 36 m depth transect, except the organic carbon is assumed to be derived from landslide plumes rather than river plumes.

The effects that the sedimentation event had on the Te Angiangi Marine Reserve marine life is investigated in Chapter 6.

Chapter 6

INTERTIDAL ECOLOGY

6.1 INTRODUCTION

Coastal landslides along the southern Hawke's Bay coastline, which occurred as a consequence of the April 2011 storm, resulted in a localised sedimentation event at the Te Angiangi Marine Reserve and adjacent immediate coastline. As described in Chapter 1, this set the scene for a unique assessment of the short term ecological response and possible effects along the landslide affected coastline encompassing the already established marine reserve. Furthermore, there was an array of information with varying degrees of quantitative detail available, which permitted some ecological characterisation of the status of the intertidal reefs inside and outside of the Te Angiangi Marine Reserve.

A preliminary survey of the intertidal marine ecology from within and outside the reserve was carried out in order to assess the impact on the marine organisms in response to the high sedimentation event. The context of this study is unique as (1) it is a natural sedimentation event caused by coastal landsliding within and adjacent to a marine reserve (this is unprecedented in New Zealand), and (2) because there is pre- and post-reserve data available (noting surveys are irregular in occurrence and they have used inconsistent methodologies). Nevertheless, the data available for the marine ecosystem in this area is valuable in its very presence. This is because of the reserves remote location, and the reserve is representative of a less well studied coastal ecosystem of eastern New Zealand characterised by soft mudstone reefs and highly turbid coastal waters. The previous surveys provide baseline time series data (which collectively represent pre-April 2011 storm event data), that can be used with certain limitations, for comparison with data gathered from the current survey (representing post-event data), which then allows the ecological consequences of the April 2011 storm event to be assessed.

An important aspect of this intertidal survey is that it has taken advantage of the fact that a marine reserve has been influenced by the sedimentation event, which

permits an opportunity to examine any resilience that may be afforded to the reserve ecosystem by virtue of a presumably naturally more robust balance of interacting biological components. It also takes advantage of the fact that there is time series information available. However, it is important to note that this work is not intended to be a comprehensive ecological review of the Te Angiangi Marine Reserve.

This chapter expands on an otherwise geologically oriented study by examining the possible consequences of catastrophic landslides on coastal marine ecosystems. It condenses and summarises the marine ecological aspects of this project, and is based around the intertidal survey completed after the April 2011 sedimentation event. The results obtained from the post April 2011 intertidal survey are outlined to highlight any trends in the distribution and abundance of the representative species selected, and provide a platform for further study which would extend into the subtidal region of the coast. The results are summarised to demonstrate ecosystem pattern inside and outside the marine reserve, and a preliminary analysis is carried out to explore any inconsistencies in the demographics of the key species.

The aims of the post-event intertidal survey are to (1) examine the effects and response of coastal marine ecosystems to catastrophic scale sedimentation, evidenced by changes in intertidal community structure, and (2) detect any resilience, provided as a result of marine protection, of intertidal communities to sedimentation.

Along with addressing these aims, this chapter reviews information relating to coastal sedimentation and effects on marine organisms; it examines the biology of ecologically and commercially important species present along the Hawke's Bay coastline - paua, kina and seagrass; it examines the conservation ecology of marine reserves in New Zealand in general, and Te Angiangi Marine Reserve in particular; and finally, the chapter examines the potential protection or resilience marine reserves may afford their included ecosystems in the face of physical disturbance.

6.2 BACKGROUND INFORMATION

6.2.1 Coastal sedimentation

What is coastal sedimentation?

Coastal sedimentation is a process where terrestrial sediment, primarily consisting of clay, silt, detritus and most commonly sand, is delivered to the coast (Airoldi, 2003). Principle sources of sediment are derived from rivers, erosion of cliffs and resuspension and transport of sediments. It is important to remember that sedimentation is a natural process which occurs in all marine environments, from soft sediment to rocky shores. Sedimentation can be beneficial to normal ecosystem functioning, for example, organic particulate matter and nutrients (an important food source to many organisms) can be delivered to the coastal marine environment through the sedimentation process (Airoldi, 2003).

Although sedimentation is a natural process, it becomes accelerated primarily due to human activities, for example, through land use change in catchments, particularly the removal of vegetation for forestry, agriculture the development of houses and infrastructure. Accelerated or increased sedimentation as a result of human related activities is now recognised as a significant source of disturbance in coastal marine environments (e.g. Cummings et al., 2009; Hewitt et al., 2003; Ellis et al., 2004; Lohrer et al., 2004; Thrush et al., 2004; Lohrer et al., 2006a; Gillespie, 2007).

Disturbances in the marine environment

Disturbance events in marine ecosystems vary considerably in frequency, scale and effect (Ellis et al., 2000), but are generally viewed as uncommon, irregular events that may cause abrupt changes in the structure of natural communities (Sousa, 1984; Allison et al., 2003). Disturbances can alter the availability of resources, such as food and space, thereby directly or indirectly influencing the structure and function of animal assemblages (Ellis et al., 2000). Disturbances can be either physical or biological in nature (often interacting), with arguably physical sources having the widest ranging effects on marine ecosystems.

Catastrophic disturbances are relatively large-scale disturbances that involve significant mortality, habitat loss and overall disruption to ecosystem functioning

(Allison et al., 2003). Examples of medium to large-scale disturbances in marine environments include algal blooms, disease epidemics, coral bleaching events, hypoxia events, oils spills, increased sedimentation and hurricanes. Frequently the source of biological anomalies such as algal blooms and coral bleaching events, are due to abrupt changes in the physical oceanic regime (temperature and nutrient changes). The nature of catastrophes means they are hard to study because they are relatively rare, they occur in unpredictable locations and at unpredictable times, and their extent is often difficult to easily quantify (Allison et al., 2003), especially if there is no prior information of relevance to the area in question.

A catastrophic sedimentation event could be defined as an event which delivers a huge volume of sediment directly to the coast (from a source such as landslides), in a relatively short amount of time. Sediment delivery into the coastal marine environment through catastrophic cliff failure and erosion of hill sides is already recognised as an important sediment source (Gorsline, 1985), and is relatively common along New Zealand coastlines (Airoldi, 2003). However, to the best of our knowledge, there are no records in New Zealand of a catastrophic sedimentation as a result of coastal landsliding in a marine reserve.

This is important because phenomena such as landslides can result in catastrophic deposition of sediments, which profoundly influences the structure and function of coastal macrobenthic communities (Ellis et al., 2000).

Effects on marine organisms

The ecological consequences of terrestrial sediment in the coastal marine environment is relatively well studied (Thrush et al., 2003; Cummings & Thrush, 2004; Ellis et al., 2004; Lohrer et al., 2004; Thrush et al., 2004; Lohrer et al., 2006a; Lohrer et al., 2006b; Cummings et al., 2009). In more recent times studies are focusing on coral reefs, in light of increased ocean acidification and coral bleaching events (e.g. Rogers, 1990), and also on investigating in freshwater environments (e.g. Ryan, 1991). However, relatively few studies have examined the effects of sediment on coastal rocky reefs (Airoldi & Cinelli, 1997; Airoldi, 2003; Gillespie, 2007). Airoldi (2003) reviews the effects of sedimentation on rocky coast assemblages, and suggests that rocky coasts are potentially one of the habitats most sensitive to increased sedimentation.

The wider ecological effects of sedimentation varies, depending on the type of organism affected and its functional role within the ecosystem. Possible sublethal effects on benthic macrofauna in general include a reduction in feeding and digestion efficiency (Ellis et al., 2000), decreased productivity due to reduced light penetration (Vermaat et al., 1997), smothering (Norkko et al., 2002) and restricted movement. Sessile organisms such as macroalgae, for example seagrass, are affected by fine suspended sediment decreasing water clarity, which hinders sufficient light penetration, and therefore its availability for use during photosynthesis (Vermaat et al., 1997). For grazers, they can either be smothered directly and buried, such that their movement becomes restricted and they unable to transport themselves away from the sediment, or they become affected by fine suspended sediment which allows fine particles to clog their respiratory systems. Mass mortality of coastal sedentary species has been observed and results in an overall change in species diversity and community structure (Sousa, 1984). This can destabilise the community by moving it away from static, or near equilibrium conditions (Sousa, 1984). An example is given of the effect of sedimentation (acting as the disturbance) on ecosystem functioning in a soft sediment ecosystem (i.e. an estuary; Figure 6.1).

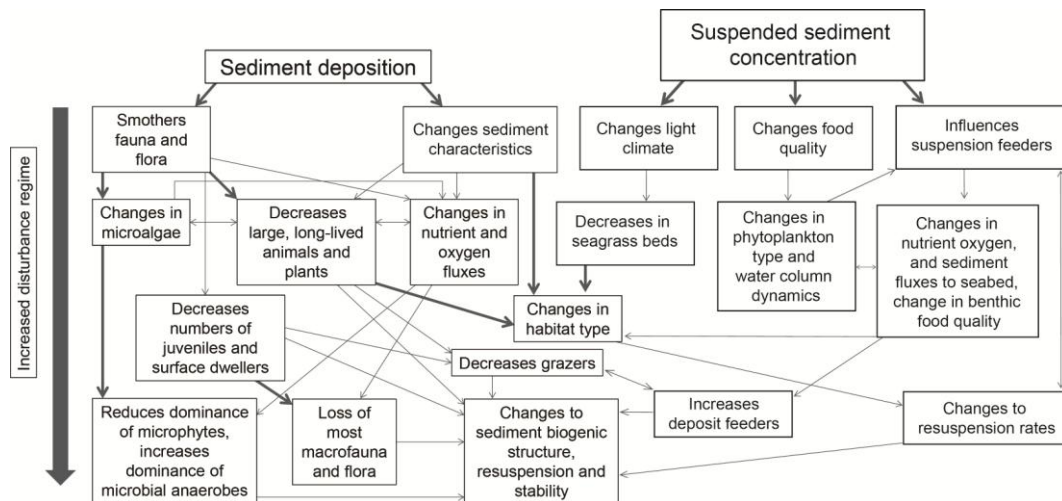


Figure 6.1. The effects of direct sediment deposition and suspended sediment concentration on a soft sediment ecosystem. As the disturbance regime increases, more effects are triggered (modified from Thrush et al., 2004).

Like the ecosystem changes exhibited in estuarine habitats (Figure 6.1), rocky coast habitats are also deeply affected by sedimentation. Rocky coast assemblage composition, structure, dynamics and overall ecosystem functioning is changed to

some degree as a result (Airoldi, 2003). Sediments that accumulate on rocky substrata are important agents of stress and disturbance, and the primary effects include burial, scour, and profound changes to bottom surface characteristics. These are then separated into direct and indirect effects. Direct outcomes are on settlement, recruitment, and growth or survival of individual species, and indirect outcomes are through changes in species diversity, resulting in changes to competition and predator-prey interactions, the latter proving to be a commonly observed and important effect (Fletcher, 1987; Fairweather & Underwood, 1991; Airoldi, 2003). For example the New Zealand kina (sea urchin *Evechinus chloroticus*) play an important role in influencing macroalgae populations, and high kina densities lead to areas void of macroalgae. If kina population is removed, macroalgae populations can re-establish, which in turn influences other organisms living in macroalgae dominated habitats (Shears & Babcock, 2002).

6.2.2 Marine reserves in New Zealand

There are 34 marine reserves established in New Zealand waters, which collectively encompass 7% of the New Zealand territorial sea (Figure 6.2). The first New Zealand marine reserve was established in 1975 at Leigh, the Cape Rodney - Okakari Point Marine Reserve. This was also one of the world's first no-take marine reserves (Ballentine & Langlois, 2008). Marine reserves are specified areas of the sea and foreshore that are protected and managed in order to preserve them in their natural state. It is the most comprehensive tool ensuring area-based biodiversity protection in the marine environment. Within most marine reserves, all marine life is protected and the removal or disturbance of any living or non-living marine resource is prohibited, unless permitted for the purpose of research and monitoring. The purpose of a marine reserve is to preserve the marine ecosystem in its natural state, primarily for the purpose of scientific study (DOC, 2001).

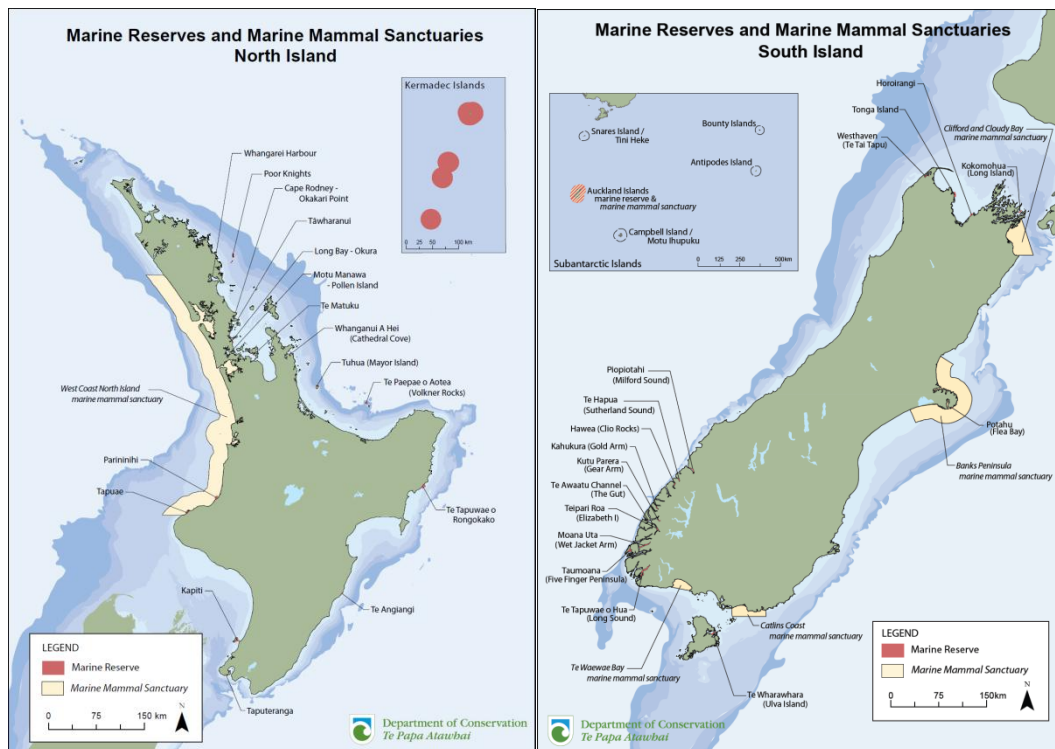


Figure 6.2. Marine reserves in New Zealand (from the DOC website).

Te Angiangi Marine Reserve

The Te Angiangi Marine Reserve (Figure 1.2) encompasses about 446 hectares, which is considered representative of the southern Hawke's Bay marine environment. It contains three general habitats - intertidal mudstone reef, subtidal mudstone reef and a subtidal boulder bank at the northern end of the reserve, adding complexity to the subtidal region of the reserve (DOC, 2001). Beyond the subtidal reef, the substrate consists of fine sand. The intertidal reef is characterised by flora: turfs of coralline algae (*Corallina officinalis*), Neptune's necklace (*Hormosira banksii*) and patches of seagrass (*Zostera capricorni*); and fauna: several species of grazing mollusc, including paua (*Haliotis* spp.) and kina (*Evechinus chloroticus*). The immediate subtidal zone consists of shallow mixed algae, dominated by brown algae (*Carpophyllum maschalocarpum* and *C. plumosum*). The shallow subtidal zone supports stands of kelp forest (*Ecklonia radiata*) with a subcanopy of encrusting and turf algae. Below 12 m encrusting invertebrates become more dominant, with hydroids becoming increasingly abundant with increasing depth. The boulder bank (extending to 36 m deep) is characterised by kelp forest, small red algae (e.g. *Plocamium costatum*), sponges (e.g. *Ancorina alata*, *Iophon* sp., *Raspailia* sp., *Callyspongia* sp., *Reniera* sp.), hydroids, bryozoans and ascidians (e.g. *Hypsistozoa fasmeriana*). Subtidal

populations of rock lobster (crayfish - *Jasus edwardsii*), kina, and grazing gastropods paua and *Cookia sulcata* are present throughout, along with reef fish: (blue cod (*Parapercis colias*), butterflyfish (*Odax pullus*), blue moki (*Latridopsis ciliaris*) and red moki (*Cheilodactylus spectabilis*) (DOC, 1994a and 2001, also see Figure 5.2).

The Te Angiangi Marine Reserve is relatively small compared to most others in New Zealand. Its 446 hectares is compared to much more generous areas of, for example, the Poor Nights Marine Reserve, which is 1890 ha, and the Fiordland marine reserves, which collectively encompass more than 10,000 ha. The Te Tapuwae o Rongokako Marine Reserve just north of Gisborne encompasses a relatively large 2450 ha, and at the other end of the spectrum, the Whangarei Harbour Marine Reserve is 253.7 ha (DOC website). The limited size of the Te Angiangi Marine Reserve has implications for recruitment of marine organisms into the reserve given the close proximity of unprotected coastal regions to the north and south. Nevertheless, the reserve is responding well to protection as evidenced by increases in those species that are usually preyed upon by humans (this is discussed in a later section). Its positive response to protection is encouraging, not only considering its size, but especially so because of illegal poaching occurring in the area (pers. observ.).

6.2.3 Marine reserve effectiveness and resilience

In New Zealand, the spatially scattered nature of marine reserves, perhaps excluding Fiordland's marine reserves, is far from adequate. Entire coastlines protected by a number of marine reserves are ideal for complete conservation and recovery (Ballentine & Langlois, 2008). However, despite whether or not marine reserves encompass entire coastlines, or just a small portion of it, it is widely known that they provide benefits for ecosystem function and health, along with supporting a platform for marine ecosystem functioning research (Ballentine & Langlois, 2008). In New Zealand, and increasingly globally, a 'reserve' effect can be evident as a result of protection, and this is commonly reflected and supported by the increased size and abundance of reserve organisms (particularly those that were formally sought by humans) and increased species diversity (e.g. Allison et al., 1998; Babcock et al., 1999; Kelly et al., 2000; Allison et al., 2003; Denny et

al., 2004; Shears & Babcock, 2004; Shears, 2007; Ballentine & Langlois, 2008; Micheli et al., 2012).

Allison et al. (1998, 2003) recognise that reserves do harbour the benefits mentioned above, and are therefore essential to marine conservation, and their efficiency can be increased by ensuring their design is scientifically sound and they are implemented well. However, their potential effectiveness is limited by large-scale ecological processes occurring within and surrounding reserves. Processes such as recruitment can occur on a very large spatial and temporal scale, which means reserve populations may not benefit directly from localised populations within the reserve. Areas immediately outside of reserves may benefit greatly from what is called the spill-over effect, where juveniles generated from within the reserve are added to populations just outside of the reserve boundary. Integrated protection of organisms within and outside reserves are needed in order for reserves to function optimally (Allison et al., 1998). Reserves with stable ecosystem functioning are more likely to withstand disturbance events, and this benefits non-reserve populations since the reserve populations are able to recover faster and continue reproducing (Micheli et al., 2012).

Empirical evidence that reserves do increase resilience of reserve populations is lacking because it is rare for disturbances to be tested within marine reserves (Allison et al., 1998; Micheli et al., 2012). However, resilience exhibited by reserve organisms after a disturbance is widely hypothesised (e.g. Ballentine & Langlois, 2008). Resilience is the ability of populations and ecosystems to adsorb disturbance while retaining their function and provision of ecosystem services, which may help combat the impacts of major disturbances (Micheli et al., 2012). Grafton et al. (2003) demonstrate that the resilience of a population is improved within a reserve. In the Grafton et al (2003) study, this was achieved by looking at the recovery time of a population, and improved resilience was defined by the amount of time taken for the population to reach within one standard deviation of the population level prior to the disturbance. A shorter period of time represents a higher level of resilience, and there is indication that resilience improves further with larger reserve size. Micheli et al. (2012) has recently studied the response of marine reserves to climate-driven hypoxia, and has shown that marine reserves increase resilience of marine populations to mass mortality. This is shown by

juvenile replenishment, which remained stable despite mass mortality of adult populations. This benefit was extended as spill over effect to non-reserve organisms (Micheli et al., 2012).

The sedimentation event which has taken place at the Te Angiangi Marine Reserve and adjacent coastline has provided a very rare natural experiment opportunity, which tests the resilience of protected marine organisms to a disturbance. The results of the current survey will provide valuable insight into the effectiveness of reserves, and it will broaden our understanding on whether marine organisms from within a marine reserve are more resilient to disturbances because of any potential reserve protection effects, of which empirical evidence is largely lacking (Micheli et al., 2012).

6.2.4 Biology of paua, kina and seagrass

It has been demonstrated that within New Zealand marine reserves, grazers such as kina and paua are particularly important to monitor because these species readily undergo changes in distribution and abundance once human predation pressure has been removed (DOC, 2001). Paua, kina and seagrass are therefore key species examined in the current intertidal survey, hence it is important to understand their life cycles, recruitment patterns, and preferred habitats. These aspects need to be considered when explaining and drawing conclusions on the findings of the survey.

Paua (*Haliotis* spp.)

Paua (New Zealand abalone) is a large marine gastropod belonging to the phylum Mollusca and the family Haliotidae (Costales et al., 2009). There are three species of paua found in New Zealand's waters, the most common is the black-foot paua (*Haliotis iris*; Figure 6.3), the less common is the yellow-foot paua (*Haliotis australis*), and the rare white-foot paua (*Haliotis virginia*). The first two species are harvested commercially from wild populations and are found at the Te Angiangi Marine Reserve. All three species are harvested recreationally (Freeman, 2006).



Figure 6.3. The most common species of paua in New Zealand, the black-foot *Haliotis iris* (from nabis.govt.nz).

Paua are herbivorous, feeding primarily on drift algae and other macroalgae (algae ranging in size from mm to m). They usually do not feed on plants attached to the substrate, and *Haliotis iris* forage mostly at night. Juvenile paua feed on diatoms until they are about 10 mm in length. Main predators of the paua are starfish (*Astrosole scabra*), blue cod (*Parapercis colias*), snapper (*Pagrus auratus*), rock lobster (*Jasus edwardsii*) and octopus (*Amphioctopus* sp.) (Costales et al., 2009).

Paua larval dispersal longevity is relatively short - paua larvae will settle between 3 to 10 days. This means that the larval population can have limited dispersal from the spawning adult population (Freeman, 2006). However, this does depend on the local hydrodynamics, which may allow larvae to be dispersed locally or much further away from the spawning population. This has implications for paua recruitment, as the juvenile paua population could then be reflective of the adult paua population. Newly settled larvae paua live in reduced flow environments, mostly on crustose coralline algae habitats, where they can attach and grow. Once they become juveniles (40 to 45 mm in shell length) they move to and live in cryptic habitats, such as beneath rocks and boulders, until they are between 60 to 70 mm in shell length (3 to 5 years old) and have reached sexual maturity. They are then relatively exposed and found most abundantly in water depths less than 5 m, and are found generally up to 10 m water depth (Freeman, 2006). They are

found in beneath rocks or ledges in crevices and rock pools, and have a muscular foot used to attach themselves securely to a hard surface, thereby enabling them to withstand constant and severe hydrodynamic forces. The legal size for paua is 125 mm shell length, which encompasses the range from when paua reach sexual maturity to a couple of years after, to allow the population to spawn before they are fished. Legal sized paua are typically only found in pockets along the northern and central coastline of the North Island (Freeman, 2006).

Paua is an important invertebrate macrograzer in many of New Zealand's marine communities and they often coexist and compete with sea urchins, or kina. Kina (*Evechinus chloroticus*) also feed on drift algae and sometimes their grazing activity is thought to decrease space available to newly settling paua larvae.



Figure 6.4. The New Zealand sea urchin, or kina *Evechinus chloroticus* (from forestandbird.org.nz).

They are found throughout the rocky intertidal and shallow subtidal shores of New Zealand, living and hiding in ledges of crevices and rock pools in water depths less than 14 m. Kina are also herbivores, feeding on encrusting algae, drift algae and macroalgae, with a particular affinity for kelp (*Ecklonia radiata*). Therefore, kina have a significant influence on and can be responsible for algae distributions on shallow reefs, and when they are in high abundance. When abundant, they can produce 'barrens' of reef completely void of algae. Main predators of kina are rock lobster (*Jasus edwardsii*), starfish (*Astrosole scabra*), snapper (*Pagrus auratus*), and octopus (*Amphioctopus* sp.), and their spines and cryptic nature are designed to protect from predation. It is observed that marine

reserves can regulate kina abundance through the increase of their predators, due to the reserve effect (Shears & Babcock, 2002). Kina do not have a minimum size at which they can legally be harvested by humans, and the size at which they reach sexual maturity varies from 30 to 75 mm in test diameter (the diameter of their shell or test, not including their spines; James, 2006).

Kina larval dispersal longevity is far greater than that of paua. Kina larvae are dispersed by hydrodynamic forces for at least 30 days before they settle, and therefore can be dispersed far from the spawning population. Indeed larvae produced from the Te Angiangi Marine Reserve population may be transported as far away as Gisborne, where larval populations from the marine reserve there (Te Tapuwae o Rongokako Marine Reserve) could potentially intermix (Freeman, 2006). It is therefore likely that any larvae produced in the Te Angiangi Marine Reserve do not settle and become part of the Te Angiangi Marine Reserve population. It has already been suggested by Oldman et al. (2006) that reefs to the north outside of the marine reserve are likely receiving large numbers of larvae derived from spawning populations within the marine reserve as a result of local hydrodynamics (section 5.2.3.2). Larval kina then metamorphose into juvenile kina and remain cryptic for 2 to 3 years, then become emergent at sizes more than 30 mm test diameter. They are classified as adults at more than 30 mm test diameter (SITO, 2006).

Seagrass (*Zostera capricorni*)

New Zealand seagrass is represented by one genus, *Zostera*, which belongs to the family Zosteraceae. (Turner & Schwarz, 2006). There has been difficulty in the taxonomic differentiation between seagrass species within New Zealand and also between New Zealand and Australian species, and as a result some New Zealand and Australian seagrass species have been merged and are now referred to as *Zostera capricorni* (Turner & Schwarz, 2006). The current, and previous surveys, deal with *Zostera capricorni* (Figure 6.5).



Figure 6.5. Seagrass *Zostera capricorni*, surrounded by Neptune's necklace (*Hormosira banksii* top and bottom right corners of the photo) within a 0.25 m² quadrat.

Seagrass occurs predominantly intertidally in New Zealand, but occasionally occurs in shallow subtidal areas of sheltered estuaries, and therefore are found at depths ranging from 2 to 12 m water depth. The depth at which they are found is mostly related to the light intensity, since they need sufficient light for photosynthesis. The most extensive seagrass beds occur in soft substrates (sand and mud) where they can form continuous expanses of vegetation, or a mosaic of patches of various sizes (Turner & Schwarz, 2006). Seagrass beds are also distributed as a function of the tidal regime, and are usually found in abundance in the region extending from the low shore (the seaward edge of the intertidal platform) to the middle shore (although extensive subtidal beds can be found in the far north). They require a protective water layer in order to prevent desiccation, so are often not found in the high shore (terrestrial edge of the intertidal platform) (Turner & Schwarz, 2006).

Seagrass are flowering plants which are specifically adapted to living in a submerged marine environment. They require an adequate rooting substrate, since they have an extensive system of roots which allow the plants to withstand wave action and tidal currents, and also aid in extracting nutrients and minerals from sediment pore-waters. They require sufficient immersion in seawater (to avoid desiccation) and sufficient light: their leaves retrieve oxygen and capture light, and each stem typically has between 3 and 5 leaves per shoot (Turner & Schwarz, 2006).

Seagrass perform a variety of functions within coastal ecosystems, and can therefore be considered a valuable component in an overall coastal ecosystem functioning (Turner & Schwarz, 2006). They are representative of areas of high productivity since they themselves are highly productive, and provide food sources and habitat for many organisms utilising seagrass beds. The habitat provided within seagrass beds is low-energy, since seagrass beds increase bottom friction thereby decreasing current speeds, which facilitates the deposition and retention of sediment. This in turn stabilises bottom sediments and provides protection against erosion. This is a very important function of seagrass, mainly because their ability to trap and retain terrestrially derived sediment then improves water clarity and quality (Turner & Schwarz, 2006). However, excess or an increased sedimentation rate (including changes in the proportion of fines) may have detrimental effects. If the point at which seagrass can retain sediment is exceeded, excess suspended sediment in the water column decreases light penetration which may cause harm or death.

6.2.5 Te Angiangi Marine Reserve previous survey work

The Te Angiangi Marine Reserve was established in 1997, and marine surveys have been carried out in the area since 1990. Data has been gathered on key intertidal and subtidal species during surveys conducted by the Department of Conservation and more recently by Victoria University of Wellington students. Data collected before 1997 act as pre-reserve data or baseline data, and data collected after 1997 act as post-reserve or monitoring data, all of which is described in several published and unpublished reports (Table 6.1).

Table 6.1. Pre-reserve and post-reserve surveys done on the reef platform, paua and kina, and seagrass, and their associated references.

		Intertidal				Reference
			Reef platform	Paua / Kina	Seagrass	
Pre-reserve / baseline data	1990	Mar-Jun	✓			Creswell & Warren, 1990
	1994	May	✓			DOC, 1994b
Reserve established	1997	Aug				
Post-reserve / monitoring data	1999 ¹	Sept		✓		Freeman, 2001 & 2006
	2000	Sept		✓		Freeman, 2001 & 2006
	2001	Sept		✓		Freeman, 2001 & 2006
	2002	Sept		✓		Freeman, 2006
	2003	Sept		✓		Freeman, 2006
	2008	Sept		✓		Victoria University of Wellington students - reference unknown
	2009 ²	Feb		✓	✓	Paua/kina - Costales et al., 2009. Seagrass - Flemming et al., 2009 (VUW)
	2010	Feb			✓	Butler et al., 2010 (VUW)
	2011	Sep, Nov-Dec		✓	✓	This thesis

¹ Monitoring of intertidal populations of paua and kina began in 1999.

² Monitoring of seagrass began in 2009.

Because the focus of this project is on the intertidal marine assemblages, subtidal surveys are not discussed in detail here. In brief, several extensive subtidal surveys have been carried out at both reserve and non-reserve sites since 1995 on paua, kina, crayfish (or spiny lobster *Jasus edwardsii*), and reef fish (blue cod (*Parapercis colias*), butterfish (*Odax pullus*), blue moki (*Latridopsis ciliaris*) and red moki (*Cheilodactylus spectabilis*); Freeman & Duffy, 2003). Data collected during these surveys is used to estimate fish density, community compositions, size frequency distributions, habitat descriptions, along with crayfish density, size and sex frequency and distributions (DOC, 2001).

Pre-reserve surveys

Creswell and Warren (1990) conducted the first intertidal and subtidal survey of the area, from Kairakau to Whangaehu for intertidal, and Kairakau to Aramoana for the subtidal work. Following this survey, in 1994, three years prior to the legal protection of the area, an intertidal survey of the reef platform within the proposed

reserve area was conducted by DOC (2001). These two studies are the only ones that have described in detail all species present of the intertidal platform.

Post-reserve surveys

Regular intertidal and subtidal monitoring was carried out since establishment of the reserve until 2003 to assess the response of organisms to the protection afforded by the reserve. Between 1999 and 2003, intertidal populations of paua (*Haliotis* spp.) and kina (*Evechinus chloroticus*) were monitored at sites within and outside of the reserve (Freeman, 2001 and 2006). In September 1999, populations of paua and kina in intertidal crevices and channels were examined at three sites: Blackhead, the marine reserve and Aramoana. 10 channels were sampled at each site. For each channel, all paua and kina were measured, either *in situ* or by carefully removing the animal. Kina test diameter and paua shell length was recorded to the nearest millimetre. In September 2000, 2001, 2002 and 2003 this survey was repeated (Freeman, 2006).

Victoria University of Wellington students examined intertidal populations of paua and kina in 2008 (data was not obtained from this survey), and they were re-examined again by Victoria University students in 2009 (Costales et al., 2009). In 2009, four sites were established: two within and two outside the reserve (one at Blackhead and one at Aramoana). These sites roughly matched the sites used in previous surveys. At each site two intertidal shore heights were sampled - the low (seaward edge of the platform) and middle shore. At each shore height three 10 m x 10 m transects were laid out where channels were present, and all channels searched for all paua and kina which were then measured.

Also in 2009, the first survey focusing solely on seagrass (*Zostera capricorni*) in the area was carried out, with the aim of establishing a seagrass monitoring program (Flemming et al., 2009). This study involved sampling seagrass beds from four sites: two within and two outside of the reserve (one at Blackhead and one at Aramoana). Three transects were established at each site, one in each of the low (seaward edge of the platform), middle, and high (terrestrial edge of the platform) areas of the platform. Within each of these transects, 10 x 0.25 m² quadrats were haphazardly placed and used to estimate the percent of seagrass

cover, percent of green seagrass, the average blade length, shoot density, any invertebrates were counted and identified, and the presence of epiphytes noted.

One year after this survey, Butler et al. (2010) re-examined seagrass but using different methodology. Three sites within the reserve and two outside (one at Blackhead and one at Aramoana) were established. At each site a 25 m wide by 100 m long area was measured out and all seagrass patches within this area were measured (maximum width by maximum length). Within the same area for each site, 10 randomly selected patches were used to estimate shoot density using a 0.25 m² quadrat for each patch.

Main conclusions made from the 1999 to 2003 intertidal paua and kina survey data, are (1) densities of kina remained low but stable within the marine reserve, in contrast with kina density at non-reserve sites which were variable and occasionally high. In 2001 kina were significantly larger within the marine reserve, compared to non-reserve sites and marine reserve populations in 1999 and 2000; and (2) densities and mean size of paua was higher within the marine reserve. The mean size of paua within the reserve increased between 1999 and 2001 and remained stable until 2003 (Freeman, 2006). Conclusions made from the 2009 and 2010 seagrass survey data are: (1) intertidal reef platform elevation attributes (i.e. low, middle or high shore height on the intertidal platform), was the main factor influencing seagrass cover, greenness, blade length and density, rather than any potential reserve effects (Flemming et al., 2009); (2) total seagrass coverage was significantly higher at non-reserve sites, although this is likely not related to any potential reserve effects, but rather lack of sufficient sampling size (Butler et al., 2010); and (3) since there are no pre-reserve seagrass survey data, it is hard to detect any potential reserve effects in both of these studies.

These data generally indicate the reserve was functioning well, or at least beginning to take effect before the catastrophic sedimentation event occurred in April 2011. It then could be hypothesised that since populations within the reserve are naturally more stable and of greater abundance than the adjacent unprotected coastline, that the protected populations would exhibit an increased resilience to the sedimentation and that populations would remain stable (with perhaps a slight decrease) compared to unprotected populations exposed to the same

sedimentation event. This is a major hypothesis of this chapter and will be examined in a later section.

6.3 SURVEY DESIGN

The sampling design used in the current survey builds on the previous DOC monitoring design for intertidal paua and kina, and the Costales et al. (2009) intertidal paua and kina survey. It was designed to encompass the varied designs of previous seagrass survey designs to permit some across survey comparison.

Firstly, the number of sites used for sampling were increased and balanced, so there were an equal number of reserve and non-reserve sites. Consequently, four reserve sites two in the southern half and two in the northern half were established, along with four non-reserve sites two at Blackhead and two at Aramoana (Figure 6.6). The sites are labelled from A to H, A being the most southern site and H being the most northern (Figure 6.6). The placement of the sites in the current survey generally matched the location of the sites used in all previous surveys. However, site selection was influenced by the location and the vertical and horizontal extent on the landslide debris, which in some places, particularly in the northern half of the reserve, buried a significant portion of the intertidal platform. It was also nearly impossible to re-sample the exact same channels sampled during previous paua and kina surveys, but the sites encompassed the general location of most channels.

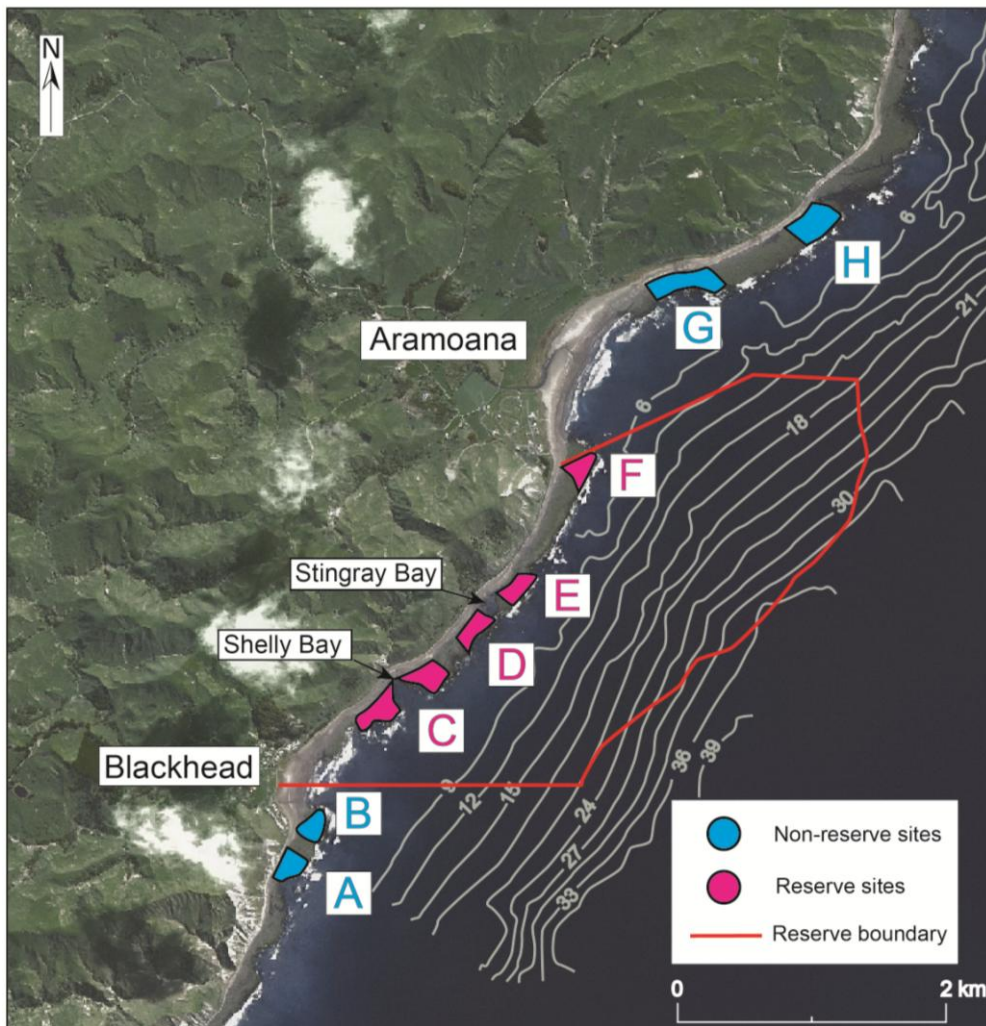


Figure 6.6. Locations of non-reserve and reserve sites used in the 2011 intertidal survey.

At each of these sites paua, kina and seagrass were examined (Table 6.2). The number of channels originally sampled for paua and kina by DOC were doubled, so 20 channels were sampled altogether at each site. This was split so 10 channels were sampled in the low (seaward edge of the platform) and 10 in the middle shore, as per the Costales et al. (2009) survey design.

The seagrass sampling design combined both Flemming et al. (2009) and Butler et al. (2010) designs. To recap: Flemming et al. (2009) used quadrats placed at different shore heights (low, middle and high) to estimate the percent of seagrass cover, percent of green seagrass, the average blade length, and shoot density at four sites altogether. Butler et al. (2010) established five sites altogether and measured all seagrass patches within a 25 m x 100 m transect at each site. Shoot density was also estimated from quadrats within each transect. The current survey combined these two designs together, so at each site three 25 m x 100 m transects

were sampled, an area of 7500 m² altogether. Within each transect: (1) all seagrass patches were measured, maximum width and maximum length, and (2) ten 0.25 m² quadrats were haphazardly placed and used to estimate the percent of seagrass cover, percent of green seagrass, the average blade length, shoot density, any invertebrates were counted and identified.

Table 6.2. A list of sampling undertaken at each site. The number of seagrass transects sampled varied due landslide debris extending onto the intertidal platform, which reduced the area available for sampling. Sites E and F were severely impacted by debris, and therefore any area available was measured out and sampled.

		# Paua/kina channels sampled		Seagrass		
	Site	Middle shore	Low shore	# Transects	Total area sampled (m ²)	# Quadrats
Non-reserve	A	10	10	1	2500	0
	B	10	10	3	7500	10
Reserve	C	10	10	1	2500	10
	D	10	10	3	7500	10
	E	10	10	1	15752	10
	F	10	10	1	8400	10
Non-reserve	G	10	10	3	7500	9
	H	10	10	3	7500	10

Multiple BACI

The current survey loosely represents a Multiple Before After Control Impact (MBACI) design, which is a design that can be applied in a situation where there is more than one impacted site, and multiple impact and control locations which can be sampled at multiple times before and after the impact (Kingsford & Battershill, 1998). However, it is not a complete MBACI experiment due to lack of control reserve locations, since the most of the intertidal platform was impacted by sediment. Sites C and D arguably could be classed as reserve control locations (in a separate nested design) since these sites evidenced low levels of direct sediment deposition..The two non-reserve sites to the south at Blackhead are impacted sites, as there was significant sedimentation from landslides present at both sites. Most of the intertidal platform at the marine reserve was inundated with sediment and therefore the reserve sites are also impacted sites (but have come from a different start point with respect to the abundance of key intertidal species present). The two non-reserve sites to the north at Aramoana were not impacted by sedimentation, and act as non-reserve control locations.

Multi-stressor experiment

Stress is a commonly used to describe different physiological or ecological conditions at the extremes of environmental gradients, for example: the conditions of organisms at the interfaces of differing zones across wave-exposure gradients in rocky intertidal communities. Stress can also describe the response of a biological community to a disturbance event that is foreign to the ecosystem, or is natural but is of a significant frequency or intensity as to cause ‘abnormal’ tensions (Ellis et al., 2000). The community response will depend on the intensity and extent of the stress, and the resistance and resilience of the community once the stress has been lifted (Ellis et al., 2000). A stressor is an event, external stimulus, or environmental condition which causes stress to an organism.

This survey can also be viewed as an investigation into a multi-stressor situation or ‘natural experiment’, where the individual and combined effects of the stressors sedimentation and human predation are examined (Table 6.3).

Table 6.3. Human predation and sedimentation stressors acting upon areas to the south at Blackhead (BH), the marine reserve (MR) and to the north at Aramoana (ARA).

	BH	MR	ARA
Sedimentation	+	+	-
Human predation	+	-	+

At Blackhead, there are both sedimentation and human predation stressors acting on the paua and kina populations. At the marine reserve there is only the sedimentation stressor, since the reserve is protected from human predation. At Aramoana there was no significant landsliding and therefore only a human predation stressor (although the location would likely have received some current derived sediments from the adjacent coast, even if only relatively temporarily during the height of storm events). The individual and combined stressors will be considered when assessing the findings of the survey and drawing conclusions.

6.4 FIELD METHODS

The survey was completed over three excursions, the first in early September 2011 (2-9th), the second in late November (29-30th) and early December 2011 (1st), and the third in mid December 2011 (13-14th). Paua and kina populations, and seagrass properties were examined in the first trip for sites A-D, the second for sites E-F, and the third for sites G-H.

6.4.1 Paua and kina

20 channels were chosen on the intertidal platform of each site- 10 in the lower section of the platform and 10 in the middle section of the platform. Channels were chosen based on their habitat suitability for paua and kina to live in, and varied in length from 3-10 m (average 8.3 m), width 0.2-2.5 m (average 0.81 m) and depth 0.05-0.5 m (average 0.26 m). One or two GPS points were taken at each channel, then thoroughly searched for all paua and kina and every individual found was measured using a calliper and recorded. If the individual could not be carefully removed then it was measured *in situ* to the nearest 5 or 10 mm. Paua shell length and kina test diameter was measured, both to the nearest mm if they were able to be safely removed from the channel (Figure 6.7).



Figure 6.7. Paua on the underside of a rock about to be measured using callipers.

6.4.2 Seagrass

Several aspects of seagrass were examined: patch size, seagrass cover, percent of green seagrass, blade length and shoot density. These aspects are used as indicators of seagrass abundance and health at each site.

Average patch size and cover

Firstly, three 25 m x 100 m transects were laid out using measuring tapes. If the site was not large enough (i.e. space was limited by landslide debris which had extended onto platform) any area that was available was measured out. The 100 m length of the transects attempted to include the first occurrence of seagrass at the high section of the reef and the last occurrence at the low section. It generally encompassed the entire middle section of the intertidal reef. To get an estimate of seagrass cover and mean patch size on the intertidal platform, all seagrass patches within the transects were measured using a measuring tape along its maximum width and the maximum length, and recorded. Ten x 0.25 m² quadrats were haphazardly placed on random patches of seagrass within the transects and used to estimate the percent seagrass cover within the quadrat, and percent of green seagrass (as opposed to brown or dying seagrass). Blade length, and average blade density was measured from counts made on seagrass clumps within 8cm² subquadrats (Figure 6.8). Any invertebrates found within the quadrat were counted, identified and recorded. A GPS point was taken at the position of each quadrat.



Figure 6.8. A 0.25 m² quadrat used to measure seagrass parameters. Outlined in the red circle is a smaller 8 cm² quadrat used to estimate shoot density.

Percent cover

The percent of total seagrass coverage was visually estimated within the quadrat to the nearest five percent.

Percent green

The percent of green seagrass was visually estimated by comparing green blades with total blades within the quadrat to the nearest five percent.

Average shoot density

3 x 8 cm² quadrats were haphazardly placed within the 0.25 m² quadrat and used to estimate shoot density. Each blade in the small quadrat was counted by counting one stem and multiplying it by 3 (since each stem typically had 3 blades) and recorded.

Average blade length

To estimate average blade length, 10 blades were randomly chosen and measured using a ruler along their vertical axes from the base of the stem to the tip, and recorded.

6.5 STATISTICAL METHODS

Paua, kina and seagrass data from the current survey, along with raw data on the size of paua and kina counted in the 1999 to 2003 DOC monitoring surveys (for multi-year comparisons) were analysed and are presented graphically (using STATISTICA Version 11).

The results focus on paua and kina size and abundance. T-tests were used to establish the magnitude of differences between reserve and non-reserve paua and kina from the current survey. The data did not violate the assumptions of the test.

Paua and kina density estimates for the multi-year comparisons were obtained by dividing the number of paua/kina sampled by the length of the channel they were sampled from. Standardising numbers of paua/kina to the average number counted per metre provides a more accurate comparison to be made between the 2011 and 1999-2003 survey results. The current survey sampled 80 channels within the reserve, 40 at Blackhead, and 40 at Aramoana, compared to the 10 channels sampled at each of these locations in the DOC surveys. This is taken into consideration when interpreting the results.

6.6 RESULTS

6.6.1 Intertidal 2011 survey results

The 2011 intertidal paua and kina results are presented for each shore height at each site. Sites A, B, G and H represent non-reserve populations and sites C, D, E and F represent reserve populations.

6.6.1.1 Paua

Total paua abundance and size results from the middle and low shore for each site are shown in Figure 6.9.

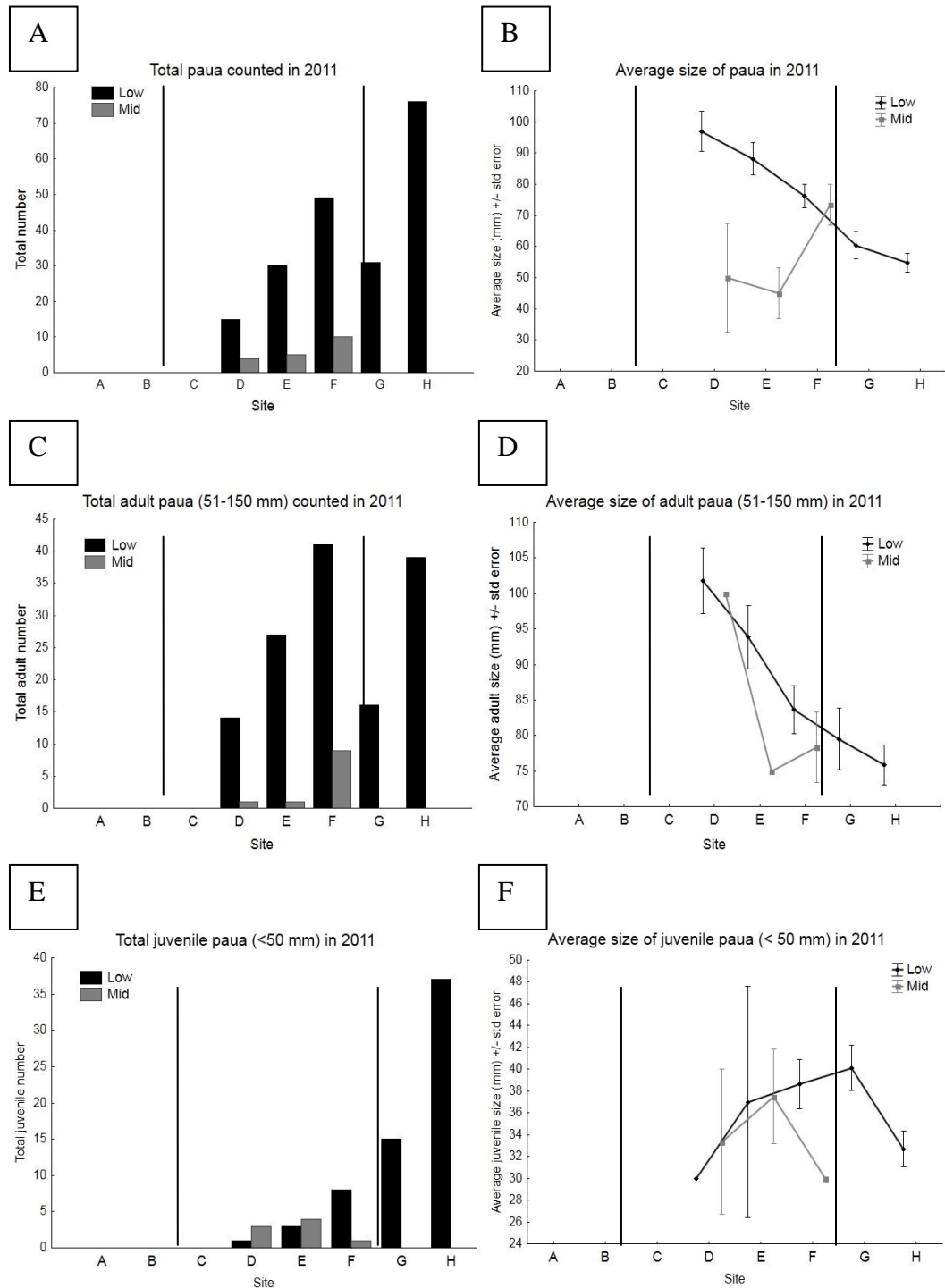


Figure 6.9. Paua abundance and size at each of the low and middle shore heights for each site. Reserve (C, D, E, F) and non-reserve (A, B, G, H) sites are delineated by the black vertical lines. Shown is the total paua counted (A) and their average size (B). This total is divided into adult (>50 mm length) and juvenile number (<50 mm length; C and E respectively) and average size (D and F respectively).

The number and size of paua sampled in the low shore are greater than those sampled in the middle shore height. This is most likely because the low shore contain more of paua's preferred habitat. Abundance generally increases from south to north. Adult (>50 mm) paua (Figure 6.9D) is larger within the reserve compared to outside the reserve, and the number and size of juveniles (< 50 mm; Figure 6.9E and F) generally increases from south to north, except for at site H where there is a large number of small juveniles.

When sites are grouped into reserve and non-reserve locations, in total, more paua were found within the reserve ($n = 113$) compared to outside the reserve ($n = 107$), and all the paua found outside the reserve were from Aramoana since no paua were found at Blackhead (despite there being suitable habitat at that location). A greater number of adult paua were found within the reserve ($n = 93$) compared to outside the reserve ($n = 55$), while a greater number of juvenile paua were found outside the reserve ($n = 52$), compared to the number of juvenile paua found inside the reserve ($n = 20$).

This difference in population composition is reflected in the average size of all paua sampled outside the reserve ($56.4 \text{ mm} \pm 25.4 \text{ SD}$), which was significantly smaller than the average size of all paua sampled within the reserve ($79.6 \text{ mm} \pm 28.5 \text{ SD}$; $t = -6.33$, $p < 0.001$).

6.6.1.2 Kina

Total kina abundance and size results from the middle and low shore for each site are shown in Figure 6.10.

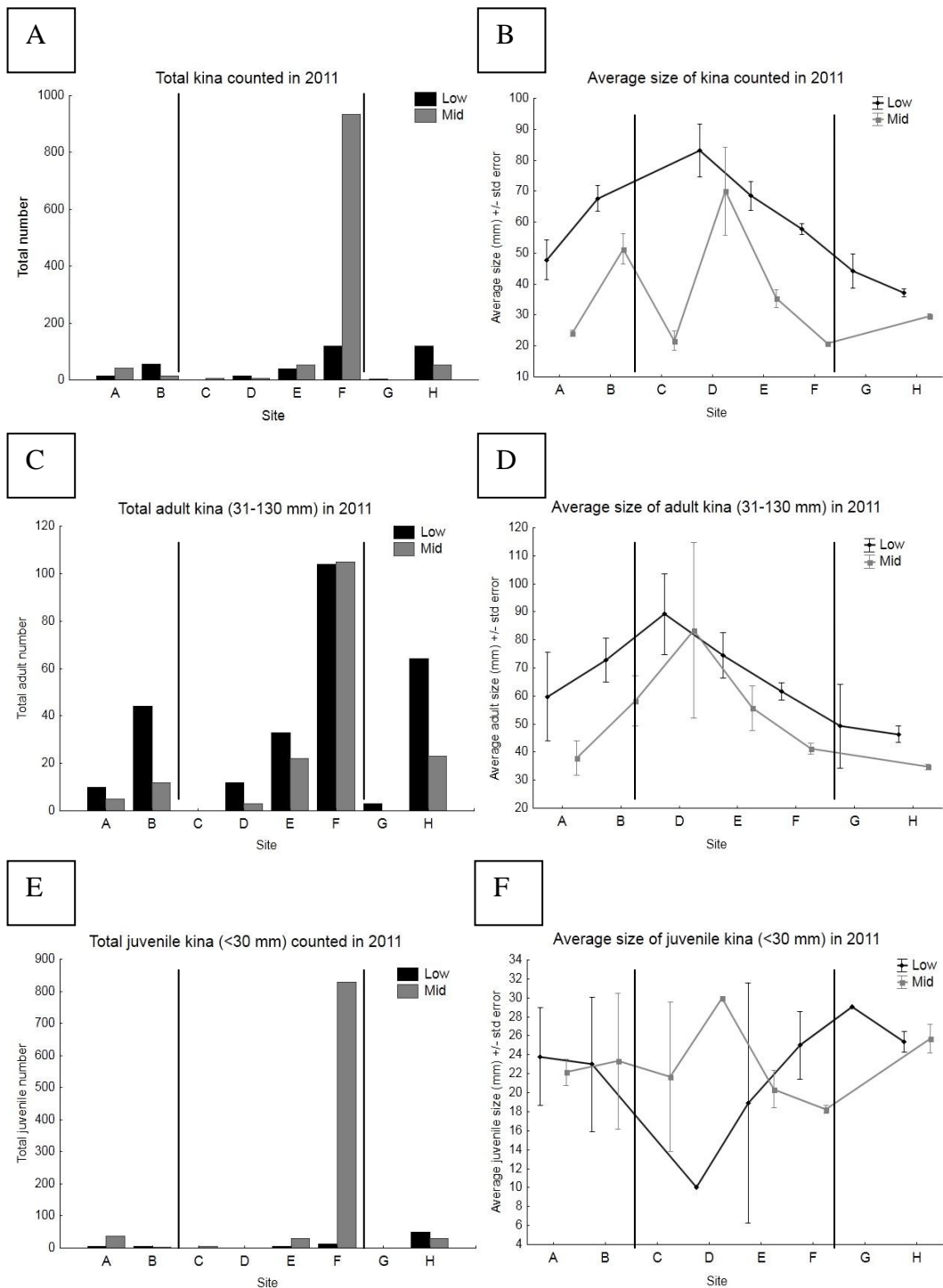


Figure 6.10. Kina abundance and size at each of the low and middle shore heights for each site. Reserve (C, D, E, F) and non-reserve (A, B, G, H) sites are delineated by the black vertical lines. Shown is the total paua counted (A) and their average size (B). This total is divided into adult (>30 mm in size) and juvenile number (<30 mm in size; C and E respectively) and average size (D and F respectively).

Kina were more abundant within the reserve, and when the influence of the high number of juvenile (<30 mm) kina sampled at site F is removed (Figure 6.10C), more kina were found at the low shore height compared to the middle shore height. Juvenile kina were generally larger in the middle shore height within the reserve, while adult (>30 mm) kina were larger at the low shore height at all sites. The kina abundance trends appear typical of a marine reserve effects with high numbers in the centre of the reserve dropping toward either boundary.

When sites are grouped into reserve and non-reserve locations, in total, more kina were found within the reserve ($n = 1161$) compared to outside the reserve ($n = 292$). A greater number of adult kina were found within the reserve ($n = 279$), compared to outside the reserve ($n = 161$), while a greater number of juvenile kina were also found within the reserve ($n = 882$), compared to the number of juvenile kina found outside the reserve ($n = 131$).

This difference in population composition is reflected in the average size of all kina sampled outside the marine reserve ($40.4 \text{ mm} \pm 27.7 \text{ SD}$), which was significantly larger than the average size of all kina sampled within the marine reserve ($27.5 \text{ mm} \pm 19.9 \text{ SD}$; t -value = 9.66, $p < 0.001$). The large number of juveniles sampled from within the reserve (site F, Figure 6.10E) heavily influenced the average size of all kina within the reserve.

Overall, paua and kina size and abundance of reserve and non-reserve populations has yielded some interesting results (Table 6.4), the implications of which will be discussed in a later section

Table 6.4. Main paua and kina results for reserve and non-reserve populations sampled in the 2011 survey.

	Reserve	Non-reserve
	Paua	
Average size (mm)	79.6	56.4
Total number	113	107
Adult number (>50 mm)	93	55
Juvenile number (<50 mm)	20	52
	Kina	
Average size (mm)	27.5	40.4
Total number	1161	292
Adult number (>30 mm)	279	161
Juvenile number (<30 mm)	882	131

6.6.1.3 Seagrass

Seagrass results are divided into transect and quadrat results. The transect data provide a percent of seagrass cover over large spatial scales and average patch size for each site, therefore providing an indication of overall abundance at each site. The quadrat results show the percent of seagrass cover and greenness, and average blade length and shoot density at each site, therefore providing an indication of health at each site.

Transects

The percent of seagrass cover and the average patch size (m²) derived from the transects are given for each site (Table 6.5 and Figure 6.11).

Table 6.5. Seagrass transect results. Shown is the total area sampled at each site, the area and percent of seagrass found within that area, and the mean patch size for each site. A comparison of the total percent seagrass cover between reserve and non-reserve sites is also shown.

Location	Site	Site area (m ²)	Total seagrass cover (m ²)	Seagrass cover %	Average patch size (m ²)
BH	A	2500	65.4	2.61	5.94
BH	B	7500	325.8	4.34	3.88
MR	C	2500	25.7	1.03	2.85
MR	D	7500	399.6	5.33	3.00
MR	E	15752	946.3	6.01	7.15
MR	F	8400	849.5	10.11	8.33
ARA	G	7500	336.6	4.49	3.78
ARA	H	7500	1051.2	14.02	2.63
	Total area	59,152	4,000	6.76	
	Reserve area	34,152	2,221	6.50	
	Non-reserve area	25,000	1,779	7.12	

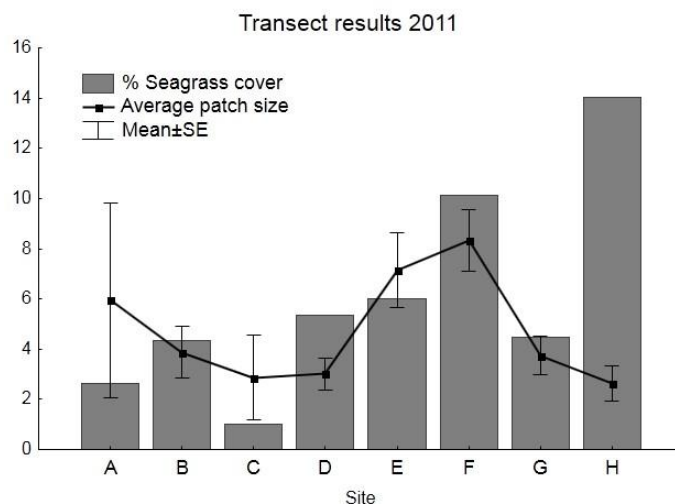


Figure 6.11. Seagrass cover and average patch size at each site.

Transect results show a general trend where seagrass cover increases from south to north, with site F (reserve site) and site H (non-reserve site) showing the most cover. Site F also has the largest average patch size, in comparison with site H, which has the smallest average patch size. This indicates that site H displayed a high abundance of small patches. However, about 50% of seagrass patches that

were measured at that site were dead, or in poor health. About 20% and 80% of seagrass at non-reserve sites B and G respectively were also dead or in poor health.

Seagrass quadrats

The percent of seagrass cover, and the percent of that seagrass which was green for each site is shown in Figure 6.12A. The average blade length and average shoot density for each site is shown in Figure 6.12B.

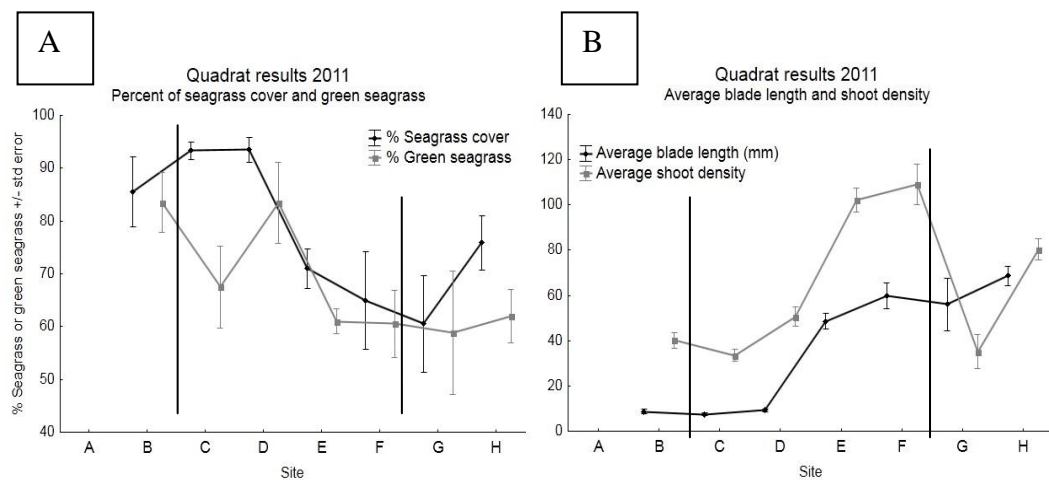


Figure 6.12. Seagrass quadrat results for each site. Shown is the percent of seagrass cover within the quadrat, and the percent of that seagrass which was green (A). B shows the average blade length and average shoot density (shoot density was estimated using small 3 x 8 cm² quadrats). Reserve (C, D, E, F) and non-reserve (A, B, G, H) sites are delineated by the black vertical lines.

Seagrass quadrat results give an indication of seagrass health at each site. Generally, seagrass cover within the 0.25 m² quadrat, and percent of green seagrass decreased from south to north. The average blade length and shoot density increased within the reserve sites, and the average shoot density increased from south to north.

6.6.2 Multi-year comparisons

Comparisons are made for paua (Figure 6.13) and kina (Figure 6.14) for the years 1999 to 2003 and 2011 (the current survey). Sites from the current survey were grouped into three locations - Blackhead (BH), the marine reserve (MR) and Aramoana (ARA), and compared to density estimate and size data for the same locations from the years 1999 to 2003.

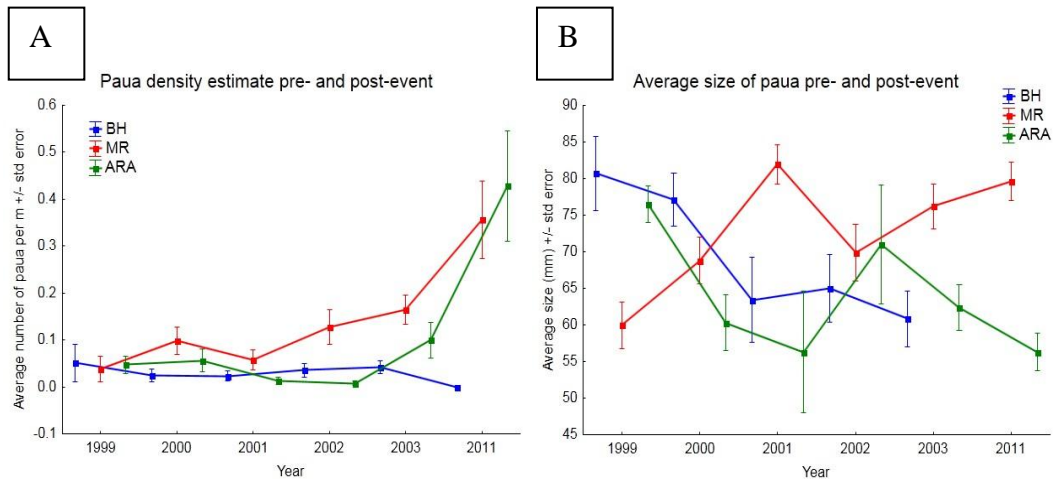


Figure 6.13. An estimate of paua density and average paua size at non-reserve locations Blackhead (BH) and Aramoana (ARA), and marine reserve location (MR), in years 1999 to 2003 (pre-event) and 2011 (post-event).

From 1999 to 2003, paua density remains high and stable at MR, while at BH and ARA density remains stable and lower compared to MR. Paua density increases in 2011 at ARA and is higher than MR density for that year. The average paua size is variable over the years, but MR paua are larger from 2001 onwards and BH paua size is steadily decreasing. In 2011, ARA paua size decreases.

Kina density at MR is low and stable compared to BH and ARA over the years, but increases dramatically in 2011. BH density remains stable, and ARA density decreases in 2011. The average kina size at BH and ARA vary over the years, compared to at MR, which has remained high and relatively stable. In 2011 the average size decreases at all locations, and dramatically so at MR.

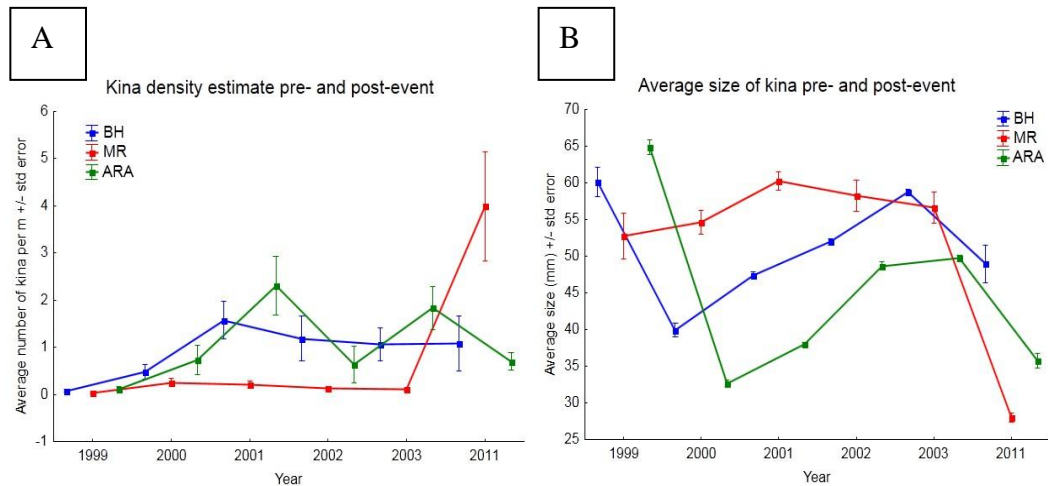


Figure 6.14. An estimate of kina density and average kina size at non-reserve locations Blackhead (BH) and Aramoana (ARA), and marine reserve location (MR), in years 1999 to 2003 (pre-event) and 2011 (post-event).

6.7 DISCUSSION

No paua were found at Blackhead to the south of the reserve. The lack of paua population could reflect the multiple-stressors impacting on the reefs there. Community response to stress depends on the intensity of the stress applied balanced against the resistance and resilience of the community after the stress has been lifted (Ellis et al., 2000). Human predation at the Blackhead reef is common (pers. observ.), partly because Blackhead is more readily accessible than Aramoana to the north. Combined with sedimentation from large landslides on that reef could mean that more stress was applied to the population than its resilience or ability to resist it, causing it to decrease dramatically. Presumably, the paua population had not yet recovered at the time of sampling in 2011.

There was a greater number of reproducing adult paua sampled within the reserve (Table 6.4), and there was a greater number of juveniles sampled outside the reserve at Aramoana. This is likely a spill-over effect, where the spawning adult population within the reserve is still reproducing, and are replenishing populations

to the north. This is supported by larval dispersal modelling (Oldman et al., 2006), which indicates reefs to the north of the reserve are likely to benefit from spawning populations within the reserve. Population resilience means that populations of a greater abundance and containing many reproducing adults are able to maintain larval production and therefore local recruitment (Micheli et al., 2012). The fact that the number of adult paua within the reserve remained high after the sedimentation event could represent an increased resilience of the adult reserve paua population.

For the reserve population to serve as a source of larvae, it must be able to replenish itself and adjacent areas (Halpern, 2003). If populations to the north of the reserve are indeed being replenished by spawning reserve populations, this could indicate the need to extend protection offered by the marine reserve, so protection encompasses areas to the north where recruitment is likely happening. This would allow the reserve population to replenish itself and increase populations even further to the north through spill-over effects, which could lead to more stabilised populations along a greater length of coastline.

Kina patterns of size and abundance suggest that a large recruitment event occurred within the reserve (site F) after the sedimentation event. Either the subtidal spawning population within the reserve generated these recruits, or they have settled within the reserve and are from a spawning population from another location. Why the juveniles have settled and are so abundant in the reserve is difficult to explain. The high juvenile number may only be high because of lack of kina predators such as crayfish, the populations of which may have been negatively affected by the sedimentation event. Populations of crayfish are known to increase in abundance within reserves (Ballentine & Langlois, 2008) and are thought to have some influence in the abundance of kina (Freeman, 2006). If the crayfish population decreased after the sedimentation event, it could be possible that in their absence that kina were able to recover faster due to lack of predation on the population. A subtidal survey would have provided insight and further explanation of this aspect.

If the kina juveniles have come from spawning populations within, or from the immediate area adjacent to the reserve, this could then be an indication of

resilience shown by the adult kina population, in that there are still many reproducing kina present within the reserve. However, the average size of kina within the reserve was 27.5 mm, which is at the lower end of the range of the typical spawning size for kina, and the long larval longevity (more than 30 days, which means factors such as currents can transport larvae over a large and variable temporal and spatial scale), means that recruitment seen in the reserve unlikely came from the kina reserve population. Even though the recruitment event may not be explained by adult kina within the reserve, the adult population sampled is still greater than the non-reserve adult population (Table 6.5), indicating there may still be a resilience trend.

The current survey, along with the multi-year results, have demonstrated that the paua and kina populations within the reserve are likely showing an increased resilience to the sedimentation event. The populations were high and stable enough when the sedimentation event occurred, so that after the impact their numbers were maintained and they were able to continue to reproduce. This is particularly well seen with the 2011 paua populations within and outside the reserve, and is also displayed well in the paua multi-year pattern (Figure 6.13). However, it must be noted that the multi-year density estimates are estimates only with some earlier sampling designs lacking in adequate replication. The 2011 density estimates are expected to have more accuracy in estimating a true mean with tighter variance because the numbers of channels sampled in 2011 were much higher compared to the number DOC channels.

Seagrass are important indicators of coastal primary productivity. They are highly productive and support numerous detritus and herbivore based food webs (Turner & Schwarz, 2006). While seagrass habitat may have arguable relevance to paua and kina population demography, it does indicate a higher general level of healthy functional intertidal reef inside the reserve compared to locations to the north and south. It is likely that subtidal algal ecosystems will also reflect this situation, and hence explain to some extent the more abundant grazing invertebrate communities (kina and paua) found inside the reserve. Whether this is a consequence of reserve protection, or other biophysical conditions acting on the various intertidal reef sites, remains unclear. All sites however, would have been affected more or less to a similar degree for at least a short period of time by substantial sediment

inundation, during the worst periods of storm activity that led to the slope failures. Subsequent tides have since modified the sedimentary regime in the intertidal area along this coast.

The current survey has provided a platform for further study relating to resilience of marine reserve organisms to disturbances. There are little studies providing conclusive evidence of resilience shown by populations within a marine reserve to disturbances (Micheli et al., 2012), let alone studies on disturbance events occurring in marine reserves. Therefore, with further examination, this study can increase the understanding of whether marine reserves play a role in increasing resilience of marine reserve populations when exposed to a disturbance.

This study could be repeated in order to gain a better understanding of temporal influence on the population during recovery of the sedimentation event, and should be conducted in conjunction with a survey of subtidal paua, kina, crayfish and reef fish populations, which are likely to be subject to longer periods of sedimentary input especially in deeper reef areas. This would help explain recruitment patterns within the reserve and adjacent non-reserve coastline, and provide further understanding of factors influencing the size and abundance of reserve organisms.

Chapter 7

DISCUSSION AND SUMMARY

This chapter provides an overall discussion of work carried out and a summary of the main conclusions drawn. The chapter integrates the conclusions made through the previous chapters to examine any interrelationships between the April 2011 catastrophic sedimentation event and possible ecological resilience of Te Angiangi Marine Reserve habitats, as evidenced by population demographics of key intertidal species within.

7.1 MAPIRI FORMATION MUDSTONE

7.1.1 Important characteristics

Joints and weakness

The Mapiri mudstone, of late Miocene age, is by nature a highly jointed rock. The mudstone bedrock exhibits a complex set of joints, ranging in scale from metres to centimetres apart, the former observed as the master joint cracks across the intertidal platform (Figure 3.2A). The smaller scale joints facilitate effective *in situ* weathering of mudstone boulders in a spheroidal manner (Figure 3.21). Once the small joint blocks are released they are readily further eroded by wetting and drying and wave action to produce fine sized particles. The joints are a particularly important feature in the presence of swelling smectite minerals, because they allow ready access of percolating water which further weakens the already relatively weakly indurated rock. The Mapiri mudstone was likely deposited in a slope basin environment, and was not subjected to especially deep burial, resulting in a weakly cemented (carbonate content about 10%) rock. Correlative mudstones at nearby Cape Turnagain have very low Schmidt hammer values of <10, supportive of the Mapiri mudstone too being an extremely weak rock (Kennedy & Dickson, 2007). The Mapiri mudstone siliciclastic material, including its high clay mineral content of illite and smectite, were likely mainly detritally derived from the erosion of older mudstones.

Smectite rich composition

Another important feature of the Mapiri mudstone is that it contains abundant clay minerals that are dominated by illite and smectite (Figure 3.11). The source of the common smectite in the Mapiri mudstone was likely mainly from erosion of older Tertiary mudstones present in the catchment area adjacent to the Te Angiangi Marine Reserve (Figure 2.5 and 2.6). Of significance are the Wanstead Formation lithologies which contain smectite clays known to cause slope instability and erosion (Lee et al., 2011). The ability of smectite minerals to expand and contract during wetting and drying means that its occurrence in soft rocks can significantly weaken them. The jointed nature of the Mapiri mudstone means water can penetrate quite deeply into the deposit, not just within the soil zone, and so the “active smectite” component becomes an important factor in weakening the rock.

Source of mud and fine sand

Erosion of the Mapiri mudstone through slope failures ultimately led to the delivery of fine sediment into the nearshore marine environment, including the area encompassing the Te Angiangi Marine Reserve. The joint controlled spheroidal weathering of the mudstone tended to release (sub) rounded clasts of mudstone that were further eroded and broken down under the influence of shoreline wave action. This process released the fine sized particles occurring in the offshore area (Figure 5.11). The Mapiri mudstone is rich in clay minerals, but nevertheless is texturally classified as a ‘sandy silt’ (Figure 3.20). In total and on average, it contains about 42% sand, about 42% silt, and about 16% clay sizes. This sand content includes about 10% very fine sand, 13-14% each of fine and medium sand, and 3-6% coarse sand (Table 3.4). Accordingly, the Mapiri mudstone is itself a viable source of both the finer sandy and mud sized material occurring in the subtidal sediments within and about the marine reserve (Chapter 5).

7.2 CATASTROPHIC LANDSLIDES

The landslides, which were the point source of the sediment delivered into the reserve and adjacent coastline, were catastrophic failures present along a significant part of the reserve hill side. 14 major landslides are recorded, generating an estimated total of 150,000 m³ of debris. The Te Angiangi Marine

Reserve is located within the much faulted and tectonically active zone of coastal ranges on the North Island East Coast (Figure 2.3), where relatively young and soft Neogene rocks are deformed due to extensive folding and fracturing. This is particularly evident in the reserve catchment, where the Mapiri Formation is influenced structurally by a series of complex folds and faults (Figure 2.5). The resulting geomorphology of the study area is mostly steep undulating hill sides, a significant proportion of which has been cleared of vegetation for the purpose of pastoral farming (Lacoste et al., 2009).

The external triggering factor initiating the landslides in the reserve and adjacent coastline was intense rainfall (650 mm) which fell between the 25-28 April 2011. This coincided also with a M4.5 scale earthquake centred only 10 km offshore from Pourerere at a depth of 20 km. The Mapiri mudstones location within a tectonically active subduction margin, along with subaerial erosion and tectonic influences, resulted in undulating steep hill sides. But most importantly, its soft and jointed nature and high smectite clay content are intrinsic features which, along with the above external triggering, caused the landslides which devastated the Te Angiangi Marine Reserve coastline in April 2011.

7.3 EXTENT OF SIGNIFICANT SEDIMENTATION

The local geology adjacent to the marine reserve, the soft Mapiri Formation mudstone, has been observed to erode quickly and effectively into fine size particles (Chapter 3). It is likely that the landslide debris, a large proportion of which consists of the soft mudstone (the rest being soil), weathers quickly into fine sediment, which then facilitates its easy dispersal and deposition from suspension far offshore. Hydrodynamic forces act to transport and disperse the sediment over large spatial scales, and the subtidal sediment survey undertaken at the marine reserve and adjacent nearshore area showed that mud sized particles become increasingly common with depth and distance offshore, with the muddiest samples found at the offshore limit of the nearshore region at about 40 m depth. This agrees with the study by Lewis and Gibb (1970) who showed that mud content increases significantly across the continental shelf, and that completely mud dominated sediments occur by about 100 m water depth (Figure 5.1).

The amount of time that the coastal marine organisms were exposed to sediment derived from the coastal landslides could therefore be relatively short. This means the effect of sedimentation on organisms is likely to be at a smaller scale than if the full amount of sediment delivered to the shore remained in place for longer periods, if hydrodynamic forces in the area had less of an influence. Therefore, ecosystem responses to sedimentation events are likely to be site specific (Norkko et al., 2002). For example, if catastrophic slope failures occurred within a sheltered embayment (e.g. an estuary) where hydrodynamic influences were relatively less persistent and vigorous, sediment transport out of the embayment could take several orders of magnitude longer in time than if the sedimentation event was to occur at a exposed location like the Te Angiangi Marine Reserve (Norkko et al., 2002).

7.4 TE ANGIANGI MARINE RESERVE RESPONSE TO SEDIMENTATION

7.4.1 Sedimentation and subsequent smothering of the intertidal platform

Paua and kina

The sedimentation event which occurred at the Te Angiangi Marine Reserve and adjacent coastline will have affected the intertidal habitats of the adjacent coastline and arguably had a significant effect on marine invertebrate species such as paua and kina as well as their habitat (algal lined rocky pools and fissures), especially in the higher intertidal reaches. Their subsequent rates of recovery inside and outside of the marine reserve are the subject of this study (Figure 7.1).

As demonstrated in Chapter 6, sedimentation has indeed had an effect on the intertidal paua and kina populations, and their response to the event is reflected in their size and abundance at reserve compared to non-reserve locations. For example, the lack of paua found at Blackhead, despite there being suitable paua habitat, is likely an artefact of the combined sedimentation and human predation stressors acting on the population there. It is hypothesised that at the time of the sedimentation event, the majority of organisms living on the mid-shore platform would have perished due to habitat destruction (e.g. sediment infilling channels where paua and kina live) and direct smothering (Figure 7.1B).

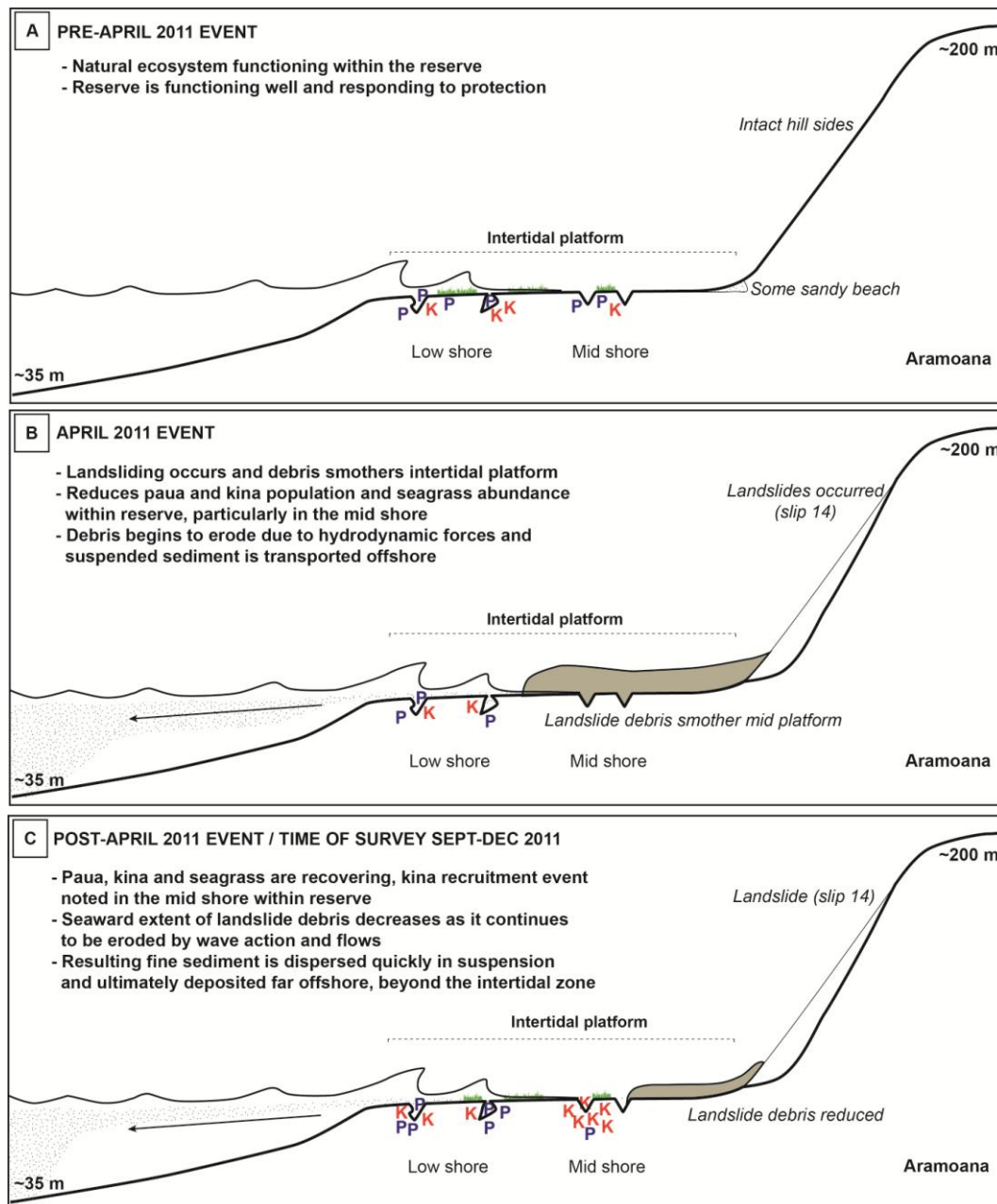


Figure 7.1. Schematic diagrams outlining the response to the 2011 sedimentation event on marine reserve populations. The blue 'P' (paua) and red 'K' (kina) are used to demonstrate the relative abundance of paua and kina in the low and mid shore before, during and after the event. Green patches of grass represent seagrass abundance before, during and after the event. Before the event (A), the reserve was functioning well and contained a presumably more robust ecological balance of interacting biological components. When the sedimentation event happened (B), landslide debris smothered a significant portion of the intertidal platform within the reserve and reduced paua and kina populations and seagrass abundance. The landslide debris began eroding into fine sized particles and being transported offshore. After the sedimentation event (C), the marine reserve populations began to recover, and landslide debris on the intertidal platform continues to rapidly reduce.

The response of reserve and non-reserve populations of paua, kina and seagrass was then predicated by the amount of sedimentation occurring at those locations, and the speed by which it was eliminated from the intertidal reefs by hydrodynamic forces. The ecological 'starting point' in terms of the robustness of

the habitat at those locations (quasi natural at the reserve or human predated at non-reserve locations) before the sedimentation event, together with the maturity of the populations of kina and paua present, may have been a factor influencing their response (albeit this latter hypothesis is difficult to substantiate without much more comprehensive pre-event information). At Blackhead, the response is clear. The ongoing human predation stress, with the additional sedimentation stress, has arguably led to a dramatic drop in the paua population. This observation is supported by the fact that previous monitoring surveys have found paua there in the past.

Paua and kina demographics within the reserve are demonstrating upward trends in the number of their average sizes. Abundance and average sizes (Figures 6.9 and 6.10) show a typical bell shaped curve, where the peak in the centre represents reserve sites. This provides further confirmation of the likelihood of human predation at reserve boundaries, and supports that the reserve populations are coping well with any sedimentation impacts. These observations hint at a resilience afforded by marine reserve status, as shown by the greater abundance of adult paua and kina found within the reserve compared to non-reserve locations (Table 6.4). The abundance of juveniles suggests that the reproductive output of paua and kina has remained steady, although it is unclear whether the origin of kina juveniles is sourced from inside the reserve. What is relevant however is that the intertidal reserve habitat appears to be more conducive to supporting recruitment of juveniles compared to non-reserve locations.

Overall, reserve populations of the species examined are indicating a reserve effect, and this reserve effect is presumably overriding any negative sedimentation effects. It is therefore tempting to accept the hypothesis that marine reserves do indeed afford resilience to environmental stressors (especially since empirical evidence of the effectiveness of marine reserves against disturbances is lacking (Micheli et al. (2012))), but there could be alternate arguments for the observations made. It could be that the geomorphology and nearshore current patterns of the reserve location was always more likely to attract recruiting kina and paua, or that simple stochastic events such as patchy recruitment episodes, and or variable longevity of fine sediments remaining on the different areas of reef (sampling and

surveys occurred some months after the sedimentation event occurred) have resulted in the patterns observed.

Seagrass

There was also an observed response in seagrass cover in areas directly smothered by landslide debris. In the areas severely affected, the intertidal platform was almost completely bare of macroalgae, including Neptune's necklace (*Hormosira banksii*), which is otherwise of common occurrence on this reef (pers. observ.). This decrease is probably due to a reduction in light caused by the suspended fine sediment, or a consequence of direct smothering, resulting in significant loss of seagrass (Figure 7.1B). At the time of the survey, seagrass had recovered well (Figure 7.1C), and this could be indicative of an improvement in overall community structure and health. This is because seagrasses are sensitive to fine sediment and other disturbance, and are characteristic of highly productive ecosystems (Turner & Schwarz, 2006).

Once the landslide debris began to reduce, and the sedimentation stress began to ease, seagrass was able to begin re-establishment. Presence of sediments may have even been favourable, since seagrass needs extensive soft sediment substrates to establish their root system, which might explain the abundance of seagrass that was sampled in the survey. While seagrasses are not likely to directly influence kina and paua populations, the relevance of examining this habitat was to assess wider ecosystem health for each reef region examined inside and outside the reserve. Conditions that would be deleterious to seagrass would also likely be deleterious to macroalgae that characterise paua and kina habitat. There may also be some benefit in the likely sediment trapping effects from extensive seagrass meadows that would benefit adjacent habitats.

7.5 PRE-EXISTING RESILIENCE IN EAST COAST

POPULATIONS AND A MARINE RESERVE EFFECT

Landsliding along the East Coast of North Island is common (Pettinga, 1980; Gibb, 1978; section 4.3), and it is clearly evident that previous landsliding has occurred on the coastal hills adjacent to the Te Angiangi Marine Reserve (Figures 4.3A and 4.5). Sediment delivery into the marine environment through coastal

landslides is therefore a common occurrence (Airoidi, 2003). One of the primary means of sedimentation in the coastal marine environment is delivery through fluvial systems (Griffiths & Glasby; 1985; Foster & Carter, 1997; Brackley et al., 2010; Parra et al., 2012). There are large river systems that discharge to the north of the Te Angiangi Marine Reserve at Hawke Bay and Poverty Bay, which carry large amounts of fine suspended sediment (Griffiths & Glasby; 1985). Given the susceptibility and occurrence of landsliding along the southern Hawke's Bay coastline, as well as sediment contributions from rivers draining the catchments, it could be said that marine populations in affected areas are already somewhat resilient to sedimentation. However, the small amount of literature relating to marine ecology along the southern Hawke's Bay coastline, apart from data gathered from the Te Angiangi Marine Reserve monitoring efforts, remains insufficient to permit any detailed evaluation of ecological trends that may suggest enhanced recovery of populations (either from reserve or non-reserve locations) along the Hawkes Bay coastline.

In isolated areas where the risk of human predation of the marine biota is smaller, the marine populations are likely to exist in a more stable or more naturally balanced ecosystem state, such that the concept of resilience to other disturbances such as sedimentation can be entertained. This study has shown that there is a significant within 'reserve effect', in that the paua and kina species studied appear to be recovering more effectively inside the Te Angiangi Marine Reserve, than those populations outside. As discussed above, there are a number of alternate arguments for this and it is not within the scope of this study to make a definitive conclusion. The work does however create a platform for further investigation, which could most effectively be carried out with subtidal survey extensions to the work presented here.

This study set out to examine possible linkages between a significant sedimentation inundation event and aspects of coastal intertidal ecosystem response. In conjunction, the study encompassed the unique opportunity to examine population responses from inside and outside of a marine reserve. It is a multi-disciplinary examination of a highly complex interaction and can be used as a platform for future work.

REFERENCE LIST

- Airoldi, L. (2003). The effects of sedimentation on rocky coast assemblages. *Oceanography and Marine Biology: an Annual Review*, 41, 161-236.
- Airoldi, L., & Cinelli, F. (1997). Effects of sedimentation on subtidal macroalgal assemblages: an experimental study from a Mediterranean rocky shore. *Journal of Experimental Marine Biology and Ecology*, 215(2), 269-288.
- Allison, G. W., Gaines, S. D., Lubchenco, J., & Possingham, H. P. (2003). Ensuring persistence of marine reserves: catastrophes require adopting an insurance factor. *Ecological Applications*, 13(sp1), 8-24.
- Allison, G. W., Lubchenco, J., & Carr, M. H. (1998). Marine reserves are necessary but not sufficient for marine conservation. *Ecological applications*, 8(1), 79-92.
- Andrew, N. L. (1988). Ecological aspects of the common sea urchin, *Evechinus chloroticus*, in northern New Zealand: a review. *New Zealand journal of marine and freshwater research*, 22(3), 415-426.
- Babcock, R. C., Kelly, S., Shears, N. T., Walker, J. W., & Willis, T. J. (1999). Changes in community structure in temperate marine reserves. *Marine Ecology Progress Series*, 189, 125-134.
- Ballantine, W. J., & Langlois, T. J. (2008). Marine reserves: the need for systems. *Challenges to Marine Ecosystems*, 35-44.
- Barnes, P. M., & de Lepinay, B. M. (1997). Rates and mechanics of rapid frontal accretion along the very obliquely convergent southern Hikurangi margin, New Zealand. *Journal of geophysical research*, 102(11), 24,931 - 24,952.
- Barnes, P. M., Lamarche, G., Bialas, J., Henrys, S., Pecher, I., Netzeband, G. L., . . . Crutchley, G. (2010). Tectonic and geological framework for gas hydrates and cold seeps on the Hikurangi subduction margin, New Zealand. *Marine Geology*, 272(1), 26-48.
- Barnes, P. M., Nicol, A., & Harrison, T. (2002). Late Cenozoic evolution and earthquake potential of an active listric thrust complex above the Hikurangi subduction zone, New Zealand. *Geological Society of America Bulletin*, 114(11), 1379-1405.
- Beanland, S., Melhuish, A., Nicol, A., & Ravens, J. (1998). Structure and deformational history of the inner forearc region, Hikurangi subduction margin, New Zealand. *New Zealand journal of geology and geophysics*, 41(4), 325-342.
- Bjolykke, K. (1998). Clay mineral diagenesis in sedimentary basins-a key to the prediction of rock properties. Examples from the North Sea Basin. *Clay minerals*, 33(1), 15-34.

- Bland, K. J., & Kamp, P. J. J. (2006). *Geological structure of the forearc basin in central Hawke's Bay, eastern North Island*. Paper presented at the New Zealand Petroleum Conference.
- Blott, S. J., & Pye, K. (2001). GRADISTAT: A grain size distribution and statistics package for the analysis of unconsolidated sediments. *Earth Surface Processes and Landforms*, 26, 1237-1248.
- Boggs, S. (2006). *Principles of sedimentology and stratigraphy: fourth edition*. New Jersey, U.S.A: Pearson Prentice Hall.
- Brackley, H. L., Blair, N. E., Trustrum, N. A., Carter, L., Leithold, E. L., Canuel, E. A., . . . Tate, K. R. (2010). Dispersal and transformation of organic carbon across an episodic, high sediment discharge continental margin, Waipaoa Sedimentary System, New Zealand. *Marine Geology*, 270(1), 202-212.
- Brodie, J. W. (1960). Coastal surface currents around New Zealand. *New Zealand journal of geology and geophysics*, 3(2), 235-252.
- Butler, H., Clegg, E., Le Vaillant, C. and Thomas, L. (2010). Te Angiangi Marine Reserve seagrass monitoring program. Unpublished report for the Department of Conservation by postgraduate students, Victoria University of Wellington.
- Carroll, D., & Starkey, H. C. (1971). Reactivity of clay minerals with acids and alkalies. *Clays and clay minerals*, 19, 321-335.
- Cashman, S. M., Kelsey, H. M., Erdman, C. F., Cutten, H. N. C., & Berryman, K. R. (1992). Strain partitioning between structural domains in the forearc of the Hikurangi subduction zone, New Zealand. *Tectonics*, 11(2), 242-257.
- Chester, R. (1993). *Marine Geochemistry*. London: Chapman and Hall.
- Chiswell, S. M. (2000). The Wairarapa coastal current. *New Zealand Journal of Marine and Freshwater Research*, 34(2), 303-315.
- Chiswell, S. M. (2003). Circulation within the Wairarapa Eddy, New Zealand. *New Zealand journal of marine and freshwater research*, 37(4), 691-704.
- Costales, et. al. (2009). *Paua and kina monitoring report*. Unpublished monitoring survey undertaken by postgraduate students. Victoria University of Wellington.
- Creswell, P. D., & Warren, E. J. (1990). The flora and fauna of the southern Hawke's Bay coast. East Coast Hawke's Bay Conservancy: the Department of Conservation.
- Crozier, M. J., Eyles, R. J., Marx, S. L., McConchie, J. A., & Owen, R. C. (1980). Distribution of landslips in the Wairarapa hill country. *New Zealand journal of geology and geophysics*, 23(5-6), 575-586.
- Crozier, M. J., Gage, M., Pettinga, J. R., Selby, M. J., & Wasson, R. J. (1992).

The Stability of Hillslopes. In J. M. Soons & M. J. Selby (Eds.), *Landforms of New Zealand second edition*. Auckland, New Zealand: Longman Paul.

Cummings, V. J., & Thrush, S. F. (2004). Behavioural response of juvenile bivalves to terrestrial sediment deposits: implications for post-disturbance recolonisation. *Marine Ecology Progress Series*, 278, 179-191.

Cummings, V. J., & Thrush, S. F. (2004). Behavioural response of juvenile bivalves to terrestrial sediment deposits: implications for post-disturbance recolonisation. *Marine Ecology Progress Series*, 278, 179-191.

Cummings, V. J., Vopel, K., & Thrush, S. (2009). Terrigenous deposits in coastal marine habitats: influences on sediment geochemistry and behaviour of post-settlement bivalves. *Marine Ecology Progress Series*, 383, 173-185.

Denny, C. M., Willis, T. J., & Babcock, R. C. (2004). Rapid recolonisation of snapper *Pagrus auratus*: Sparidae within an offshore island marine reserve after implementation of no-take status. *Marine Ecology Progress Series*, 272, 183-190.

Department of Conservation website: www.doc.govt.nz/conservation/marine-and-coastal/marine-protected-areas/

Department of Conservation (1994a). Te Angiangi Marine Reserve Intertidal baseline survey. Collection of survey notes held at the East Coast Hawke's Bay Conservancy.

Department of Conservation. (1994b). Te Angiangi (Aramoana – Blackhead, Central Hawke's Bay) marine reserve application. *Hawke's Bay Conservancy Series*, 7, 86.

Department of Conservation. (2001). Te Angiangi Marine Reserve: Biological Monitoring Plan. East Coast Hawke's Bay Conservancy: Technical Support (Marine & Freshwater).

Department of Conservation. (2003). Te Angiangi Marine Reserve Operational Plan. Napier, New Zealand: Hawke's Bay Conservancy.

Department of Conservation. (2008). Te Angiangi Marine Reserve brochure, Central Hawke's Bay. Department of Conservation.

Dymond, J. R., Ausseil, A. G., Shepherd, J. D., & Buettner, L. (2006). Validation of a region-wide model of landslide susceptibility in the Manawatu–Wanganui region of New Zealand. *Geomorphology*, 74(1), 70-79.

Ellis, J., Nicholls, P., Craggs, R., Hofstra, D., & Hewitt, J. (2004). Effects of terrigenous sedimentation on mangrove physiology and associated macrobenthic communities. *Marine Ecology Progress Series*, 270, 71-82.

Ellis, J. I., Norkko, A., & Thrush, S. F. (2000). Broad-scale disturbance of intertidal and shallow sublittoral soft-sediment habitats; effects on the

- benthic macrofauna. *Journal of Aquatic Ecosystem Stress and Recovery*, 7(1), 57-74.
- Erdman, C. F., & Kelsey, H. M. (1992). Pliocene and Pleistocene stratigraphy and tectonics, Ohara Depression and Wakarara Range, North Island, New Zealand. *New Zealand journal of geology and geophysics*, 35(2), 177-192.
- Fairweather, P. G., & Underwood, A. J. (1991). Experimental removals of a rocky intertidal predator: variations within two habitats in the effects on prey. *Journal of Experimental Marine Biology and Ecology*, 154(1), 29-75.
- Field, B. D., Uruski, C. I. and others (1997). *Cretaceous-Cenozoic geology and petroleum systems of the East Coast Region, New Zealand*. Institute of Geological and Nuclear Sciences monograph 19. 301, 7 enclosures. Lower Hutt, New Zealand: Institute of Geological and Nuclear Sciences Limited.
- Flemming, et. al. (2009). *Seagrass monitoring proposal*. Unpublished monitoring survey undertaken by postgraduate students. Victoria University of Wellington
- Fletcher, W. J. (1987). Interactions among subtidal Australian sea urchins, gastropods, and algae: effects of experimental removals. *Ecological Monographs*, 89-109.
- Folk, R. L. (1954). The distinction between grain size and mineral composition in sedimentary-rock nomenclature. *The Journal of Geology*, 344-359.
- Folk, R. L. (1968). *Petrology of sedimentary rocks*. Austin, Texas: Hemphill.
- Folk, R. L., & Ward, W. C. (1957). Brazos River bar: a study in the significance of grain size parameters. *Journal of Sedimentary Petrology*, 27, 3-26.
- Foster, G., & Carter, L. (1997). Mud sedimentation on the continental shelf at an accretionary margin—Poverty Bay, New Zealand. *New Zealand Journal of Geology and Geophysics*, 40(2), 157-173.
- Freeman, D. J. (2001). *Te Angiangi Marine Reserve intertidal paua and kina monitoring 1999-2001*. Unpublished report by the Department of Conservation.
- Freeman, D. J. (2006). *Te Angiangi and Te Tapuwae o Rongokako Marine Reserves: Intertidal paua and kina monitoring*. Department of Conservation Technical Support Series Number: 26.
- Freeman, D. J., & Duffy, C. A. J. (2003). *Te Angiangi Marine Reserve, Reef Fish Monitoring, 1995-2003*. Gisborne, New Zealand: Department of Conservation.
- Funnell, G., Hancock, N., Williston, T., & Drury, J. (2005). *Tuingara to Blackhead Point Habitat Mapping NIWA Client report HAM2004-094*: National Institute of Water and Atmospheric Research.
- Game, E. T., Watts, M. E., Wooldridge, S., & Possingham, H. (2008). *Planning*

for persistence in marine reserves: a question of catastrophic importance. *Ecological applications*, 18(3), 670-680.

Garner, D. M. (1961). Hydrology of Coastal Waters, 1955 (New Zealand Oceanographic Institute Memoir No. 8, Department of Scientific and Industrial Research Bulletin 138). Wellington, New Zealand: Department of Scientific and Industrial Research.

Garner, D. M. (1969). The geopotential topography of the ocean surface around New Zealand. *New Zealand journal of marine and freshwater research*, 3(2), 209-219.

Geological and Nuclear Sciences. (2011). GeoNet Magnitude 4.5 earthquake, Hawke's Bay region, New Zealand Retrieved April, 2011, from <http://lists.geonet.org.nz/pipermail/eqnews/2011-April/004711.html>

Gibb, J. G. (1978). Rates of coastal erosion and accretion in New Zealand. *New Zealand Journal of Marine and Freshwater Research* 12, 429-456.

Gibb, J. G. (1981). Coastal hazard mapping as a planning technique for Waiapu County, East Coast, North Island, New Zealand. In W. a. S. T. Publication (Ed.), (pp. 63). Wellington, New Zealand: Water and Soil Division, Ministry of Works and Development.

Gillespie, P. (2007). Potential effects of high sediment loads on the marine environment of the East Coast of the North Island, East Cape - Hawke Bay: A review of existing information. Nelson, New Zealand: Cawthron.

Glade, T. (2003). Landslide occurrence as a response to land use change: a review of evidence from New Zealand. *Catena*, 51(3), 297-314.

Gorsline, D. S. (1985). Some thoughts on fine-grained sediment transport deposition. *Sedimentary Geology*, 41, 113-130.

Grafton, R. Q., Van Ha, P., & Kompas, T. (2003). On marine reserves: rents, resilience and 'Rules of thumb'.

Griffiths, G & Glasby, G (1895). Input of river-derived sediment to the New Zealand Continental Shelf: I. Mass. *Estuarine, Coastal and Shelf Science*, 21, 773-787.

Halpern, B. S. (2003). The impact of marine reserves: do they work and does reserve size matter? *Ecological Applications*, 13(1), 117-137.

Heath, R. A. (1985). A review of the physical oceanography of the seas around New Zealand—1982. *New Zealand journal of marine and freshwater research*, 19(1), 79-124.

Hewitt, J. E., Cummings, V. J., Ellis, J. I., Funnell, G., Norkko, A., Talley, T. S., & Thrush, S. F. (2003). The role of waves in the colonisation of terrestrial sediments deposited in the marine environment. *Journal of Experimental Marine Biology and Ecology*, 290(1), 19-47.

- James, P. (2006) Biology of kina (*Evechinus chloroticus*). *A learning resource, Unit Standard 20305*: Seafood Industry Training Organisation.
- John, O., Jimin, H., Graham, R., & Scott, S. (2006). Larval dispersal from Te Taonga O Ngati Kere and Te Angiangi Marine Reserve: numerical model simulations. Hamilton, New Zealand: National Institute of Water & Atmospheric Research.
- Jones, H. (2008). Coastal sedimentation: What we know and the information gaps. Prepared for Environment Waikato: Environment Waikato Technical Report 2008/12. Hamilton, New Zealand: Waikato Regional Council
- Jones, K., Page, M., & Levick, S. (2011). Processing and classifying satellite imagery to assess the April 2011 storm induced landsliding in Hawke's Bay *GNS Science Consultancy Report 2011/265*: GNS Science.
- Kamp, P. J. J. (1992). Landforms of Hawke's Bay and their origin: A plate tectonic interpretation. In J. M. Soons & M. J. Selby (Eds.), *Landforms of New Zealand second edition* (pp. 344-366). Auckland, New Zealand: Longman Paul.
- Kelly, S., Scott, D., MacDiarmid, A. B., & Babcock, R. C. (2000). Spiny lobster, *Jasus edwardsi*, recovery in New Zealand marine reserves. *Biological Conservation*, 92, 359-369.
- Kelly, S., Scott, D., MacDiarmid, A. B., & Babcock, R. C. (2000). Spiny lobster, *Jasus edwardsi*, recovery in New Zealand marine reserves. *Biological Conservation*, 92, 359-369.
- Kennedy, D. M., & Dickson, M. E. (2007). Clifed coasts of New Zealand: perspectives and future directions. *Journal of the Royal Society of New Zealand*, 37(2), 41-57.
- Kiest, K. (1993). *The Influence of sediment from landslide plumes on sessile kelp forest assemblages*. MSc, San Jose State University.
- Kingsford, M., & Battershill, C. (1998). *Studying temperate marine environments: A handbook for ecologists*. Christchurch, New Zealand: Canterbury University Press.
- Lacoste, A., Loncke, L., Chanier, F., Bailleul, J., Vendeville, B. C., & Mahieux, G. (2009). Morphology and structure of a landslide complex in an active margin setting: The Waitawhiti complex, North Island, New Zealand. *Geomorphology*, 109, 184-196.
- Lee, J. M., Bland, K. J., Townsend, D. B., & Kamp, P. J. J. (2011). Geology of the Hawke's Bay Area. Institute of Geological & Nuclear Sciences 1:250 000 Geological Map 8.
- Lee, J. M., Begg, J. G. (2002). Geology of the Wairarapa Area. Institute of Geological & Nuclear Sciences 1:250 000 Geological Map 11.

- Lewis, K. B. (1971). *Marine geology of the Turnagain area*. PhD, Victoria University of Wellington.
- Lewis, K. B., & Gibb, J. G. (1970). Turnagain sediments. New Zealand Oceanographic Institute Chart, Coastal Series, 1:200,000
- Lewis, K. B., & Pettinga, J. R. (1993). The emerging, imbricate frontal wedge of the Hikurangi margin. In P. F. Balance & H. G. Reading (Eds.), *Sedimentation in Oblique-slip Mobile Zones* (pp. 225-247). Oxford: Blackwell Scientific Publications.
- Li, G., Peacor, D. R., & Coombs, D. S. (1997). Transformation of smectite to illite in bentonite and associated sediments from Kaka Point, New Zealand; contrast in rate and mechanism. *Clays and Clay Minerals*, 45(1), 54-67.
- Lillie, A. R. (1953). The geology of the Dannevirke Subdivision *New Zealand Geological Survey Bulletin No. 46*. Wellington, New Zealand: Department of Scientific and Industrial Research.
- Lohrer, A. M., Hewitt, J. E., & Thrush, S. F. (2006b). Assessing far-field effects of terrigenous sediment loading in the coastal marine environment. *Marine Ecology Progress Series*, 315, 13.
- Lohrer, A. M., Thrush, S. F., Hewitt, J. E., Berkenbusch, K., Ahrens, M., & Cummings, V. J. (2004). Terrestrially derived sediment: response of marine macrobenthic communities to thin terrigenous deposits. *Marine ecology. Progress series*, 273, 121-138.
- Lohrer, A. M., Thrush, S. F., Lundquist, C. J., Vopel, K., Hewitt, J. E., & Nicholls, P. E. (2006a). Deposition of terrigenous sediment on subtidal marine macrobenthos: response of two contrasting community types. *Marine Ecology Progress Series*, 307, 115-125.
- Micheli, F., Saenz-Arroyo, A., Greenley, A., Vazquez, L., Montes, J. A. E., Rossetto, M., & De Leo, G. A. (2012). Evidence That Marine Reserves Enhance Resilience to Climatic Impacts. *PloS one*, 7(7), e40832.
- Moon, V. (2010). *ERTH241-10A (HAM): Engineering geomorphology*. Earth and Ocean Sciences, University of Waikato. Hamilton, New Zealand.
- Moore, M. D., & Reynolds, R. C. (1997). *X-ray diffraction and the identification and analysis of clay minerals*. Oxford: Oxford University Press.
- Morrisey, S., Turner, S., & MacDiarmid, A. B. (1998). Subtidal assemblages of soft substrata. In M. Kingsford & C. Battershill (Eds.), *Studying temperate marine environments: a handbook for ecologists*. Christchurch, New Zealand: Canterbury University Press.
- National Institute of Water and Atmospheric Research. (2011a). National climate summary Retrieved April, 2011, from <http://www.niwa.co.nz/our-science/climate/publications/all/cu/new-zealand-climate-update-143-a-may-2011/current-climate---april-2011>.

- National Institute of Water and Atmospheric Research. (2011b). Climate Statistics, Summary of the records of temperature, rainfall and sunshine, April 2011, from <http://www.niwa.co.nz/our-science/climate/publications/all/cu/new-zealand-climate-update-143-a-may-2011/current-climate---april-2011>.
- Norkko, A., Thrush, S. F., Hewitt, J. E., Cummings, V. J., Norkko, J., Ellis, J. I., . . . MacDonald, I. (2002). Smothering of estuarine sandflats by terrigenous clay: the role of wind-wave disturbance and bioturbation in site-dependant macrofaunal recovery. *Marine Ecology Progress Series*, 234, , 23-42.
- Nyman, S. L., Nelson, C. S., & Campbell, K. A. (2010). Miocene tubular concretions in East Coast Basin, New Zealand: Analogue for the subsurface plumbing of cold seeps. *Marine Geology*, 272(1), 319-336.
- Olge, B. A. (1953). Geology of the Eel River Valley Area, Humboldt County, California *Bulletin 164*. Ferry Building, San Francisco: Department of Natural Resources, Division of Mines.
- Ollier, C. D. (1971). Causes of spheroidal weathering. *Earth-Science Reviews*, 7(3), 127-141.
- Parker, K. R., & Wiens, J. A. (2005). Assessing recovery following environmental accidents: environmental variation, ecological assumptions, and strategies. *Ecological applications*, 15(6), 2037-2051.
- Parra, J. G., Marsaglia, K. M., Rivera, K. S., Dawson, S. T., & Walsh, J. P. (2012). Provenance of sand on the Poverty Bay shelf, the link between source and sink sectors of the Waipaoa River sedimentary system. *Sedimentary Geology*, 280 208-233.
- Pettinga, J. R. (1980). *Geology and Landslides of the Eastern Te Aute District, Southern Hawke's Bay*. PhD, University of Auckland, Auckland, New Zealand.
- Pettinga, J. R. (1982). Upper Cenozoic structural history, coastal southern Hawke's Bay, New Zealand. *New Zealand journal of geology and geophysics*, 25(2), 149-191.
- Pettinga, J. R. (1987a). Waipoapoa Landslide: a deep seated complex block slide in Tertiary weak-rock flysh, Southern Hawke's Bay, New Zealand. *New Zealand Journal of Geology and Geophysics*, 30, 401-414.
- Pettinga, J. R. (1987b). Ponui Landslide: a deep seated wedge failure in Tertiary weak-rock flysh, Southern Hawke's Bay, New Zealand. *New Zealand Journal of Geology and Geophysics*, 30, 415-430.
- Pettinga, J. R. (2004). Three-stage massive gravitational collapse of the emergent imbricate frontal wedge, Hikurangi Subduction Zone, New Zealand. *New Zealand journal of geology and geophysics*, 47, 399-414.
- Pickrill, R. A., & Mitchell, J. S. (1979). Ocean wave characteristics around New

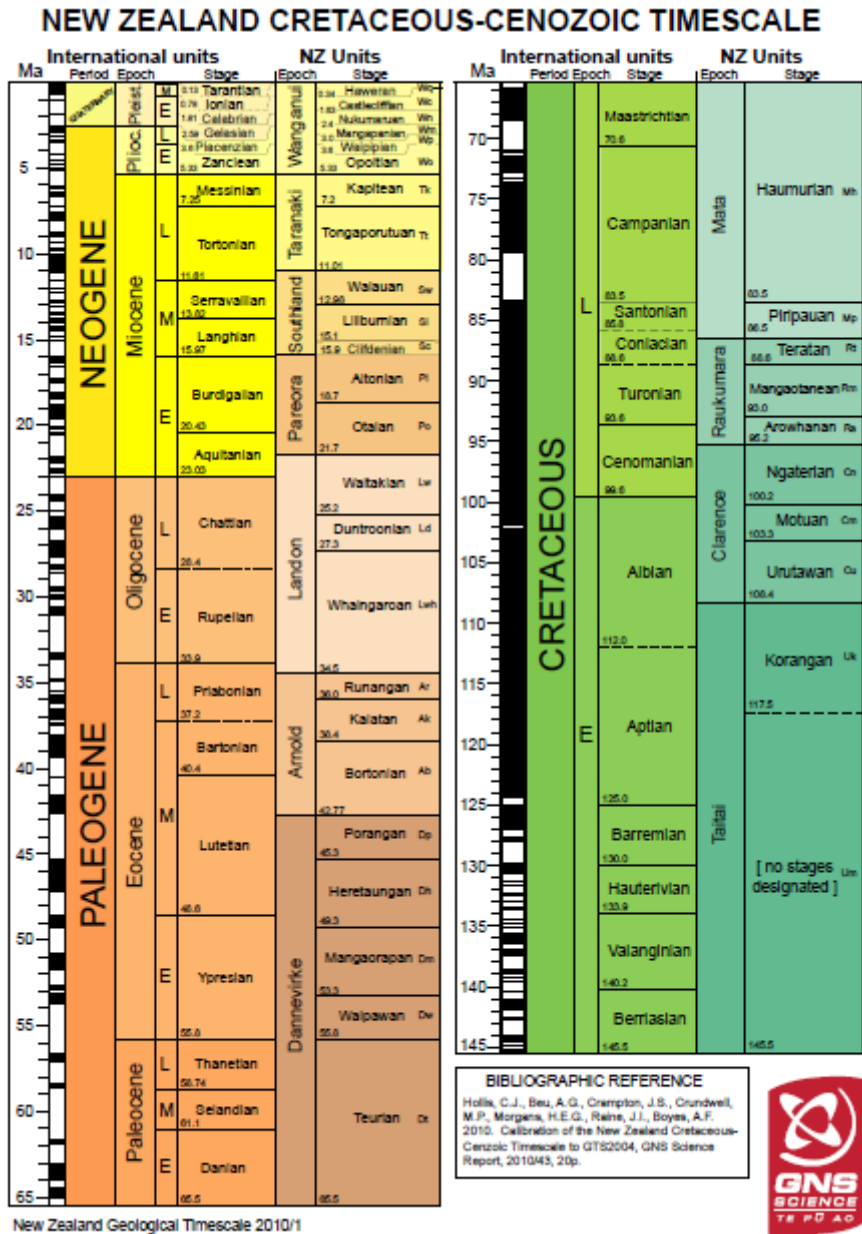
Zealand. *New Zealand Journal of Marine and Freshwater Research*, 13(4), 501-520.

- Prothero, D. R., & Schwab, F. (2003). *Sedimentary geology: an introduction to sedimentary rocks and stratigraphy*. New York, U.S.A: W.H. Freeman and Company.
- Rait, G., Chanier, F., & Waters, D. W. (1991). Landward-and seaward-directed thrusting accompanying the onset of subduction beneath New Zealand. *Geology*, 19(3), 230-233.
- Rogers, C. S. (1990). Responses of coral reefs and reef organisms to sedimentation. *Marine ecology progress series*, 62(1), 185-202.
- Ryan, P. A. (1991). Environmental effects of sediment on New Zealand streams: a review. *New Zealand journal of marine and freshwater research*, 25(2), 207-221.
- Selby, M. J. (1970). *Slopes and slope processes*. Hamilton, New Zealand: Waikato Branch of the New Zealand Geographical Society (Inc.).
- Selby, M. J. (1993). *Hillslope materials and processes*. Oxford: Oxford University Press.
- Shears, N. T. (2007). Shallow subtidal reef communities at the Poor Knights Islands Marine Reserve after eight years of no-take protection. Northland Conservancy, New Zealand: Department of Conservation.
- Shears, N. T., & Babcock, R. C. (2002). Marine reserves demonstrate top-down control of community structure on temperate reefs. *Oecologia*, 132(1), 131-142.
- Shears, N. T., & Babcock, R. C. (2004). Indirect effects of marine reserve protection on New Zealand's rocky coastal marine communities. Wellington, New Zealand: Department of Conservation.
- Sousa, W. P. (1984). The role of disturbance in natural communities. *Annual Review of Ecology and Systematics*, 15, 353-391.
- Thrush, S. F., Hewitt, J. E., Cummings, V. J., Ellis, J. I., Hatton, C., Lohrer, A., & Norkko, A. (2004). Muddy waters: elevating sediment input to coastal and estuarine habitats. *Frontiers in Ecology and the Environment*, 2(6), 299-306.
- Thrush, S. F., Hewitt, J. E., Norkko, A., Cummings, V. J., & Funnell, G. A. (2003). Macrobenthic recovery processes following catastrophic sedimentation on estuarine sandflats. *Ecological Applications*, 13(5), 1433-1455.
- Turner, S., & Schwarz, A. M. (2006). Management and conservation of seagrass in New Zealand: an introduction. Wellington, New Zealand: New Zealand Department of Conservation.

- Varnes, D. J. (1978). Slope movement types and processes. In R. L. Schuster & R. J. Krizek (Eds.), *Special Report 176: Landslides: Analysis and Control* (pp. 11-33). Washington D. C.: Transportation and Road Research Board, National Academy of Science.
- Velde, B. (1992). *Introduction to clay minerals: chemistry, origins, uses and environmental significance*. London: Chapman and Hall.
- Vermaat, J. E., Agawin, N. S. R., Fortes, M., Uri, J., Duarte, C. M., Marba, N., . . . Van Vierssen, W. (1997). The capacity of seagrasses to survive increased turbidity and siltation: the significance of growth form and light use. *Ambio*, 26, 499-504.
- von Hochstetter, F. (1867). *New Zealand: its physical geography, geology and natural history*: JG Cotta.

APPENDICES

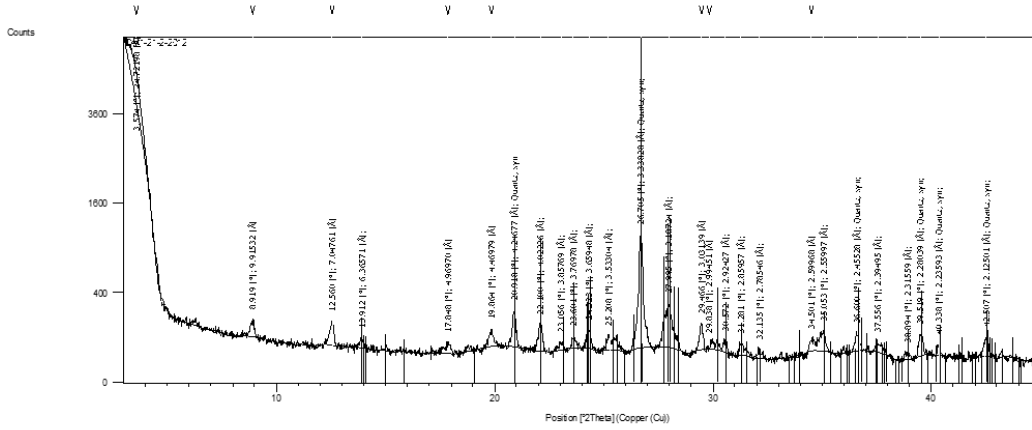
APPENDIX 1. GEOLOGICAL TIMESCALE



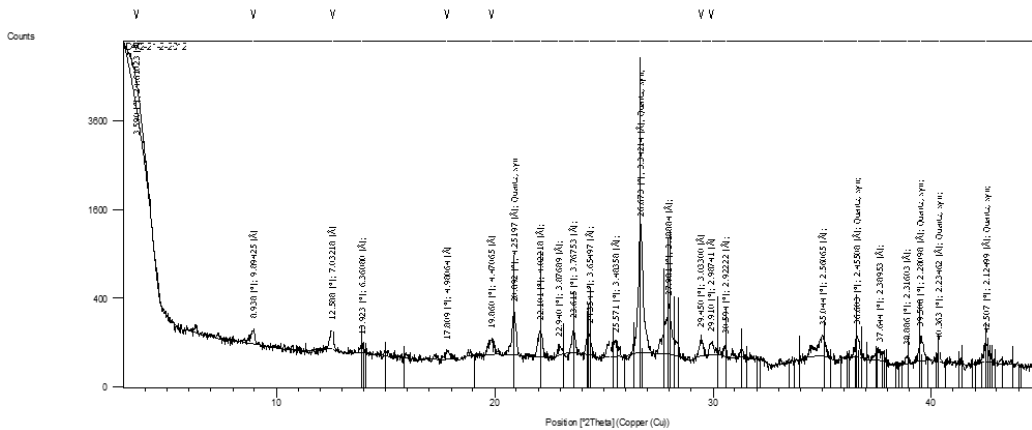
APPENDIX 2. BULK AND CLAY MINERALOGY XRD CHARTS

Bulk mineralogy XRD charts.

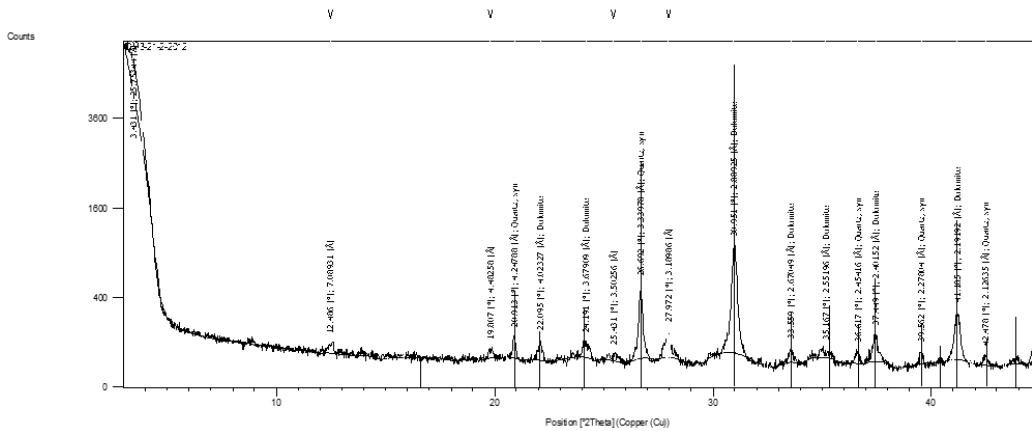
DM1 mudstone



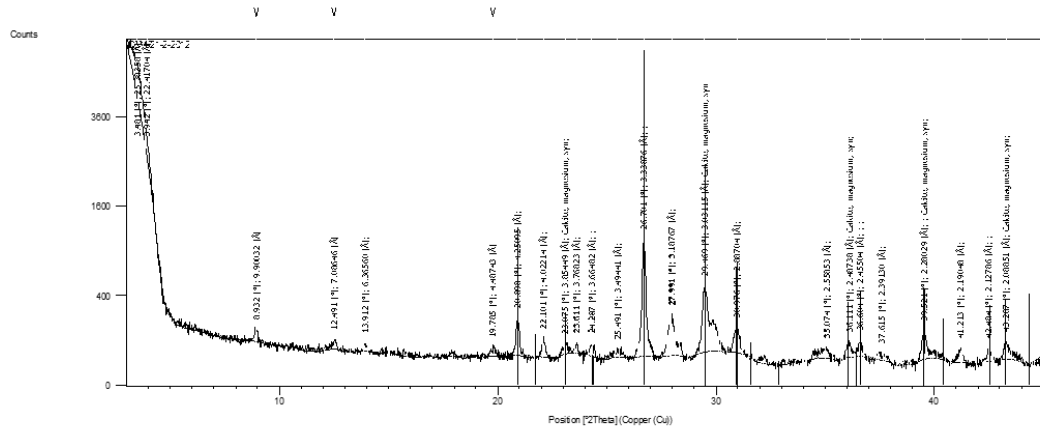
DM2 mudstone



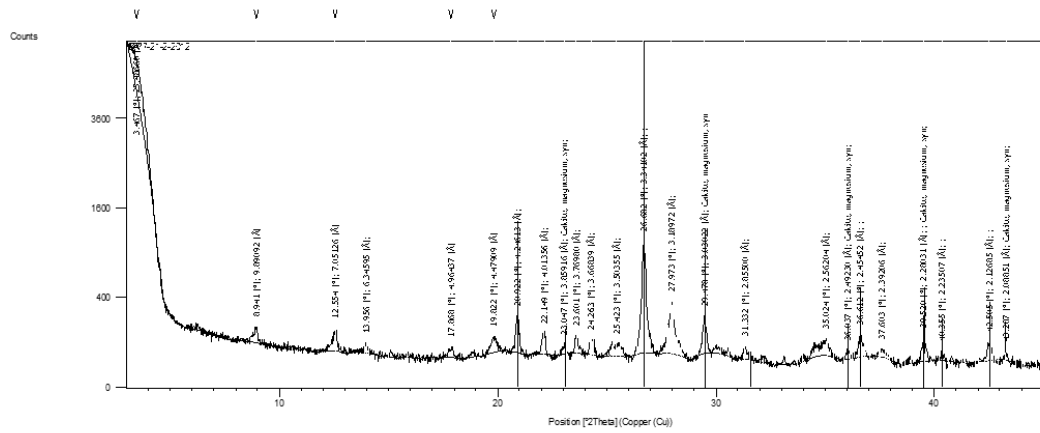
DM3 dolomitic concretion



DM4 calcitic concretion

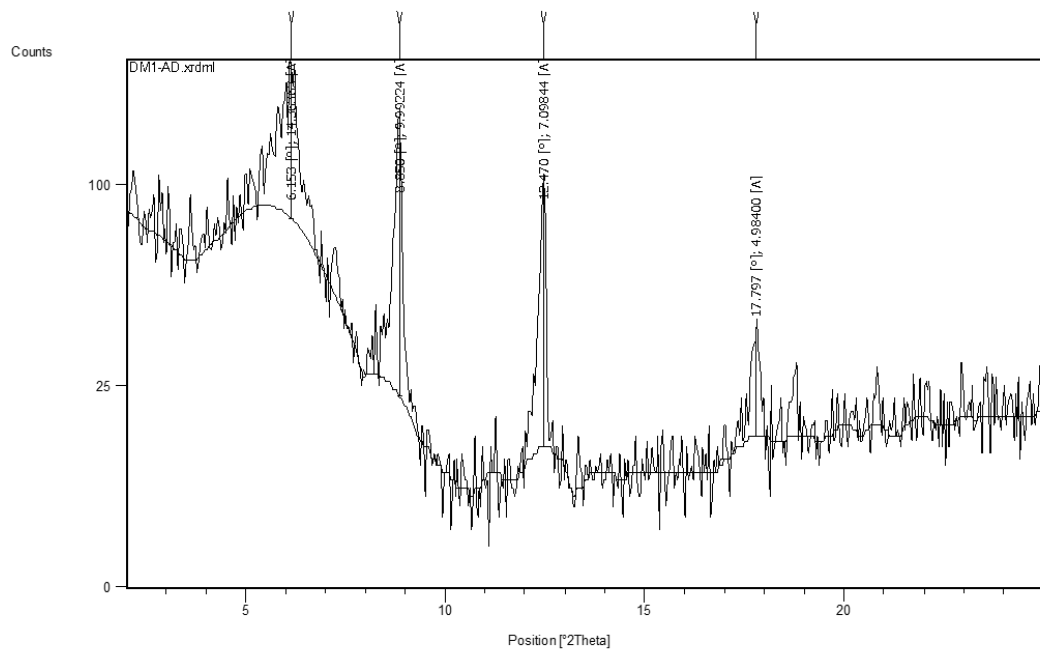


DM7 mudstone

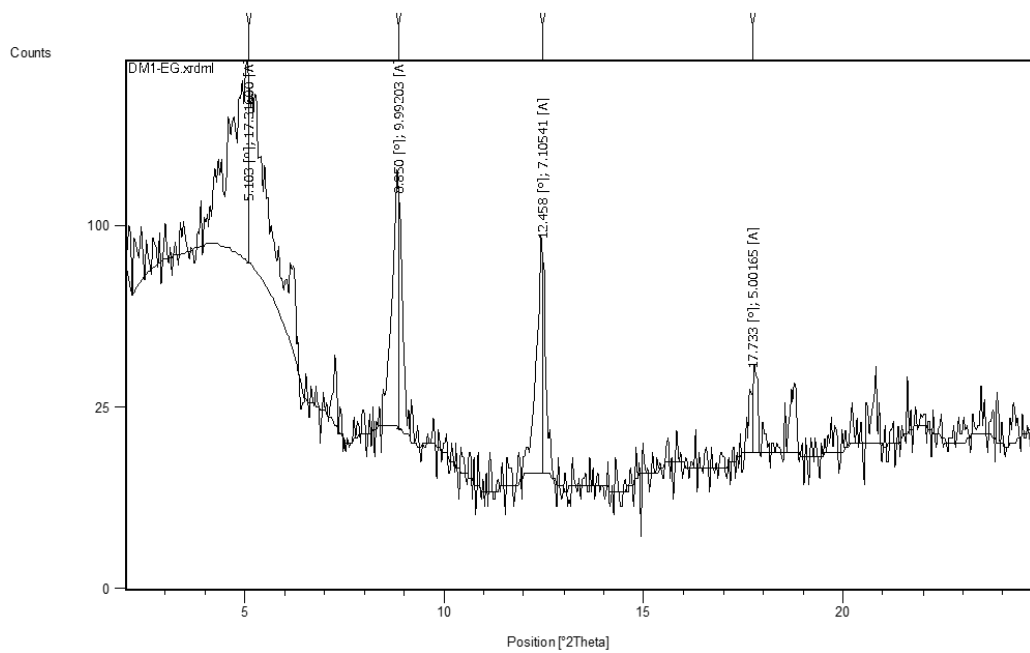


Clay mineralogy XRD charts.

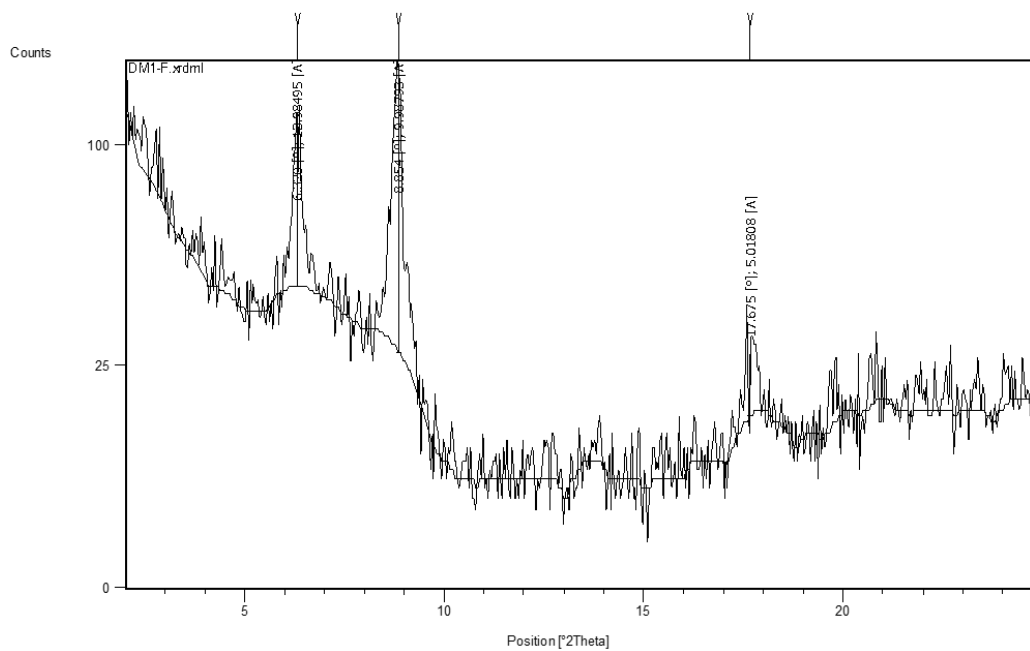
DM1 mudstone air dry mount



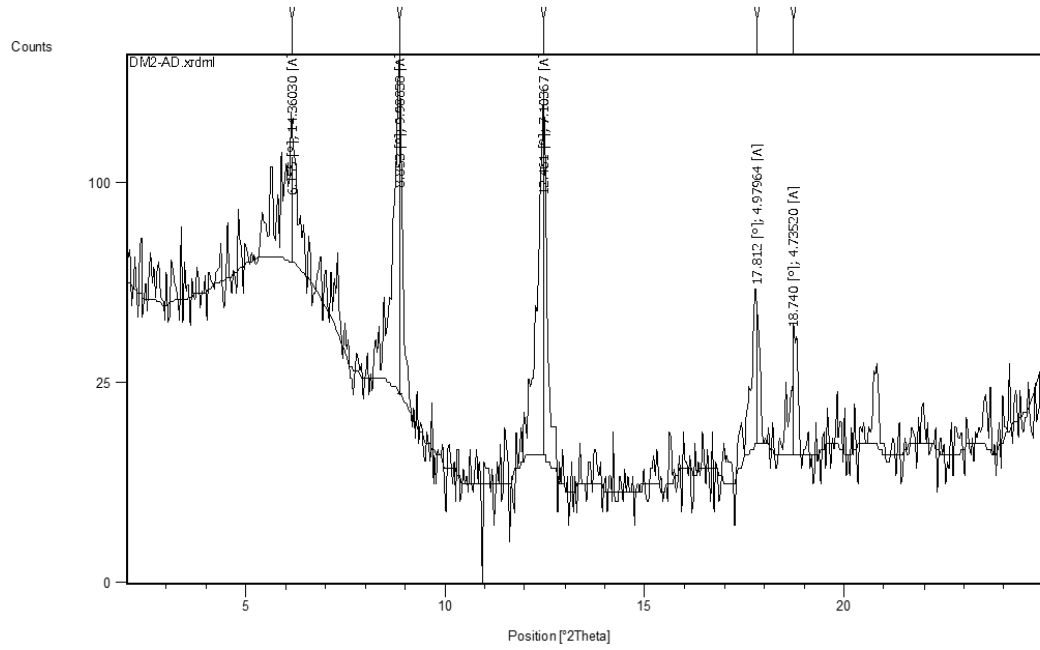
DM1 mudstone glycolated mount



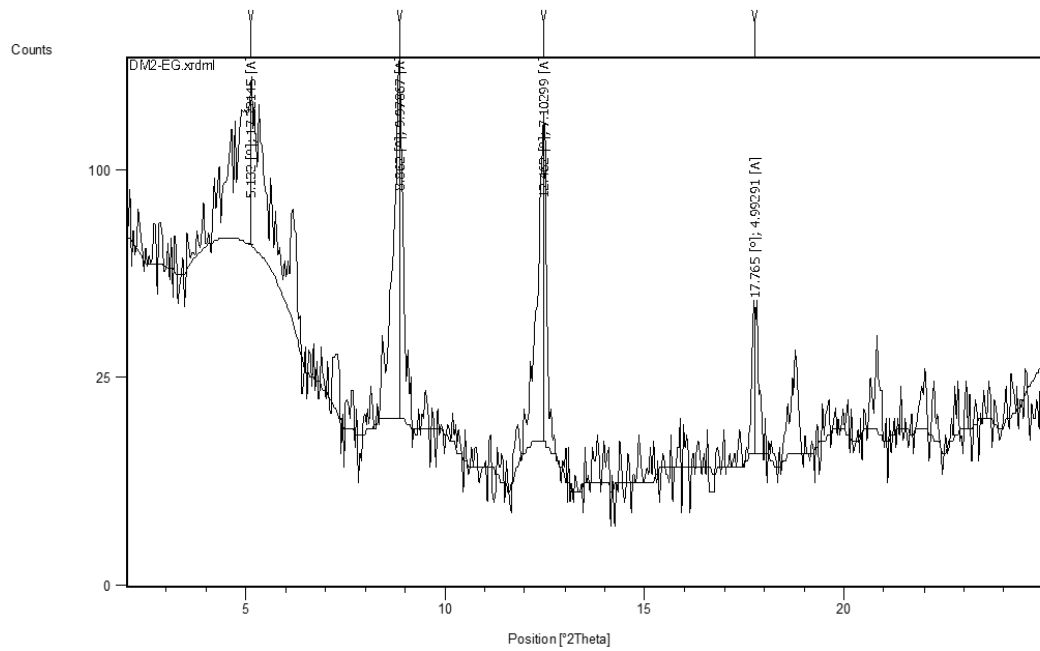
DM1 mudstone heated mount



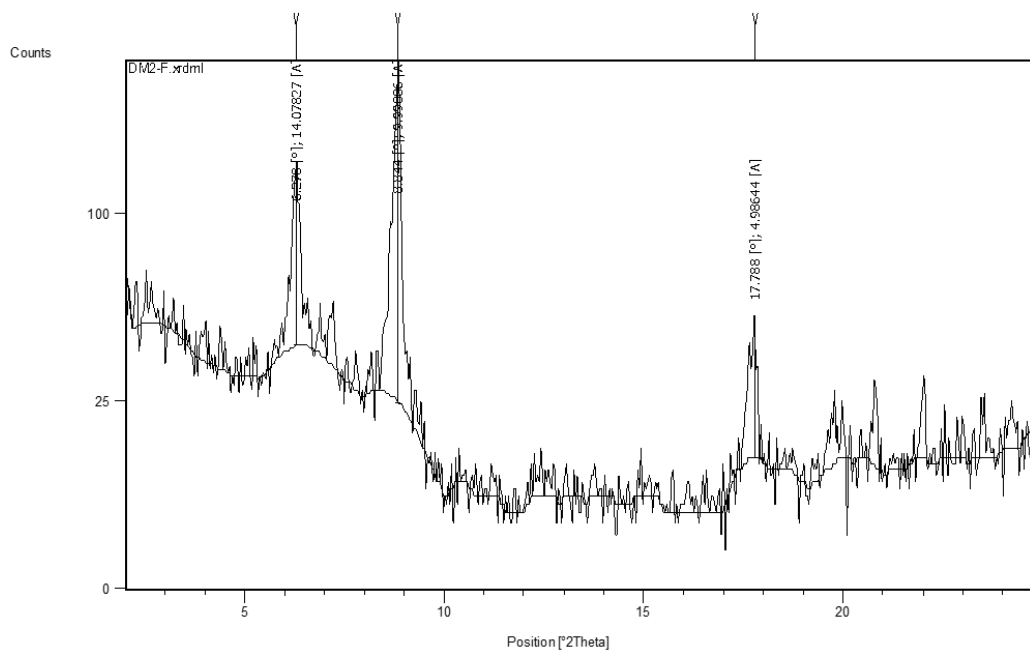
DM2 mudstone air dry mount



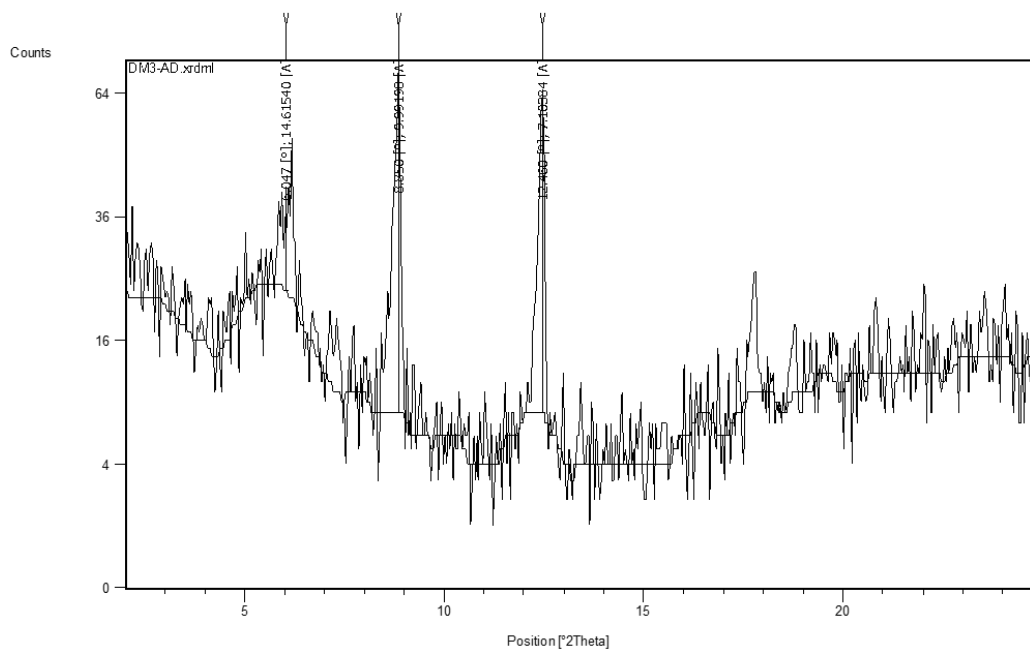
DM2 mudstone glycolated mount



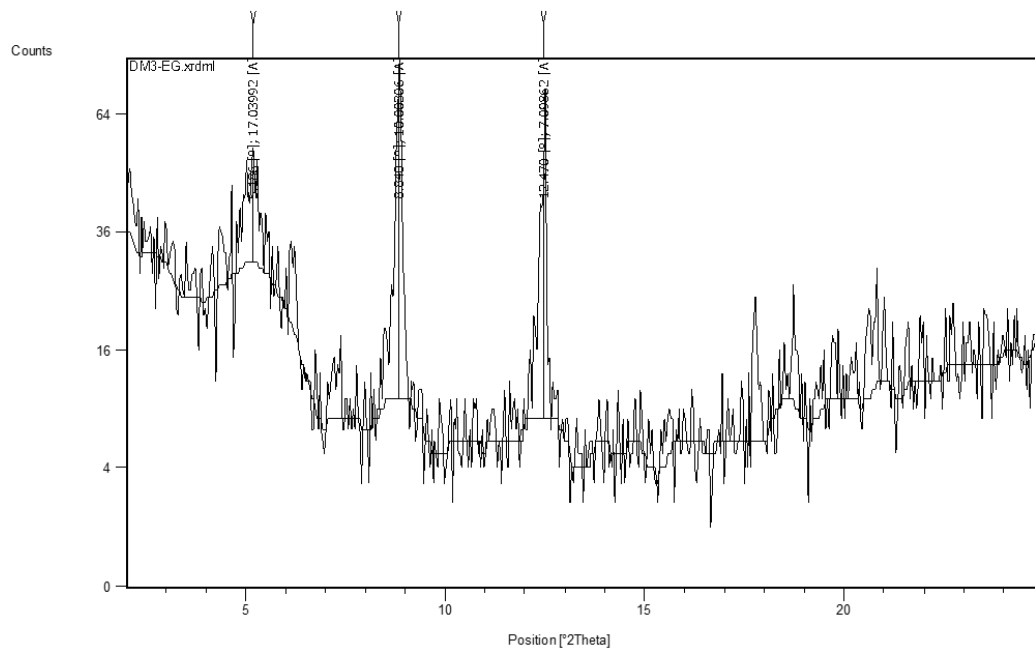
DM2 mudstone heated mount



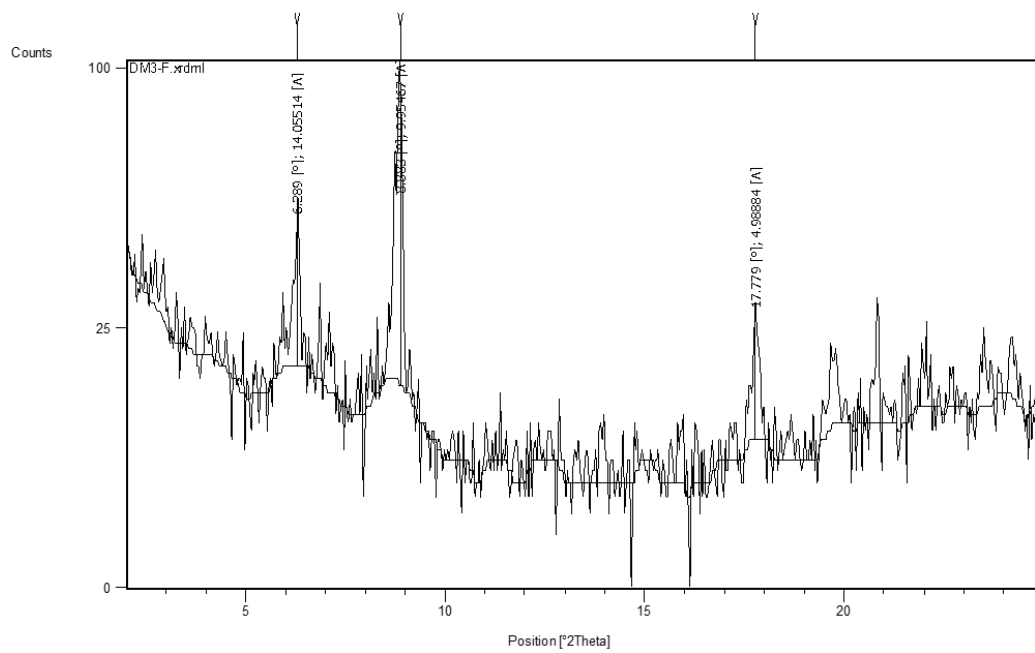
DM3 dolomitic concretion air dry mount



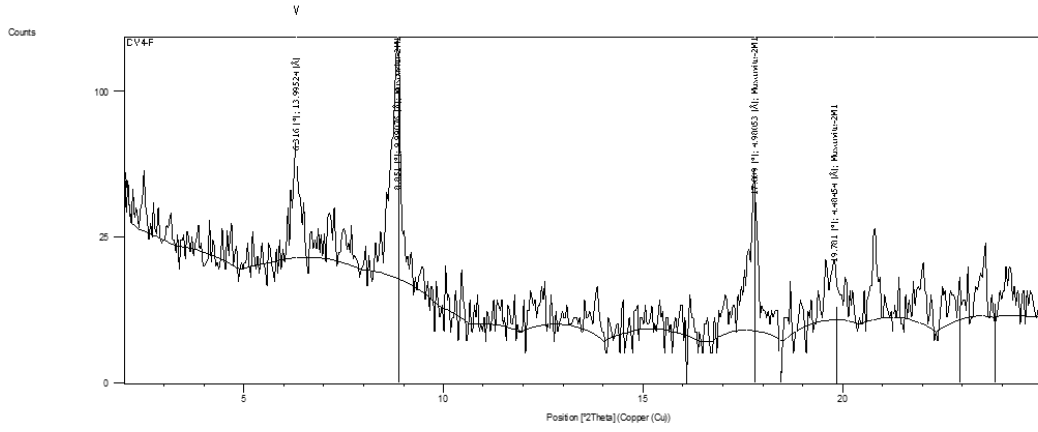
DM3 dolomitic concretion glycolated mount



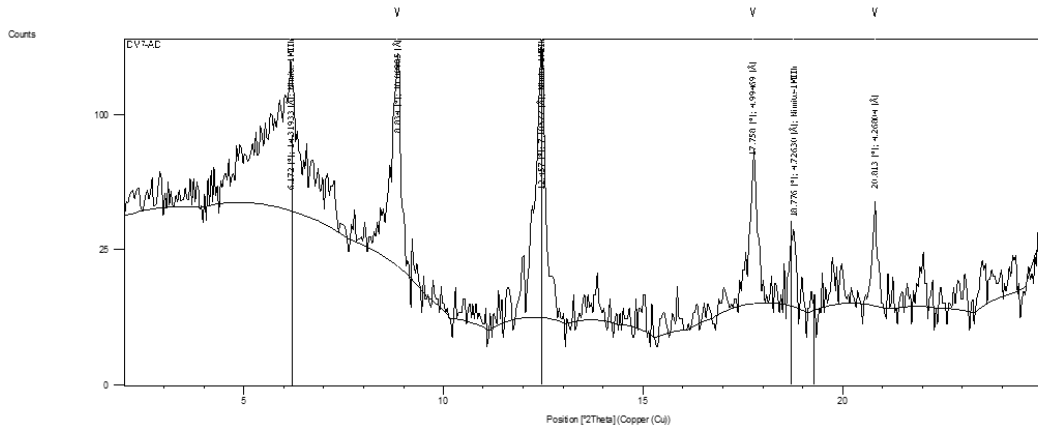
DM3 dolomitic concretion heated mount



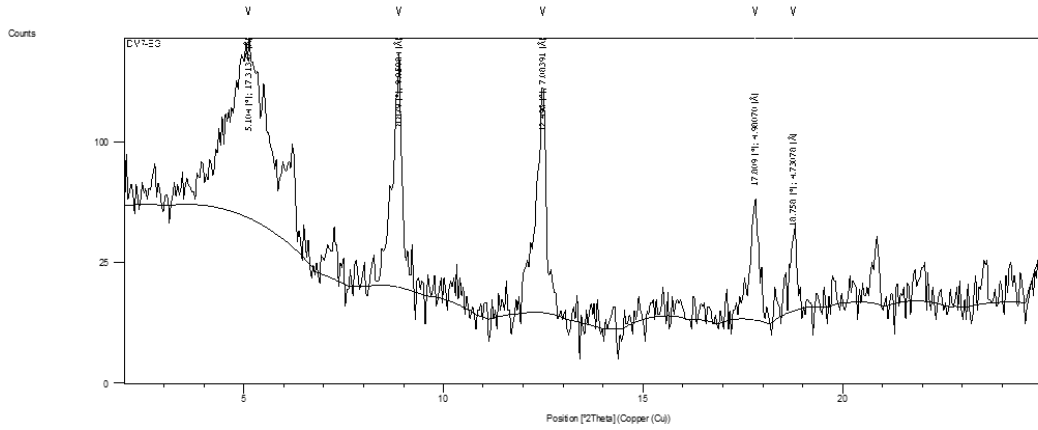
DM4 calcitic concretion heated mount



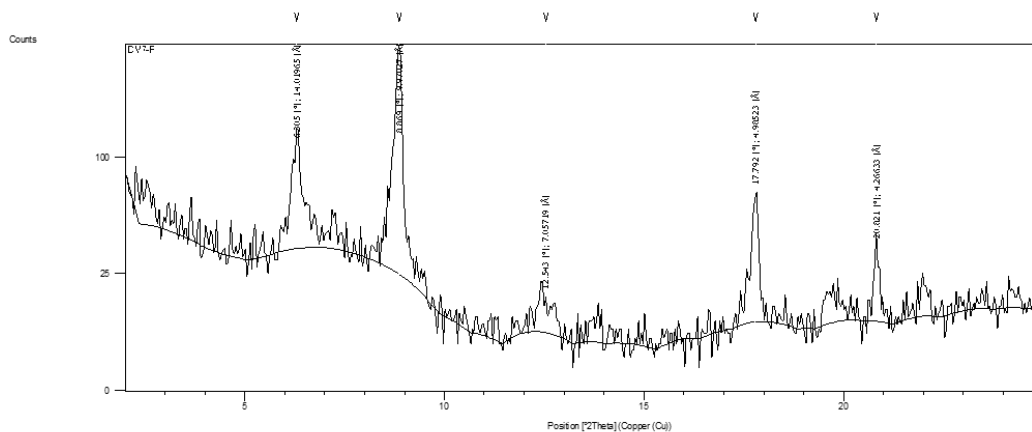
DM7 mudstone air dry mount



DM7 mudstone glycolated mount



DM7 mudstone heated mount



APPENDIX 3. XRD MINERALOGY

Summary of clay mineral analysis from both oriented and unoriented powder mounts. The main peak positions seen in each sample and their closest corresponding clay mineral are shown, along with the shape or intensity of the peak in the treated oriented samples. B=broad, Sh=sharp, L=large, M=medium, S=small, u = unoriented mount, o = oriented mount.

DM1 Mudstone	17-17.6 Å	14-14.7 Å	9.9-10 Å	7-7.1 Å	Other
Bulk (u)	-	14	10	7	
Air dry (o)	-	14.4	10	7.1	
Glycolated (o)	17.2 (B/M)	14.7 (Sh/T)	10 (Sh/L)	7.1 (Sh/L)	5 Å = 002 of 10 Å
Heated (o)	-	14 (Sh/M)	10 (Sh/L)	-	5 Å = 002 of 10 Å
DM2 Mudstone					
DM2 Mudstone	17-17.6 Å	14-14.7 Å	9.9-10 Å	7-7.1 Å	Other
Bulk (u)	-	14	10	7	
Air dry (o)	-	14.4 (B/M)	9.9 (Sh/L)	7.1 (Sh/L)	
Glycolated (o)	17.3 (B/L)	14.7 (Sh/S)	10 (Sh/L)	7.1 (Sh/L)	
Heated (o)	-	14 (Sh/M)	10 (Sh/L)	-	5 Å = 002 of 10 Å
DM7 Mudstone					
DM7 Mudstone	17-17.6 Å	14-14.7 Å	9.9-10 Å	7-7.1 Å	Other
Bulk (u)	-	14	10	7	
Air dry (o)	-	14.3 (B/M-L)	10 (Sh/L)	7 (Sh/L)	
Glycolated (o)	17.3 (B/L)	14.7 (Sh/S)	10 (Sh/M-L)	7.1 (Sh/M-L)	
Heated (o)	-	14 (Sh/M)	10 (Sh/L)	7.1 (B/S)	5 Å = 002 of 10 Å
DM3 Concretion					
DM3 Concretion	17-17.6 Å	14-14.7 Å	9.9-10 Å	7-7.1 Å	Other
Bulk (u)	-	-	10	7	
Air dry (o)	-	14.6 (B/M)	10 (Sh/L)	7.1 (Sh/L)	
Glycolated (o)	17 (B/M)	14.7 (Sh/S)	10 (Sh/L)	7.1 (Sh/L)	
Heated (o)	-	14 (Sh/M)	10 (Sh/L)	-	5 Å = 002 of 10 Å
DM4 Concretion					
DM4 Concretion	17-17.6 Å	14-14.7 Å	9.9-10 Å	7-7.1 Å	Other
Bulk (u)	-	-	9.9	7	
Air dry (o)	-	14.4 (B/M)	10 (Sh/L)	7.1 (Sh/L)	
Glycolated (o)	17.6 (B/S)	14.7 (Sh/S)	9.9 (Sh/L)	7.1 (Sh/L)	
Heated (o)	-	14 (Sh/M)	10 (Sh/L)	-	5 Å = 002 of 10 Å

The semi-quantitative results of bulk mineralogical analysis by XRD of the mudstone and concretion samples. The relative abundance of minerals in these samples are represented as A=abundant, C=common, S=some and -=absent.

	Clays	Quartz	Plagioclase	Low-Mg calcite	High-Mg calcite	Dolomite
	4.48 Å	3.34 Å	3.19 Å	3.04 Å	2.97 Å	2.89 Å
DM1 mst	A	C	S-C	S	-	-
DM2 mst	A	C	S-C	S	-	-
DM7 mst	A	C	S-C	S-C	-	-
DM3 concret	A	C	S	-	-	A
DM4 concret	A	C	S	C	S	S

APPENDIX 4. XRF GEOCHEMISTRY

Major element results. Results are in weight percent of the sample. Totals do not equal 100 due to H₂O(OH) loss in clay and CO₂ loss in carbonate. * Fe₂O₃ is total Fe and includes FeO.

Element	DM1	DM2	DM7	DM3	DM4
SiO ₂	63.25	57.95	61.14	27.51	34.90
TiO ₂	0.68	0.57	0.67	0.28	0.37
Al ₂ O ₃	15.87	14.09	15.29	7.64	9.01
Fe ₂ O ₃ *	5.62	4.64	5.44	3.43	3.79
MnO	0.07	0.06	0.07	0.07	0.11
MgO	3.15	3.04	3.08	16.49	6.07
CaO	4.36	2.30	5.90	19.15	23.65
Na ₂ O	2.36	7.43	2.30	0.35	0.34
K ₂ O	2.89	2.59	2.74	1.35	1.49
P ₂ O ₅	0.17	0.14	0.17	0.17	0.32
Total	98.41	93.48	96.80	76.45	80.04

Trace element results. Light grey numbers indicate measured values lower than the detectable limit by the XRF machine. Care should be taken with values less than 3 ppm due to a 1-5% measurement error on trace element analysis. Results are in parts per million (ppm).

Element	DM1	DM2	DM7	DM3	DM4
S	7476	4742	7397	1934	513
Cl	119	47440	944	2890	1310
V	115	88	112	49	60
Cr	75	63	76	33	42
Co	16.4	18.7	14.6	12.9	12.9
Ni	32.8	26	33	14.4	25
Cu	8.8	6.1	8.1	1.5	2
Zn	87	76	86	40	47
Ga	19.1	16.9	18.1	9.8	11.8
Ge	1.2	1.3	1.4	0.4	1.1
As	2.5	2	1.7	0.8	0.8
Se	1	0.8	0.8	0.6	0.9
Br	2.8	33	4.9	7.2	5.2
Rb	115	101	110	53	60
Sr	338	254	356	632	494
Y	18.7	20	23	9.7	17.8
Zr	163	178	165	78	118
Nb	9.3	9.2	9.3	5	5.8
Mo	1.9	2.1	2.9	< 1.0	< 1.0
Sn	2.1	1.5	1.5	0.5	0.5
Sb	< 0.9	< 0.9	< 0.9	< 0.9	< 0.9
Ba	520	500	487	300	329
La	17.7	19.4	18.9	10	13.5
Ce	45	45	47	22	31
Nd	17.8	21	23	< 10	12
Hf	9.1	6.6	7	3.6	3.6
Ta	4.3	4.2	3	< 3.0	< 3.3
W	22	33	27	51	33
Tl	1.8	1.6	1.4	1.1	1.2
Pb	14.6	13.5	13.4	7.3	8.7
Bi	0.8	0.8	< 0.5	0.8	1.2
Th	15.3	14.2	13.4	8.3	11.4
U	6.5	10	7.2	4.9	10.5

APPENDIX 5. GRAIN SIZE RESULTS

Folk & Ward (1957) equations and classifications used to classify rock samples.

Skewness		Kurtosis			
$Sk_G = \frac{\ln P_{16} + \ln P_{84} - 2(\ln P_{50})}{2(\ln P_{84} - \ln P_{16})} + \frac{\ln P_5 + \ln P_{95} - 2(\ln P_{50})}{2(\ln P_{25} - \ln P_5)}$		$K_G = \frac{\ln P_5 - \ln P_{95}}{2.44(\ln P_{25} - \ln P_{75})}$			
Mean		Standard Deviation			
$M_G = \exp \frac{\ln P_{16} + \ln P_{50} + \ln P_{84}}{3}$		$\sigma_G = \exp \left(\frac{\ln P_{16} - \ln P_{84}}{4} + \frac{\ln P_5 - \ln P_{95}}{6.6} \right)$			
Sorting (σ_G)	Skewness (Sk_G)	Kurtosis (K_G)			
Very well sorted	< 1.27	Very fine skewed	-0.3 to +1.0	Very platykurtic	< 0.67
Well sorted	1.27 – 1.41	Fine skewed	+0.1 to +0.3	Platykurtic	0.67 – 0.90
Moderately well sorted	1.41 – 1.62	Symmetrical	+0.1 to +0.1	Mesokurtic	0.90 – 1.11
Moderately sorted	1.62 – 2.00	Coarse skewed	+0.1 to +0.3	Leptokurtic	1.11 – 1.50
Poorly sorted	2.00 – 4.00	Very coarse skewed	+0.3 to +1.0	Very leptokurtic	1.50 – 3.00
Very poorly sorted	4.00 – 16.00			Extremely	> 3.00
Extremely poorly sorted	> 16.00			leptokurtic	

Udden-Wentworth grain size classes used to classify rock and sediment samples.

Millimeters	μm	Phi (ϕ)	Wentworth size class	
4096		-20	Boulder (-8 to -12 ϕ)	Gravel
1024		-12		
256		-10		
64		-8	Pebble (-6 to -8 ϕ)	
16		-6	Pebble (-2 to -6 ϕ)	
4		-4		
3.36		-2	Gravel	
2.83		-1.75		
2.38		-1.50		
2.00		-1.25		
1.68		-1.00		
1.41		-0.75		
1.19		-0.50		
1.00		-0.25	Very coarse sand	
0.84		-0.00		
0.71		0.25	Coarse sand	
0.59		0.50		
0.50		0.75		
1/2	500	1.00	Medium sand	Sand
0.42	420	1.25		
0.35	350	1.50		
0.30	300	1.75		
1/4	250	2.00		
0.210	210	2.25	Fine sand	
0.177	177	2.50		
0.149	149	2.75		
1/8	125	3.00	Very fine sand	
0.105	105	3.25		
0.088	88	3.50		
0.074	74	3.75		
1/16	63	4.00	Coarse silt	
0.0625	63	4.25		
0.0530	53	4.50		
0.0440	44	4.75		
0.0370	37	5	Medium silt	
1/32	31	6		
1/64	15.6	7	Fine silt	
1/128	7.8	8	Very fine silt	
1/256	3.9	9	Clay	Mud
0.0020	2.0	10		
0.00098	0.98	11		
0.00049	0.49	12		
0.00024	0.24	13		
0.00012	0.12	14		
0.00006	0.06	14		

APPENDIX 6. SEDIMENT SURVEY DEPLOYMENT INFORMATION

The coordinates, depth, and time recorded at each deployment during the subtidal sediment survey. Also shown is the sediment sample name collected from each successful deployment.

Transect	Deployment #	Depth (m)	GPS #	E	S	Date	Time	Sed. Sample	Sample name
1	3	~7-8	004	176°49'51.95"	40°10'40.71"	27/03/2012	8.50am	-	
1	4	10	003	176°49'58.78"	40°10'40.75"	27/03/2012	8.40am	✓	T1-4
1	5	14-15	005	176°50'13.47"	40°10'47.91"	27/03/2012	9.00am	-	
1	6	20	006	176°50'24.27"	40°10'49.98"	27/03/2012	9.15am	-	
1	7	25	007	176°50'30.54"	40°10'52.37"	27/03/2012	9.30am	-	
1	8	30	008	176°50'34.93"	40°10'54.02"	27/03/2012	9.40am	-	
1	9	35	009	176°50'45.43"	40°10'57.01"	27/03/2012	10.00am	-	
1	10	40	010	176°50'51.17"	40°10'58.07"	27/03/2012	10.10am	✓	T1-10
								2	
2	1	6	056	176°49'58.20"	40°10'27.58"	17/04/2012	8.45am	✓	T2-1
2	4	~9	058	176°50'6.37"	40°10'29.66"	17/04/2012	8.50am	✓	T2-4
2	5	15	059	176°50'17.66"	40°10'34.51"	17/04/2012	8.55am	✓	T2-5
2	6	20	060	176°50'25.46"	40°10'36.94"	17/04/2012	9.00am	✓	T2-6
2	7	25	061	176°50'46.92"	40°10'44.70"	17/04/2012	9.10am	-	
2	8	30	062	176°50'49.57"	40°10'45.54"	17/04/2012	9.15am	-	
2	9	35	063	176°50'52.48"	40°10'47.21"	17/04/2012	9.20am	-	
2	10	40	064	176°50'59.79"	40°10'50.30"	17/04/2012	9.25am	✓	T2-10
								5	
3	3	8	011	176°50'27.74"	40°10'0.74"	27/03/2012	10.35am	✓	T3-3
3	4	10	012	176°50'29.49"	40°10'4.36"	27/03/2012	10.40am	✓	T3-4
3	5	15	013	176°50'34.84"	40°10'12.68"	27/03/2012	10.48am	✓	T3-5
3	6	20	014	176°50'44.28"	40°10'18.92"	27/03/2012	10.55am	✓	T3-6
3	7	25	015	176°50'51.36"	40°10'25.26"	27/03/2012	11.04am	✓	T3-7
3	8	30	016	176°50'54.45"	40°10'30.19"	27/03/2012	11.10am	✓	T3-8
3	9	35	017	176°50'56.42"	40°10'34.97"	27/03/2012	11.19am	✓	T3-9

3	10	40	018	176°50'59.53"	40°10'37.60"	27/03/2012	11.37am	✓	T3-10	
									8	
4	4	12	049	176°50'51.12"	40°9'43.09"	16/04/2012	4.27pm	✓	T4-4	
4	5	15	050	176°50'56.22"	40°9'45.72"	16/04/2012	4.31pm	✓	T4-5	
4	6	20	051	176°51'5.69"	40°9'51.11"	16/04/2012	4.36pm	✓	T4-6	
4	7	25	052	176°51'13.38"	40°9'55.06"	16/04/2012	4.40pm	✓	T4-7	
4	8	30	053	176°51'19.93"	40°9'59.55"	16/04/2012	4.44pm	✓	T4-8	
4	9	35	054	176°51'25.89"	40°10'3.49"	16/04/2012	4.49pm	✓	T4-9	
4	10	40	055	40°10'7.47"	40°10'7.47"	16/04/2012	4.53pm	-		
									6	
5	4	10	019	176°50'59.17"	40°9'23.09"	27/03/2012	11.57am	✓	T5-4	
5	5	15	020	176°51'7.48"	40°9'27.53"	27/03/2012	12.03pm	✓	T5-5	
5	6	20	021	176°51'16.65"	40°9'33.75"	27/03/2012	-	-		
5	7	25	031	176°51'21.87"	40°9'34.94"	16/04/2012	2.15pm	✓	T5-7	
5	8	30	032	176°51'30.89"	40°9'37.39"	16/04/2012	2.20pm	✓	T5-8	
5	9	35	033	176°51'36.57"	40°9'41.85"	16/04/2012	2.30pm	✓	T5-9	
5	10	40	034	176°51'48.85"	40°9'45.64"	16/04/2012	2.40pm	✓	T5-10	
									6	
6	5	15	065	176°51'16.73"	40°9'10.89"	17/04/2012	9.43am	✓	T6-5	
6	6	20	066	176°51'30.56"	40°9'15.01"	17/04/2012	9.49am	-		
6	7	25	067	176°51'33.65"	40°9'16.37"	17/04/2012	9.51am	✓	T6-7	
6	8	30	068	176°51'47.49"	40°9'19.38"	17/04/2012	9.56am	✓	T6-8	
6	9	35	069	176°51'57.41"	40°9'22.03"	17/04/2012	10.00am	✓	T6-9	
6	10	40	070	176°52'10.14"	40°9'26.48"	17/04/2012	10.05am	✓	T6-10	
									5	
7	1	7	041	176°51'25.98"	40°8'32.64"	16/04/2012	3.34pm	✓	T7-1	
7	4	10	042	176°51'34.23"	40°8'42.50"	16/04/2012	3.42pm	✓	T7-4	
7	5	15	043	176°51'44.20"	40°8'47.27"	16/04/2012	3.47pm	✓	T7-5	
7	6	25	045	176°51'53.12"	40°8'52.47"	16/04/2012	3.55pm	✓	T7-6	
7	7	20	044	176°52'3.72"E	40°8'56.68"	16/04/2012	3.51pm	✓	T7-7	
7	8	30	046	176°52'11.17"	40°9'1.50"	16/04/2012	3.59pm	✓	T7-8	

7	9	35	047	176°52'18.78"	40° 9'5.83"	16/04/2012	4.04pm	✓	T7-9
7	10	40	048	176°52'27.35"	40° 9'10.86"	16/04/2012	4.08pm	✓	T7-10
								8	
8	6	20	035	176°52'19.56"	40° 8'31.29"	16/04/2012	2.58pm	✓	T8-6
8	7	25	036	176°52'29.15"	40° 8'37.32"	16/04/2012	3.04pm	✓	T8-7
8	8	30	037	176°52'34.03"	40° 8'42.48"	16/04/2012	3.12pm	-	
8	8	30	038	176°52'34.67"	40° 8'44.00"	16/04/2012	3.12pm	-	
8	9	35	039	176°52'41.26"	40° 8'49.19"	16/04/2012	3.16pm	-	
8	10	37	040	176°52'49.30"	40° 8'53.98"	16/04/2012	3.23pm	-	
								2	
							Total:	42	

APPENDIX 7. SUBTIDAL SEDIMENT GRAIN SIZE DATA

	µm	T1-4	T1-10	BH1	T2-1	T2-4	T2-5	T2-6	T2-10	T3-3	T3-4	T3-5	T3-6	T3-7	T3-8	T3-9	T3-10	SB1	T4-4	T4-5	T4-6	T4-7	T4-8	T4-9
Clay	0.05-3.90	0	4.66	0	0	0	0	0	6.51	0	0	0	1.43	2.43	15.91	0	21.88	0	0	0	0	2.19	3.52	6.18
Silt	7.80-63	0	14.00	0.00	0.00	0.00	0.00	0.01	15.20	0.00	0.00	0.09	2.55	3.09	19.17	0.00	55.40	0.00	0.00	0.01	0.02	4.10	5.35	14.50
Very fine sand	74-125	15.25	40.98	14.00	25.48	19.03	26.26	33.86	41.89	11.18	20.51	38.52	36.42	34.62	23.73	29.95	12.10	16.10	16.76	32.31	34.98	42.60	37.76	35.61
Fine sand	149-250	80.41	39.44	82.01	72.90	78.11	72.48	65.61	34.36	79.41	77.24	58.60	57.70	58.85	36.74	67.81	9.73	70.99	79.63	66.01	62.55	49.31	48.81	37.48
Medium sand	300-500	4.34	0.91	3.99	1.62	2.85	1.26	0.53	2.04	9.41	2.25	2.80	1.91	1.02	4.45	2.23	0.89	12.91	3.60	1.66	2.46	1.81	4.55	6.22
Coarse sand	590-1000	0	0	0	0	0	0	0	0	0	0	0	0	0	0	0	0	0	0	0	0	0	0	0.003214
	>2000	0	0	0	0	0	0	0	0	0	0	0	0	0	0	0	0	0	0	0	0	0	0	0
Mode (µm)		191.69	149.71	195.22	176.24	186.66	174.21	165.84	139.79	208.84	185.50	163.88	164.20	164.40	173.20	171.84	40.19	205.54	190.50	169.15	167.55	155.29	160.98	153.28
St Dev (µm)		51.88	71.38	50.55	47.58	49.52	46.24	43.30	74.89	59.77	48.46	56.30	60.23	59.00	97.78	50.84	67.50	70.51	50.76	49.36	53.66	63.71	76.42	92.39
Wentworth size class (based on mode)		Fine sand	Fine sand	Fine sand	Fine sand	Fine sand	Fine sand	Fine sand	Fine sand	Fine sand	Fine sand	Fine sand	Fine sand	Fine sand	Fine sand	Fine sand	Coarse silt	Fine sand						
%Sand		100	81.33	100	100	100	100	99.99	78.29	100	100	99.91	96.02	94.48	64.92	100	22.72	100	100	99.99	99.98	93.71	91.13	79.31
%Silt		0	14.00	0	0	0	0	0.01	15.20	0	0	0.09	2.55	3.09	19.17	0.00	55.40	0	0	0.01	0.02	4.10	5.35	14.50
%Clay		0	4.66	0	0	0	0	0	6.51	0	0	0	1.43	2.43	15.91	0	21.88	0	0	0	0	2.19	3.52	6.18
%Clay / %Silt		0	0.33	0	0	0	0	0	0.43	0	0	0	0.56	0.79	0.83	0	0.39	0	0	0	0	0.53	0.66	0.43
Textural classification (Folk, 1968)		Sand	Silty sand	Sand	Sand	Sand	Sand	Sand	Silty sand	Sand	Sand	Sand	Sand	Sand	Muddy sand	Sand	Sandy silt	Sand	Sand	Sand	Sand	Sand	Sand	Silty sand

	µm	T5-4	T5-5	T5-7	T5-8	T5-9	T5-10	ARA 1	T6-5	T6-7	T6-8	T6-9	T6-10	T7-1	T7-4	T7-5	T7-6	T7-7	T7-8	T7-9	T7-10	T8-6	T8-7	
Clay	0.05-3.90	0	0	1.46	1.60	3.38	7.60	0	0	0	0	5.49	7.63	0	0	0	0	0	2.40	3.42	16.20	0	0	
Silt	7.80-63	0.00	0.00	2.73	2.85	11.60	19.08	0.00	0.00	0.02	0.00	10.20	20.85	0.00	0.00	0.00	2.38	0.04	3.86	9.01	25.56	0.01	0.01	
Very fine sand	74-125	21.85	31.09	37.73	41.96	41.84	37.29	4.83	23.92	35.83	27.27	39.87	40.89	19.33	23.36	30.75	36.19	33.39	33.36	38.52	27.92	28.59	31.12	
Fine sand	149-250	74.67	65.85	56.21	52.03	38.67	29.49	82.42	74.64	62.32	71.64	41.70	28.01	78.02	73.14	65.78	58.20	62.13	56.42	44.93	26.22	69.25	65.55	
Medium sand	300-500	3.49	3.06	1.86	1.56	4.51	6.20	12.75	1.43	1.83	1.10	2.74	2.62	2.65	3.50	3.47	3.24	4.44	3.96	4.12	4.11	2.16	3.32	
Coarse sand	590-1000	0	0	0	0	0	0.335554	0	0	0	0	0	0	0	0	0	0	0	0	0	0	0	0	
	>2000	0	0	0	0	0	0	0	0	0	0	0	0	0	0	0	0	0	0	0	0	0	0	
Mode (µm)		185.60	172.91	162.22	156.27	145.01	133.44	224.56	179.32	166.93	172.58	153.20	126.68	185.87	183.41	173.49	167.33	172.69	170.25	159.55	148.02	174.98	173.80	
St Dev (µm)		52.62	54.59	60.61	59.78	79.84	101.86	58.80	46.65	51.72	45.76	75.96	78.50	48.99	53.22	55.81	61.65	60.26	70.79	77.19	94.60	50.61	55.66	
Wentworth size class (based on mode)		Fine sand	Fine sand	Fine sand	Fine sand	Very fine sand/fine sand	Very fine sand/fine sand	Fine sand	Fine sand	Very fine sand/fine sand	Fine sand	Very fine sand/fine sand	Fine sand	Fine sand										
%Sand		100	100.00	95.80	95.55	85.02	73.32	100	100.0	99.98	100.0	84.31	71.52	100	100	100	97.62	99.96	93.74	87.57	58.24	99.99	99.99	
%Silt		0	0.00	2.73	2.85	11.60	19.08	0	0	0.02	0	10.20	20.85	0	0	0.00	2.38	0.04	3.86	9.01	25.56	0.01	0.01	
%Clay		0	0	1.46	1.60	3.38	7.60	0	0	0	0	5.49	7.63	0	0	0	0	0	2.40	3.42	16.20	0	0	
%Clay / % Silt		0	0	0.54	0.56	0.29	0.40	0	0	0	0	0.54	0.37	0	0	0	0	0	0.62	0.38	0.63	0	0	
Textural classification (Folk, 1968)		Sand	Sand	Sand	Sand	Silty sand	Silty sand	Sand	Sand	Sand	Sand	Muddy sand	Silty sand	Sand	Sand	Sand	Sand	Sand	Sand	Sand	Silty sand	Muddy sand	Sand	Sand